Advanced Self - Reporting Polymer Systems with Tailored Properties

Zur Erlangung des akademischen Grades einer

DOKTORIN DER NATURWISSENSCHAFTEN

(Dr. rer. nat.)

von der KIT-Fakultät für Chemie und Biowissenschaften

des Karlsruher Instituts für Technologie (KIT)

genehmigte

DISSERTATION

von

M. Sc. Christina Maria Geiselhart

aus Weingarten, Deutschland

1. Referent: Prof. Dr. Christopher Barner-Kowollik
2. Referent: Prof. Dr. Pavel Levkin

Tag der mündlichen Prüfung: 08.02.2021

To my family

"A diamond doesn't start out polished and shining. It once was nothing special, but with enough pressure and time, becomes spectacular."

Solange Nicole

Die vorliegende Arbeit wurde im Zeitraum von April 2017 bis Februar 2021 am Institut für Technische Chemie und Polymerchemie am Karlsruher Institut für Technologie (KIT) – Universitätsbereich unter der Betreuung von Dr. Hatice Mutlu und Prof. Dr. Christopher Barner-Kowollik angefertigt.

Erklärung

Ich erkläre hiermit, dass ich die vorliegende Arbeit im Rahmen der Betreuung durch Dr. Hatice Mutlu und Prof. Dr. Christopher Barner-Kowollik selbstständig verfasst und keine anderen als die angegebenen Quellen und Hilfsmittel verwendet habe. Wörtlich oder inhaltlich übernommene Stellen sind als solche kenntlich gemacht und die Satzung des Karlsruher Instituts für Technologie (KIT) zur Sicherung guter wissenschaftlicher Praxis wurde beachtet.
Des Weiteren erkläre ich, dass ich mich derzeit in keinem weiteren laufenden Promotionsverfahren befinde und auch keine vorausgegangenen Promotionsversuche unternommen habe.

Ort, Datum Christina Geiselhart

Abstract

Polymeric compounds that mimic the stimuli-responsive behaviour of natural organisms have emerged as powerful tools for the design of innovative, smart, human-made materials. One important class thereby are self-reporting polymeric materials. These materials visually report changes or damages caused by different stimuli (e.g. mechanical forces, temperature, pH, light or chemicals) immediately without the need of sophisticated instruments.

On this premise, in the present thesis two different systems of self-reporting polymeric materials were investigated. The first one is based on a polymeric system with chemiluminescent (CL) properties, i.e. the system emits light in the visible range as a direct response to chemical stimuli. Therefore, statistical copolymers of methyl methacrylate (MMA), pentafluorophenyl acrylate (PFP-A) and 4-vinyl benzylchloride (VBC) were synthesized via free radical polymerization (FRP). Subsequently, post-polymerization modifications (PPM) were conducted to introduce the desired properties to the polymer. Substitution of the PFP-moieties with luminol as luminophore enabled the CL reaction output, while modification of the VBC units with the organic superbase 1,5,7-triazabicyclo[4.4.0]dec-5-ene (TBD) provided the required basic environment for the successful CL reaction of luminol. In the presence of randomly methylated β-cyclodextrin (β-CD), the TBD-units were encapsulated and supramolecular assemblies mimicking biomolecule-substrate interactions were formed. Upon the addition of chemical stimuli (e.g. reactive oxygen species (ROS)), the host-guest interactions were disrupted and the luminol moieties were oxidized to the excited 3-aminophthalhydrazide units, which emitted a striking blue-green light when returning to the ground state. Additionally, as a positive side-effect, the CL emission of luminol was enhanced by the β-CD. The novel self-reporting polymeric system and its CL properties were characterised by 1D and 2D nuclear magnetic resonance (NMR) spectroscopy, dynamic light scattering (DLS), UV/Vis spectroscopy and CL measurements.

However, light is not only able to self-report the presence of certain stimuli, but also acts as stimulus itself. Thereupon focuses the second system of the investigated self-reporting polymeric materials. By means of the Passerini Multi-Component-Reaction (MCR), photo-sensitive tetrazole-containing monomers were synthesized that subsequently allowed a direct

reversible-deactivation radical polymerization (RDRP). Depending on the tetrazole species, the obtained polymer was folded and post-modified under irradiation with UV- (λ_{em} = 320 nm) or visible (λ_{em} = 420 nm) light. Light irradiation leads to the release of N_2 from the tetrazole and subsequently, to the formation of a nitrile-imine dipole. This nitrile-imine dipole can react with various substrates such as amino acids, boronic acid derivatives, alcohols or thiols. Most importantly, the dipole can react with alkene moieties (e.g. maleimides) to form highly fluorescent pyrazolines. Since this photoreaction, i.e. the nitrile-imine mediated tetrazole-ene cycloaddition (NITEC), leads to a colour change of the reaction mixture (from almost colourless to a strong yellow), the reaction progress can be readily monitored by the naked eye as well as by absorbance and fluorescence measurements. The synthesis of the monomers, polymers and photoproducts were characterised via NMR spectroscopy, SEC, UV/Vis- and fluorescence spectroscopy.

Zusammenfassung

Polymere Materialien, die das stimuli-responsive Verhalten von natürlichen Organismen nachahmen, haben sich als nützliches Werkzeug für das Design innovativer, intelligenter, synthetischer Materialien herausgestellt. Eine wichtige Klasse hierbei sind die selbst-berichtenden Materialien, welche Veränderungen oder Schäden durch verschiedene Stimuli (z. B. mechanische Kräfte, Temperaturen, pH, Licht oder Chemikalien) sofort und ohne komplexe Instrumente visuell anzuzeigen können.

Unter dieser Prämisse wurden in der vorliegenden Doktorarbeit zwei verschiedene Systeme selbst-berichtender polymerer Materialen untersucht. Eines davon basiert auf einem Polymersystem mit chemilumineszenten (CL) Eigenschaften, also einem System, welches sichtbares Licht als direkte Antwort auf chemische Stimuli ausstrahlt. Dafür wurden mittels der freien radikalischen Polymerisation (FRP) statistische Copolymere aus Methylmethacrylat (MMA), Pentafluorophenylacrylat (PFP-A) und 4-Vinyl-Benzylchlorid (VBC) hergestellt. Anschließend wurde das Polymer mit den gewünschten Eigenschaften durch Post-Polymerisationsmodifikationen (PPM) versehen. Substitution der PFP-Einheiten mit Luminol als Luminophor ermöglichte die CL als Reaktionsprodukt, wohingegen die Modifikation der VBC-Einheiten mit der organischen Superbase 1,5,7-Triazabicyclo[4.4.0]dec-5-en (TBD) die notwendige Basizität für die erfolgreiche CL sicherstellte. In der Gegenwart von statistisch methyliertem β-Cyclodextrin (β-CD) wurden die TBD-Gruppen eingeschlossen und supramolekulare Einheiten analog zu Biomolekül-Substrat-Wechselwirkungen gebildet. Durch die Zugabe von chemischen Stimuli (bspw. reaktive Sauerstoffspezies) wurden die Wirts-Gast-Bindungen gelöst und die Luminol-Einheiten zu angeregten 3-Aminophthalhydrazid-Einheiten oxidiert, welche bei der Rückkehr in den Grundzustand strahlend blaugrünes Licht emittierten. Als positiver Nebeneffekt wurde durch das β-CD zusätzlich die CL Emission von Luminol erhöht. Das neue selbst-berichtende Polymersystem und seine CL-Eigenschaften wurden mittels 1D und 2D nuklearer magnetischer Resonanzspektroskopie (NMR), dynamischer Lichtstreuung (DLS), UV/Vis-Spektroskopie sowie CL-Messungen charakterisiert.

Licht kann jedoch nicht nur die Gegenwart von chemischen Stimuli anzeigen, sondern auch selbst als Stimulus agieren. Darauf basiert das zweite System der untersuchten selbst-

berichtenden polymeren Materialien. Zunächst wurden mittels der Passerini Multikomponenten-Reaktion licht-sensitive Monomere mit Tetrazol-Einheiten synthetisiert, welche anschließend eine radikalische Polymerisation mit reversibler Deaktivierung ermöglichten. Abhängig von den Tetrazol-Derivaten konnte das erhaltene Polymer durch Bestrahlung mit UV- (λ_{ex} = 320 nm) oder sichtbarem (λ_{ex} = 420 nm) Licht gefaltet und post-modifiziert werden. Die Bestrahlung mit Licht führt zu der Freisetzung von N_2 aus dem Tetrazol und ein Nitril-Imin Dipol wird generiert. Dieser Nitril-Imin Dipol kann mit verschiedenen Substraten, z.B. Aminosäuren, Borsäurederivaten, Alkoholen oder Thiolen reagieren. Am wichtigsten jedoch ist die mögliche Reaktion des Dipols mit Alkengruppen (bspw. Maleimide), bei der stark fluoreszierende Pyrazoline entstehen. Da diese Photoreaktion, genauer gesagt die Nitril-Imin vermittelte Tetrazol-En Cycloaddition (NITEC), zu einer Farbänderung der Reaktionslösung (von fast farblos bis stark gelb) führt, kann der Reaktionsverlauf einfach mit dem bloßen Auge, Absorbanz- oder Fluoreszenzmessungen beobachtet werden. Die Synthese der Monomere, Polymere und die Produkte der Photoreaktion wurden mittels NMR Spektroskopie, GPC, UV/Vis- und Fluoreszenz-Spektroskopie analysiert.

Publications and Conference Contributions

Publications Arising from this Thesis

Passerini Multi-Component Reactions Enabling Self-Reporting Photo-Sensitive Tetrazole-Polymers. C. M. Geiselhart, H. Mutlu, C. Barner-Kowollik, *in preparation.*

Untapped Toolbox of Luminol Based Polymers. C. M. Geiselhart, C. Barner-Kowollik, H. Mutlu, ***Polym. Chem.*** **2021**, https://doi.org/10.1039/D1PY00034A.

Prevent or Cure – The Unprecedented Need for Self-Reporting Materials. C. M. Geiselhart, H. Mutlu, C. Barner-Kowollik, ***Angew. Chem*****. 2020**, https://doi.org/10.1002/anie.202012592.

Chemiluminescent Self-Reporting Supramolecular Transformations on Macromolecular Scaffolds. C. M. Geiselhart, H. Mutlu, P. Tzvetkova, C. Barner-Kowollik, ***Polym. Chem.*** **2020**, *11*, 4213.

A Guanidine-Based Superbase as Efficient Chemiluminescence Booster. C. M. Geiselhart, C. W. Schmitt, P. Jöckle, H. Mutlu, C. Barner-Kowollik, ***Sci. Rep*****. 2019**, *9*, 14519.

Other Publications

Degradable Redox-Responsive Novel Polyolefin Derivatives. C. M. Geiselhart, W. Xue, C. Barner-Kowollik, H. Mutlu, ***Macromolecules.*** **2021**, accepted.

Untapped Potential for Debonding on Demand: The Wonderful World of Azo-Compounds. H. Mutlu, C. M. Geiselhart, C. Barner-Kowollik, ***Mater. Horiz*****. 2018**, *5* 162.

Polybutadiene Functionalization via an Efficient Avenue. C. M. Geiselhart, J. T. Offenloch, H. Mutlu, C. Barner-Kowollik, ***ACS Macro Lett*****. 2016**, *5*, 1146.

Conference Contributions

Organic Superbases as Efficient Chemiluminescence Booster (Poster Presentation)

C. M. Geiselhart, C. W. Schmitt, P. Jöckle, P. Tzvetkova, H. Mutlu, C. Barner-Kowollik, *Macromolecular Colloquium Freiburg*, February 26th – 28th 2020.

Table of Contents

1 Introduction

Natural organisms such as plants, animals or the human body, inherit the possibility to sense, report and eventually, heal any damages immediately in a visible manner. Plants, for example, respond to a deficiency of water with a colour change and falling leaves, while marine phytoplankton or glow-worms emit light in the visible range due to environmental changes or as mating call; biological mechanisms in the human body visually indicate injuries by the red colour of bleeding wounds or the colour change of bruises on the skin and autonomously start the healing process. These properties of natural organisms have inspired scientists to create fascinating smart, stimuli-responsive polymeric materials in order to fulfil the ever-growing demands on our daily lives technologies. Depending on the initial synthesis strategy, the smart material alters its properties in the presence of certain stimuli (such as mechanical forces, magnetic fields, ultrasound, temperature, pH, solvation, light or chemicals).[1-5]

For example, the successful transfer from natural self-healing properties to synthetic materials has been reported.[6-10] On the one hand, polymeric materials with either non-covalent (such as hydrogen bonding, supramolecular complexes or ionomers) or covalent segments allowing reversible (de-)bonding reactions (e.g. Diels Alder, thiol-ene, addition or condensation reactions) have been developed.[11-16] On the other hand, containers (e.g. microcapsules or microchannels) filled with a healing agent into polymeric materials were dispersed into polymeric materials.[13, 17-19] Upon physical damage, the (non-)covalent bonds or the containers break and the healing process takes place, either by inducing the reverse bonding reaction or release of the healing agent form the containers. However, there are also drawbacks such as complex monomer / polymer synthesis, necessity of close proximity for the functional groups, the requirement of external triggers to induce the bonding reaction or the irreversible breaking of the containers. Therefore, self-healing materials would highly benefit from the ability to report the existence and exact location of damages immediately, particularly in a visible way. The latter would not only allow to monitor damaged areas and their healing process very carefully, but also to apply necessary external triggers in a fast and precise manner to the damaged area to increase the life-time and safety of human-made materials. Consequently, the class of stimuli-responsive materials was expanded by the development of

self-reporting systems that visually indicate any changes or damages due changes in colour, fluorescence or chemiluminescence, as illustrated in Scheme 1.1.[3-4, 20-22]

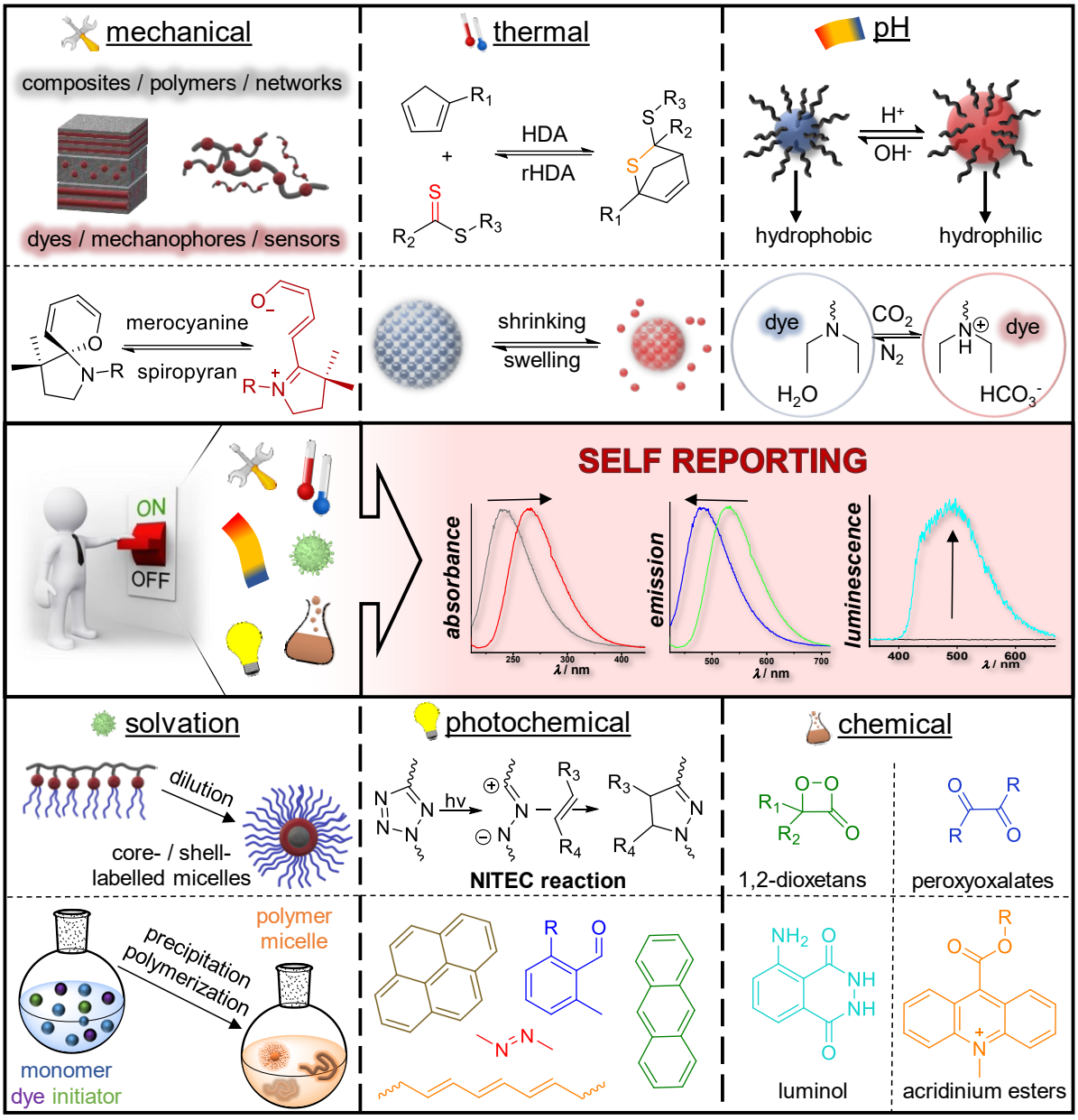

Scheme 1.1: Overview of stimuli (e.g. mechanical, thermal, pH, solvation, photochemical and chemical) employed to switch on / off self-reporting properties of human-made materials, which are visualized by a change in colour, fluorescence or chemiluminescence, respectively.[4]

Advantageously, various stimuli-responsive components are ideally suited for the design of self-reporting materials such as dye-filled containers (microcapsules or fibres),[23-26] fluorescent guest-molecules encapsulated by supramolecular host molecules (e.g. rotaxanes or cucurbiturils)[27-28] as well as diverse chromophores (e.g. mechanophores, fluorophores, thermochromic substances or luminophores).[29-38] Embedded into polymeric materials, these

compounds alter their optical appearance due to broken interactions or structural changes triggered by mechanical forces, temperature, pH, solvation, light or chemicals (refer to Scheme 1.1). Depending on the applied stimuli-responsive functionality, the self-reporting output can even be triggered by several stimuli simultaneously.[21, 39-41] This is especially useful for outdoor materials or materials exposed to harsh and changing environments (e.g. different weather conditions throughout the seasons, heating / air conditioning or pollutions). Clearly, such self-reporting materials hold great potential for the development of innovative, smart stimuli-responsive materials with applications in e.g. nanotechnology, engineering, biology, medicine or sensor technology.

Among the plethora of stimuli-responsive components with self-reporting properties, chemiluminescence (CL) as a direct visual indication output offers advantages such as high sensitivity and real-time monitoring without the need of an external light source or complicated instrument setups.[42-45] Unfortunately, the CL quantum yields are rather low compared to bioluminescent quantum yields and thus, (high) excess of additives such as catalysts or enhancers is required.[46-47] Therefore, the first aim of the present doctoral thesis was the development of a simplified, yet efficient self-reporting CL system (Chapter 3.1). In order to simplify conventional CL systems, a polymeric system was designed that contained all the necessary functionalities for a successful CL reaction output in the same backbone, as illustrated in Scheme 1.2 (top). Luminol was chosen as the most prominent representative luminophore,[48-50] and, since it is well known that the luminol-CL requires additional bases or catalysts,[29, 51-52] the organic superbase 1,5,7-triazabicyclo[4.4.0]dec-5-ene (TBD) was selected as second functionality. Additionally, supramolecular assemblies were formed in the presence of randomly methylated β-cyclodextrin (Me-β-CD) to mimic the binding behaviour of biological substrates.

However, light is not only a powerful tool to monitor ROS in a self-reporting manner, but is also important as stimulus itself to trigger a self-reporting output. Indeed, light as trigger offers the unique advantages of spatiotemporal controllability, short reaction times already at ambient temperatures and an easy fine-tuning of the desired wavelength by carefully choosing the photo-sensitive substrate.[53-57] Additionally, protein-like structures can be obtained by light-induced intramolecular folding of polymers with tethered photo-sensitive moieties such as anthracene, pyrene-substituted oxime esters, benzophenone, nitroxides or tetrazoles.[58-62] By incorporating photo-sensitive substrates responsive to different

wavelengths, the folding of the polymer can be achieved in a light-controlled orthogonal way.[63-65] While such a strategy is appealing, the synthetic approach towards such λ-orthogonal photo-sensitive polymers is challenging and often requires a multi-step synthesis. Accordingly, the second aim of the present thesis is to simplify the synthesis of such polymers (Chapter 3.2). As photo-sensitive compound, the tetrazole-moiety has been chosen due to the facile fine-tuning of the photo-responsiveness.[66-67] Therefore, different light-responsive tetrazole-monomers were synthesized using the Passerini multi-component reaction (MCR) and subsequently polymerized via reversible-deactivation radical polymerization (RDRP) protocols (refer to Scheme 1.2, bottom). Irradiation with either UV- or Vis-light in the presence of suitable alkenes (e.g. maleimides) induced the folding process, which self-reports due to the formation of the highly fluorescent pyrazoline-adduct.

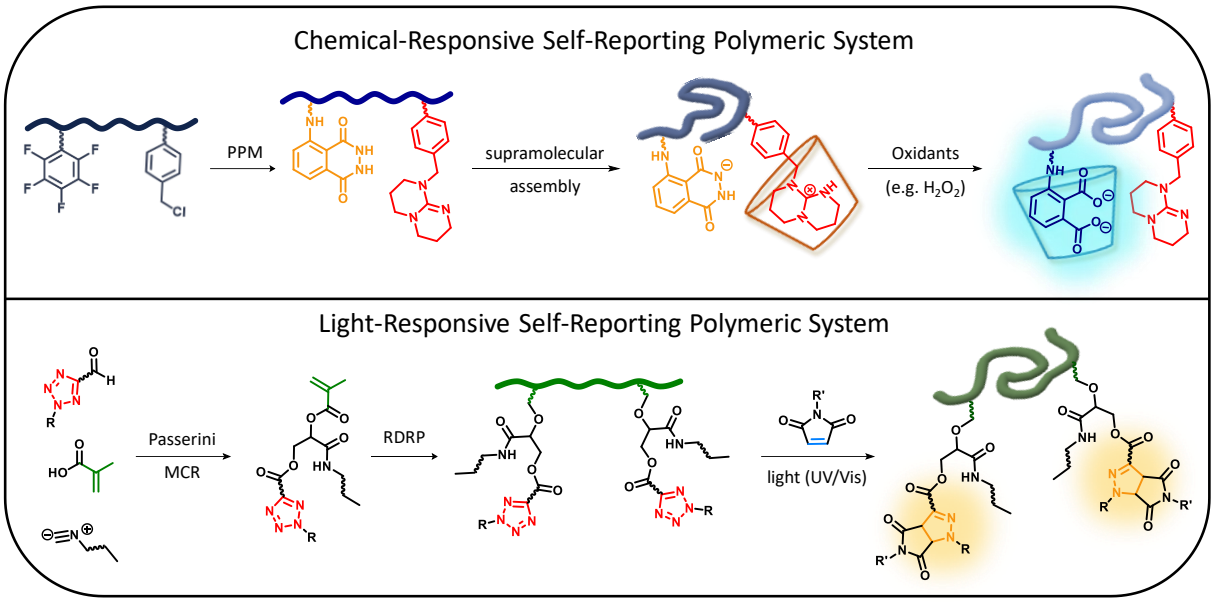

Scheme 1.2: Overview of the two self-reporting polymeric systems investigated in the current thesis: the chemiluminescent luminol-based polymer responsive to chemicals (top) and the fluorescent tetrazole-based polymer responsive to light (bottom).

2 Theoretical Background

To aid a better understanding of the topics discussed in the present PhD thesis, the underlying theoretical principles are subsequently covered. First, the relevant synthesis and modification techniques of polymeric materials are introduced (Chapter 2.1). Subsequently, the theory for photochemistry (Chapter 2.2) and tetrazoles (Chapter 2.2.3) are described. Finally, chemiluminescence (Chapter 2.3) and the applied organic compounds as handles for the CL output (i.e. luminol (Chapter 2.4.1), organic superbases (Chapter 2.4.2) and host-guest complexes (Chapter 2.4.3)) are addressed.

2.1 Polymers – Synthesis and Modification Techniques

Although materials with high molecular weights have been known since the 19th century from natural products such as cellulose, rubber, resins or proteins,[68-70] the molecular nature of such materials was not understood before the findings of Hermann Staudinger in 1920.[71] His research into the chemical and physical properties of "macromolecules" not only earned him the Nobel prize in 1953,[72] but also paved the way for the synthesis of diverse polymeric materials.[73-75] Today, several polymerization strategies are available for the synthesis of polymers with specific, tailor-made properties. These can be divided into two major categories, namely the step-growth and the chain growth polymerizations with various subclasses,[76-77] as illustrated in Scheme 2.1. Characteristic for the different polymerization techniques is the dispersity $Đ$ as the ratio between the molar mass average (M_w) and the number average (M_n) (Equation 2.1).[77-78]

$$Đ = \frac{M_w}{M_n}$$

Equation 2.1: Dispersity $Đ$ defined as ratio between the mass average M_w and the number average M_n.

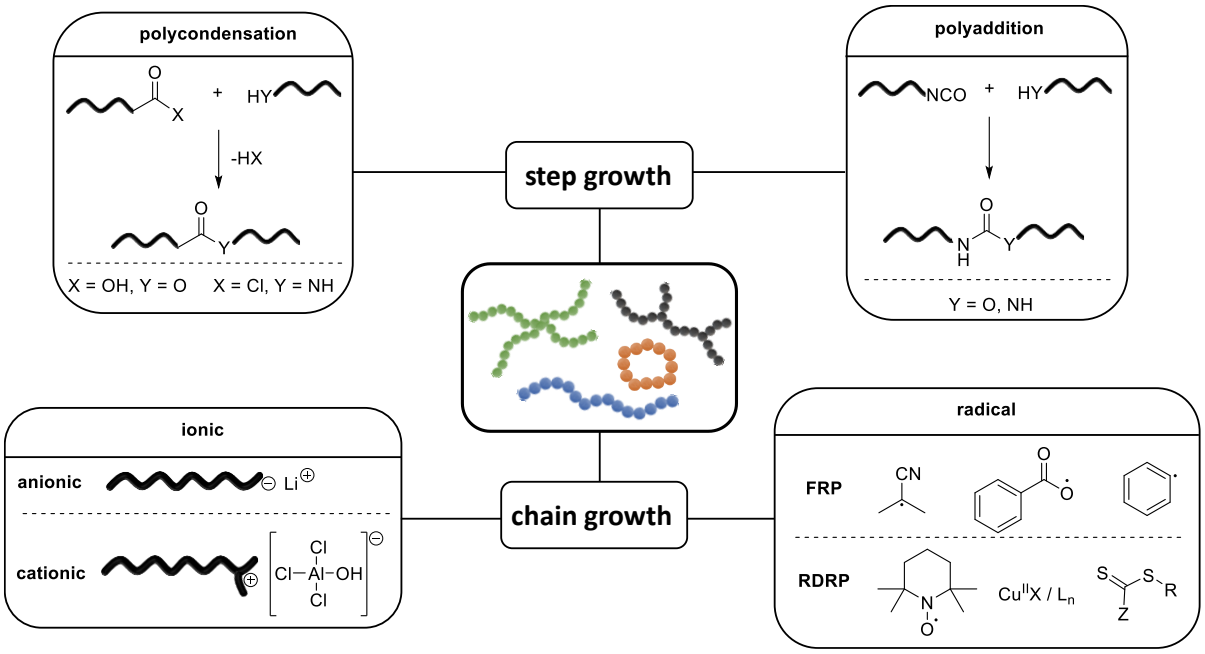

Scheme 2.1: Two main categories of polymerization strategies and their respective subclasses.

Perfectly defined polymers, in which all chains are of identical length have a *Đ* value of 1.0 and are almost exclusively found in natural polymers (e.g. peptides, DNA). In synthetic polymers, the closest *Đ* values to 1 are obtained via anionic polymerization (*Đ* < 1.1), followed by polymers synthesized via reversible-deactivation radical polymerization (RDRP) (*Đ* = 1.1 – 1.4). Higher values are usually obtained via free radical polymerizations (FRP) (*Đ* > 1.5).

However, research into designing perfectly defined synthetic polymers is of growing interest to obtain polymeric materials with dispersity values analogue to natural polymers.[79-84] One approach therefore applies proteins as precursors for the synthesis of well-defined polymeric materials.[85-88] Another approach is based on the synthesis of (polydisperse) RDRP-polymers, which are subsequently separated into well-defined fractions (*Đ* < 1.1) by flash column chromatography.[81, 89-90] Furthermore, ring-opening metathesis polymerization,[91-92] single-chain nanoparticle formations,[93] multi-component reactions,[94-96] iterative synthesis strategies[97-98] or photochemical approaches[99-102] were successfully applied for the formation of well-defined polymers.

While a detailed comparison of all these techniques would be beyond the scope of the present doctoral thesis, the focus in the following chapters lies on the two relevant techniques of the second category, i.e. the FRP (Chapter 2.1.1) and the reversible addition-fragmentation chain transfer (RAFT) polymerization (Chapter 2.1.2). Furthermore, the synthesis of highly functional monomers via multi-component reactions (MCRs) will be described (Chapter 2.1.3).

However, it is not always possible to introduce all desired functionalities directly during the polymerization process due to solubility issues, undesired side reactions or instability at the applied reaction conditions. Therefore, methods have been developed to introduce functional moieties into polymeric materials without affecting the initial polymeric backbone by various (orthogonal) post-polymerization modification (PPM) reactions (Chapter 2.1.4).

2.1.1 Free Radical Polymerization (FRP)

The free radical polymerization (FRP) is one of the most detailed investigated polymerization techniques in industry and academia. This is attributed to the broad range of available monomers and initiators. As depicted in Scheme 2.2, the mechanism involves four steps.[103-104] Initially, radicals are generated by the thermal or photochemical decomposition of the initiator and the first monomer is added. The efficiency *f* of the initiation is thereby critical for the success of the subsequent propagation step.[103]

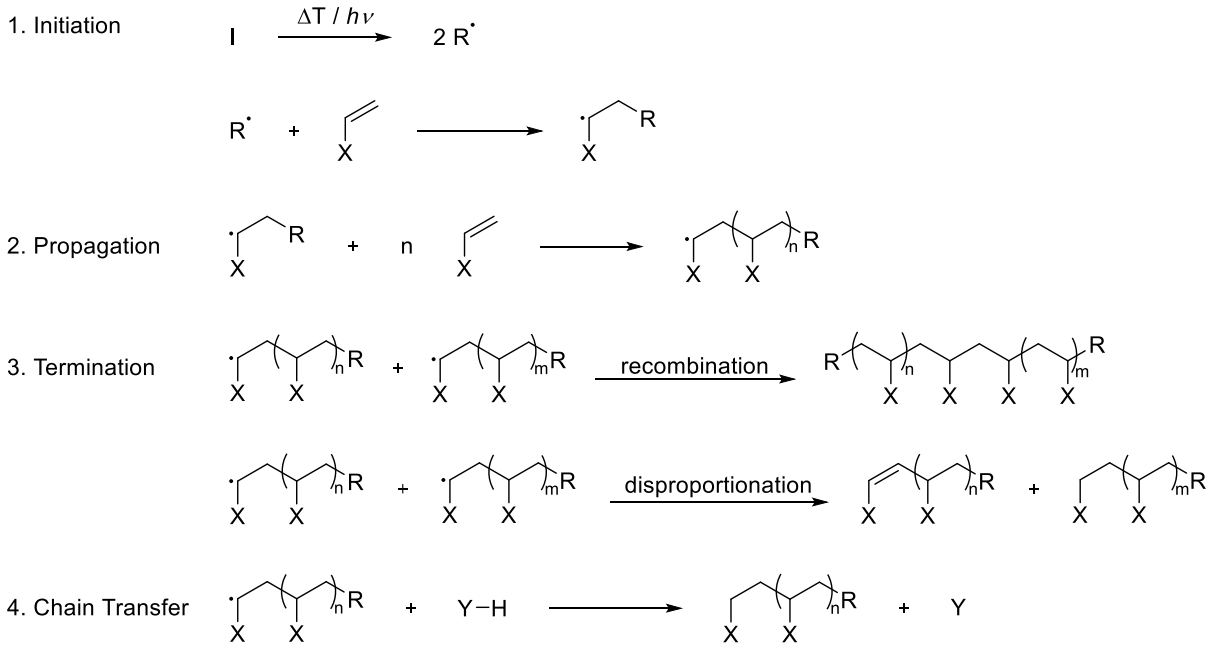

Scheme 2.2: The four steps of the FRP process, i.e. initiation, propagation, termination and chain transfer.

While *f* = 1 would be the optimum efficiency, the values of the subsequent propagation are typically lower due to several side effects such as recombination (within or outside the solvent cage), branching or crosslinking reactions. Thus, the values for *f* range from 0.3 (for less efficient initiators) to 0.8 (for efficient initiators) depending on the solvent, temperature and

viscosity of the reaction mixture. Commonly applied initiators belong either to the class of azo compounds (e.g. 2,2'-azobisisobutyronitrile (AIBN), 4,4'-azobis(4-cyanovaleric acid) (V-501)) or peroxide derivatives (e.g. benzyl peroxide (BPO), di-*tert*-butylperoxide (DTBP)).[77, 103] Once the initiation step has taken place, the chain is growing in the propagation step by adding further monomers until the growing chains are terminated. The termination involves three steps:[103]

1. translational diffusion (the propagating polymer chains need to converge);
2. segmental diffusion (the radical chain ends have to rearrange themselves to be in a suitable distance for the third step);
3. chemical reaction (the radicals finally terminate either via disproportionation or recombination reactions).

Obviously, the termination reaction is a highly diffusion-controlled process and thus, critically depending on the polymer chain length and viscosity of the reaction mixture, respectively. Moreover, the last step of the termination is reliant on the applied monomers due to steric effects of the radical species and (facile) abstraction of β-hydrogens. For example, olefin monomers with electron-withdrawing groups (such as methyl methacrylate) are mainly terminating via disproportionation, whereas monomers such as styrene favourably undergo recombination reactions.[105] Thereby, the nature of the termination reaction has great influence on the final polymer structure. While the recombination leads to the formation of inactive polymer chains with typical dispersity values of $Đ \sim 1.5$, the disproportionation results in saturated and unsaturated polymer chains. The latter can undergo further reactions, which results in usually higher dispersity values of $Đ \sim 2$.[105]

Yet, the limiting factor for the maximum degree of polymerization DP_n is the type of chain transfer reaction, which can occur to all present species, i.e. monomer, polymer, solvent or initiator. The respective calculations for the DP_n can be carried out by means of the Mayo equation (Equation 2.2).[77, 103] Certainly, chain transfer agents can be added on purpose to the reaction mixture in order to influence the DP_n, for instance to yield branched polymers or to introduce further functional groups to the chain end-termini.

$$\frac{1}{\overline{DP_n}} = (1+\lambda)\frac{k_t[R]}{k_p[M]} + C_M + C_A\frac{[A]}{[M]}$$

Equation 2.2: Mayo equation with DP_n = degree of polymerization, λ = recombination / disproportionation ratio, k_t = termination rate coefficient, k_p = propagation rate coefficient, $C_{M,A}$ = transfer to monomer / agent constant.

2.1.2 Reversible Addition Fragmentation Chain Transfer (RAFT) Polymerization

To overcome the drawbacks of FRP such as lack of control over the molecular weight, termination and chain transfer reactions as well as the resulting high *Đ* values, RDRP methods have been developed.[81, 106-109] These RDRP methods combine the benefits of the anionic polymerization (e.g. low *Đ* values, well-defined functional polymer chains) with the advantages of FRP (e.g. simple reaction procedures, various initiating possibilities, high tolerance towards functional groups). Mainly, this is accomplished by establishing an equilibrium between active radicals and dormant species with the equilibrium lying on the side of the dormant species.[110] Thus, termination reactions are minimized and the propagation possibility is equally distributed over all chains. The most important methods emerged are the atom transfer radical polymerization (ATRP),[111-113] the nitroxide-mediated polymerization (NMP)[114-116] and the reversible addition-fragmentation chain transfer (RAFT)[117-119] polymerization. In contrast to ATRP and NMP however, the concentration of active radical species in the RAFT polymerizations is not reduced but rather controlled by special RAFT agents, e.g. dithioesters, dithiobenzoates, trithiocarbonates or xanthogenates (refer to Scheme 2.3).[117-118, 120-121]

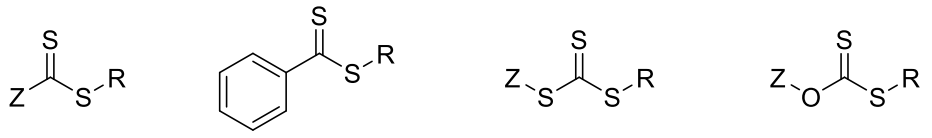

Scheme 2.3: Commonly applied RAFT agents, e.g. dithioester, dithiobenzoate, trithiocarbonates and xanthogenates.

Thus, the RAFT polymerization proceeds rather fast and can be triggered by common initiators such as AIBN or BPO. The mechanism is depicted in Scheme 2.4.[77, 117, 120-121] Similar to the mechanism of the FRP, the first step is the dissociation of the initiator into radical species and the addition of the first monomers. Then, a pre-equilibrium is generated between propagating polymer chains $P_n^{\cdot}$ and the macro-RAFT species, which in turn releases initiating fragments $R^{\cdot}$. These fragments reinitiate chain growth reactions to form the polymer chains $P_m^{\cdot}$. In the main equilibrium, a radical intermediate is formed between the macro-RAFT species and the

polymer chains $P_n^{\cdot}$ and $P_m^{\cdot}$. As is obvious from Scheme 2.4, the intermediate is symmetrical and therefore allows the dissociation to both sides equally. This leads to proportionally growing polymer chains with narrow mass distributions.

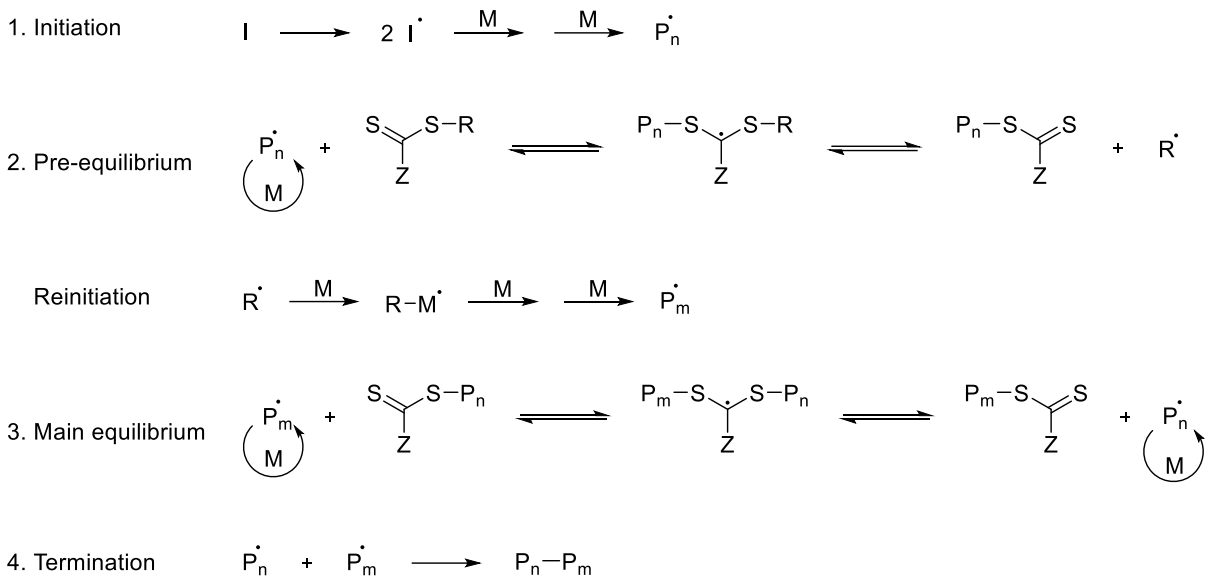

Scheme 2.4: Mechanism of the RAFT polymerization including the initiation, the pre-equilibrium, reinitiation, the main equilibrium and the termination.

Although the radical concentration is not lowered, the generation of termination products is strongly reduced by the competing reversible chain transfer. Most important for a successful RAFT polymerization is the choice of the RAFT agent.[77, 120-121] The RAFT agents possess a R- and Z-group, which need to be individually chosen for the desired monomer to be polymerized. While the R group is essential for the fragmentation reaction in the pre-equilibrium, it also has to reinitiate chain growth reactions again. On the other hand, the Z-group needs to ensure that the formation of the radical intermediate is favoured and yet allow the release of the polymer chains to enable chain propagation. As orientation for suitable R- and Z-groups, charts as shown in Scheme 2.5 are available for several monomers.[118, 121]

While the right choice of the R- and Z-groups might still be challenging, the RAFT polymerization offers several advantages such as the synthesis of linear, block, comb or star polymers, short reaction times, mild conditions and a broader range of applicable monomers than ATRP or NMP.

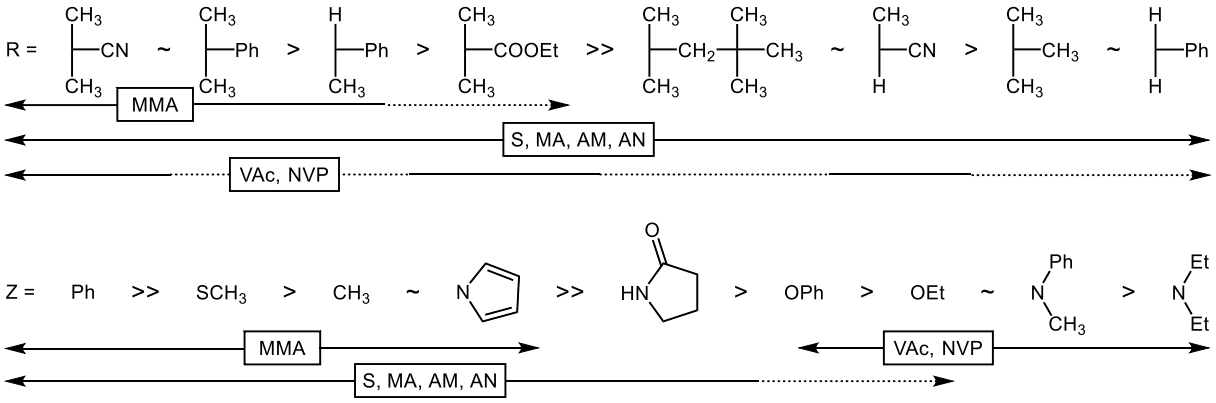

Scheme 2.5: Charts of R- and Z-groups to support the choice of suitable RAFT agent depending on the respective monomer.

2.1.3 Passerini Multi-Component Reaction (P-MCR)

Multi-component reactions (MCRs) have proven to be a powerful tool for the synthesis of highly functionalized molecules in a one-pot reaction setup providing atom economy, mild conditions, facile reaction protocols accompanied by high reaction yields.[122-126] Consequently, such MCRs are widely applied for the synthesis of natural products, drug molecules, organic or polymeric (macro)molecules. Well-known representatives are the Biginelli,[127] Hantzsch,[128] Strecker,[129] Mannich,[130] Kabachnik-Fields,[131] metal-catalysed (e.g. Cu, Pd),[132-133] Ugi[134] or Passerini[135] MCRs (refer to Scheme 2.6). As the examples clearly show, the MCR products incorporate most atoms of the starting materials. Additionally, the products can be either linear or cyclic with various heteroatoms (e.g. N, O, S, P), depending on the applied MCR.

Among the different MCRs, the Ugi and the Passerini MCRs belong to a noteworthy subclass based on isocyanides (red structure in the Ugi reaction in Scheme 2.6). [136-137] Isocyanides combine both nucleophilic and electrophilic properties due to the two mesomeric resonance structures depicted in Scheme 2.7.[138-139] The carbon atom in the left resonance structure in Scheme 2.7 has a carbene-like configuration and thus undergoes electrophilic reactions. While carbenes are known to prefer a bent geometry, high-level quantum calculations support a linear structure.[140] On the other hand, the second resonance structure (right structure in Scheme 2.7) has a zwitterionic character with a formal positive charge on the nitrogen and a formal negative charge on the triply bonded carbon atom.

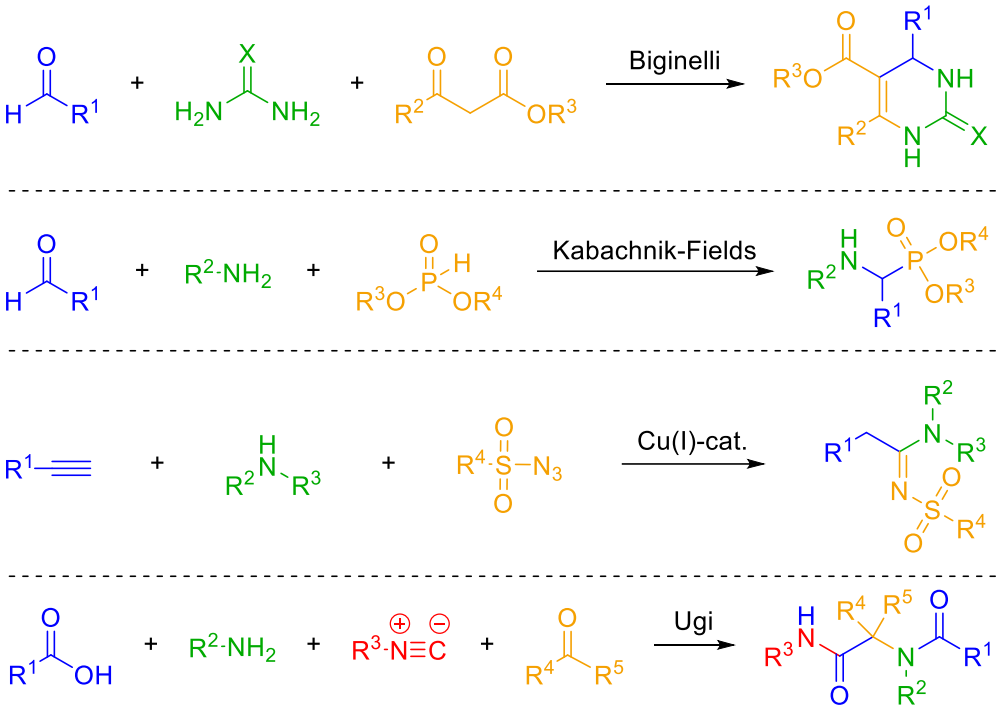

Scheme 2.6: Representatives of important MCRs: the Biginelli, Kabachnik Fields, Cu(I)-cat. and Ugi MCR.

This zwitterionic character is responsible for the nucleophilic properties of the isocyanides, since a nucleophilic attack leads to a conversion of the carbon into an electrophilic species and facilitates subsequent α-addition at the same position. Additionally, the zwitterionic character as well as the α-acidity can be easily influenced by suitable substituents at the α-position of the isocyanide. Due to the special reactivity behaviour with tuneable properties, the isocyanides are indispensable for the synthesis of highly functional heterocyclic compounds.[141-143]

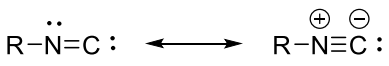

Scheme 2.7: Mesomeric resonance structures of isocyanides.

Of particular interest for the present thesis is the Passerini MCR (P-MCR), which was the first isocyanide-based MCR reported by Passerini in 1921.[144] As pictured in Scheme 2.8, the P-MCR involves an isocyanide (red), a carboxylic acid (green) and an aldehyde (blue, rarely also a ketone) and is usually conducted highly concentrated in aprotic solvents at ambient temperature.[145]

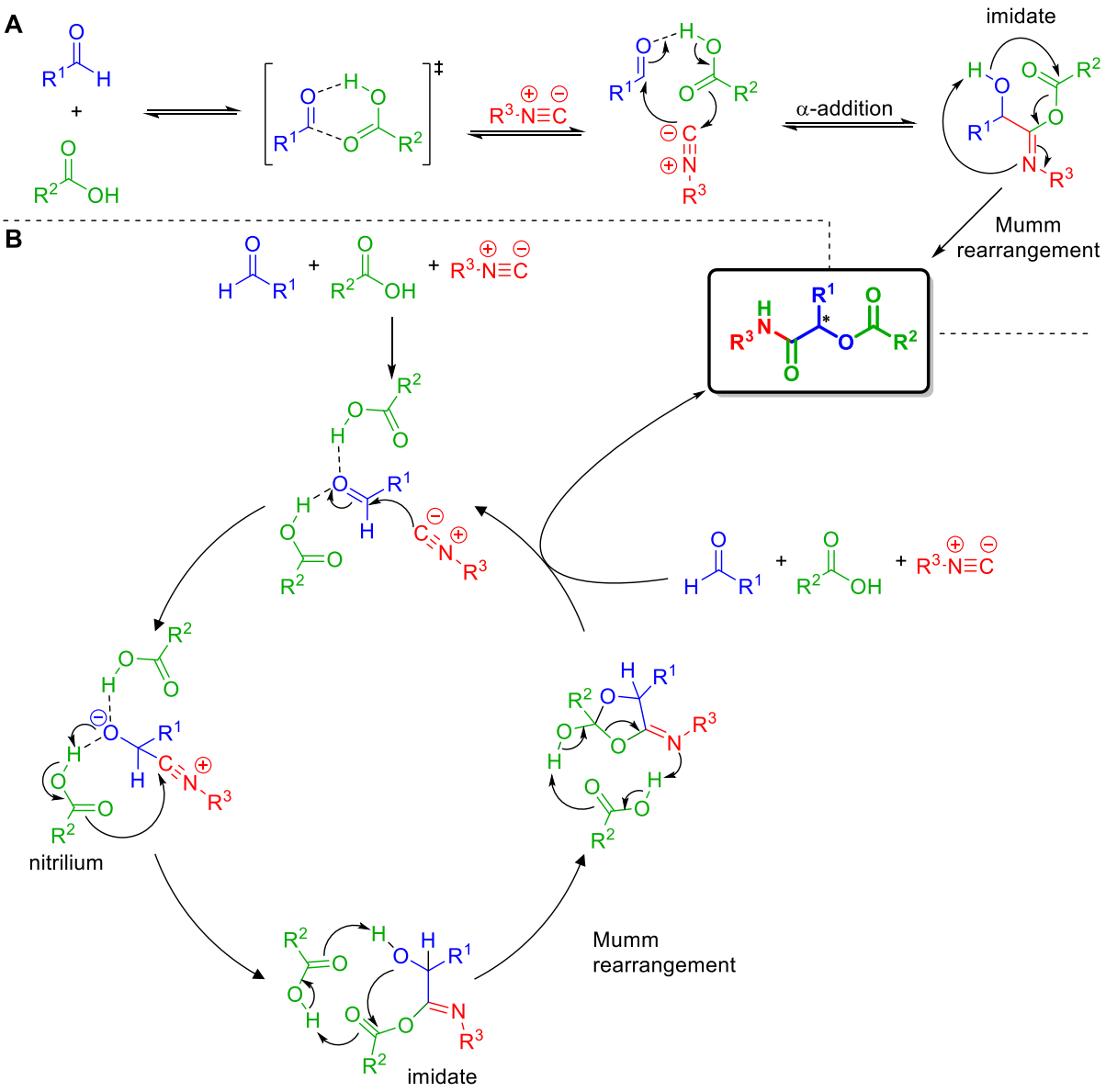

Scheme 2.8: Suggested mechanisms for the P-MCR by Baker and Ugi (**A**) and Morokuma and coworkers (**B**).

While extensive research has been conducted ever since its discovery, the exact mechanism has not yet been fully verified. Until recently, the mechanism depicted in Scheme 2.8A was considered as one of the most presumable ones. This mechanism was suggested by Baker (1951) and Ugi (1961) based on kinetic studies.[146-147] First, the carboxylic acid and the aldehyde form a six-membered transition state, which subsequently reacts with the isocyanide in an α-addition to yield an imidate species. The imidate undergoes an irreversible Mumm rearrangement and the final α-acyloxyamide is obtained. Interestingly, the Mumm rearrangements leads to the formation of a stereocenter, which allows control over the stereochemistry by applying chiral starting materials. Recently, further mechanical details were obtained by means of high level density functional theory (DFT) calculations and the

mechanism illustrated in Scheme 2.8B was suggested.[144] The first step is thereby similar to the former one, however two carboxylic acid molecules are involved instead of only one. Addition of the isocyanide in the α-position leads to the formation of the nitrilium species, which was theoretically proven to be stable in solution by the DFT calculations. Cleavage of one of the carboxylic acids yields the imidate species. Apparently, the second carboxylic acid acts as organo-catalyst and decreases the barrier for the subsequent Mumm rearrangement yielding the P-MCR product.

Besides the broad variety of organic hetero-atom containing molecules accessible via the P-MCR, also the successful synthesis of diverse polymers was achieved.[148-150] This can be realized by substituting two of the three components by dual functional ones (Scheme 2.9). Thus, three different types of polymers are obtained: amide substituted polyesters (Scheme 2.9A), alternating poly(ester amide)s (Scheme 2.9B) or polyamides with ester side chains (Scheme 2.9C).[150] Showing similar tolerance towards a broad variety of functional groups as the P-MCR, highly functionalized polymers were obtained via the Passerini-MCP ranging from poly(ester amide)s,[151] poly(caprolactone)s,[152] hydrogels,[153] H_2O_2-[154] or reduction-[155] sensitive polymers to photo-sensitive polymers.[156]

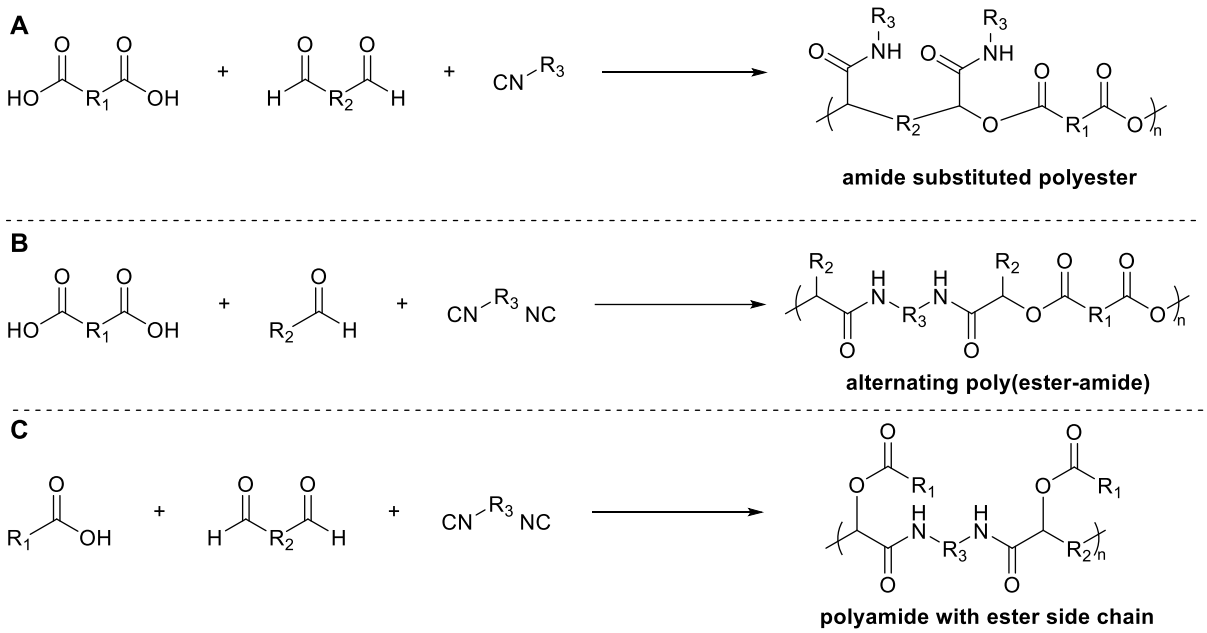

Scheme 2.9: P-MCP for the synthesis of amide substituted polyesters (**A**), alternating poly(ester amide)s (**B**) and polyamides with ester side chains (**C**).

Therefore, both the P-MCR and the P-MCP promise to be a powerful tool for the synthesis of tetrazole-containing substrates, which laid in the synthesis scope of the present work.

2.1.4 Post-Polymerization Modification (PPM)

Despite the advantages of the aforementioned RDRP or MCR methods for the synthesis of tailor-made polymers, it is not always possible to introduce all targeted functionalities directly into the polymer backbone during the polymerization process. Reasons therefore may be different solubility properties, stability issues at the required polymerization conditions or interference of the functional moieties with e.g. the initiator or RAFT agent or other present functionalities. Fortunately, these drawbacks can be overcome by post-polymerization modification (PPM) reactions.[157-159] These PPMs are typically based on organic reactions such as thiol-ene[160] or thiol-*para*-fluoro click reactions,[161] *N*-bromosuccinimide (NBS) initiated electrophilic MCRs,[162] copper(I)-cat. alkyne-azide cycloadditions (CuAAC)[163] or Diels Alder cycloaddition,[164] as shown in Scheme 2.10.

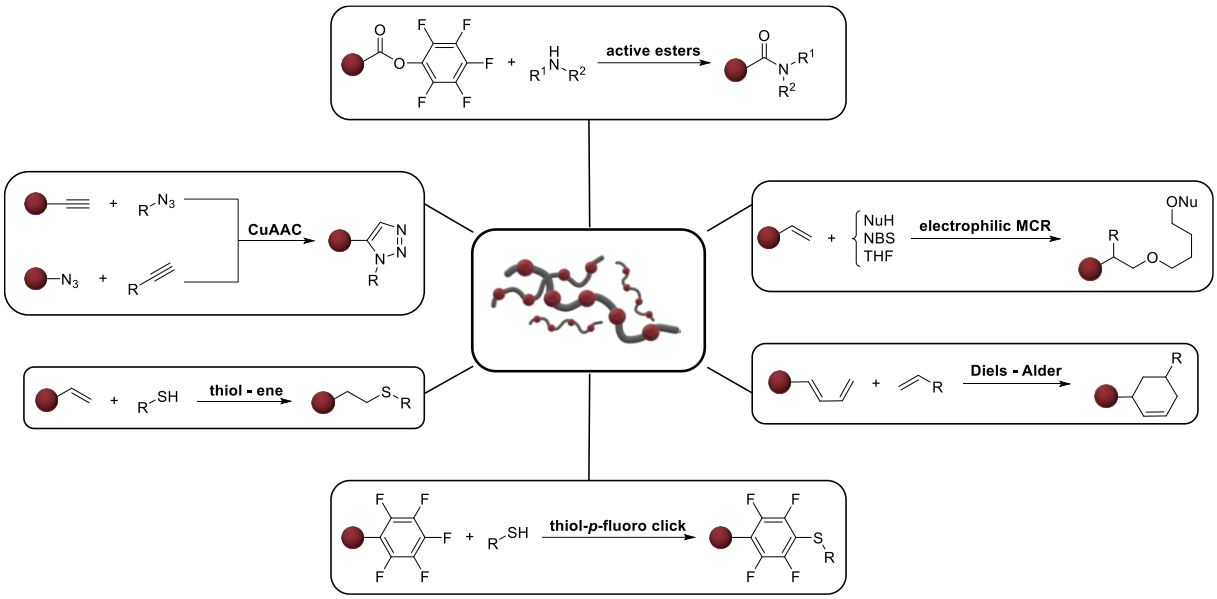

Scheme 2.10: Examples for PPM reactions: Diels-Alder cycloaddition, nucleophilic substitutions, electrophilic MCRs, CuAAC, thiol-*p*-fluoro click reaction, thiol-ene reaction and active esters.

Furthermore, the chemistry of active esters has gained much attention for the synthesis of well-defined multi-functional polymers by PPMs.[165-167] This approach allows the modification of ester moieties in the polymer backbone with diverse amine derivatives under mild conditions. Beneficially, different active ester moieties can be simultaneously polymerized

(e.g. via FRP or RAFT) and subsequently post-modified in a selective manner. For example, active ester monomers with a pentafluorophenyl acrylate (PFP-A, green structure in Scheme 2.11) and a pentafluorophenyl methacrylate (PFP-MA, blue structure in Scheme 2.11) unit not only allowed the synthesis of homopolymers, but also of copolymers for the orthogonal modification with various functionalities. This is attributed to the differential reaction behaviour of the acrylate and the methacrylate functionality.[168]

Additionally, the successful PPM can be easily observed via ^{19}F NMR analysis due to the change in the fluorine resonances before and after the PPM. These advantages have herein been taken as inspiration for the synthesis of a polymeric self-reporting system based on chemiluminescence with all required functionalities combined in a single polymeric backbone.

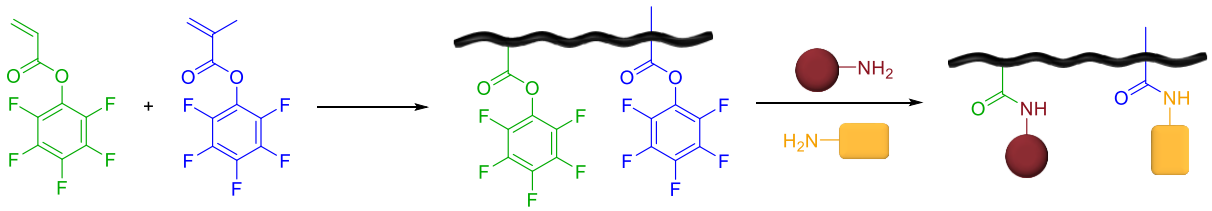

Scheme 2.11: Copolymer of PFP-A (green) and PFP-MA (green) enabling subsequent PPM with different amine derivatives (red / orange).

2.2 Photochemistry

2.2.1 Basic Principles

Photochemistry typically involves light with a wavelength λ between 200 and 1000 nm.[169] Depending on λ, the light is divided into three main classes (and the respective subclasses) according to its frequency v [Hz] and energy E [kJ mol^{-1}], as listed in Table 2.1.[169-170]

Table 2.1: Classes and subclasses of light suitable for photochemical reactions and the respective wavelengths λ, frequencies v and energies E.

class	subclass	λ [nm]	v [Hz x 10^{14}]	E [kJ mol^{-1}]
NIR		780 – 1000	3.0 – 3.8	120 – 150
Vis	red	620 – 780	3.8 – 4.8	150 – 190
	orange	585 – 620	4.8 – 5.1	190 – 205
	yellow	575 – 585	5.1 – 5.2	205 – 208
	green	490 – 575	5.2 – 6.1	208 – 244
	blue	420 – 490	6.1 – 7.1	244 – 285
	violet	380 – 420	7.1 – 7.9	285 – 315
UV	A	315 – 380	7.9 – 9.5	315 – 380
	B	280 – 315	9.5 – 10.7	380 – 427
	C	200 – 280	10.7 – 15.0	427 – 598

Hereby, λ is inversely proportional to v (Equation 2.3A), while the latter is proportionally connected to E via the Planck's constant h (6.63 x 10^{-34} J s) (Equation 2.3B).[169]

$$v = \frac{c}{\lambda} \quad (2.3.a) \qquad\qquad E = hv \quad (2.3.b)$$

Equation 2.3A and **B**: Correlations between the frequency v, the wavelength λ and the energy E (c = speed of light in vacuum = 2.998 x 10^{8} m s^{-1}, h = Planck's constant = 6.63 x 10^{-34} J s).

Upon light-irradiation of a molecule with a specific energy E (see Table 2.1and Equation 2.3), the molecule is promoted from the electronic ground state into electronically excited states.

Since the electronic excitation proceeds faster than molecular vibration processes (10^{-15} s *vs.* 10^{-12} s), the position of the nuclei is basically unchanged. Therefore, the maximum overlap of vibrational states and the possibility for electronic transitions before and after excitation is obtained vertically when plotting the energy *vs* nuclear coordinates, also known as the Franck-Condon principle (refer to Figure 2.1A).[169-171]

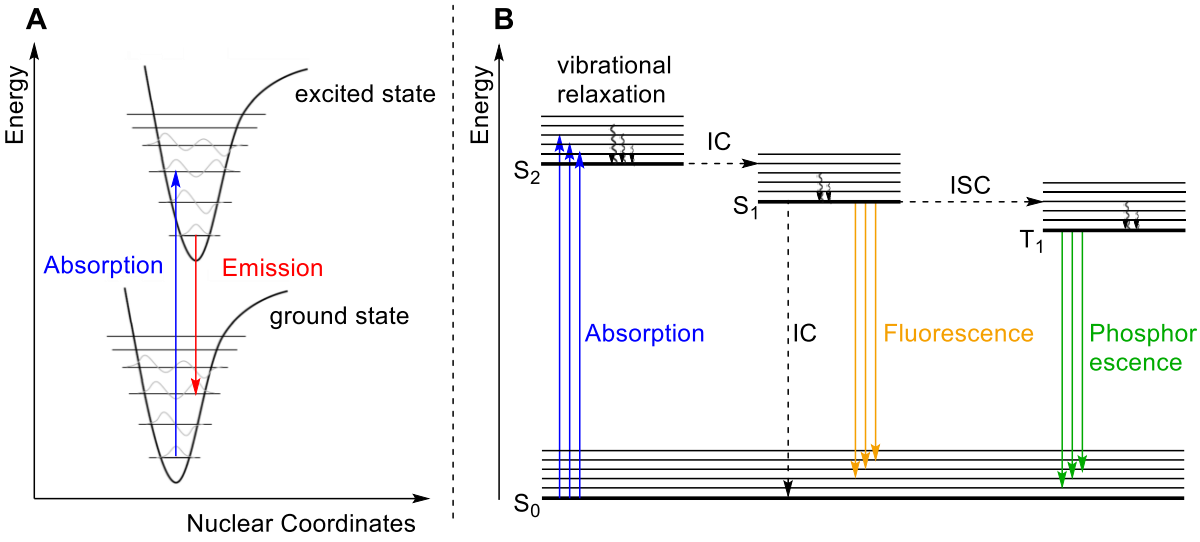

Figure 2.1A: Franck – Condon Principle. **B**: Jablonski diagram displaying the ground state S_0 and electronically excited states (S_1, S_2, T_1) and their respective vibrational states. The photophysical processes for radiative (straight arrows) and non-irradiative (dashed arrows) are illustrated.

The first process required for photochemical reactions is absorption (blue arrow in Figure 2.1A). Important for the absorption is the Beer-Lambert's law (Equation 2.4).[171] At a given concentration c and the optical path length d, the initial light intensity I_0 decreases when passing through the sample to the transmitted intensity I depending on the molar extinction coefficient ε_v. The higher ε_v, the better are the light-absorbing properties of the sample.

$$A = log_{10}\frac{I_0}{I} = \varepsilon_v cd$$

Equation 2.4: Beer-Lambert's law with A = absorbance, I_0 and I = incident and transmitted light intensities, ε_v = molar extinction coefficient, c = concentration of the sample and d = optical path length.

From the excited states, there exist several pathways for the molecule to return to the ground state, either by chemical deactivation reactions or by photophysical processes. The photophysical processes are illustrated in a simplified Jablonski diagram in Figure 2.1B.[172-173]

In the diagram, the electronic levels (bold lines) and the respective vibrational states (thin lines) of the ground state S_0 and the excited states S_1, S_2 and T_1 are displayed.

On the one hand, molecules can release the absorbed energy ($S_0 \rightarrow S_n$, blue arrows) via non-irradiative pathways:[169-173]

- Vibrational relaxation (wavy arrows) within an excited state to the respective ground state accompanied by the release of heat
- Internal conversion (IC) (dashed arrows) from an excited state into a lower electronic state of the same spin multiplicity (e.g. $S_2 \rightarrow S_1$)
- Intersystem crossing (ISC) (dashed arrow), when the relaxation from an excited state proceeds between states of different spin multiplicities (e.g. $S_1 \rightarrow T_1$)

On the other hand, the energy release take place via radiative pathways:

- Fluorescence ($S_1 \rightarrow S_0$, orange arrows)
- Phosphorescence ($T_1 \rightarrow S_0$, green arrows)

The latter however is a spin-restricted process only possible after ISC and occurs with a delayed emission. Furthermore, non-irradiative, competing deactivation processes with other molecules can occur (e.g. bimolecular collision, energy transfer).

2.2.2 Photochemical Reactions

The first synthetic photochemical reaction was reported in 1834 by Trommsdorff, who observed a colour-change of the colourless Santonin into yellow compounds upon exposure to UV-light as illustrated in Scheme 2.12.[174-176]

Since then, extensive research has been conducted in the field of photochemical reactions due to the unique advantage of spatial and temporal control of such reactions.[56, 177-178] The photo-reaction takes place precisely at the irradiated area and only as long as the irradiation is turned

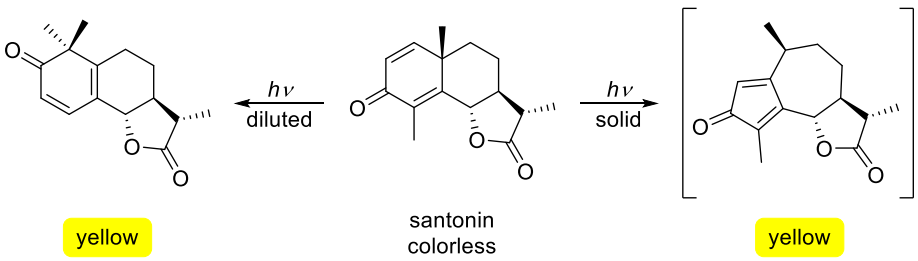

Scheme 2.12: The first reported photochemical reaction of Santonin by Trommsdorff in 1834.

on. Thus, photochemical reactions have become a powerful synthetic tool in biology, physics and synthetic chemistry.[179-180] An overview of possible photochemical reaction is given in Scheme 2.13. For example, aldehydes or ketones can undergo a Norrish type I or II photoreactions,[181-182] whereas the [2+2] cycloaddition[179] is ideally suited for the synthesis of (hetero-) cyclobutanes (Paterno-Büchi reaction).[183] Other molecules such as anthracene,[184] cinnamic acid,[185] styryl-pyrene[186] and the respective derivatives undergo dimerization reactions upon exposure to light. Additionally, photo-sensitive protecting groups have emerged to enable orthogonal organic synthesis strategies with simple deprotection procedures.[65]

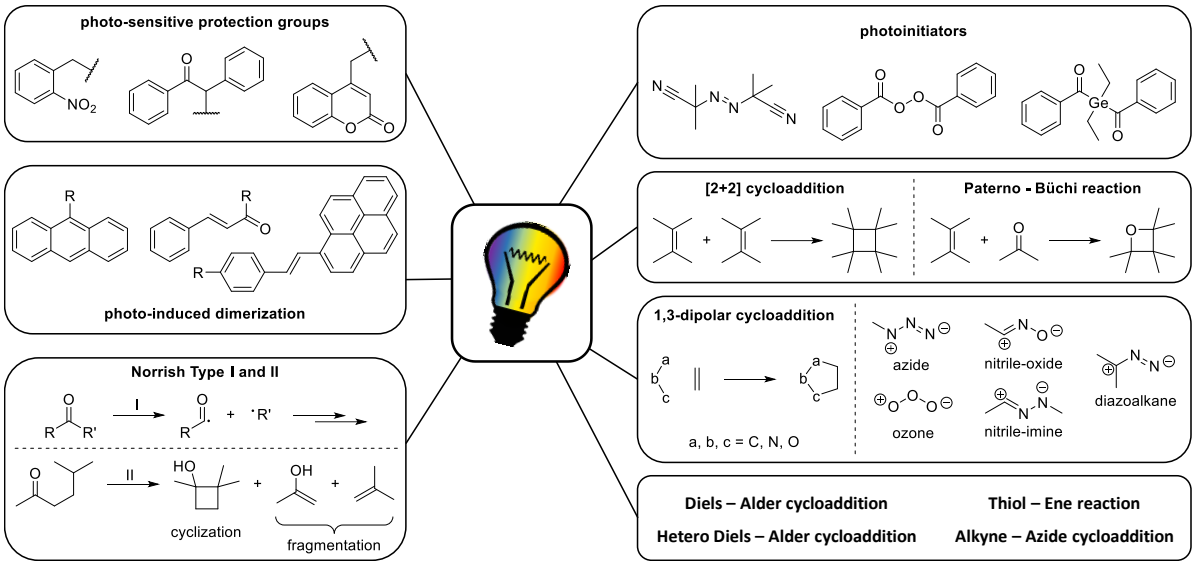

Scheme 2.13: Examples of photochemical reactions and photo-sensitive compounds.

However, photochemistry is not only restricted to organic synthesis but can also be adapted for polymer synthesis by means of photosensitive initiators such as AIBN, DBPO or acylgermanes.[65, 187] Moreover, the thiol-ene reaction is ideally suited for radical-mediated polymerization reactions or network formations by applying multi-functional thiols and ene-derivatives as illustrated in Scheme 2.14A-B.[178, 188-190] Additionally, polymers such as poly(butadiene) were successfully post-modified via the thiol-ene reaction.[191] Noteworthy, also competing intramolecular cyclization reactions can accompany the latter process to deliver unusual macromolecular topologies, as demonstrated in Scheme 2.14C.[189] Related thiol-based photoreactions relevant for polymer functionalization are the thiol-yne (Scheme 2.14D)[192-194] and the thiol-Michael reaction (Scheme 2.14E).[195-197]

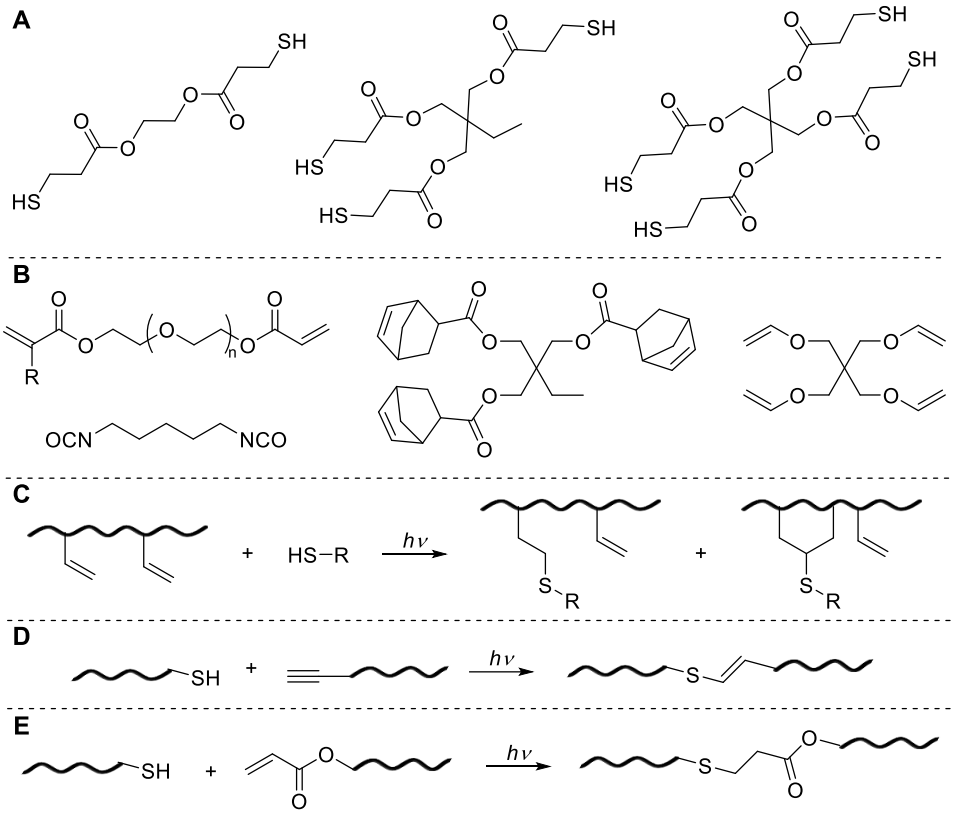

Scheme 2.14: Commonly applied multi-functional thiols (**A**) and enes (**B**) in the thiol-ene-polymerization. Reaction pathways of the thiol-ene PPM of poly(butadiene) with the competing intramolecular cyclization (**C**), the thiol-yne polymer ligation (**D**) and the thiol-Michael polymer ligation (**E**).

Besides, the aforementioned photochemical dimerization reactions have been thrivingly used for the (reversible) ligation of polymers,[198-200] the formation of networks,[201] the synthesis of hydrogels[202] or nanoparticles[203] as well as patterning of surfaces.[198, 204] In a similar manner, the light-induced (hetero) Diels-Alder reaction has proven to be a powerful tool in polymer science. As depicted in Scheme 2.15A, a phenacyl sulfide at a polymer chain end releases acetophenone upon irradiation with UV-light (λ = 355 nm), which results in the formation of a highly reactive thioaldehyde.[205-206] This thioaldehydes subsequently reacts with a suitable diene via the hetero Diels-Alder cycloaddition. Importantly, the thioaldehydes cannot only react with dienes, but also with e.g. amines, hydroxylamines or thiols,[207] making thioaldehydes a useful ligation method in polymer chemistry. On the other hand, *ortho*-methyl benzaldehyde (*o*-MBA) and its derivatives have been successfully applied in the photo-induced Diels-Alder reaction, as shown in Scheme 2.15B. Upon exposure to light, *ortho*-quino dimethanes ("photoenols") are formed that can undergo the Diels-Alder reaction in the presence of e.g. maleimides, fumarates or acrylates. Both the *o*-MBA and the alkene derivative can be

positioned at polymer chain ends, which makes this *o*-MBA based Diels-Alder reaction an efficient polymer ligation technique.[178, 205, 208-215]

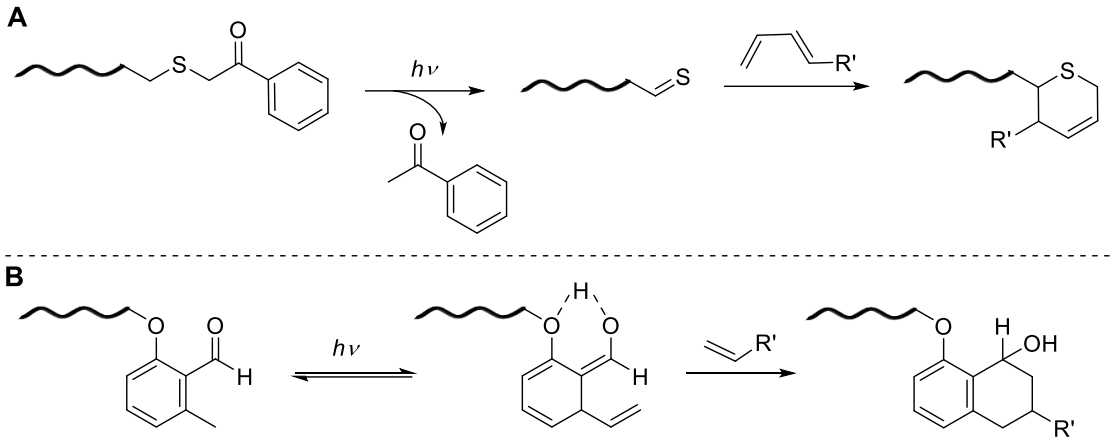

Scheme 2.15: Light-induced (hetero) Diels Alder reactions based on thiolaldehydes (**A**) and *o*-methoxy benzaldehyde (**B**).

Another important class of photoreactions are the 1,3-dipolar cycloadditions.[216-219] Here, a heterocyclic 1,3-dipole (such as diazoalkane, azide, ozone or nitrile-imine) reacts with e.g. an alkene to form a five-membered heterocyclic product. Of special interest in the field of polymer chemistry is the photo-induced copper(I)-catalysed azide alkyne cycloaddition (CuAAC), displayed in Scheme 2.16.[178, 220] During the reaction, an azide 1,3-diple is generated, which reacts with an alkyne to yield the five-membered cyclic 1,2,3-triazole, catalysed by Cu(I). This reaction offers several advantages such as short reaction times, regioselectivity, tolerance towards various functional groups as well as compatibility with several solvents for the reaction process.[220] Consequently, the reaction has become an efficient photochemical approach for polymer synthesis and modification as well as surface functionalization.[221-225]

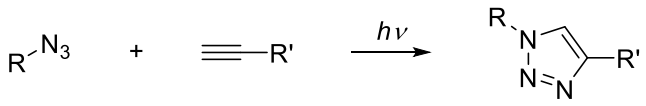

Scheme 2.16: General reaction pathway of the CuAAC yielding the five-membered cyclic 1,2,3-triazole.

One other prominent example of 1,3-dipolyar cycloadditions for photochemical-based polymer reactions involves the generation of a nitrile-imine dipole, which can react with a broad variety of functional groups. Since this reaction is also relevant for the tetrazole-chemistry, it will be further discussed in the following Chapter 2.2.3.

2.2.3 Tetrazoles

In 1885, Baldin discovered the formation of a five-membered heterocyclic compound by the reaction of dicyanophenylhydrazine with nitrous acid and termed it “tetrazole”.[226] Since then, tetrazoles have become valuable chemical motifs in various fields such as medicine, pharmacology, photography, rocket propellants or (bio-)chemistry. This is attributed to their stability despite the high amount of nitrogen atoms (e.g. penatzoles are highly unstable and explosive compounds), their bioisosterism to carboxylic acids or amides along other physicochemical properties.[226]

One of such physicochemical properties is the photochemical behaviour of tetrazoles. Upon irradiation with light, the tetrazoles is promoted to an electronically excited state, which undergoes ISC and a highly reactive nitrile imine is obtained after the release of nitrogen (refer to Scheme 2.17).[227-228]

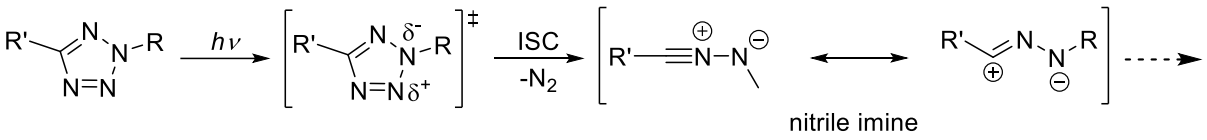

Scheme 2.17: Photochemical reaction of a 2,5-disubstituted tetrazole, yielding a highly reactive nitrile imine.

This nitrile imine is a highly reactive 1,3-dipol and can subsequently react with a broad variety of functional groups (e.g. water, acetonitrile, thiols, amines, acids, heterocycles or aryl boronic acid derivatives),[229-236] as depicted in Scheme 2.18.

Of special interest for the present work is the nitrile-imine mediated tetrazole-ene cycloaddition (NITEC). Herein, the nitrile-imine reacts with an ene and a five-membered pyrazoline adduct is obtained.[237-239] This pyrazoline is highly fluorescent and hence, the conversion and product formation can be monitored in a self-reporting manner via colour and fluorescence changes. Beneficially, the photo-responsiveness of the tetrazoles can be easily fine-tuned by suitable substituents at the *N*-position (refer to Scheme 2.19). While the 2,5-diphenyltetrazole or 2-methoxyphenyl-5p-phenyl tetrazole react under irradiation within invasive harsh UV light (e.g. 290 nm and 320 nm, respectively),[67, 240] push-pull substituents lead to a red-shift (bathochromic shift) of the photo-responsiveness.[241-242] For example, dimethylaniline as substituent allows photoreactions at milder UV-light, namely 365 nm.[241]

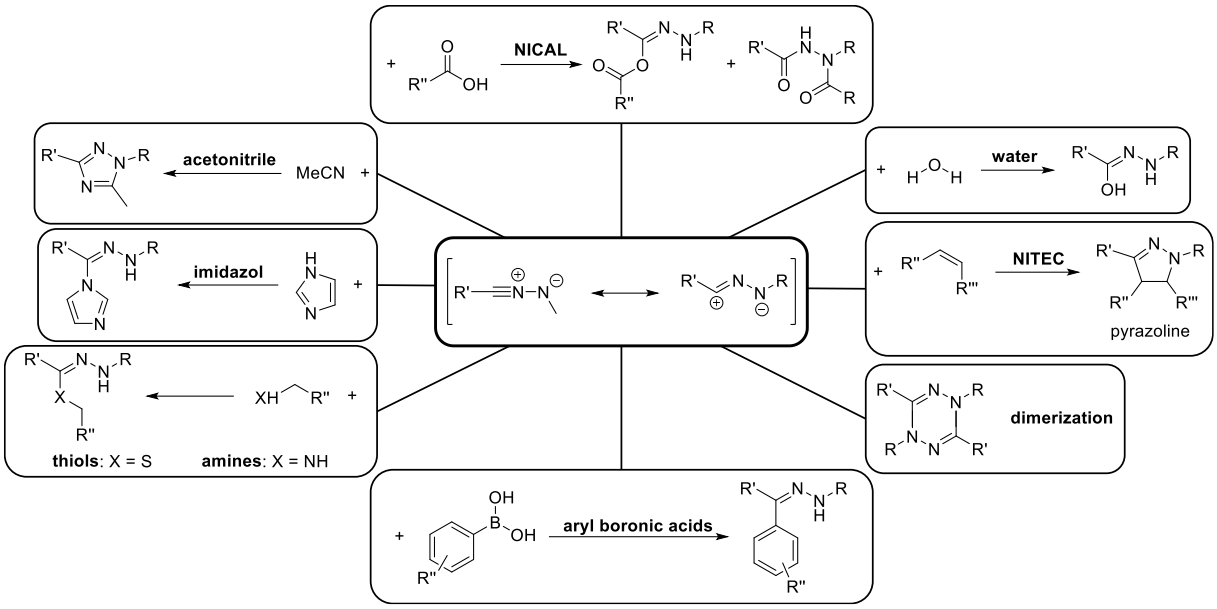

Scheme 2.18: Overview of possible reactions of the nitrile imine intermediate.

By means of substituents with larger delocalized π-systems, e.g. pyrene, the photoreaction can even be triggered in the visible light range (410 nm).[243] This is important especially for biochemical or biomedical applications to avoid tissue damage by the harsh irradiation conditions.

Due to all these properties, tetrazoles have also been recognized as powerful tools in the field of polymer chemistry. The incorporation of tetrazole moieties into polymeric materials not only allows PPMs with the reactions displayed in Scheme 2.18 in order to obtain highly functionalized polymers,[233, 244-248] but also the intramolecular chain folding in the presence of suitable linkers via the NITEC reaction.[60, 249-250] Such 3D-folded polymers have great potential as protein-mimicking materials and thus, they find applications in e.g. drug delivery, contrast agents, sensors, nanoreactors or catalysis.[93, 251-253] Unfortunately, the synthesis for tetrazole-containing polymers is challenging and requires several steps and / or complex monomer synthesis strategies.

Therefore, the aim of the present work was to find a facile, efficient synthesis strategy for tetrazole-containing polymers. Taking inspiration of the adjustable photo-responsiveness of the tetrazoles, two tetrazole-functionalities responsive to different wavelengths are supposed to be incorporated into the same polymeric backbone. In this way, the folding (or PPM) of the polymer can be conducted in a light-controlled, self-reporting manner.

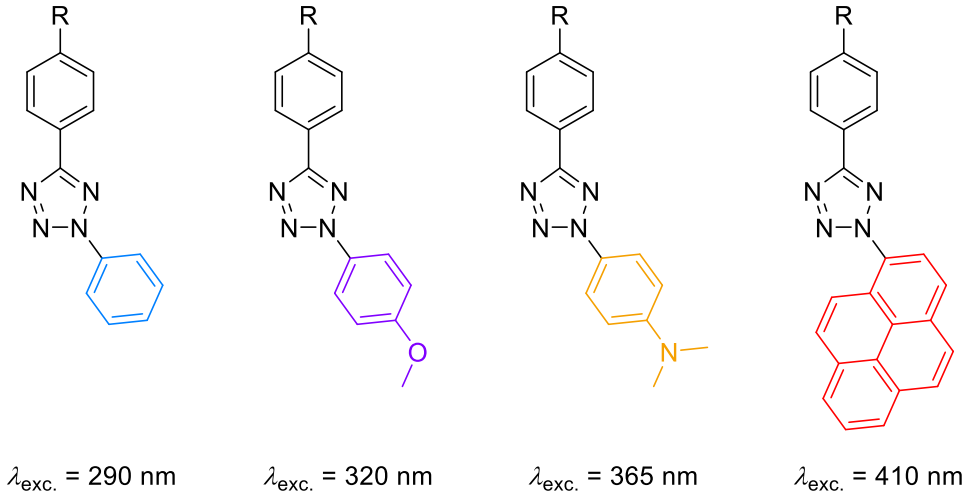

Scheme 2.19: Tetrazoles with different photochemical properties due to the respective substituents at the *N*-position of the tetrazole.

2.3 Chemiluminescence

The emission of light evoked by a chemical reaction is termed chemiluminescence (CL).[254] Such a reaction generates electronically excited states, which emit light upon relaxing back into the ground state. To successfully produce CL however, the reaction has to fulfil specific criteria:[46, 255]

1. In order to provide the required energy for the electronically excited states, the reaction needs to be exothermic. According to the free energy ΔG (refer to Equation 2.5), 40-70 kcal mol^{-1} are necessary for CL occurring in the visible light range (400-750 nm).

$$-\Delta G \geq \frac{hc}{\lambda_{ex}} = \frac{28\,600}{\lambda_{ex}}$$

Equation 2.5: calculation formula for the free energy ΔG required for the CL reaction (*h*: Planck constant, *c*: speed of light, λ_{ex}: wavelength)

2. Once the chemical reaction affords the necessary energy, the electronically excited state needs to be favoured. If the energy is radiated e.g. via heat, no light will be emitted during the reaction.
3. Finally, the relaxation into the ground state needs to be achieved via photon emission and not via other deactivation processes such as dissociation, isomerization or inter-/ intramolecular energy transfer.

Conceding that criteria 1-3 are fulfilled, there are two pathways of the CL emission to take place: either direct or indirect,[255] as illustrated in Scheme 2.20.

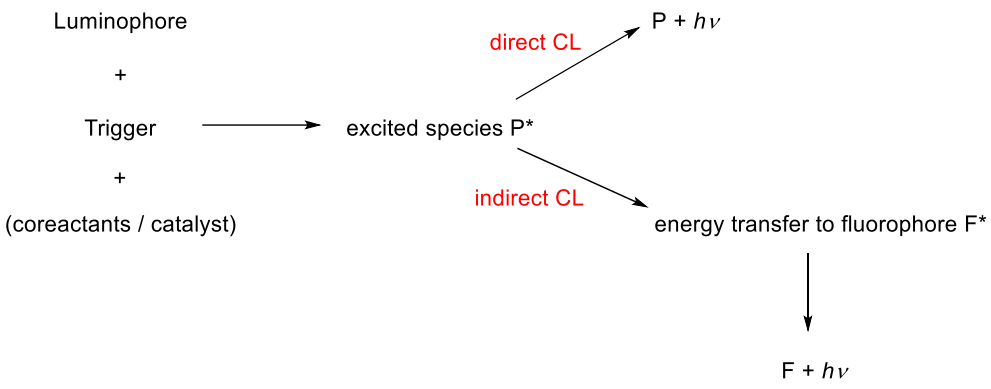

Scheme 2.20: direct and indirect CL emission pathways.

If the excited species P* in the CL reaction is the light emitting species itself, the process is termed direct CL (e.g. 1,2-dioxetanes, luminol, acridinium esters). However, the excited species P* can also transfer the energy to a fluorophore molecule F* that emits light instead of P* when returning to the ground state. In this case, the process is termed indirect CL (e.g. the CL of peroxyoxalates (PO)). For both the direct and indirect CL process, the efficiency of the CL, i.e. the amount of photons emitted per reacting molecule, is defined as the CL quantum yield Φ_{CL}, represented in Equation 2.6.[46, 256]

$$\Phi_{CL} = \Phi_R \times \Phi_{ES} \times \Phi_F$$

Equation 2.6: CL quantum yield Φ_{CL} (Φ_R: chemical reaction yield, Φ_{ES}: yield in the excited state, Φ_F: fluorescence quantum yield).

Typically, Φ_{CL} is rather low (< 1%) due to either a low reaction yield (Φ_R) or a low emission of the emitting species (Φ_F).[255, 257] Fortunately, the light emission can be enhanced by suitable substitution of the luminophore, addition of a catalysts or a more effective fluorophore as energy transfer acceptor, or by the choice of solvent. The CL emission of POs for example highly depends on the applied fluorophore.[258-259] Oxidation of a PO (e.g. bis(2,4,6-trichlorophenyl)oxalate (TCPO)) by active species (e.g. peroxides or microorganisms) leads to a decomposition into an unstable, energy-rich dioxetanone, which further decomposes into CO_2, as displayed in Scheme 2.21A. No CL emission takes place unless the energy of the dioxetanone is transferred onto an additional fluorophore, e.g. 9,10-diphenylanthracence (DPA) via a chemical-induced electron-exchange luminescence (CIEEL) process. So, by carefully choosing the fluorophore, the intensity as well as the emission wavelength of the CL reaction can be adjusted from the UV/Vis to the NIR spectral range. Dioxetane formation and its decomposition into CO_2 also plays a critical role in the CL reaction mechanism of acridinium esters.[30, 260-261] In contrast to the POs however, no additional fluorophore is required. Acridinium esters are oxidized to dioxetanones by e.g. peroxides and CO_2 is released, leading to the highly emissive acridone-species as illustrated in Scheme 2.21B. Hereby, the kinetics and the efficiency of the light emission depend on the pK_a value of the leaving group R. Substituents that increase the pK_a value and donate electrons (e.g. methyl, methoxy) show a slower reaction and longer CL signal than substituents decreasing the pK_a value and withdrawing electrons (e.g. halogens, CN).

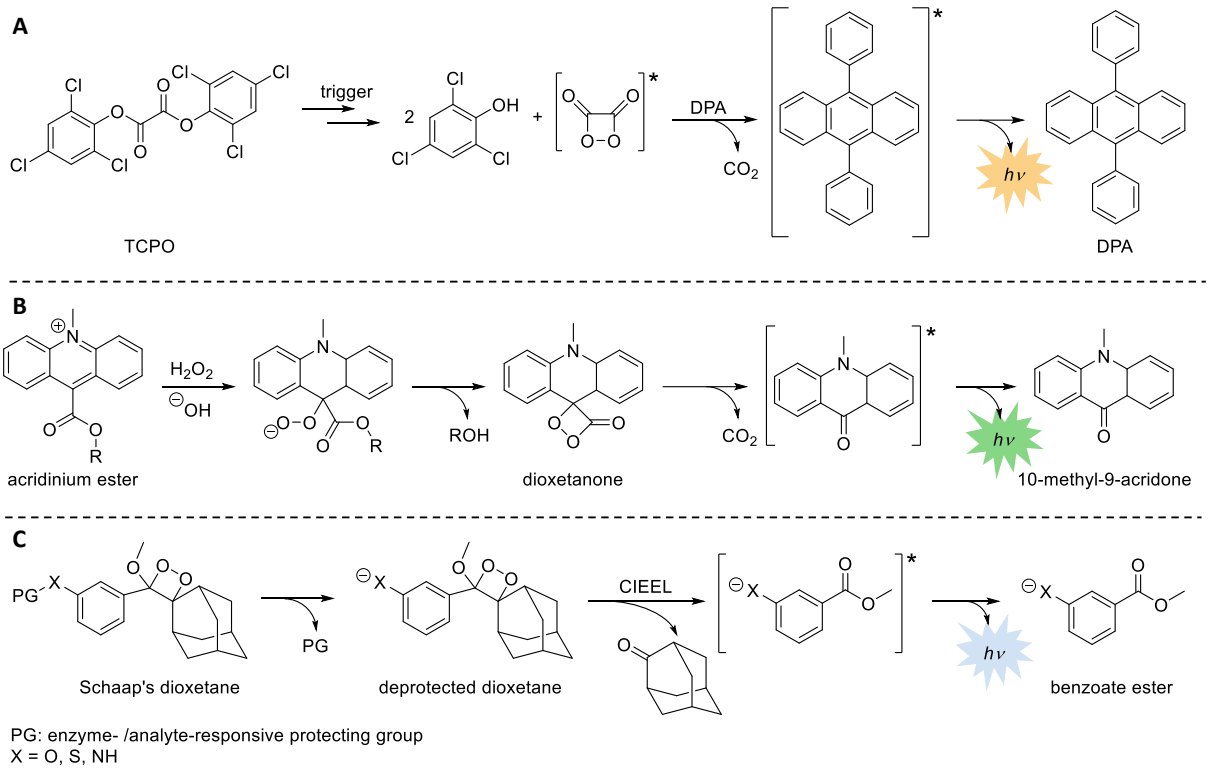

Scheme 2.21: CL reaction mechanism of **A**: POs (i.e. TCPO) in the presence of DPA as fluorophore, **B**: acridinium esters and **C**: Schaap's dioxetane.

Similarly, the choice of the substituents influences the CL emission of 1,2-dioxetanes. The research upon efficient 1,2-dioxetane derivatives is based on Schaap's dioxetane, which consists of a dioxetane enclosed by both an adamantly and phenyl moiety. Additionally, a protecting group (PG) is attached to the phenyl unit, as shown in Scheme 2.21C.[32, 46, 262] Cleavage of the PG destabilizes the dioxetane and triggers the CIEEL process, in which the dioxetane decomposes into 2-adamantone and a benzoate ester in the excited state. The latter returns to the ground state accompanied by the emission of light. Depending on the PG, the CL process can be started by thermal, chemical or mechanical stimuli. Moreover, the CL emission of 1,2-dioxetanes was highly enhanced by introducing additional electron-withdrawing groups at the *ortho*-position of the phenol ring or by forming supramolecular complexes in the presence of cyclodextrin.[254, 263-266] These versatile possibilities to tune the CL emission of dioxetanes by introducing suitable substituents onto the luminophore were taken as inspiration for the present thesis to improve the CL emission of the most applied luminophore in forensic science, namely luminol (Chapter 2.4.1).

2.4 Organic Compounds as Handles for Self-Reporting CL-Materials

2.4.1 Luminol

Since the discovery of luminol and its chemiluminescent properties by Albrecht in 1928,[46] people have been fascinated by its striking blue light, especially due to the application as blood detector in forensic sciences. This is attributed to the catalytic effect of the iron containing hemin in the blood.[267-268] By means of such catalysts (e.g. metal ions, enzymes or nanoparticles)[269-271] the Φ_{CL} of luminol can be raised to ~ 4% in aqueous alkaline media. In aprotic media (such as DMSO or DMF) Φ_{CL} can even be raised to ~ 9% in the presence of a strong base (e.g. NaOH, KOH).[46-47] The mechanism of the chemiluminescence reaction is shown in Scheme 2.22.[46]

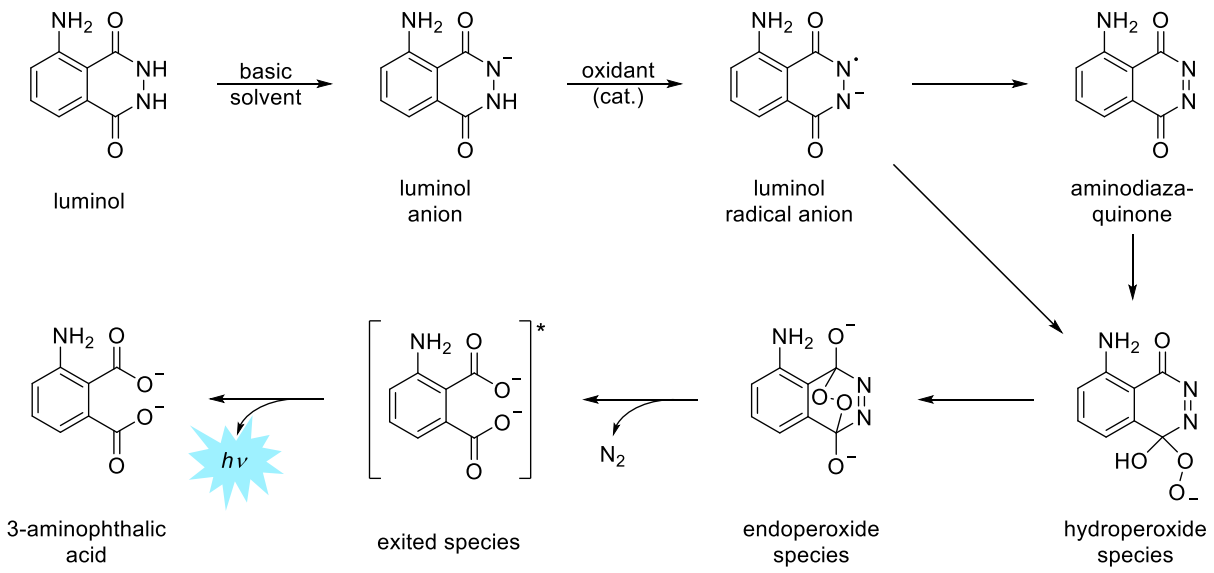

Scheme 2.22: CL reaction pathway of luminol in basic solution triggered by an oxidant.

In basic solution, the luminol is present in its deprotonated state as luminol anion. Oxidation by ROS (such as H_2O_2, NO, $ROO^{\cdot}$ or $ClO_2^{\cdot}$) leads to the formation of the radical anion, which further reacts to the hydroperoxide species either directly or via the aminodiazaquinone. Subsequently, the endoperoxide species is generated, from which nitrogen is released and the excited 3-aminophthalic acid (3-APA) is obtained. Finally, the excited 3-APA returns to the

ground state accompanied by the emission of light (λ = 430 nm). This mechanism needs to be considered if the CL properties are meant to be enhanced by altering the luminol structure. Since the heterocyclic ring is crucial for the CL (refer to Scheme 2.22), its modification results in a loss of the CL. Modification of the aromatic ring on the other hand, for example by expanding the aromatic system or by introducing electron-donating functionalities, can increase the light emission.[257, 272] Beneficially, modification of the aromatic ring also enabled the synthesis of luminol-containing polymeric systems with CL properties either via electropolymerization[273-276] (refer to Scheme 2.23A) or chemical polymerization[277-279] (see Scheme 2.23B).

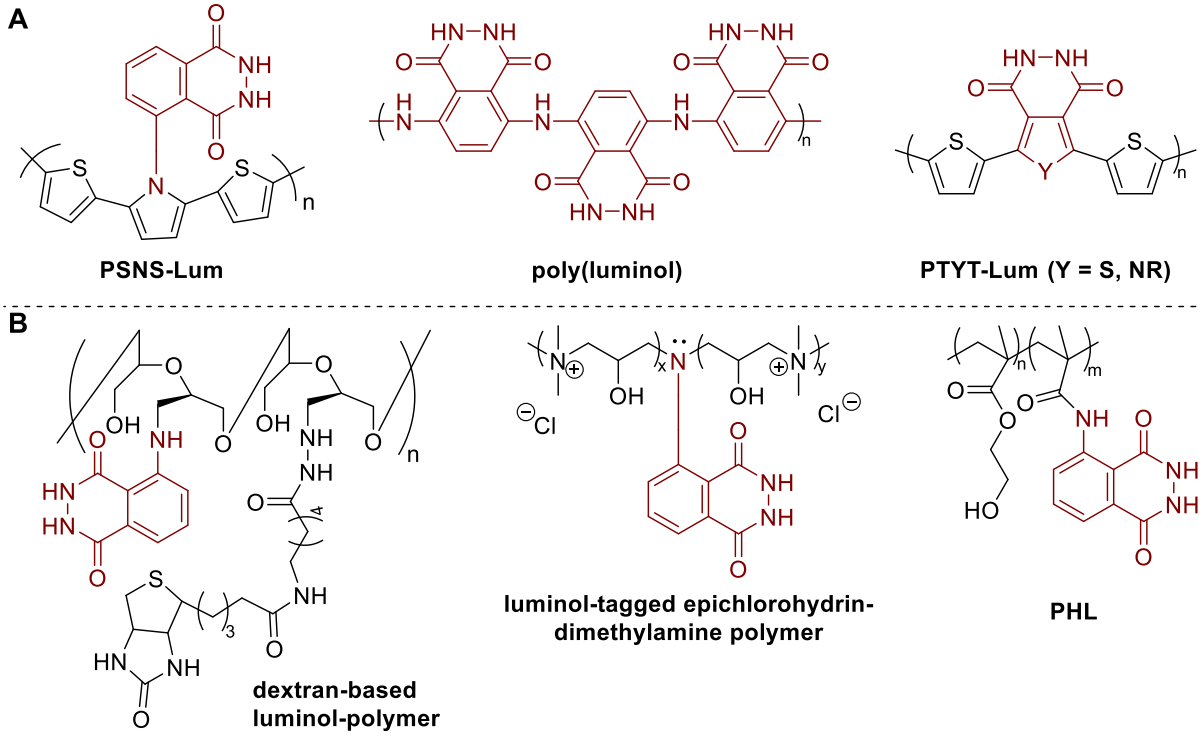

Scheme 2.23: Examples of luminol-polymers obtained via electropolymerization (**A**) and chemical polymerization (**B**).

Nevertheless, these systems still require the presence of additives such as bases and the aforementioned catalysts. Unfortunately, they suffer from certain drawbacks such as high costs, toxicity or air sensitivity of metal catalysts, limited stability and lifetime of enzymes, dependence on particle size and distribution of nanoparticles or harsh conditions (e.g. up to 1000 eq. of base).[280-281] Therefore, the development of a new, easy-to-handle and efficient luminol-CL system is targeted in the present thesis to overcome these drawbacks by means of the organic superbases.

2.4.2 Organic Superbases

Superbases are by definition compounds with high basicity properties similar to lithium diisopropylamide (LDA, pK_a = 36 in THF) or other comparable ionic metal-containing bases.[282-284] However, also non-ionic compounds such as phosphazenes, amidines or guanidines with pK_a values higher than the one of the proton sponge 1,8-bis(dimethylamino)naphthalene (DMAN, pK_a = 16.8 in THF) as displayed in Scheme 2.24 are referred to as organosuperbases.[283-284]

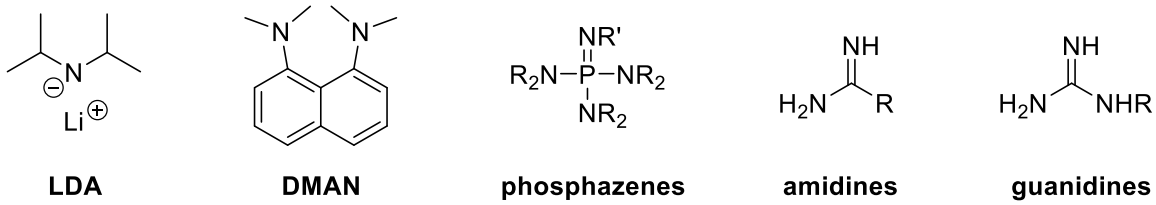

Scheme 2.24: Chemical structures of the superbases LDA, the proton sponge DMAN and the basic structures of phosphazenes, amidines and guanidines.

These superbases find widespread applications as ionic liquids, peptide mimetics or catalysts in organic chemistry (e.g. in polycondensations, Michael or Wittig reactions, ring-opening polymerizations)[285-293] due to their good solubility in organic media, high stability at low temperatures and ambient conditions.[294-296]

Among them, guanidines are of special interest for biochemical applications. Guanidine functionalities (orange coloured units in Scheme 2.25A) are found in several natural compounds (e.g. guanine, arginine, agmatine or creatine),[297-299] which play crucial roles in biological enzymatic reactions. Furthermore, synthetic guanidines with bio-mimicking properties were developed for applications in pharmaceutical drugs (e.g. Rosuvastidin for the treatment of cardiovascular issues, Imanitib as anticancer drug or Cimetidine for peptic ulcer treatment), sweeteners, disinfectants, insecticides or catalysts.[300]

In a similar manner, guanidine derivatives such as 1,1,3,3-tetramethylguanidine (TMG) or its cyclic counterpart, i.e. 1,5,7-triaza-bicyclo[4.4.0] dec-5-ene (TBD) (refer to Scheme 2.25A), are also of particular interest in organic chemistry[289, 301-308] due to the resonance stability of the conjugated acid depicted in Scheme 2.25B.[286] Beneficially, guanidines do not only serve as catalyst in polymerization reactions, but can also be implemented directly into polymers.

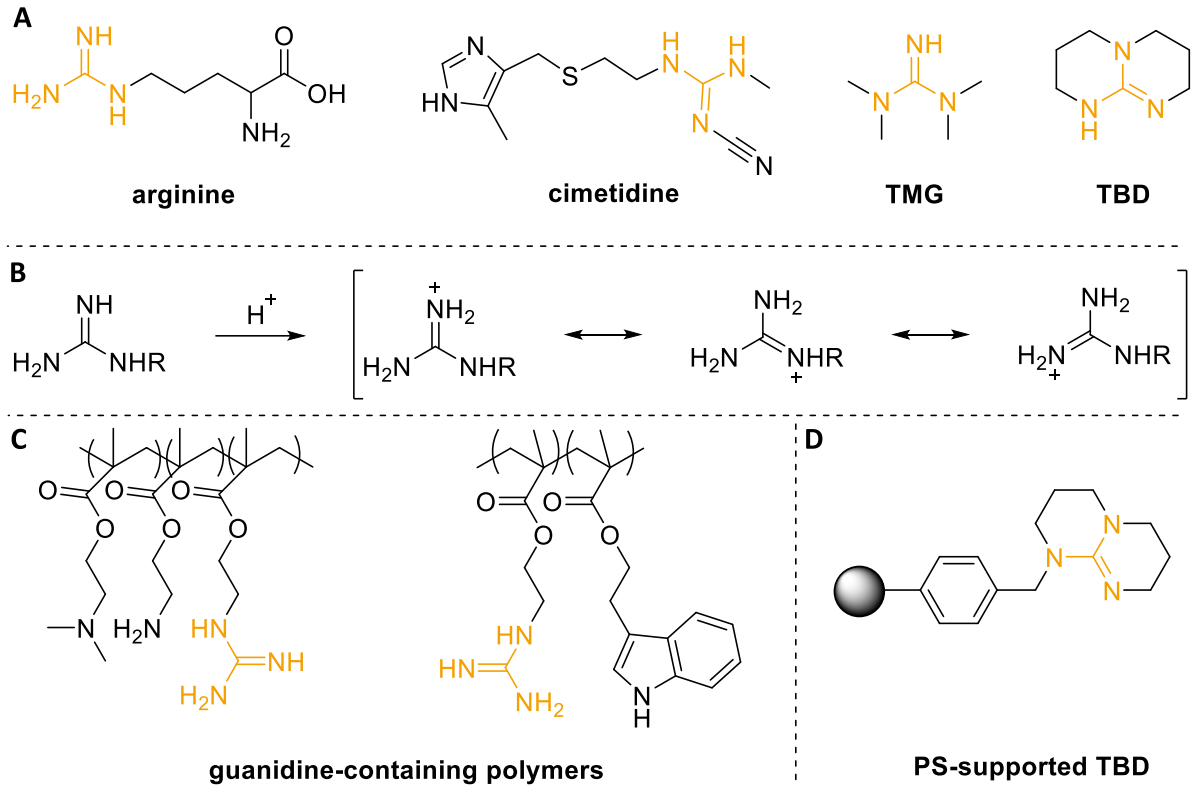

Scheme 2.25A: Example of guanidine derivatives: arginine, cimetidine, TMG and TBD. **B**: Resonance stability of the conjugated guanidinium ion. **C**: Structures of synthesized guanidine-polymers. **D**: Structure of polystyrene-supported TBD.

Indeed, the synthesis of several peptide- mimicking polymers was reported (Scheme 2.25C).[309-312] Furthermore, TBD was incorporated into polystyrene (refer to Scheme 2.25D), which resulted in a polymer-supported catalytic resin that is stable at ambient conditions, easy to handle and simple to recover by filtration. Besides the application as mediator in organic reactions such as alkylations, esterifications or dehalogenations, this resin was also able to catalyse several reactions (e.g. Henry, aldol-) condensations, Michael addition or regioselective synthesis of lysophospholipids at ambient temperature under very mild conditions.[313-316]

All these beneficial synthetic properties (such as high basicity and catalytic activity) along the possibility of incorporating these structures into polymeric backbones inspired the investigation of such guanidine-compounds in the context of the chemiluminescent reaction of luminol.

2.4.3 Host-Guest Chemistry

The formation of host-guest inclusion complexes as part of supramolecular chemistry has emerged as effective tool for the design of dynamic soft matter materials with stimuli-responsive (e.g. bioactive, self-assembling, self-healing or self-reporting) properties.[317-320] Therefore, host molecules such as rotaxanes, cucurbit[n]urils, calix[n]arenes, pillar[n]enes or cyclodextrins (CDs) (refer to Scheme 2.26) have been used to encapsulated suitable guest molecules.[321-330]

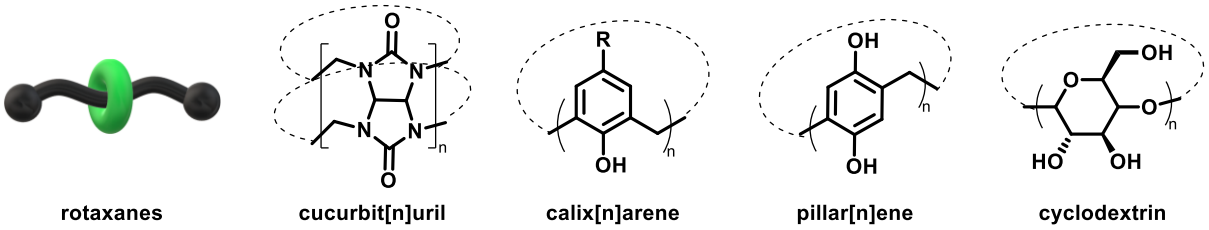

Scheme 2.26: Host molecules for supramolecular complex formations: rotaxanes, cucurbit[n]urils, calix[n]arenes, pillar[n]arenes and cyclodextrins.

Among the broad plethora of host molecules, CDs are of special interest in the food, cosmetic or pharmaceutical industry due to their non-toxicity, biocompatibility and large-scale production.[331-335] The production of CDs is mainly based on starch, which is degraded by the enzyme cyclomaltodextrin glucanotransferase into CDs with different amounts of α-1,4-linked glycosyl units. With six units, α-CD is the smallest one with an inner diameter of 4.7-5.3 Å, followed by the seven-membered β-CD (inner diameter = 6.0-6.5 Å) and the eight-membered γ –CD (inner diameter = 7.5-8.3 Å).[336] The structure of the CDs can be described as a truncated cone with a hydrophilic shell due to the secondary CH_2OH-groups and a hydrophobic core due to the carbon backbone of the glycosyl units.[337] Thus, apolar guest molecules (e.g. adamantly, ferrocene, bipyridine-complexes or lipophilic drug molecules) can be encapsulated by CDs in aqueous media.[335, 338] Such complex formations are based on non-covalent interactions such as electrostatic or charge-transfer interactions, hydrogen bonding, Van der Waals forces or thermodynamic energy increase due to the release of solvent molecules from the CDs. Generally, these inclusion processes are reversible and can be characterized by the stability constant $K_{m:n}$ of *m* guest molecules and *n* CD molecules, as shown in Equation 2.7.[336-337]

$$m(Guest) + n(CD) \rightleftarrows Guest_mCD_n \qquad K_{m:n} = \frac{[Guest_mCD_n]}{[Guest]^m \times [CD]^n}$$

Equation 2.7: reversible process of the host-guest inclusion and the respective stability constant $K_{m:n}$ depending on the molar concentrations of the guest molecule and the CD

The higher the value of $K_{m:n}$, the more stable is the formed supramolecular complex. This can be exploited for the encapsulation of guest molecules with different $K_{m:n}$ values as illustrated in Scheme 2.27. For example, an encapsulated guest molecule with a lower $K_{m:n}$ value can be replaced by a guest molecule with a higher $K_{m:n}$ value.

Importantly, the stability and sensitivity of the complexes can be readily altered by suitable chemical modifications of the CDs (e.g. amination, etherification, esterification or alkylation), variation of the solvent or guest molecules.[335] Moreover, the reversible (de-)complexation can be influenced by tuning temperature, pH, light or redox properties.[339-342] Besides the aforementioned guest molecules that were encapsulated by CDs, also the successful complex-formation between CDs and guanidines has been reported.[343-344] Additionally, CD-derivatives have been found to enhance the CL emission of luminol.[345] Therefore, CD was chosen as host molecule to enable the supramolecular complex formation of the targeted luminol-guanidine-system.

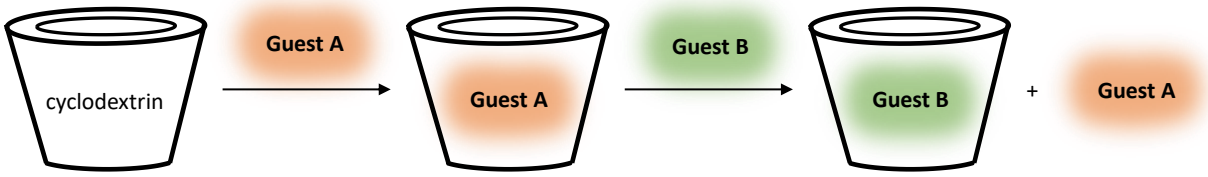

Scheme 2.27: Illustration of the supramolecular host-guest complex formation between cyclodextrin and guest A, which can be replaced by guest B having a higher $K_{m:n}$ value.

3 Results and Discussion

The aim of the current doctoral thesis is the development of polymeric, self-reporting systems. Therefore, two different approaches have been chosen, based on either photochemical or chemiluminescent (CL) processes. For the CL system, luminol was chosen as the light-emitting species. Ideally, the luminol along all required functionalities for the CL reaction are incorporated into the same polymeric backbone. The synthetic approaches and the respective results are discussed in Chapter 3.1. On the other hand, the second self-reporting approach is based on the photo-sensitive tetrazole functionality. The synthesis for the tetrazole-bearing polymers and their photochemical properties are addressed in Chapter 3.2. To enable a better understanding of the results, only the most relevant analytical data are presented, additional figures, the detailed synthesis along information about applied materials and instruments can be found in Chapter 5 and in the appendix (Chapter 6).

3.1 A Luminol-Based Self-Reporting System

The research into the polymeric luminol-based system is based on previous studies performed in our group.[346-347] Herein, luminol was successfully incorporated into the same polymeric backbone as the non-cyclic (2-aminoethyl)guanidine by orthogonal, active-ester based PPMs, as illustrated in Scheme 3.1.

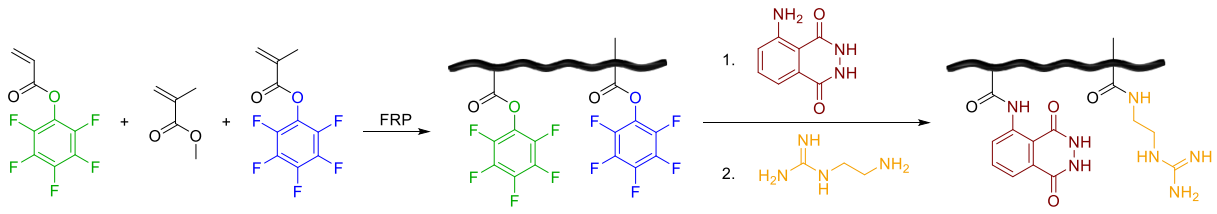

Scheme 3.1: Initial synthesis strategy for the polymer with both luminol and (2-aminoehtyl)guanidine functionalities.

However, no CL emission was obtained when an oxidant (e.g. H_2O_2) was added to the polymer dissolved in DMSO, unless an additional base (e.g. TBD) was present in the reaction mixture. At this point, the investigations of the present doctoral thesis have been initiated.

Parts of chapter 3.1 and the respective experimental parts are adopted from publications written by the author.[347-348]

3.1.1 Contest of Organic Superbases

Although the (2-aminoethyl)guanidine-functionality was apparently not able to facilitate the CL emission of luminol in a sufficient manner, the successful CL emission in the presence of additional TBD as a base clearly suggested the potential of organic superbases as mediator for the self-reporting output. Therefore, in the first step a small molecule model study with different bases has been conducted to determine the best-suited organic superbase for the luminol-CL and the underlying mechanism.[348] The applied bases belong to four different categories: a non-cyclic (TMG, pK_a (THF) = 15.6))[349] and a cyclic (TBD, pK_a (THF) = 21.0))[349] guanidine derivative, an amidine (1,8-diazabicyclo[5.4.0]undec-7-ene, DBU, pK_a (THF) = 16.9))[349] and an inorganic base (KOH, already known in the context of the luminol-CL), as illustrated in Scheme 3.2.

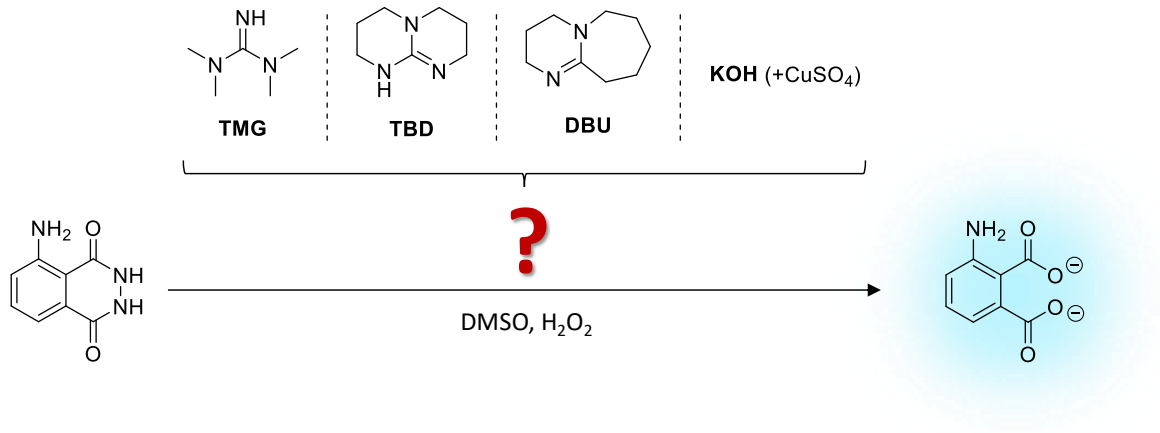

Scheme 3.2: Overview of investigated bases regarding the luminol-CL reaction in DMSO triggered by H_2O_2.

As mentioned in chapter 2.4.1, the highest Φ_{CL} of luminol are obtained in aprotic media in the presence of a strong base, thus DMSO was chosen as the solvent.

First, luminol (c = 7.5x 10^{-2} mol L^{-1}) and different equivalents of TBD (0.5, 1.0, 5.0, 10.0 and 20.0 eq.) were dissolved in DMSO and subsequently, 0.1 mL H_2O_2 (1 mol L^{-1}) were added to trigger the CL reaction. While no CL emission was observed by the naked eye in the presence of 0.5 or 1.0 eq. TBD, a strong CL emission was clearly visible at ≥ 5.0 eq. TBD. This behaviour was further investigated by UV/Vis and CL emission measurements (refer to Figure 3.1).

Indeed, the absorption has changed drastically between 1.0 (blue line in Figure 3.1A) and 5.0 eq. (red line in Figure 3.1A) TBD. The decreasing absorption bands at 295 nm and 357 nm along the increasing new bands at 329 nm and 370 nm for 5.0, 10.0 and 20.0 eq. TBD suggested the formation of the luminol mono-anion species (refer to Scheme 2.22) only in the presence of ≥ 5.0 eq. Thus, only in the presence of sufficient amount of TBD the CL emission is observed by the naked eye as well as in the CL emission measurement depicted in Figure 3.1B.

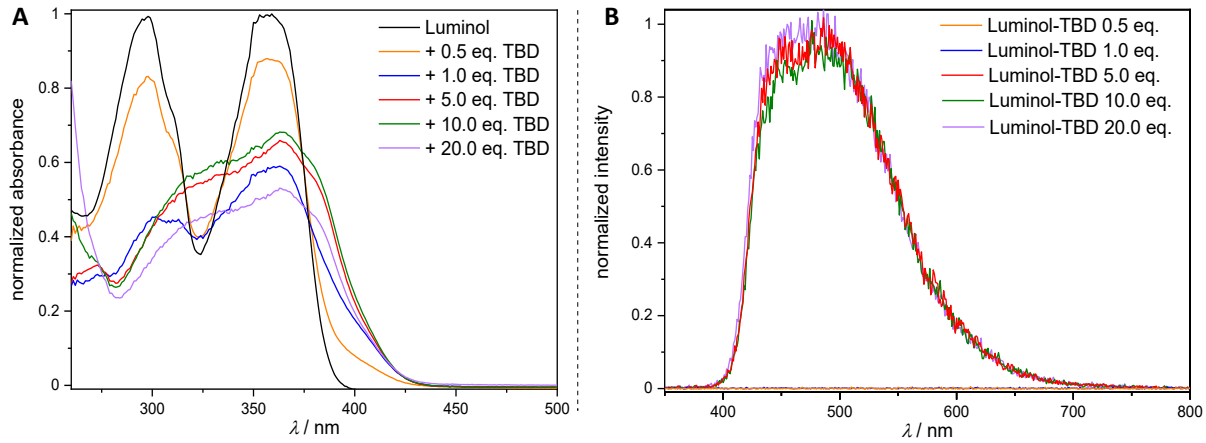

Figure 3.1A: UV/Vis spectra of luminol (c = 7.5 x 10^{-5} mol L^{-1}) in DMSO with different concentrations of TBD (c(0.5 eq.) = 3.75 x 10^{-5} mol L^{-1}, c(1.0 eq.) = 7.5 x 10^{-5} mol L^{-1}, c(5.0 eq.) = 37.5 x 10^{-5} mol L^{-1}, c(10.0 eq.) = 75.0 x 10^{-5} mol L^{-1}, c(20.0 eq.) = 150.0 x 10^{-5} mol L^{-1}). **B**: CL emission of luminol (c=7.5*10^{-2} mol L^{-1}) in DMSO with different concentrations of TBD (c(0.5 eq.)=3.75x10^{-2} mol L^{-1}, c(1.0 eq.)=7.5x10^{-2} mol L^{-1}, c(5.0 eq.)=37.5x10^{-2} mol L^{-1}, c(10.0 eq.)=75x10^{-2} mol L^{-1}, c(20.0 eq.)=150x10^{-2} mol L^{-1}) at ambient temperature, triggered by H_2O_2.

Having established the required amount of superbase to enable the CL reaction of luminol (i.e. 5.0 eq., since no significant change in the absorption and CL emission was observed between 5.0 eq. and ≥ 10.0 eq. TBD), the other bases (TMG, DBU and KOH) were tested under similar conditions. Evidently, luminol in the presence of KOH shows a similar absorbance behaviour as in the presence of TBD, contrary to the absorbance in the presence of TMG and DBU (Figure 3.2A). This behaviour is also reflected in the CL emission (Figure 3.2B). While no CL emission is observed in the presence of TMG and only a rather low emission is obtained in the presence of DBU, a clear CL emission is measured in the presence of KOH. Interestingly, the CL emission for the luminol-TBD system is up to five times higher than the CL emission of luminol-KOH system (green line in Figure 3.2B) and about two times higher than for the $CuSO_4$-catalysed luminol-KOH system (orange line in Figure 3.2B). The different CL emission behaviour between the luminol-TBD system and the systems with either KOH or DBU can be explained by the outstanding basic and catalytic properties of the guanidine-superbases (refer to Chapter

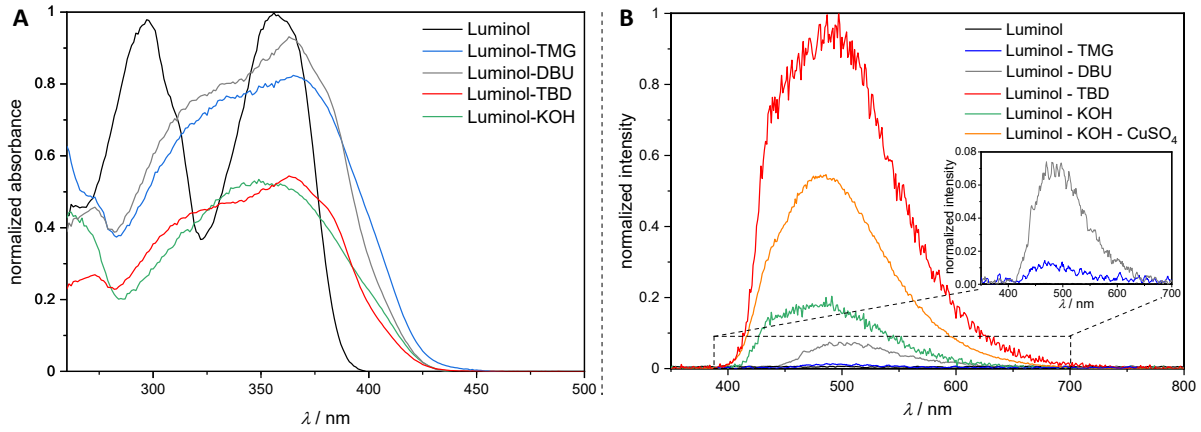

Figure 3.2A: UV/Vis spectra of luminol-CL-systems in DMSO (c(lum)=7.5x10^{-5} mol L^{-1}, c(base)=37.5x10^{-5} mol L^{-1}) at ambient temperature (without the addition of H_2O_2). **B**: CL emission of luminol-base systems in DMSO (c(luminol)=7.5x10^{-2} mol L^{-1}, c(base)=37.5x10^{-2} mol L^{-1}, c($CuSO_4$)=4.5x10^{-2} mol L^{-1}) at ambient temperature, triggered by 0.1 mL H_2O_2 (1 mol L^{-1}).

2.4.2). It is of critical importance to mention that both TBD and TMG belong to the class of guanidines, suggesting a high impact of the bicyclic structure of the TBD compared to the non-cyclic structure of the TMG. Indeed, it has been reported that non-cyclic guanidine functionalities are transformed to the respective urea derivatives in the presence of oxidants (e.g. H_2O_2), as depicted in Scheme 3.3.

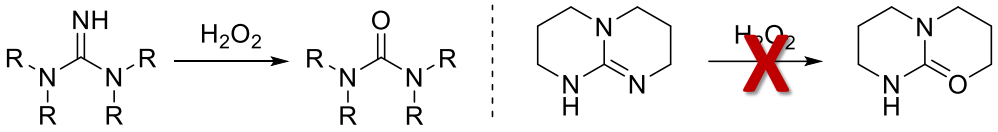

Scheme 3.3: Oxidation reaction of a non-cyclic guanidine (left) and TBD (right) triggered by H_2O_2.

Consequently, the basic and catalytic properties of the oxidized species differ from the initial guanidine compound and are no longer able to initiate the aimed CL reaction of luminol. On the other hand, TBD remains intact, i.e. it is not transformed into its corresponding urea derivative due to the steric hindrance of the bicyclic structure.

Thus, TBD sustains its properties as efficient base and catalyst for the successful CL reaction of luminol. Accordingly, TBD was chosen for the mechanistic investigations of the superbase-mediated luminol-CL reaction as well as for the design of a polymers with self-reporting CL properties.

3.1.2 Mechanism of the TBD-Mediated Luminol-CL

The manifestation of TBD as efficient mediator for the CL-reaction of luminol has raised the question for the underlying mechanism. Since typically ROS such as the hydroxyl radical •OH, the superoxide anion radical $O_2^{\bullet-}$ or singlet oxygen $^1O_2$ are involved in the luminol-CL, spin trap experiments with various radical scavengers were conducted. Indeed, the CL emission of the luminol-TBD system is clearly inhibited in the presence of radical scavengers (e.g. L-ascorbic acid (AA), NaN_3, superoxide dismutase (SOD) or thiourea (TU), refer to Figure 3.3A), indicating the participation of ROS in the TBD-mediated luminol-CL.

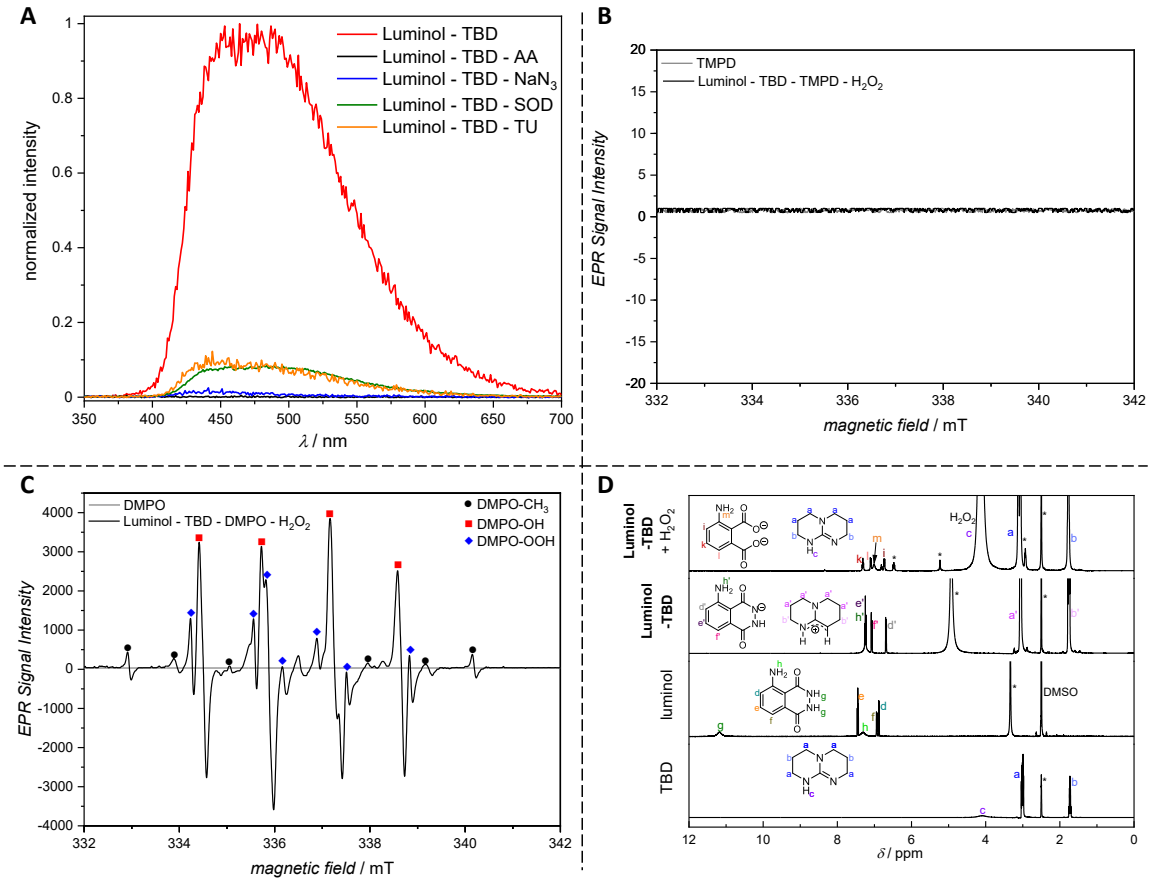

Figure 3.3A: CL emission of the luminol-TBD-system (c(luminol)=7.5x10^{-2} mol L^{-1}, c(TBD)=37.5x10^{-2} mol L^{-1}) in DMSO in the presence of radical scavengers (c=2.5x10^{-2} mol L^{-1}) at ambient temperature, triggered by H_2O_2. **B**: EPR spectra of TMPD (grey line) and the luminol-TBD-system in the presence of TMPD after addition of H_2O_2. **C**: EPR spectra of DMPO (grey line) and the luminol-TBD-system with DMPO after the addition of H_2O_2 (black line). The signals can be assigned to different DMPO-radical-products: DMPO-CH_3 (black dot), DMPO-OH (red square) and DMPO-OOH (blue rhomb). **D**: ^{1}H NMR (400 MHz) spectra of luminol, TBD, luminol-TBD and luminol-TBD + H_2O_2 in DMSO-d_6.

To enable a distinctive identification of the involved ROS, electron-paramagnetic resonance (EPR) spectroscopic analysis was carried out. On the one hand, no signal is obtained for a

reaction mixture containing luminol, TBD, H_2O_2 and 2,2,6,6-tetramethyl-4-piperidone (TMPD) as scavenger for $^1O_2$, suggesting that no $^1O_2$ is generated during the CL reaction (Figure 3.3B). On the other hand, clear EPR signals are obtained for the same mixture with 5,5,-dimethyl-1-pyrroline N-oxide (DMPO) as scavenger (Figure 3.3C).

The signals can be clearly assigned to $^{\bullet}OH$ (red square) and $O_2^{\bullet-}$ (blue rhomb) as well as to the methyl radical $^{\bullet}CH_3$ (black dot). Thus, the following mechanism is postulated (Scheme 3.4): In the first step, dissolution of luminol and TBD in DMSO leads to the formation of the luminol mono-anion and $TBDH^+$. Subsequently, $TBDH^+$ triggers the dissociation of H_2O_2 into ^-OH and $^{\bullet}OH$. Since TBD is regenerated during this reaction, the catalytic behavior of the superbase is revealed. Furthermore, $O_2^{\bullet-}$ is formed by the reaction of DMSO with ^-OH and oxygen present in the non-anhydrous solvent. In this step, the $^{\bullet}CH_3$ radicals are generated detected in the EPR spectrum (Figure 3.3C), which instantaneously react with oxygen to the dimethyl peroxide in the absence of a radical scavenger. Eventually, the generated ROS trigger the CL mechanism of luminol as already explained in chapter 2.4.1 (refer also to Scheme 2.22 and Scheme 3.4C) accompanied by the emission of a striking blue-green light.

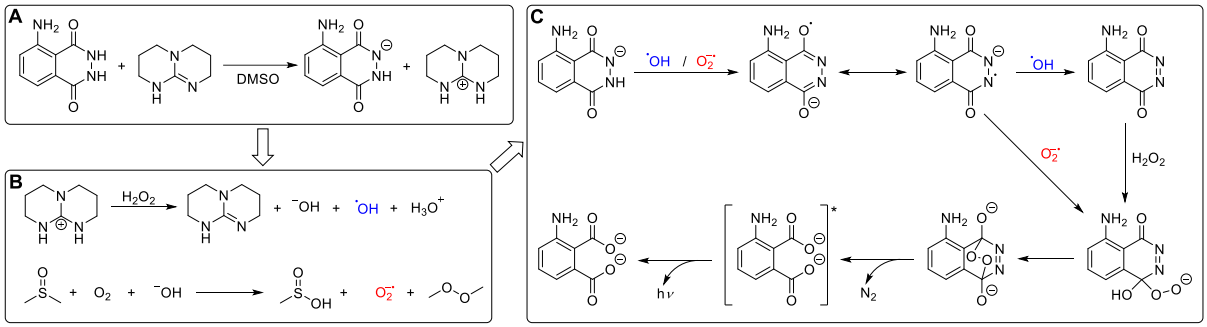

Scheme 3.4: Proposed mechanism of the TBD-mediated luminol-CL.

Additional NMR spectroscopy and GC-MS analysis supported the proposed mechanism. In the ^1H NMR spectrum (Figure 3.3D) of luminol and TBD, the resonances of the protons c and g are no longer detected and the resonances of the luminol-protons f and h are shifted to f' and h', assuming the (de-)protonation of luminol and TBD in DMSO (Scheme 3.4A). The formation of the oxidized luminol after H_2O_2 addition is assessed by the arising resonances i, k, l and m between 7.3 and 6.7 ppm, along the assigned resonances in the ^{13}C NMR spectrum (Figure 6.1) and the GC-MS analysis (Figure 6.2). While the theoretically reappearing resonance c of TBD overlaps with the resonances of H_2O_2, the unaltered resonances a and b in the ^1H and the

consistent resonances 8 and 9 in the ^{13}C NMR spectra (Figure 6.1) before and after the addition of H_2O_2 are in accordance with the implied catalytic properties of the TBD.

Based on the outstanding performance of TBD in the CL reaction of luminol without the need of any additional additives under mild conditions (i.e. ambient temperature, low-toxic solvent (DMSO), reduced amount of base (5.0 eq. instead of 20-1000 eq. as it is reported for other luminol-systems),[280-281] the synthesis of a luminol-TBD-bearing polymer was subsequently envisaged.

3.1.3 Synthesis of the Luminol-TBD-Polymer

Taking inspiration from the aforementioned luminol-(2-aminoethyl)guanidine-polymer obtained via active-ester based PPM (refer to Scheme 3.1), a similar synthesis strategy was considered for the luminol-TBD-polymer **LTP1**, as depicted in Scheme 3.5.

First, an active-ester copolymer (**AEC1**) of MMA, PFP-A and PFP-MA was synthesized via FRP with a ratio of MMA / PFP-A / PFP-MA 1 : 1 : 5 to ensure the 5.0 eq. of superbase in regards of luminol. NMR analysis (^1H and ^{19}F, Figure 6.3) confirmed the successful synthesis of **AEC1** with an apparent number average molecular weight (M_n) of 6 500 g mol^{-1} and a dispersity of $Đ$ = 1.49 (Figure 6.4A). Subsequently, the PFP-A moieties were post-modified with luminol in a solvent mixture of 1,4-dioxane and DMSO at 50°C. SEC analysis of the obtained luminol-polymer **LP1** revealed a slightly increased molecular weight of M_n = 7 400 g mol^{-1} without any side reactions, as it was indicated with a substantially similar dispersity value ($Đ$ = 1.54, Figure 6.4A). Furthermore, the substitution of the PFP-A moieties by luminol was validated via ^1H and ^{19}F NMR analysis (Figure 6.3), in which all resonances can be assigned to the respective functionalities of **LP1**. Finally, the TBD-moiety was meant to be introduced to **LP1** by PPM of the PFP-MA units to yield **LTP1**. Similar conditions as for the PPM of **AEC1** with luminol were applied.

However, a highly viscous jelly-like material was obtained, which was not soluble in any organic solvent /solvent combinations or aqueous media. Thus, no analysis or subsequent applications of the material were feasible. Possible reasons for the gelation could be undesired side reactions or cross-linking processes of **LP1** in the presence of TBD.

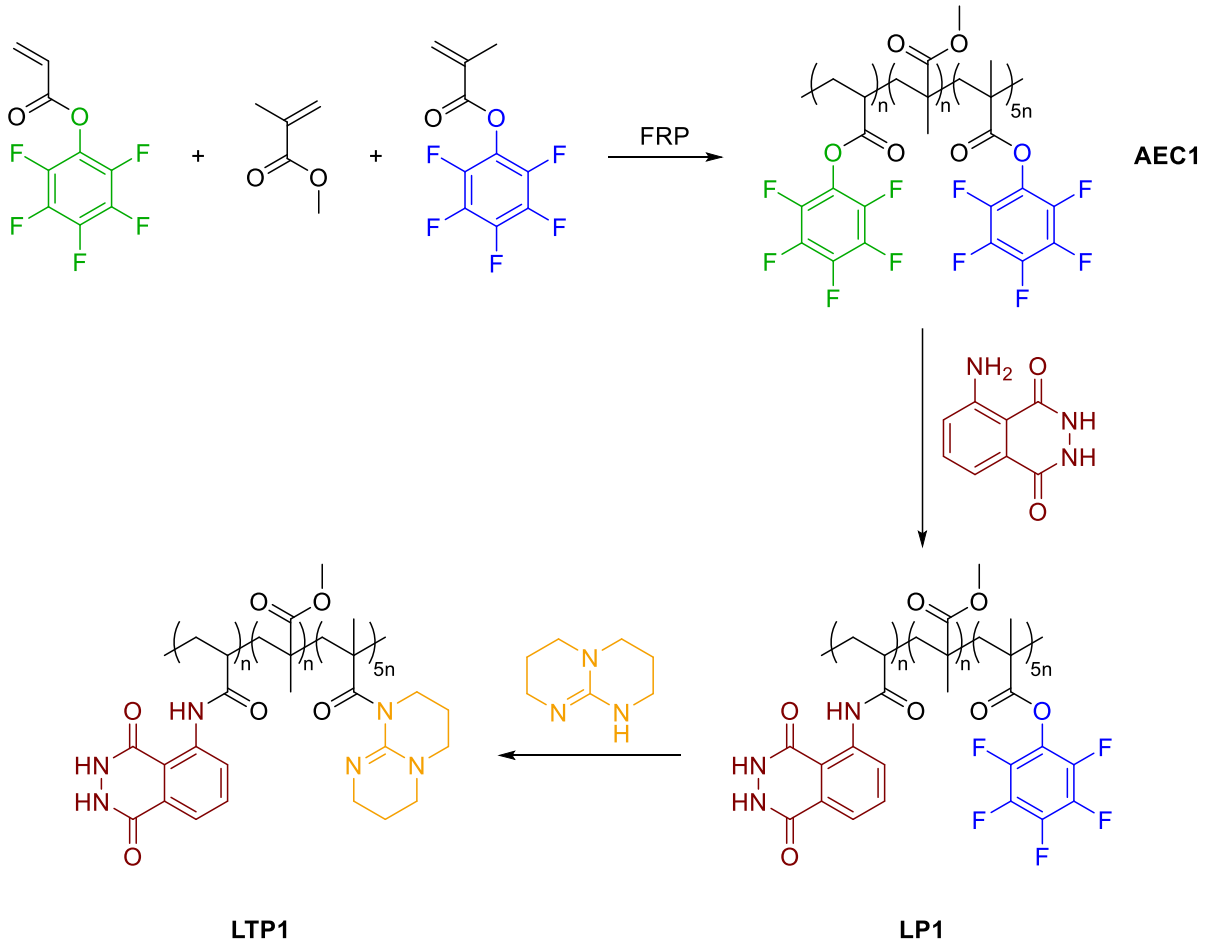

Scheme 3.5: Synthesis strategy for the luminol-TBD-polymer **LTP1** via FRP of MMA, PFP-A and PFP-MA and subsequent PPM reactions with luminol and TBD.

To overcome these problems, TBD-derivatives with an aliphatic spacer were targeted to reduce the steric hindrance of the functionalities in the polymer backbone and increase the solubility of the material. Therefore, TBD-derivatives with three different spacers of variable aliphatic chain lengths were synthesized (**TBD1**-**3**), as illustrated in Scheme 3.6A.

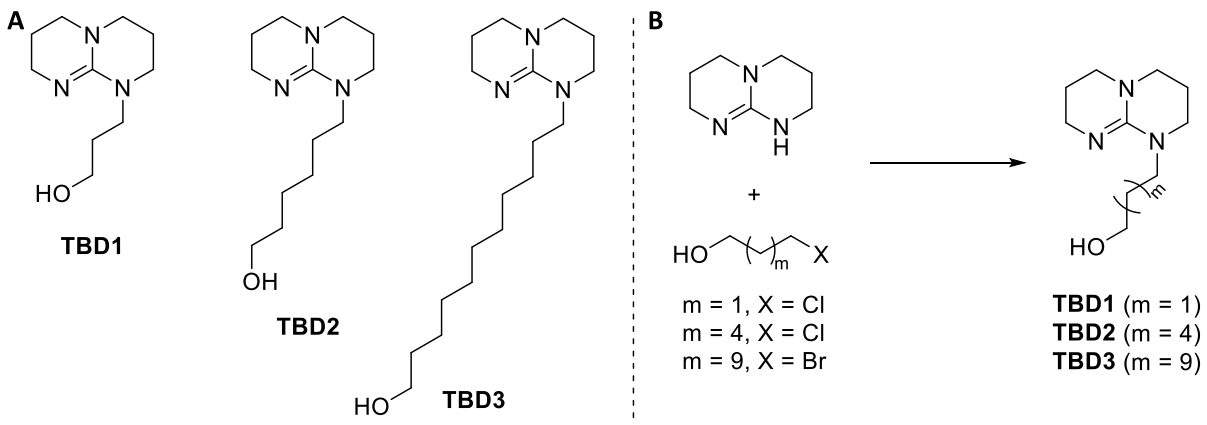

Scheme 3.6A: Structure of the TBD-derivatives **TBD1**, **TBD2** and **TBD3**. **B**: Synthesis strategy for **TBD1**-**3**.

The synthetic procedure was adopted from the literature[350] and has been modified accordingly to obtain the desired TBD-derivatives by nucleophilic substitution reaction of TBD with a halogen-alkylalcohol (refer to Scheme 3.6B). Despite the several attempts (experimental sections 5.2.1) with varying ratios of the starting materials, different solvents (THF, EtOH) and reaction times, the desired products could not be isolated or purified (e.g. by washing, recrystallization, distillation, column chromatography) in a satisfying manner with sufficient yields for the subsequent PPM of the luminol-polymer. Detailed analysis via ^{1}H and ^{13}C NMR spectroscopy (Figure 6.5-Figure 6.7) has revealed the following: there are either no resonances detectable of the products or still resonances of the starting materials next to undesired side products.

Consequently, it was aimed to incorporate spacer chains into the polymer backbone that allow subsequent PPM with TBD. Since it has been reported that PFP-A and PFP-MA can also be post-modified with alcohols, **LP1** was post-modified with 11-bromo-1-undecanol (**LP1'**) followed by the PPM with TBD (**LTP1'**), as shown in Scheme 3.7. However, there are only very low resonances of the luminol protons present after the PPM with 11-bromo-1-undecanol (**LP1'**, Figure 6.8A) and minor resonances left in the ^{19}F NMR spectrum (Figure 6.8B).

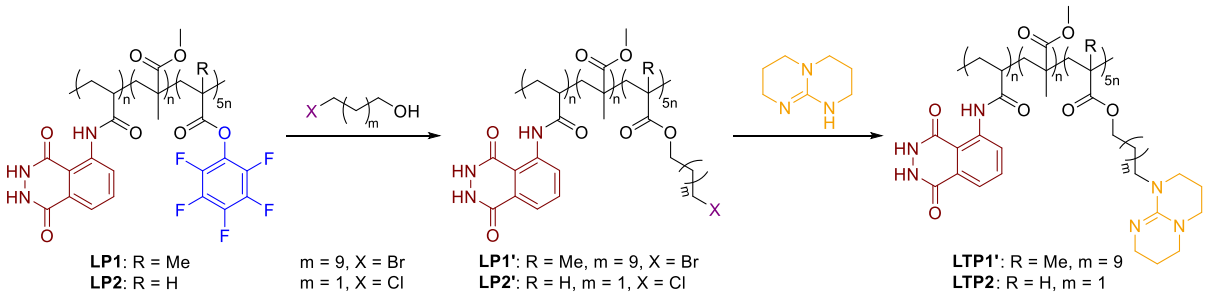

Scheme 3.7: Synthesis procedure for the luminol-TBD-polymers **LTP1'** and **LTP2**.

Due to solubility issues, no analysis of the TBD-modified polymer **LTP1'** was possible. Simultaneously, a copolymer of MMA and PFP-A (**AEC2**) was synthesized, of which only 16.6 mol% were post-modified with luminol (**LP2**) to ensure a ratio of 1 : 5 after complete conversion of the PFP-A units by 3-chloro-1-propanol (**LP2'**) or rather TBD (**LTP2**). Although NMR analysis indicated the successful synthesis of **LTP2** (no resonances present anymore in the ^{19}F NMR spectrum of **LTP2** (Figure 6.10) and new arising resonances in the ^{1}H NMR spectrum of TBD (n, o, p, Figure 6.9), SEC analysis in DMAc (Figure 6.4B) revealed a decreased M_n after complete PPM of **LP2**, indicating degradation accompanied with other undesired side

reactions. Furthermore, test reactions of the self-reporting properties of **LTP2** triggered by H_2O_2 did not result in visible or measurable CL emission.

Anew, it was essential to design an alternative synthetic strategy which facilitates the successful synthesis of the targeted luminol-TBD-polymer. Inspired by the synthesis approach previously reported for polystyrene-supported TBD resins, TBD was successfully incorporated into a polymeric material via PPM of 4-vinylbenzyl chloride (VBC). Hence, a copolymer of MMA, PFP-A and VBC was synthesized analogue to **AEC1** with a ratio of 20 : 1 : 5 (**AEC3**, Scheme 3.8).

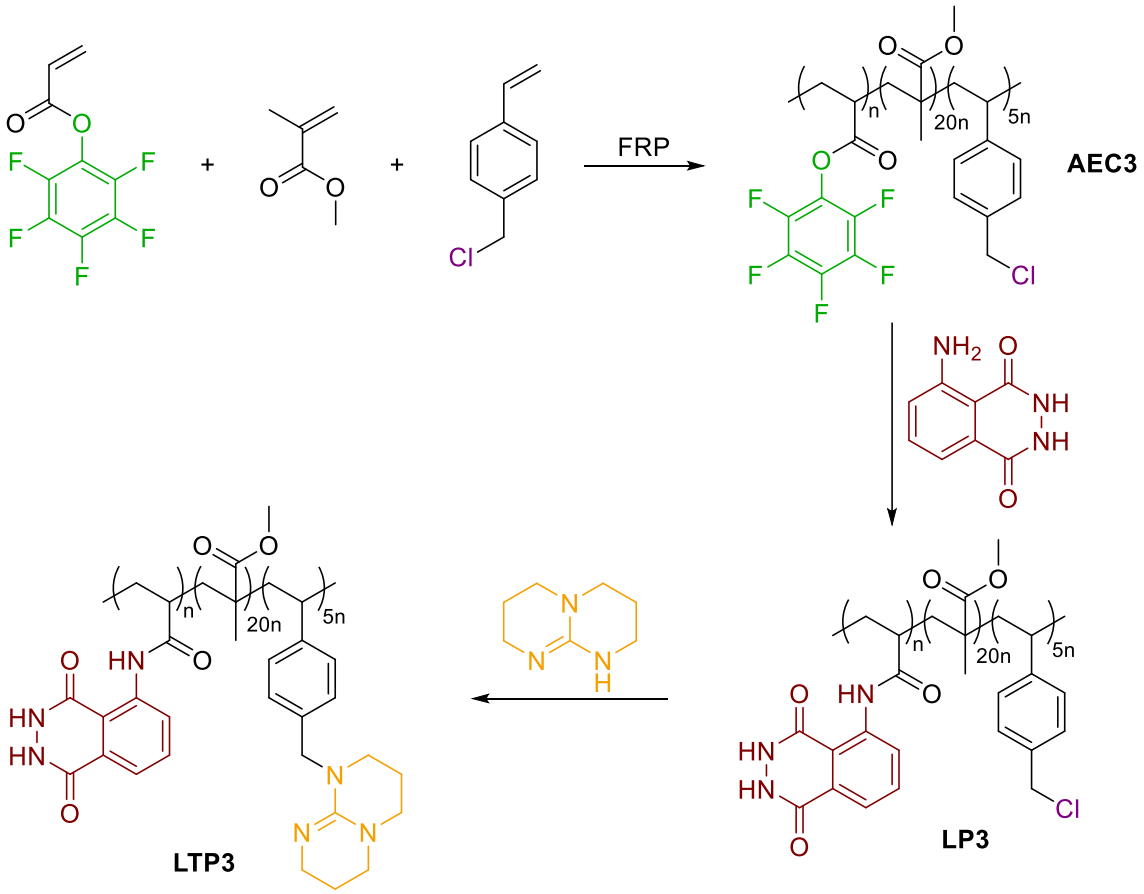

Scheme 3.8: New concept for the synthesis of the luminol-TBD-polymer **LTP3**.

The high amount of MMA (20.0 eq.) was essential to prevent undesired crosslinking reactions, and to increase the solubility of the subsequent post-modified polymer with luminol and TBD (**LTP3**, Scheme 3.8). While the PFP-A moiety was post-modified with luminol as described for the synthesis of **LP1** (Scheme 3.5), the Cl-moiety was substituted by TBD, as aforementioned, in a similar manner to the synthesis reported for the PS-supported TBD resin.[350] Beneficially,

NMR analysis of **LTP3** (Figure 3.4) confirmed the successful incorporation of both functional moieties (i.e. luminol and TBD). The resonances in the ^{1}H NMR spectrum can be assigned to the respective luminol- (e-i) and TBD- protons (most importantly n and r), whereas no resonances are detected in the ^{19}F NMR spectrum anymore due to the complete functionalization. However, **LTP3** is not soluble in suitable solvents for SEC analysis (e.g. THF or DMAc), thus no determination of M_n was possible.

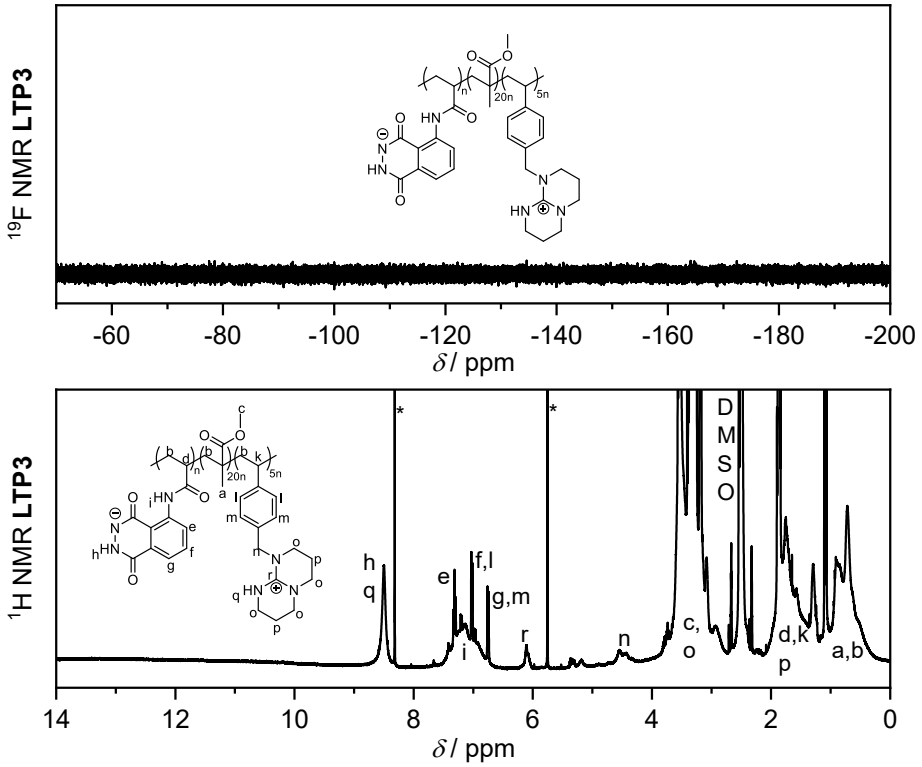

Figure 3.4: ^{1}H NMR (400 MHz) and ^{19}F NMR (377 MHz) spectrum of **LTP3** in DMSO-d_6 at ambient temperature.

3.1.4 Supramolecular Assembly

After the successful synthesis of **LTP3**, the supramolecular assembly behaviour of the polymer was investigated. Therefore, **LTP3** and randomly methylated β-cyclodextrin (Me-β-CD) were dissolved in DMSO in order to form the host-guest complex **C1** (refer to Scheme 3.9).

A first indication of the successful supramolecular assembly was obtained from ^{1}H NMR analysis (Figure 3.5A) due to the broadening of the luminol-resonances i and h in addition to the resonances o, p and q arising from the aliphatic cyclic skeletal of TBD.

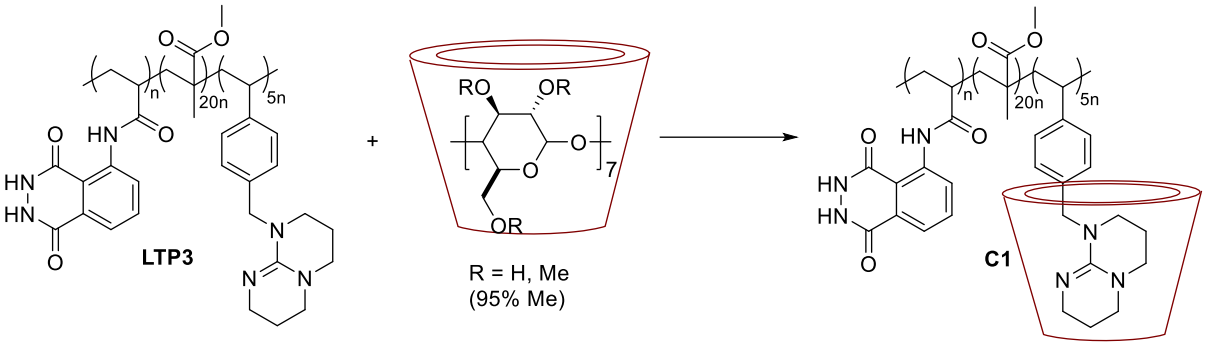

Scheme 3.9: Supramolecular assembly of **LTP3** in the presence of Me-β-CD yielding the host-guest complex **C1**.

Additional 2D NMR analysis, i.e. nuclear Overhauser effect spectroscopy (NOESY), confirmed the complexation, as illustrated in Figure 3.5B. Besides the expected NOEs at 8.5 ppm (orange circles) arising from the dipolar interactions between the Me-β-CD and TBD, cross-resonances at 7.5 ppm (red circles) and 4.5 ppm (grey circles) are detected, which can be assigned to interactions between Me-β-CD and luminol (red circles) or MMA (grey circles), respectively.

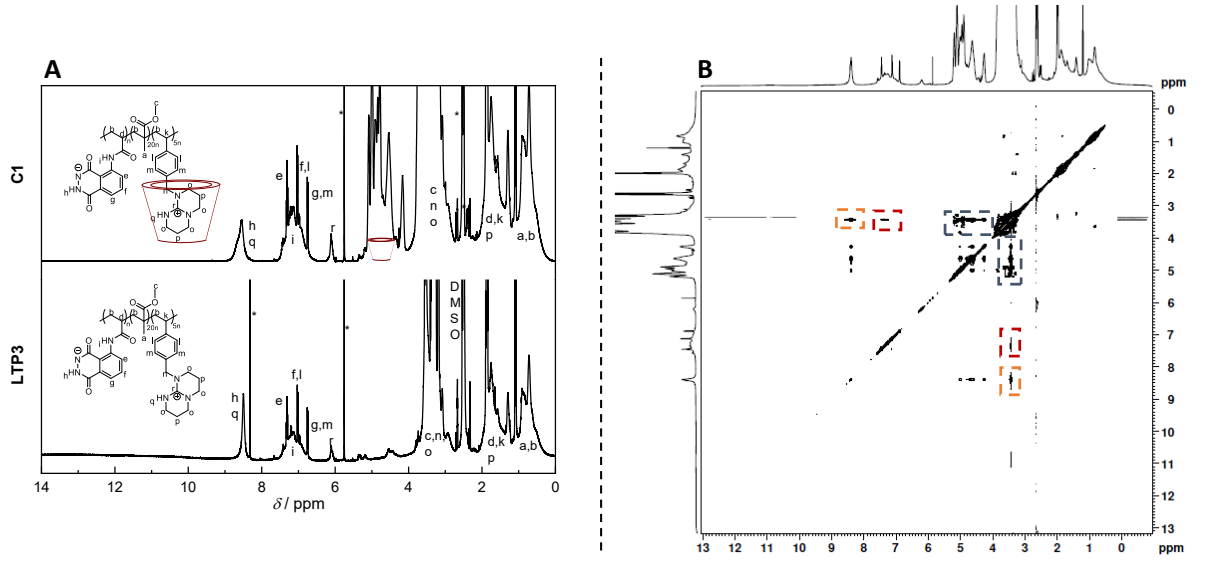

Figure 3.5A: ^{1}H NMR (400 MHz) spectra of **LTP3** and **C1** in DMSO-d_6 at ambient temperature. **B**: NOESY spectrum of **C1** in DMSO-d_6 at 300K.

Another complementary characterization technique for supramolecular assemblies is the dynamic light scattering (DLS) analysis. If the assembly is successful, one specific distribution with a diameter value between the ones of the single components prior to the complexation should be measured. Indeed, exactly this behaviour is observed for **C1** as depicted in Figure 3.6, clearly demonstrating the supramolecular assembly properties of **LTP3**.

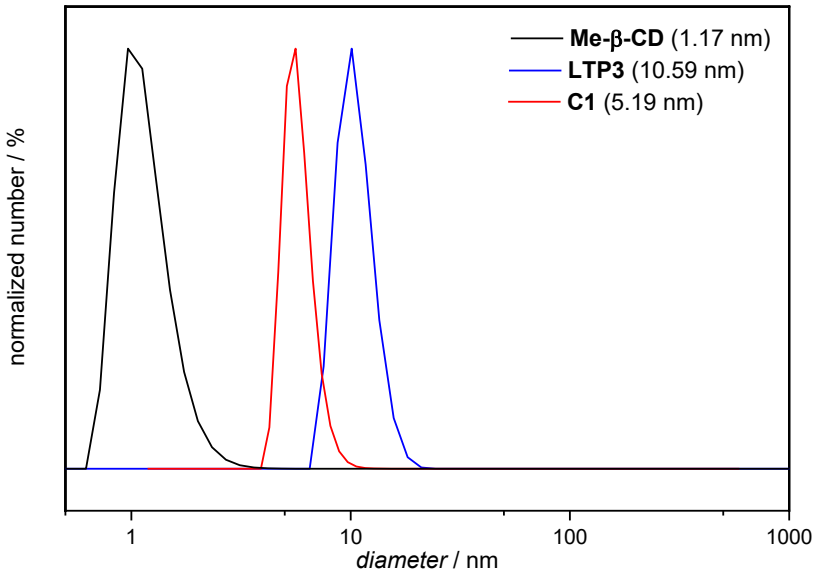

Figure 3.6: DLS traces of Me-β-CD, **LTP3** and **C1** in DMF at 20°C with a concentration of c = 1 mg mL^{-1}, respectively.

3.1.5 Self-Reporting Chemiluminescent Output

Finally, the CL-properties of **C1** were investigated. To trigger the CL reaction, H_2O_2 was added to the dissolved **C1** in DMSO to yield the oxidized complex **C2** (Scheme 3.10).

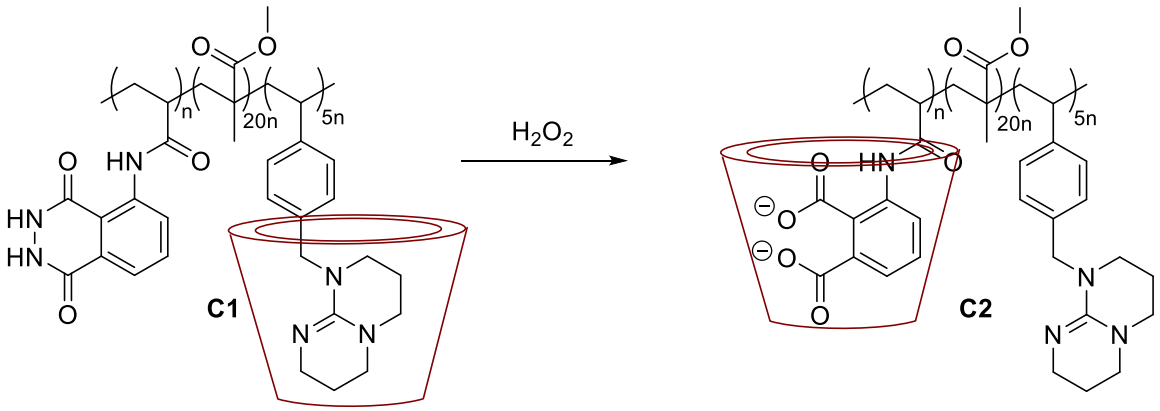

Scheme 3.10: Oxidation of **C1** by the addition of H_2O_2, yielding the supramolecular complex **C2**.

As can be seen in the UV/Vis spectra in Figure 3.7A, the initial bands at 360 and 300 nm have decreased, while the band at 260 nm increased as a result of the formation of the oxidized luminol. The oxidation also has a strong influence on the supramolecular assembly. While there is no NOE detected anymore between Me-β-CD and TBD (refer to Figure 3.7B), a cross-resonance at 10.5 ppm (grey box) between Me-β- CD and H_2O_2 or the polymer backbone is observed along a cross-resonance in the aromatic region (blue box). The NOE in the aromatic

region possibly arises from dipolar interactions between Me-β-CD and the oxidized luminol due to an apparently higher stability constant $K_{m:n}$ (see chapter 2.4.3) compared to the one between Me-β-CD and TBD. Indeed, the altered supramolecular assembly behaviour of the oxidized polymer is also supported by DLS analysis (Figure 3.7C). The diameter of the oxidized complex **C2** shows only a 7% difference to the diameter of the initial luminol-TBD-polymer **LTB3** and a 47% larger diameter than **C1**, thus supporting the NOESY results.

Most importantly, a strong CL emission is observed for **C1** (Figure 3.7D) upon the addition of H_2O_2. In comparison to the CL of the non-encapsulated **LTP3**, a (~ 140 times) higher CL for **C1** is obtained, revealing the enhancing properties of Me-β-CD regarding the luminol-CL. Beneficially, the intense CL emission was even observable by the naked eye.

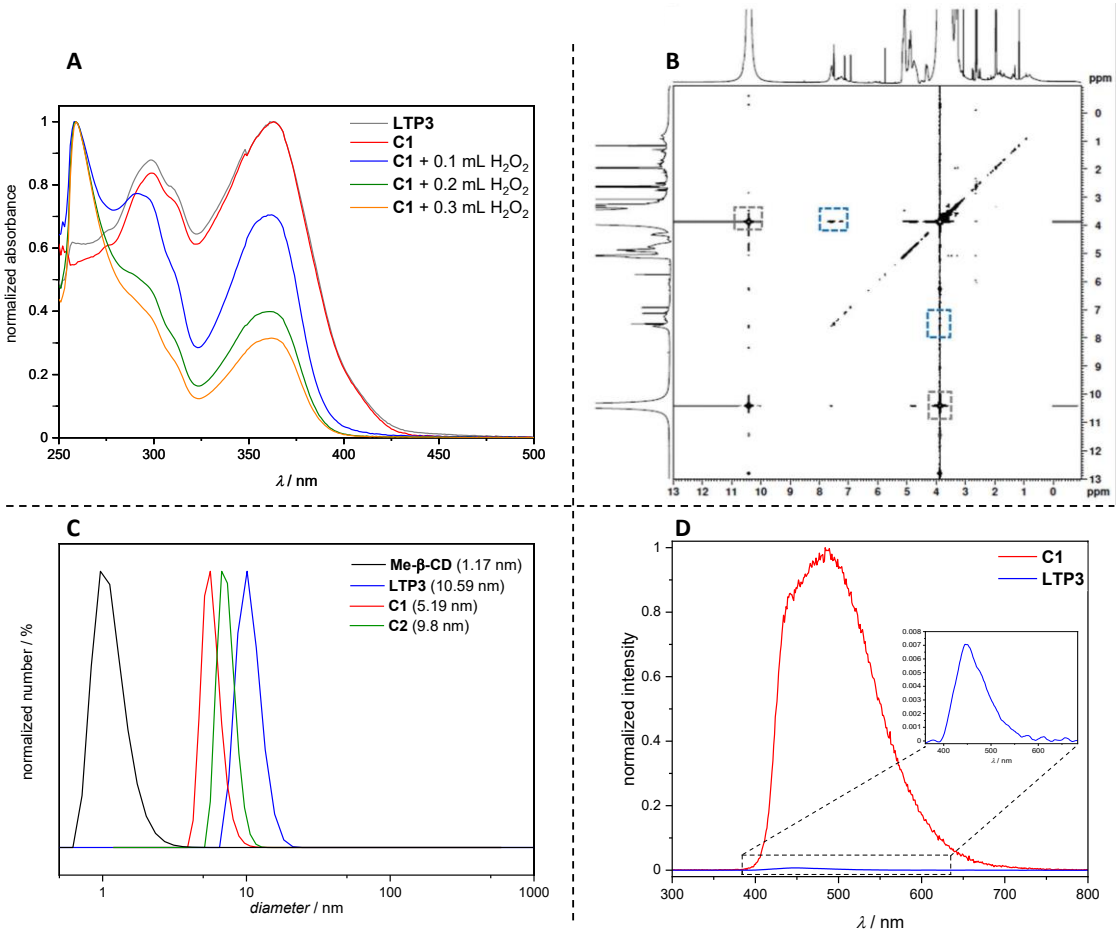

Figure 3.7A UV/Vis-spectra of **LTP3** and **C1** (c = 3.25 × 10^{-6} mmol mL^{-1}) before and after addition of H_2O_2 (1 mol L^{-1}). All spectra were recorded in DMSO at ambient temperature. **B**: NOESY spectrum of **C2** in DMSO-d_6 at 300K. **C**: DLS traces of Me-β-CD, **LTP3**, **C1** and **C2** in DMF at 20°C (c = 1 mg mL^{-1}, respectively). **D**: CL emission of **LTP3** and **C1** (c = 3.25 × 10^{-4} mmol mL^{-1}) in DMSO at ambient temperature, triggered by 0.1 mL H_2O_2 (1 mol L^{-1}).

Evidently, the luminol-TBD-polymer facilitates not only the formation of supramolecular (dis)assembly, but also displays CL properties combined in one polymeric material, which may allow *in vivo* applications for the detection of ROS without the need of additives or external triggers in a self-reporting manner. Additionally, the present work can be taken as inspiration for the design of artificial, smart materials with the ability to self-report damages or structural changes in polymeric materials.

3.2 A Self-Reporting System based on Tetrazole and its Derivatives

In the recent years, 2,5-diphenyl tetrazole and its derivatives have been deeply investigated in our group due to the versatile reactions of the photochemical inducible nitrile-imine dipole (refer to Chapter 2.2.3). Depending on the substituents of the tetrazole, this nitrile-imine dipole can be generated in a λ-orthogonal manner and, most importantly, react with a suitable ene-functionality to yield a highly fluorescent pyrazoline-adduct. Hence, the system becomes self-reporting by allowing the monitoring of the reaction progress and detection of the product via analysis of the changing fluorescent behaviour.

While diverse tetrazole-containing polymeric materials have been successfully synthesized, the tetrazole moiety was generally introduced either as pendant or polymer chain end-group into pre-synthesized polymers via PPM reactions[60, 351-352] or multiple chain extension steps[101] rather than being directly polymerized. Therefore, the second project of the current thesis focused on the investigation of synthetic protocols suitable for a direct polymerization of tetrazole and its derivatives in order to deliver self-reporting polymeric materials based on the photochemistry of tetrazoles. Ideally, such protocols should allow the simultaneous polymerization of two tetrazole-monomers with different photochemical properties (e.g. UV- or Vis-responsiveness) to enable further PPM reactions in a λ-orthogonal procedure. Inspiration was taken from the aforementioned Passerini-MCR (refer to Chapter 2.1.3) and especially its feasible application for polymer synthesis (Scheme 2.9) due to the tolerance to a broad variety of functional units.

The results discussed in the following Chapters are part of a publication in preparation.

3.2.1 Synthesis of Tetrazole-Polymers via the P-MCP

For the direct polymerization of tetrazole derivatives, the P-MCP was applied owing to the generation of synthetic enzyme-mimicking units, thus paving the way for the synthesis of man-made polymeric materials resembling natural enzyme derivatives. As stated before, the P-MCP requires two bi-functional monomers and one mono-functional monomer, the latter

being incorporated as pendant side chain (Chapter 2.1.3). Consequently, the tetrazole moiety was selected as mono-functional aldehyde-moiety in order to maintain the possibility for subsequent photo-induced PPM reactions without affecting the polymer backbone. Since successful P-MCP reactions were reported with 1,6-diisocyanohexane (DICH) and 3,3'-dithiodipropionic acid (DTDPA), [156, 353-354] they were chosen as the bi-functional monomers. Beneficially, the disulfide-bond of the acid compound provides an additional functionality for possible degradation reactions, thus the applied components allow for the synthesis of a highly-functionalized polymer (**TP1**) with two newly formed peptide-analogue bonds per repeating unit in a one-pot reaction, as illustrated in Scheme 3.11.

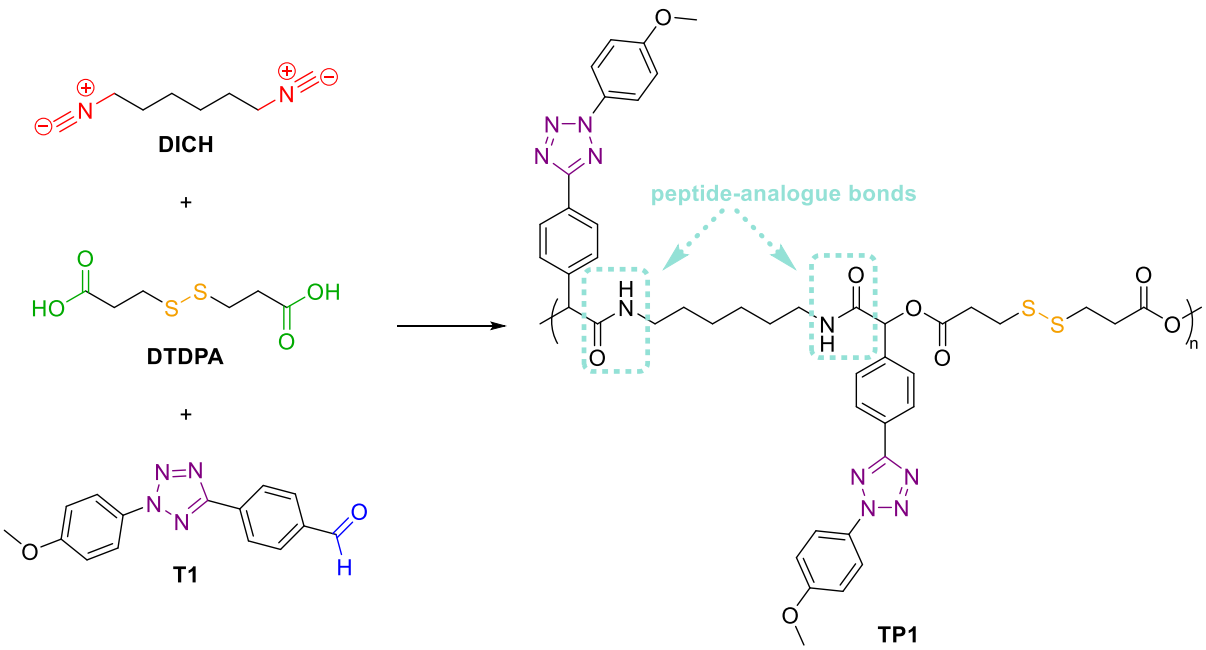

Scheme 3.11: Synthesis strategy for **TP1** via the P-MCP employing DICH, DTDPA and **T1**.

In a first reaction setup (Scheme 3.11), the monomers were dissolved in DCM as aprotic solvent[145] with a ratio of **T1** / DTDPA / DICH 2.2 : 1.0 : 1.0. However, SEC analysis of the obtained polymer **TP1** revealed no polymer formation after a reaction time of 7 days at 40°C (Figure 6.11), which may be attributed to the low solubility of **T1** in DCM at high concentrations (c = 1 M regarding one of the bi-functional monomers) required for the P-MCP. Therefore, a tetrazole-monomer **T2** has been synthesized with an aliphatic spacer moiety to increase the solubility of the monomer. The latter was achieved by an esterification of the tetrazole carboxylic acid derivative (**M1**) with 1,3-propandiol and subsequent oxidation of the obtained alcohol species (**M2**) to the desired aldehyde **T2**, as demonstrated in Scheme 3.12.

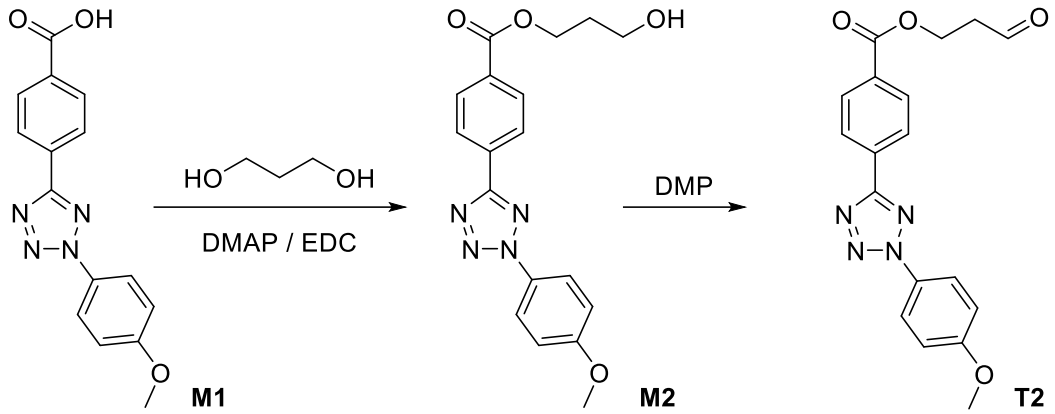

Scheme 3.12: Synthesis for the tetrazole-monomer **T2** via esterification and Dess-Martin periodinane (DMP)-oxidation.

The successful synthesis of both **M2** and **T2** was confirmed by ^{1}H and ^{13}C NMR spectroscopy, in which all the resonances are assigned to the respective compounds **M2** and **T2** (Figure 6.12). Unfortunately, similar solubility issues were observed during the P-MCP as for **T1,** and consequently , no polymer formation was observed for **TP2** (Scheme 3.13A) according to SEC analysis (Figure 6.13A).

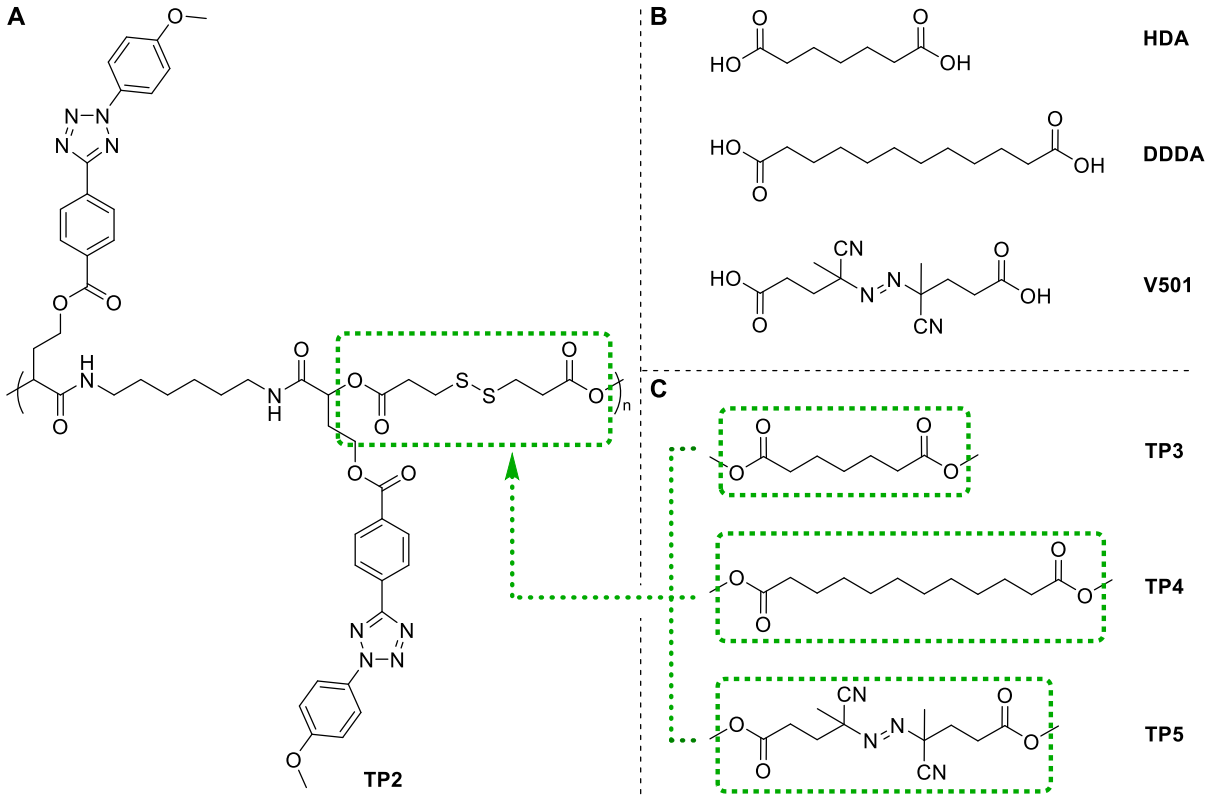

Scheme 3.13: Structures of the tetrazole-polymer **TP2** (**A**), the dicarboxylic acids (**B**) applied for the P-MCP of **T2** to yield the tetrazole-polymers **TP3** – **TP5** (**C**).

Several attempts have been made by varying reaction conditions (e.g. different solvents (DCM, $CHCl_3$, THF, toluene, *o*-chlorobenzene, polarclean, DMSO and mixtures thereof), reaction times (1-11 days), conventional heating or microwave), nevertheless, the results of the SEC analysis obtained for each performed screening experiment suggested the formation of only dimer or trimer (Figure 6.13B-D). In order to reveal whether the problem arises from the hindered structure of the tetrazole-monomer or conceivably the dicarboxylic acid, the P-MCP of **T2** has been repeated with three different dicarboxylic acids, namely heptanedioic acid (HDA), dodecanedioic acid (DDDA) and V-501, respectively (Scheme 3.13B). Since the latter is a well-known azo-initiator and generally not implemented as monomer, the stability of V-501 was tested under the applied P-MCP reaction conditions to ensure that no undesired side-reactions are triggered. Therefore, V-501 was dissolved in THF, stirred at 45°C for 3 days and subsequently analysed via NMR spectroscopy. Indeed, ^{1}H and ^{13}C NMR analysis (Figure 6.14) of V-501 before and after the heating process revealed no decomposition once exposed to high temperatures (e.g. 45 °C), thus indicating the suitability of the compound for the P-MCP. Yet again, SEC analysis (Figure 6.15) did not show any polymer formation for **TP3** – **TP5** (Scheme 3.13C). Apparently, the problem cannot be resolved by employing different dicarboxylic acid, thus suggesting that the tetrazole-monomers **T1** and **T2** are not appropriate compounds for the P-MCP. To verify this hypothesis, an additional attempt has been made with DICH and V-501 under similar reaction conditions as for **TP1** with the aromatic azo-aldehyde **A1** as comparable aldehyde-derivative to the tetrazole-aldehyde derivatives (**T1**, **T2**) (Scheme 3.14).

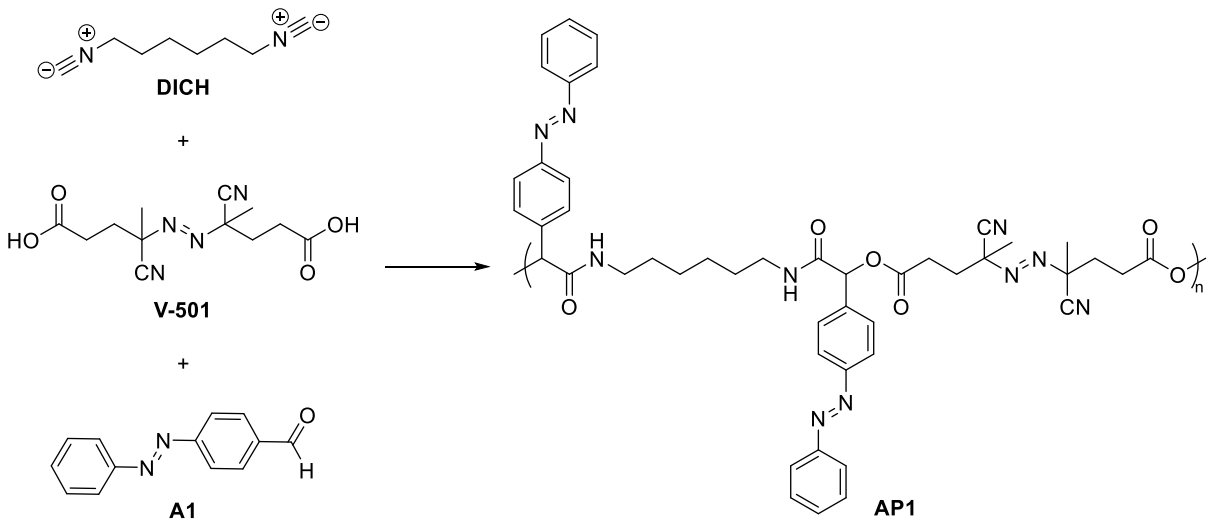

Scheme 3.14: P-MCP of DICH, V-501 and **A1**, yielding the azo-polymer **AP1**.

Interestingly, the targeted azo-polymer **AP1** was obtained with a M_n = 13 500 g mol^{-1} ($Đ$ = 1.26), as evident from the SEC analysis (Figure 6.16) and ^{1}H NMR spectroscopy (Figure 6.17). Clearly, the P-MCP is suitable for the synthesis of multi-functional polymers under the applied reaction conditions, however the electronic character of the tetrazole-monomers **T1** and **T2** implies to hinder the reactivity during the P-MCP.

Consequently, the strategy has been modified from the P-MCP to the P-MCR in order to obtain tetrazole-monomers that can be polymerized under subsequent polymerization reactions.

3.2.2 Synthesis of Tetrazole-Monomers via P-MCR

Although the P-MCP was not suitable for the polymerization of **T1** or **T2**, it is postulated that the P-MCR might be a useful method for the synthesis of tetrazole-monomers with a functionality that allows subsequent polymerization reactions. Inspiration has been taken from the work of Roth and colleagues, who applied the P-MCR to deliver PFP-derived (meth)acrylic MCR-monomers suitable for subsequent RAFT homo- and co-polymerization reactions.[355] Accordingly, methacrylic acid (MAA) was applied in the P-MCR as the carboxylic acid component to enable subsequent RAFT polymerization of the metharylic moiety. Similar to the P-MCP, a tetrazole-derivative (**T3**) was selected as the aldehyde component, while 1-pentyl isocyanide (PIC) was chosen as an aliphatic isonitrile to avoid unnecessary functionalities in the P-MCR. The P-MCR of MAA, **T3** and PIC for the synthesis of **T4** is displayed in Scheme 3.15. After a reaction time of 40 h at 45°C, ^{1}H NMR analysis (Figure 3.8, top) revealed the successful formation of **T4**, whereas there were still resonances of the starting materials detectable with considerably low reaction yield (~ 30 %).

Therefore, the reaction was repeated under similar conditions in the microwave due to the recently reported advantages of e.g. shorter reaction times, increased reaction rates and yields.[356-358] Indeed, the microwave-induced reaction yielded **T4** with a higher yield (~ 65 %) at shorter reaction times (18 h). As evident form the NMR analysis (Figure 3.8, bottom and Figure 6.18), all resonances can be assigned to **T4**. The resonances of the methacrylic protons (i.e. a at 1.99 ppm and b at 6.2-5.7 ppm) did not shift compared to MAA, indicating no reaction during the P-MCR. Furthermore, the resonance of the newly formed *CH*-bond at the chiral centre in **T4** (c at 5.6 ppm) is clearly detectable. Additionally, UV/Vis spectroscopy (Figure 6.19) revealed no change in the absorbance of the tetrazole-moiety after the P-MCR.

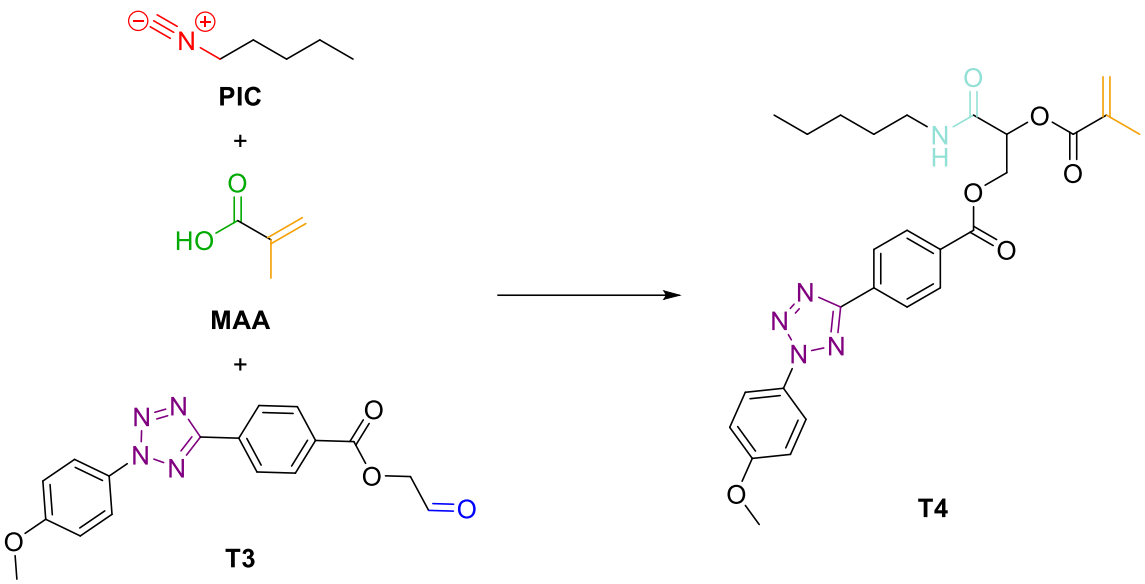

Scheme 3.15: P-MCR of PIC, MAA and **T3** to yield the tetrazole-monomer **T4.**

Motivated by these positive results, the P-MCR with PIC and MAA has been repeated with a tetrazole-monomer showing a different photochemical behaviour than **T3**. While the photoreaction of **T3** (and thus of **T4**) can be triggered in the UV-range ($\lambda_{exc.}$ = 320 nm, refer to Scheme 2.19), substitution of the tetrazole-moiety with a pyrene-chromophore allows the photoreaction to take place in the Vis-range ($\lambda_{exc.}$ = 410 nm, refer to Scheme 2.19).

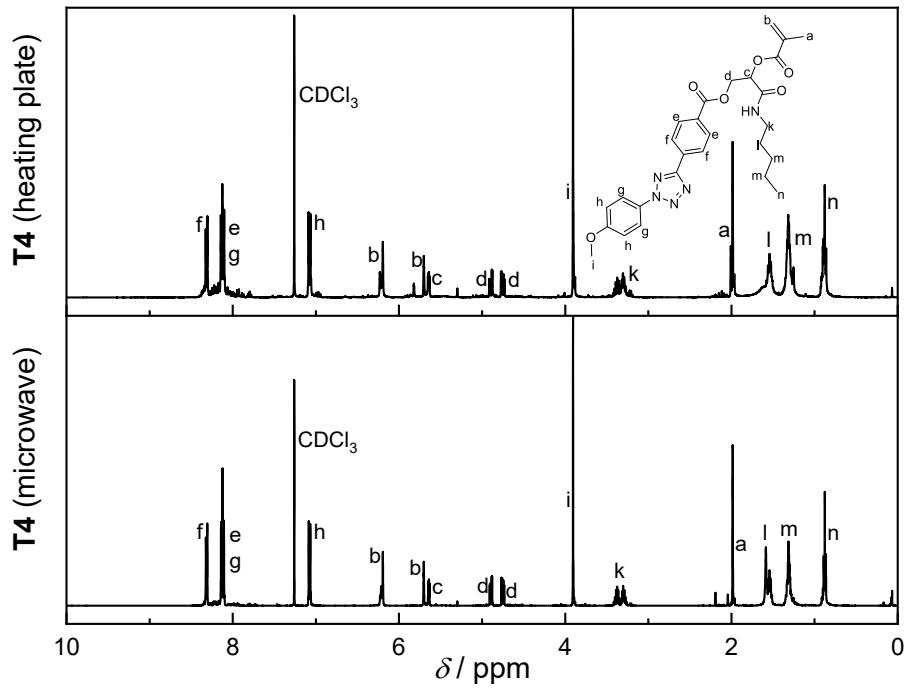

Figure 3.8: ^{1}H NMR (400 MHz) spectra of **T4** in $CDCl_3$ for the reaction on a conventional heating plate (top) and under microwave conditions (bottom).

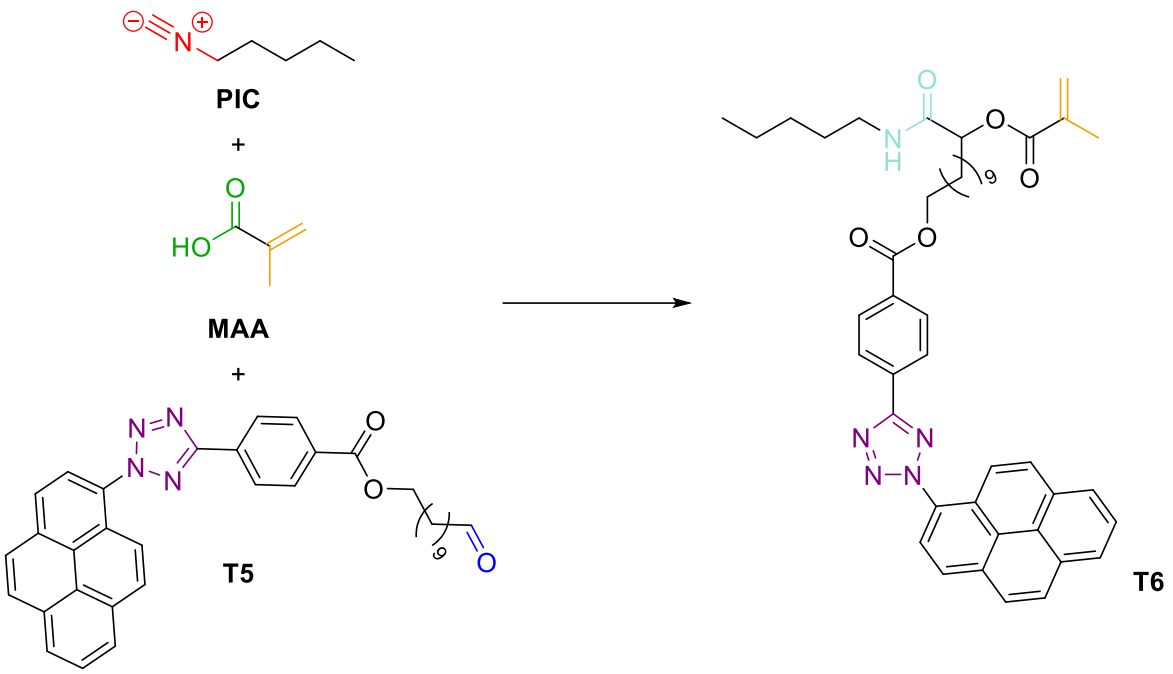

Scheme 3.16: P-MCR of PIC, MAA and the pyrene-aryl-tetrazole derivative **T5** to yield the tetrazole monomer **T6**.

Therefore, the pyrene-aryl-tetrazole (PAT) derivative **T5** was applied together with PIC and MAA in the P-MCR to yield the Vis-sensitive tetrazole-monomer **T6** with a polymerizable methacrylic functionality, as depicted in Scheme 3.16.

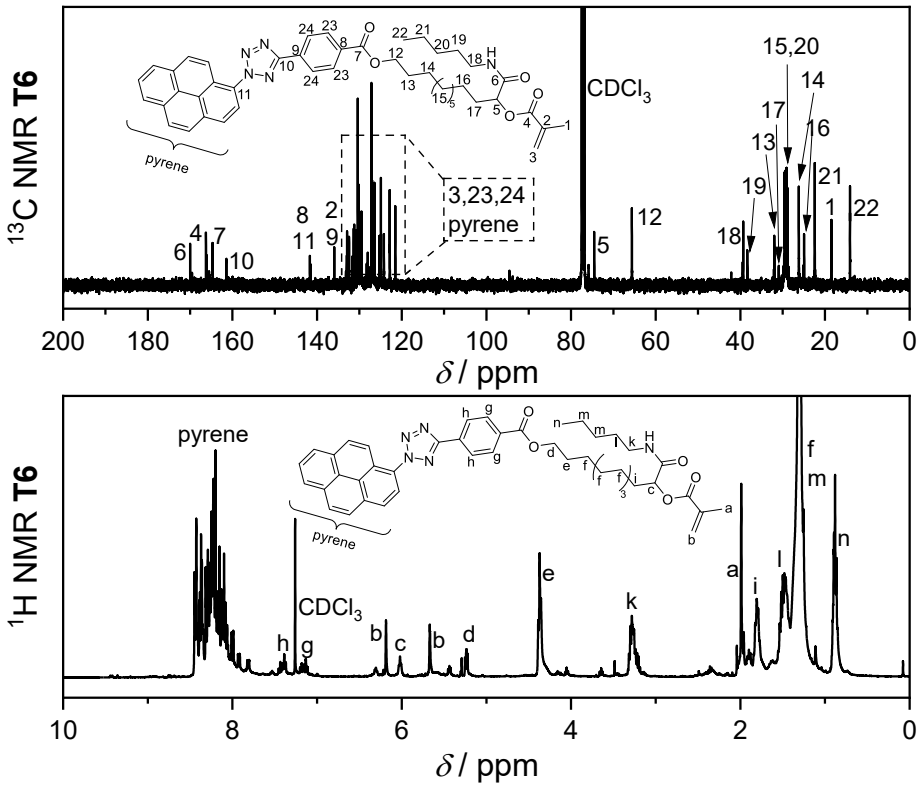

Figure 3.9: ^{1}H NMR (400 MHz) spectra and ^{13}C NMR (100 MHz) spectra of **T6** in $CDCl_3$, respectively.

Analogue to **T4**, the ^{1}H and ^{13}C NMR analysis of **T6** (Figure 3.9) revealed the successful synthesis by virtue of the newly arising resonance c at 6.0 ppm and 5 at 74.7 ppm without affecting the methacrylic units (resonances a at 2.0 ppm and b at 6.2-5.8 ppm) or the pyrene-tetrazole-moiety, supported by the intact absorbance of the photosensitive moiety in the UV/Vis spectrum (Figure 6.20).

3.2.3 RAFT-Polymerization of the Tetrazole-Monomers T4 and T6

Having confirmed the successful synthesis of **T4** and **T6** via the P-MCR, in the next step the polymerization of the respective monomers was conducted. For the polymerization reaction, the RAFT process was considered as suitable method for polymerization by virtue of the advantages described in Chapter 2.1.2 (e.g. short reaction times, mild conditions, good reaction control and tolerance towards various functional groups). With AIBN as initiator and 2-(dodecylthiocarbonothioylthio)-2-methylpropionic acid (DTMP) as chain transfer RAFT agent, the respective tetrazole monomer (**T4** or **T6**) was polymerized in the presence of methyl methacrylate (MMA) as co-monomer in 1,4-dioxane at 90°C for 2 h, as illustrated in Scheme 3.17.

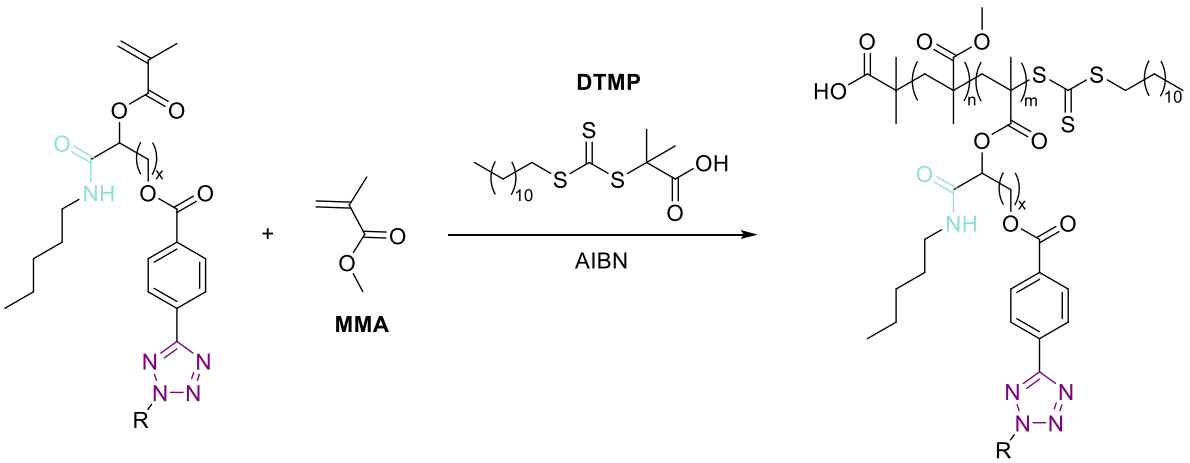

T4 (x = 1, R = 4-methoxy phenyl)
T6 (x = 10, R = pyrene)

RP1 (x = 1, R = 4-methoxy phenyl)
RP2 (x = 10, R = pyrene)

Scheme 3.17: RAFT polymerization of the respective tetrazole-monomer (**T4** or **T6**) in the presence of MMA as co-monomer, AIBN as initiator and DTMP as RAFT agent to yield the RAFT-polymers **RP1** or **RP2**, respectively.

A ratio of tetrazole-monomer / MMA of 1 : 7 was selected to achieve comparable amounts of photosensitive moieties in the polymer as in previous reported tetrazole-polymers obtained via PPM reactions.[60] The obtained RAFT-polymers **RP1** and **RP2** with peptide-analogue bonds in the side chains (mint green colour in Scheme 3.17) were characterized via SEC (Figure 6.21) and ^{1}H NMR analysis (Figure 6.22 and Figure 6.23). While the latter was meant as a handle to calculate the incorporated tetrazole amounts by comparing the resonance integrals of the MMA protons (o at ~ 3.5 ppm or p at ~ 1.8 ppm) with the integrals of the tetrazole protons (h at ~7.0 ppm, c at ~ 6.0 ppm, e' at ~ 4.3 ppm, i at ~ 3.5 ppm or a at ~ 1.8 ppm), the overlapping of the resonances did not allow a precise distinguishing of the respective protons. Therefore, the theoretical values of the tetrazole-amount in the RAFT-polymers were assumed due to the applied ratio of the monomers during the polymerization reaction. A summary of the theoretical tetrazole amounts in addition to the respective M_n values according to the SEC analysis can be found in Table 3.1.

Table 3.1: Apparent number average molecular weight and dispersity values of the RAFT polymers **RP1**-**RP3** obtained via THF-SEC and the respective theoretical % of the photosensitive moiety.

Polymer	M_n [Da]	$Đ$	T4 [%]	T6 [%]
RP1	12 700	1.22	14.3	-
RP2	12 900	1.23	-	14.3
RP3	11 400	1.41	14.3	14.3

Evidently, both polymers are obtained with similar M_n values, and thus theoretically comparable incorporated tetrazole-amounts, which is of critical importance for the comparison of their respective photochemical behaviour.

Beneficially, both **RP1** and **RP2** show no change in their absorbance (Figure 3.10), thus indicating no interference of the tetrazole-moieties with the applied components during the RAFT polymerization. Additionally, the resonance of the protons c at ~ 6.0 ppm and k at ~ 3.3 ppm in the ^{1}H NMR spectra remain intact in comparison to the tetrazole-monomers **T4** and **T6**, proving the RAFT-process as suitable polymerization method for **T4** and **T6**.

Therefore, another RAFT polymerization has been conducted with both **T4** and **T6** in order to obtain a polymer **RP3** with orthogonal photochemical properties, i.e. UV- and Vis-responsiveness (Scheme 3.18). The reaction was performed in similar manner as for **RP1** or **RP2** with a monomer ratio of MMA / **T4** / **T6** 7 : 1 : 1 to integrate a similar amount of both photoactive moieties in the polymer as for **RP1**/**2**.

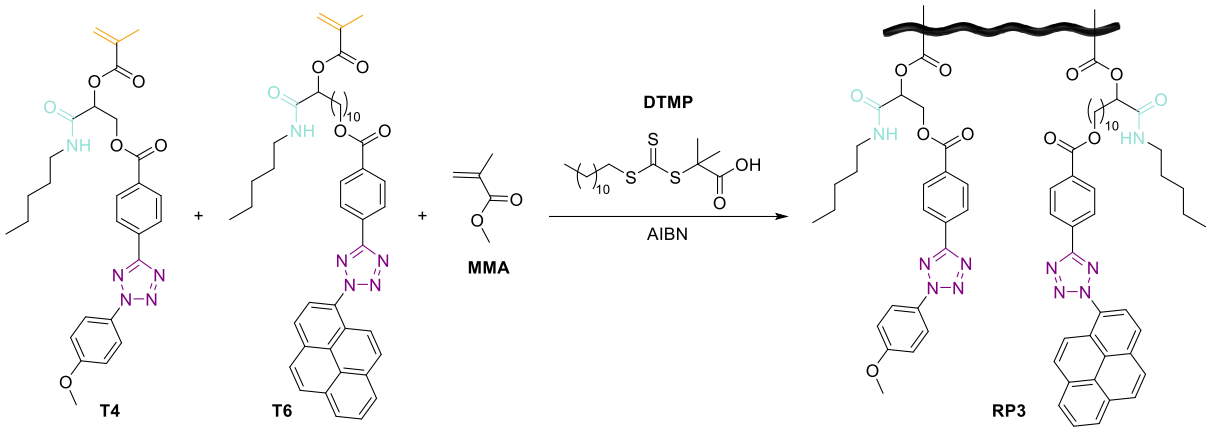

Scheme 3.18: Synthesis of the co-polymer **RP3** via RAFT-polymerization of **T4** and **T6** with MMA, AIBN and DTMP.

Indeed, SEC analysis (Figure 6.21) revealed a polymer formation with M_n = 11 400 g mol^{-1} ($Đ$ = 1.41), and the successful incorporation of the tetrazole-monomers was evident from the ^{1}H NMR spectrum (Figure 6.24), thus being comparable to **RP1** and **RP2**. Similarly to the NMR analysis of **RP1** and **RP2**, the overlap of the resonances prevented the exact calculation of the respective incorporated photo-sensitive moieties and the theoretical values were taken as shown in Table 3.1. Anew, UV/Vis spectroscopy of **RP3** revealed the unchanged absorbance of the intact tetrazole moieties (Figure 3.10).

3.2.4 Light-Controlled Orthogonal Self-Reporting Behaviour of the Synthesized RAFT Polymers

Last but not least, the self-reporting properties of the RAFT-polymers **RP1**-**RP3** were investigated. Therefore, the NITEC reaction was conducted in the presence of a maleimide as ene-functionality, which allows monitoring of the reaction progress in a self-reporting manner due to the formation of a fluorescent pyrazoline adduct.[359]

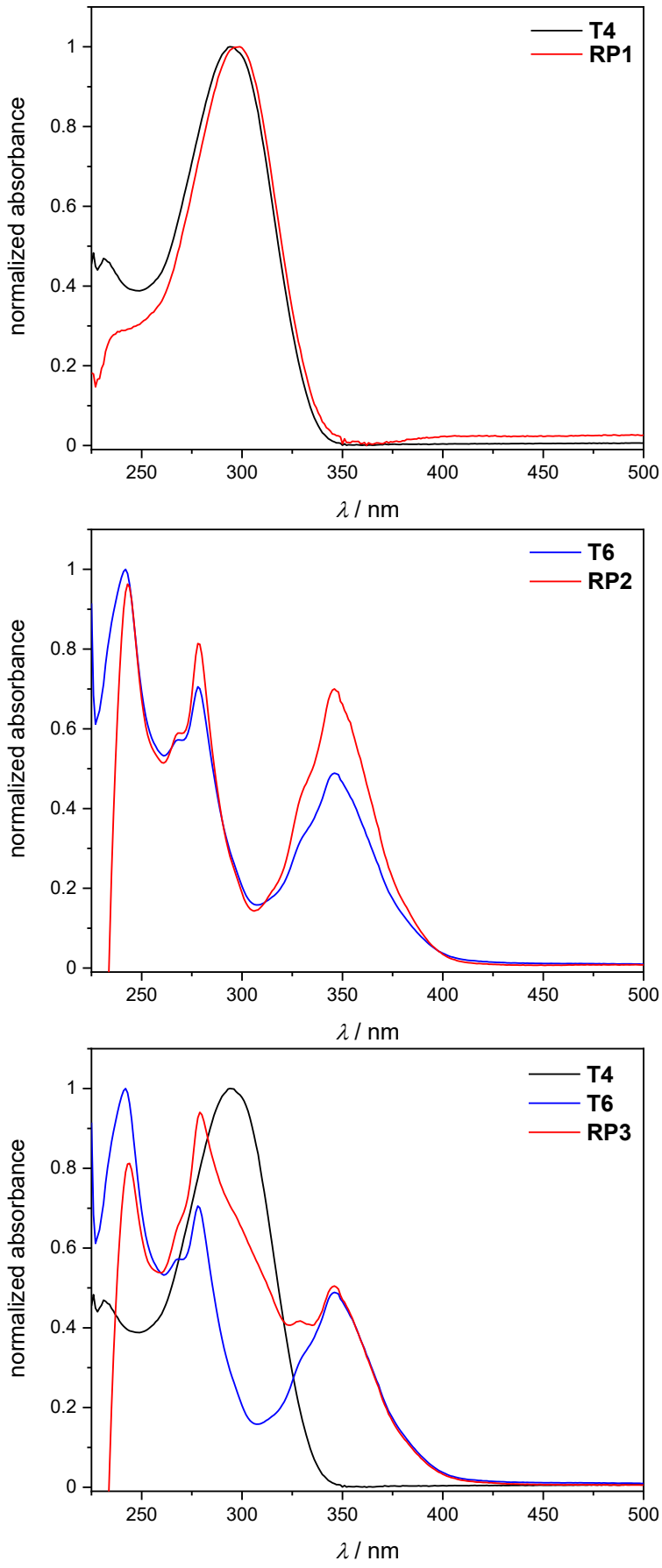

Figure 3.10: UV/Vis spectra of **T4**, **T6**, **RP1**, **RP2** and **RP3** in DCM at ambient temperature (c = 0.2 mg mL^{-1}).

Furthermore, the polymers can be folded into 3D-structured protein-mimicking materials in the presence of suitable linker molecules (refer to Chapter 2.2.3), for which the RAFT-polymers **RP1**-**RP3** would be a suitable substructure due to the peptide-analogue bonds formed in the P-MCR.

Accordingly, **RP1**-**RP3** were irradiated with light in the presence of a bi-functional maleimide (Bis-Mal) as cross-linker to obtain the folded polymers **FP1**-**FP3** in the NITEC reaction. The general reaction pathway is illustrated in Scheme 3.19 with simplified structural representations for a better visualization (the exact molecular structures can be found in the experimental part, 5.2.11). While **FP1** is obtained via UV-irradiation of **RP1** at λ_{max} = 320 nm, **RP2** is folded under irradiation with a red-shifted light source, i.e. Vis-light at λ_{em} = 410 -420 nm, yielding **FP2**.

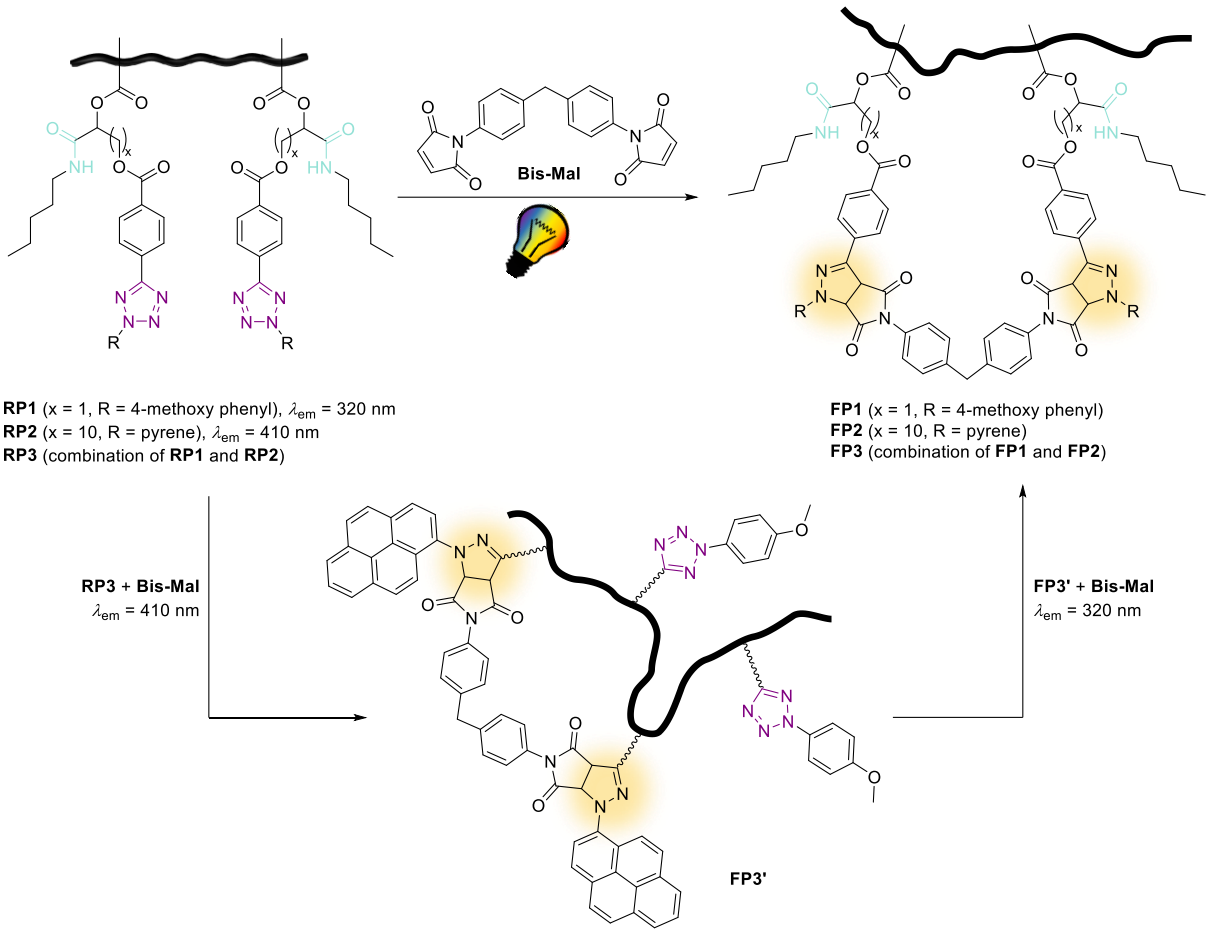

Scheme 3.19: Schematic representation of the NITEC reaction of the RAFT-polymers **RP1**-**RP3**. The folded polymer **FP1** is obtained after irradiation of **RP1** at λ_{max} = 320 nm, while **FP2** is obtained after irradiation of **RP2** at λ_{em} = 410-420 nm. For the copolymer, **RP3** was first irradiated at λ_{em} = 410-420 nm to fold the Vis-sensitive moieties (**FP3'**, displayed in a highly simplified manner for better visualization); subsequently, the UV-sensitive moieties were folded under irradiation at λ_{max} = 320 nm to yield **FP3**. The fluorescent pyrazoline-units are marked in orange.

As is evident from the UV/Vis analysis of the tetrazole-monomers **T4** and **T6** (refer to Figure 3.10), the absorption spectra partially overlap in the UV-region (< 350 nm), whereas exclusively **T6** shows an absorption at higher wavelengths (> 350 nm). Consequently, **RP3** was first irradiated at λ_{em} = 410-420 nm to fold solely the Vis-sensitive units (**FP3'**). Subsequent irradiation at λ_{max} = 320 nm leads to the complete folding in **FP3** by the reaction of the UV-sensitive moieties with the Bis-Mal.

The first indication of a successful polymer folding was already observable by the naked eye at normal daylight due to a colour change of the reaction mixtures before (**RP1**-**3**) and after (**FP1**-**3**) the photoreactions (Scheme 3.20, top). Additionally, the folded polymers possess different fluorescent properties compared to the unfolded polymers when irradiated with a hand-held UV-lamp (λ_{max} = 365 nm, Scheme 3.20, bottom), supporting the self-reporting character of the tetrazole-containing polymers.

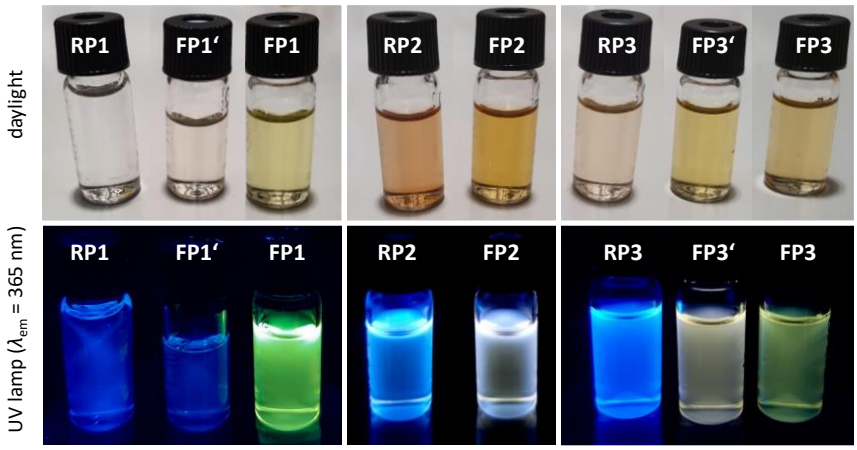

Scheme 3.20: Images of the polymers before (**RP1**-**3**) and after (**FP1**-**3**) the photoreaction at daylight (top) and under a hand-held UV-lamp (bottom, λ_{em} = 365 nm).

To ensure that the different colour is indeed related to the pyrazoline formation and not to the possible dimerization of the 1,3-dipole formed during the NITEC reaction (refer to Chapter 2.2.3), the photoreaction of **RP1** has also been conducted in the absence of the Bis-Mal or any other co-reactant. Clearly, the obtained polymer **FP1'** shows different optical properties both at daylight and under UV irradiation in comparison to **FP1**. Therefore, the colour change is certainly attributed to the pyrazoline formation. The latter was also proven by further analytical characterization methods. Indeed, the absorbance of **RP1** shows a different absorbance behaviour after the folding processes (**FP1** and **FP1'**) as is evident from the UV/Vis spectra in Figure 3.11A. As expected, the fluorescence emission of **FP1'** is very weak with an

emission maximum at 466 nm, whereas a strong fluorescence emission is observed for **FP1** with a maximum at 535 nm due to the formed pyrazoline moieties[60] (Figure 3.11D). This was also supported by ^{1}H NMR analysis (Figure 3.12). While the magnetic resonances of the polymer backbone are mainly unchanged, the aromatic protons (e-g) are broadening and, most importantly, new resonances at 5.7 and 5.1 (v and v', highlighted in red) ppm are arising that can be assigned to the pyrazoline adduct.

For **RP2** and **RP3**, the absorbance is not changing as drastically as for **RP1** after the folding process (Figure 3.11B-C); however, fluorescence analysis of the respective folded polymers **FP2**, **FP3'** and **FP3** evidently shows the formation of the pyrazoline moieties. In the fluorescence spectrum of **FP2** (Figure 3.11E), two emission maxima are detected at 472 and 547 nm. While the maximum at 472 nm is generated by the excimer formation of the pyrene units,[360-362] the maximum at 547 nm reveals the successful generation of the desired pyrazoline-moieties.

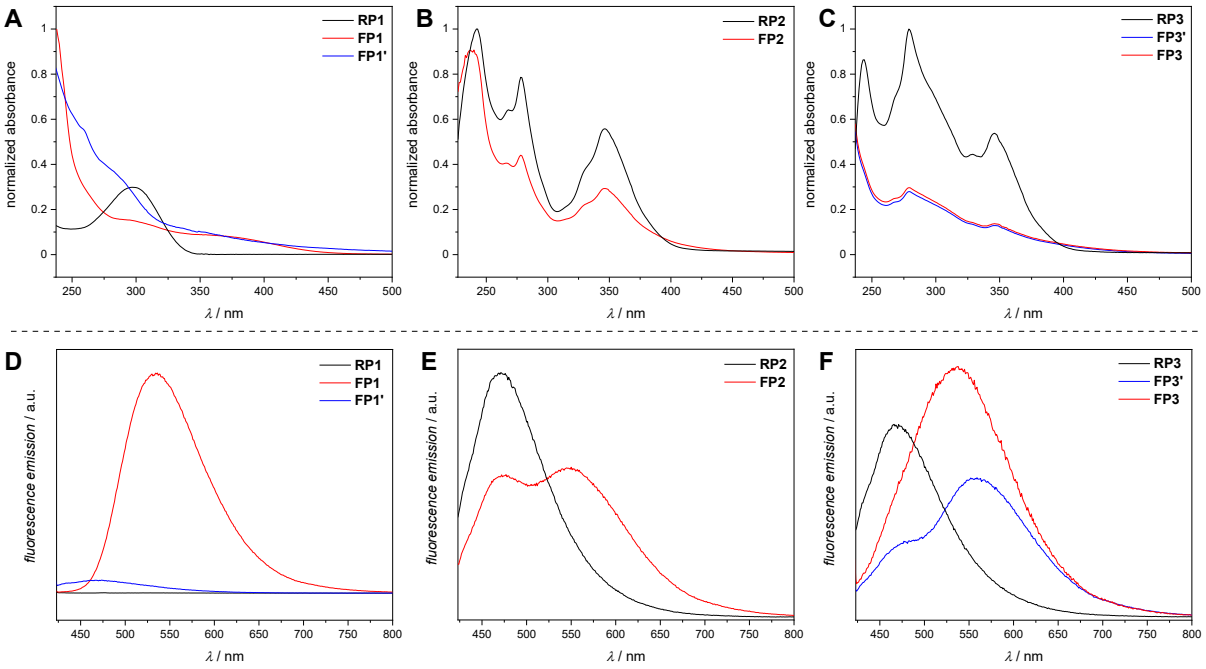

Figure 3.11A-C: UV/Vis spectra of the RAFT polymers **RP1**-**RP3** and the respective folded polymers **FP1**-**FP3** in DCM (c = 0.2 mg mL^{-1}). **D**-**F**: Fluorescence emission spectra of the RAFT polymers **RP1**-**RP3** and the respective folded polymers **FP1**-**FP3** in DCM (c = 0.2 mg mL^{-1}, λ_{exc} = 400 nm).

Similarly, two emission maxima are obtained for **FP3'** after the folding in the Vis-range due to the pyrene units and the partially modified tetrazole-moieties, whereas one broad emission is obtained after the second irradiation in the UV-range leading to the complete folding of the initial **RP3** (Figure 3.11F).

Once again, ^{1}H NMR spectroscopy supported the successful folding of **RP2** and **RP3**. The resonances of the pyrazoline-moiety in **FP2** can be clearly detected at 3.9 and 3.4 ppm (v and v', highlighted in green in Figure 3.12). In addition, the orthogonal folding of **RP3** can be monitored, as demonstrated in Figure 3.13. While after the irradiation at 410 nm the resonances of the UV-sensitive unit (protons h) remain intact at 7.1 ppm, a clear shift is observed after irradiation at 320 nm to 7.7 ppm (indicate in blue). Moreover, the protons of the two different pyrazoline units can be assigned (green and red assignments Figure 3.13.) Beneficially, the resonances of the protons c from the parent tetrazole monomers at ~ 6.1 ppm are not affected during the NITEC reaction.

Noteworthy, the resonances of the aromatic protons in all RAFT and folded polymers are more intense than e.g. the aliphatic resonance d or c at the stereo-centres of the polymers. This might be attributed to hydrogen bonding effects and coiled structures due to the peptide-analogue bonds in the polymers. This would also explain the results obtained from the SEC analysis after the respective photoreactions. In the literature, it is reported that the folded polymers show a decreased molecular weight due to the reduced hydrodynamic diameter of the folded structure.[60] However, only minor shifts in the M_n values are measured for the folded RAFT-polymers **FP1**-**FP3**, as shown in Figure 3.14.

Certainly, if the RAFT-polymers are already coiled, the intramolecular cross-linking with the bis-maleimide would not result in a drastic change of the hydrodynamic diameters. Since these results were obtained within the last stage of the PhD, more intense research needs to be conducted in the future to precisely characterize the complex polymeric structures of the RAFT polymers and the respective photo-chemically modified materials. For example, analysis of all polymeric structures via DLS or diffusion ordered spectroscopy (DOSY) could possibly give further insight into the structural behaviour. Moreover, repeating the NMR analysis with a higher concentration or more scans for the respective measurements might be valuable.

Nevertheless, the employed synthetic strategy for the tetrazole-containing polymers via direct polymerizable tetrazole-monomers was successful, and further, the simultaneous incorporation of different photochemical properties into one polymeric material was facilitated. Encouragingly, the photochemical properties allowed the monitoring of the folding-process not only with instrumental analysis, but also by the naked eye in a self-reporting manner due to the colour change of the reaction mixtures.

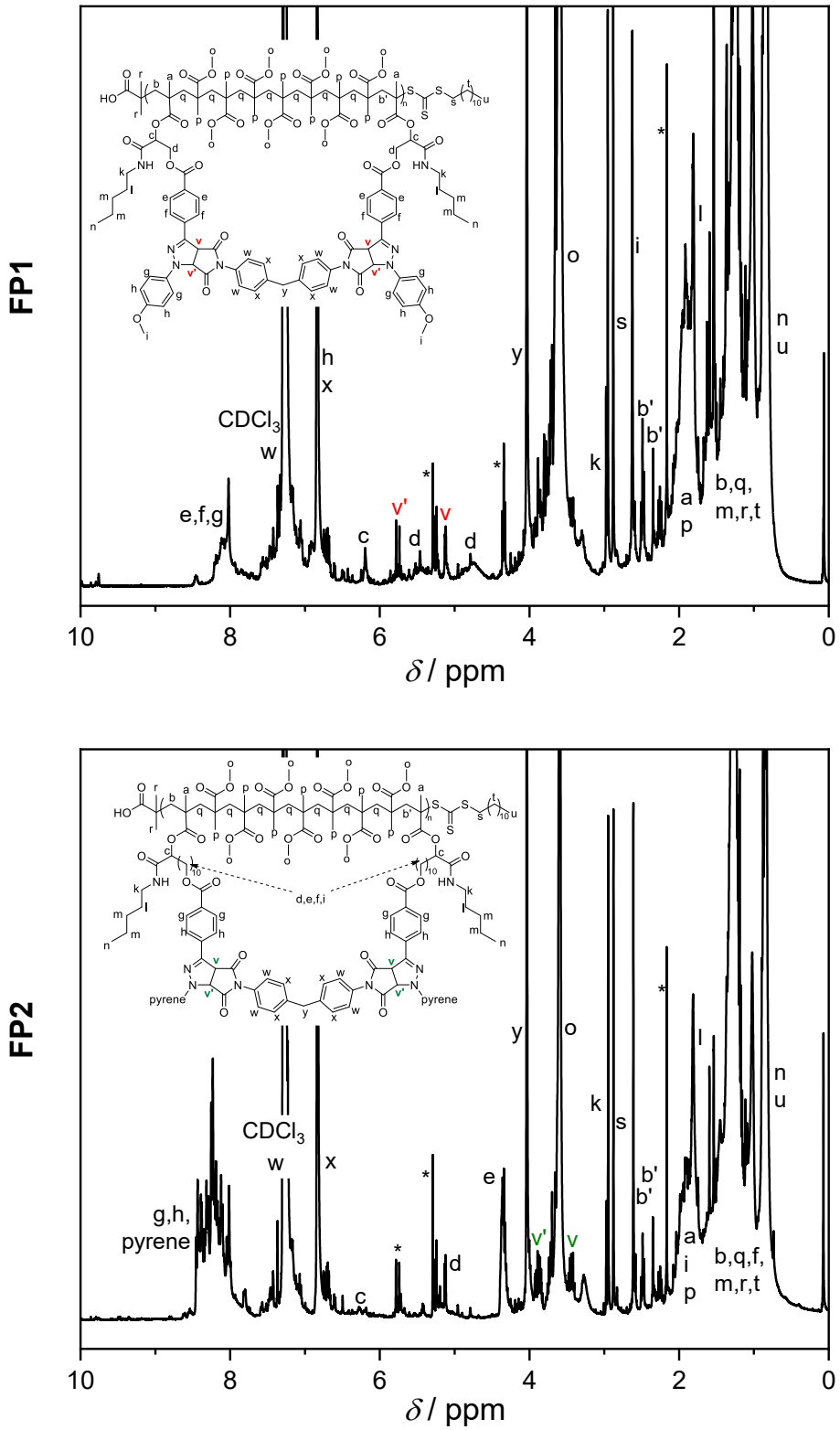

Figure 3.12: Comparative ^{1}H NMR (400 MHz) spectra of **FP1** and **FP2** in $CDCl_3$.

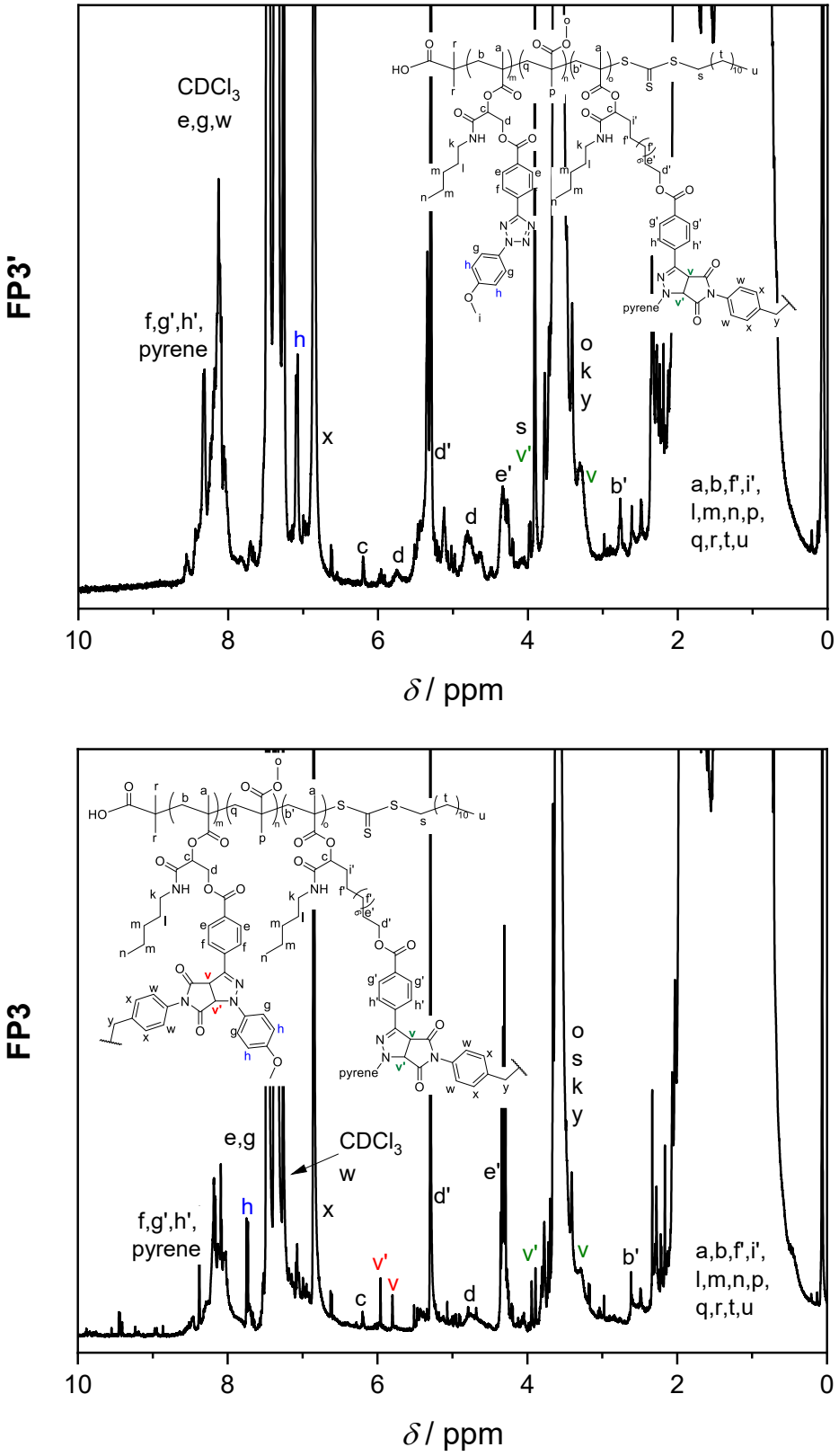

Figure 3.13: Comparative ^{1}H NMR (400 MHz) spectra of **FP3'** and **FP3** in $CDCl_3$.

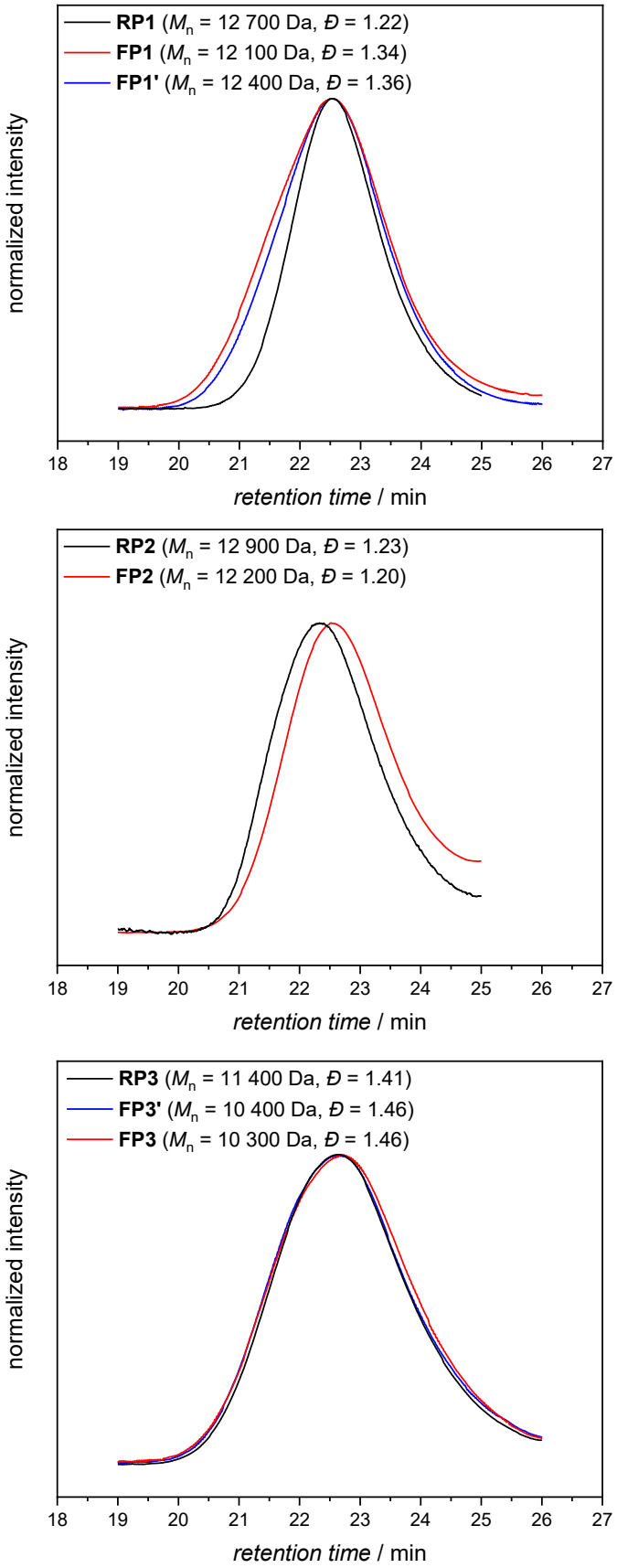

Figure 3.14: SEC elution traces of the RAFT polymers **RP1**-**RP3** and the respective elution traces of the folded polymers **FP1**-**FP3** in THF at 30°C.

4 Summary and Outlook

Within the last years, self-reporting materials responsive to a broad variety of stimuli (e.g. mechanical forces, temperature, pH, solvation, light or chemicals) have been developed.[4] In view of the many advantageous of such materials (for instance the precise detection of changes or damages, facile maintenance, prolonged lifetime and the associated cost reduction), the aim of the present doctoral thesis was the development of advanced self-reporting systems with tailored properties. Therefore, two approaches have been investigated based on different working principles, namely the chemiluminescent behaviour of luminol and the photochemical properties of tetrazole and its derivatives.

In Chapter 3.1, an efficient synthetic strategy for the incorporation of all required functionalities (i.e. a luminophore and a suitable co-reactant) enabling a self-reporting output in one polymeric material is demonstrated. For the self-reporting moiety, luminol was chosen as luminophore, whose CL is known to take place in basic (aprotic) media. Therefore, at first a small molecule model study with luminol and various organic superbases has been conducted to identify the most efficient organic superbase as co-reactant in the luminol-CL-reaction. Beneficially, the bicyclic guanidine-superbase TBD revealed an outstanding performance as co-reactant and a strong CL-emission was observed. Consequently, TBD was supposed to be incorporated into the same polymer backbone.

Indeed, after several attempts and varying synthetic strategies, the PPM approach of an active-ester copolymer allowed the incorporation of both TBD- and luminol-functionalities. Moreover, the formation of supramolecular assemblies was facilitated in the presence of Me-β-CD as host-molecule to yield biomolecule-mimicking binding behaviours. Eventually, the addition of H_2O_2 triggered the generation of ROS and thus, the oxidation of luminol to 3-APA, which emitted a striking blue light visible even by the naked eye. Clearly, the results prove the excellent self-reporting properties of the luminol-TBD-polymer. However, to enable the postulated *in vivo* detection of ROS, the solubility and applicability of the polymer system in aqueous media needs to be highly improved. One suitable approach therefore could be the synthesis of active-ester-copolymers with a water-soluble polymer backbone (e.g. poly(acrylamide) or poly(ethylene glycol)). Furthermore, luminol- and / or TBD-derivatives

with water-soluble spacer chains might be prepared via MCR protocols. Indeed, just recently a luminol-derivative was synthesized by means of the Ugi-MCR under microwave conditions exhibiting a strong CL upon addition of H_2O_2.[125] Combined with the results presented in the current work, fascinating self-reporting chemiluminescent polymeric materials based on luminol are envisaged with potential applications as imaging probe for the *in vivo* detection of ROS or in analytical sensor technologies.

The potential of such MCR protocols has also proven to be extremely valuable for the second part of the thesis. Herein, the photochemical properties of tetrazole and its derivatives were selected as the handle for the self-reporting output due to the formation of highly fluorescent pyrazoline adducts during the NITEC reaction. Similar to the synthesis of the first self-reporting system, the strategies had to be adjusted several times before the Passerini-MCR finally enabled the synthesis of tetrazole-derivatives with polymerizable moieties. Beneficially, tetrazole-derivatives with λ-orthogonal behaviour were synthesized by carefully choosing the substituents on the tetrazole moiety. Detailed analysis of the tetrazole-derivatives revealed that the tetrazole-units remain intact during the MCR, thus facilitating that the monomers are subsequently polymerized via the RAFT polymerization process. Importantly, both tetrazole-derivatives were simultaneously incorporated into the same polymeric material. Thus, a polymer with λ-orthogonal photochemical properties was obtained. Depending on the applied wavelength, only one of the tetrazole-moiety is modified. While fluorescence and ^{1}H NMR analysis clearly revealed the successful folding of the respective photo-sensitive moiety, further research and detailed analysis is necessary to precisely characterize the polymers and their molecular structures before and after the photoreaction.

Nevertheless, the successful application of the P-MCR for the synthesis of highly functional compounds might serve as inspiration for the design of a broad variety of innovative, multi-functional substances in a facile manner without the need of catalysts of additional supporting molecules during the reaction. For example, the starting materials in the P-MCR for the synthesis of the tetrazole-monomers could be altered to broaden the range of suitable subsequent polymerization methods. By applying for instance a bi-functional isonitrile and two eq. of a tetrazole-aldehyde-derivative and a carboxylic acid derivative with a terminal double bond, respectively, the obtained product would ideally lend itself for the acyclic diene metathesis (ADMET) or thiol ene polymerization. Moreover, the ene-functionality or other photo-sensitive chromophores (e.g. o-MBA) may be incorporated along the tetrazole-moiety

within a single polymerization reaction to obtain highly functional self-reporting polymeric materials.

5 Experimental Part

5.1 Materials

Unless otherwise stated, all chemicals and solvents were used as received.

Acetone (VWR, normapur), aluminium oxide (Al_2O_3, Merck, 90 active basic), 4,4'-azobis(4-cyanovaleric acid) (V501, ≥ 75 %, Sigma Aldrich), 2,2'-azobis(isobutyronitrile) (AIBN, 98.0 %, Sigma Aldrich), 11-bromo-1-undecanol (> 97 %, TCI), Celite®545 (VWR), chloroform ($CHCl_3$, 99.0-99.4 %, Merck), $CHCl_3$ (99.9 %, extra dry, stabilized, AcroSeal, Acros Organics), 6-chloro-1-hexanol (> 96.0 %, TCI), 3-chloro-1-propanol (98 %, Sigma Aldrich), copper sulfate pentahydrate ($CuSO_4 \cdot 5H_2O$, 99 %, Acros Organics), Dess-Martin periodinane (≥ 95 %, Alfa Aesar), (1,8-diazabizyclo[5.4.0]undec-7-ene (DBU, ≥ 99.0 %, Sigma Aldrich), 1,2-dichlorobenzene (99 %, Sigma Aldrich), dichloromethane (DCM, 99.9 %, extra dry, stabilized, AcroSeal, Acros Organics), DCM (99.8 %, stabilized with 0.2 % of ethanol, VWR), diethylether (VWR, normapur), diisopropylamine (DIPA, 99.5 %, Sigma Aldrich), *N*-(3-dimethylaminopropyl)-*N*-ethylcarbodiimid (EDC, ≥ 97.0 %, Sigma Aldrich), 4-(dimethylamino)pyridine (DMAP, ≥ 99 %, Sigma Aldrich), 5,5-dimethyl-1-pyrroline N-oxide (DMPO, ≥97%, Sigma Aldrich), dimethyl sulfoxide (DMSO, > 99 %, Fisher), DMSO (max. 0.025 % H_2O, VWR, normapur), 1,4-dioxane (extra dry, AcroSeal, 99.8 %, Acros Organics), 1,4-dioxane (99+ %, stabilized with ~5-10 ppm BHT, Alfa Aesar), 3,3'-dithiodipropionic acid (DTDPA, 99 %, Sigma Aldrich), dodecanedioic acid (DDDA, 99 %, Sigma Aldrich), ethanol (EtOH, VWR, normapur), EtOH absolute (max. 0.003 % H_2O, VWR), ethyl acetate (EtOAc, VWR, normapur), 1,2-ethylene glycol (99.8 %, VWR), ethylformate (98 %, Acros Organics), heptanedioic acid (HDA, ≥ 98 %, Sigma Aldrich), hexamethylenediamine (98 %, Alfa Aesar), hexane (VWR, normapur), hydrochloric acid (HCl, 32 %, VWR), hydrogen peroxide (H_2O_2, 35 %, Roth), L-ascorbic acid (AA, 98%, suitable for cell culture, Sigma Aldrich), lithium aluminium hydride ($LiAlH_4$, 95 %, Sigma Aldrich), luminol (98 %, (Alfa Aesar), magnesium sulfate anhydrous ($MgSO_4$, 99.5 %, VWR), methacrylic acid (MAA, ≥ 99 %, Sigma Aldrich), methanol (MeOH, VWR, normapur), 4,4'-methylenebis (N-phenylmaleimide) (bis-mal, 95 %, Alfa Aesar), methyl-β-

cyclodextrin (Me-β-CD, > 95 %, Cavasol W7 M, Wacker), 1-pentyl isocyanide (PIC, 97 %, Sigma Aldrich), phosphoryl trichloride ($POCl_3$, 99 %, Sigma Aldrich), polarclean (Rhodiasolv®), potassium carbonate (K_2CO_3, 99 %, Carl Roth), potassium hydroxide (KOH, ≥ 85 %, Merck), 1,3-propanediol (98 %, Sigma Aldrich), silica gel (Merck), sodium azide (NaN_3, 99%, AJA), sodium chloride (NaCl, 99.5 %, Merck), sodium hydrogen carbonate ($NaHCO_3$, 99 %, Merck), sodium hydroxide (NaOH, ≥ 99.0 %, Merck), superoxide dismutase (SOD, Sigma Aldrich), tetrahydrofuran (THF, > 99.9 %, AcroSeal, Acros Organics), THF (VWR, analytical grade), 1,1,3,3-tetramethylguanidine (TMG, 99 %, abcr), 2,2,6,6-tetramethyl-4-piperidone (TMPD, 95%, Sigma Aldrich), thiourea (TU, extra pure, Scharlau), toluene (99.8%, extra dry, AcroSeal, Acros Organics), 1,5,7-triazabicyclo[4.4.0]dec-5-ene (TBD, 98 %, Sigma Aldrich), triethylamine (TEA, ≥ 99 %, Sigma Aldrich), 4-vinylbenzyl chloride (VBC, 90%, Sigma Aldrich).

Methylmethacrylate (MMA, Sigma Aldrich, 99 %, ≤ 30 ppm MEHQ as stabilizer), pentafluorophenyl methacrylate (PFP-MA, TCI, > 97.0%) and pentafluorophenyl acrylate (PFP-A, TCI, > 98.0 %) were passed through a basic Al_2O_3 – column to remove the stabilizer before using.

4-(2-(4-methoxyphenyl)-2H-tetrazol-5-yl)benzoic acid (**M1**)[363] and 2-(dodecylthiocarbothioylthio)-2-methylpropionic acid (DTMP)[364] were synthesized according to the literature within the group. **P1** was synthesized via a reported literature procedure[243] and kindly provided by Waldemar Konrad.

5.2 Experimental Procedures

5.2.1 Synthesis of the TBD-Derivatives TBD1-TBD3

5.2.1.1 3,4,7,8-Tetrahydro-2*H*-pyrimido[1,2-*a*]pyrimidine-1(6*H*)-propanol (**TBD1**)

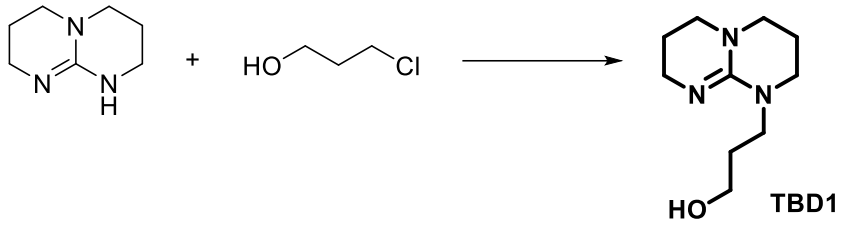

Approach a: Under anhydrous conditions, 0.2784 g TBD (2.00 mmol, 1.00 eq.) were dissolved in 3.0 mL dry THF. After the addition of 0.2111 g 3-chloro-1-propanol (2.20 mmol, 1.10 eq.), the colourless reaction mixture was put in a pre-heated oil bath at 70°C. The orange reaction was stopped after 24 h and the solvent was evaporated. Subsequently, the orange oil was dissolved in 10 mL DCM and washed with sat. $NaHCO_3$, brine and H_2O (2 x 10 mL each). The organic layer was dried over $MgSO_4$ and removal of the solvent under reduced pressure yielded an orange oil (m = 0.0119 g, 3.0 %).

^{1}H NMR (400 MHz, $CDCl_3$) δ / ppm: 5.26 (s, 1H, -*N*-C<u>*H*</u>-*N*-), 3.74 (t, 2H, *HO*-C<u>*H*$_2$</u>-), 3.64 (t, 2H, *Cl*-C<u>*H*$_2$</u>-), 3.30 (m, 4H, -*CH*$_2$-C<u>*H*$_2$</u>-*N(H)*-), 3.23 (m, 4H, -C<u>*H*$_2$</u>-*N*-C<u>*H*$_2$</u>-), 1.99 (m, 2H, *Cl*-*CH*$_2$-C<u>*H*$_2$</u>-), 1.88 (m, 2H, -*NH*-*CH*$_2$-C<u>*H*$_2$</u>-), 1.75 (m, 2H, -*N*-*CH*$_2$-C<u>*H*$_2$</u>-).

Approach b: For the second approach, the same procedure as for approach a were applied, yet with a shorter reaction time (i.e. 18 h) and a purification via vacuum distillation (3.0 x 10^{-1} mbar, 60°C), yielding a yellow sticky material (m = 0.3324 g, 84 %).

^{1}H NMR (400 MHz, DMSO) δ / ppm: 7.25 (1H, m, <u>*H*</u>*O*-*CH*$_2$-), 3.42 (m, 4H, -*N*-C<u>*H*$_2$</u>-*CH*$_2$-C<u>*H*$_2$</u>-*OH*), 3.27-3.02 (m, 8H, -*N*-C<u>*H*$_2$</u>-*CH*$_2$-C<u>*H*$_2$</u>-*N*-), 1.85 (m, 4H, -*N*-*CH*$_2$-C<u>*H*$_2$</u>-*CH*$_2$-*N*-), 1.64 (m, 2H, *N*-*CH*$_2$-C<u>*H*$_2$</u>-*CH*$_2$-*OH*).

Approach c: The reaction was conducted as described for approach a in EtOH and at 80°C. After 70 h, the reaction was stopped and the solvent was evaporated. The crude product was dissolved in 1M HCl (10 mL) and washed with Et_2O (3 x 15 mL). The aq. Layer was adjusted to pH = 14 by means of NaOH and subsequently extracted with DCM (6 x 15 mL). The combined organic layers were dried over $MgSO_4$ and the solvent was evaporated. A dark yellow oil was obtained (m = 0.3019 g, 76 %).

^{1}H NMR (400 MHz, $CDCl_3$) δ / ppm: 5.96 (1H, m, *HO-CH$_2$-*), 3.38 (m, 4H, *-N-CH$_2$-CH$_2$-CH$_2$-OH*), 3.28-3.10 (m, 8H, *-N-CH$_2$-CH$_2$-CH$_2$-N-*), 1.92-1.69 (m, 4H, *-N-CH$_2$-CH$_2$-CH$_2$-N-*), 1.61 (m, 2H, *N-CH$_2$-CH$_2$-CH$_2$-OH*).

The detailed assigned chemical shifts of approach a-c can be found in Figure 6.5.

5.2.1.2 3,4,7,8-Tetrahydro-2*H*-pyrimido[1,2-*a*]pyrimidine-1(6*H*)-hexan-1-ol (**TBD2**)

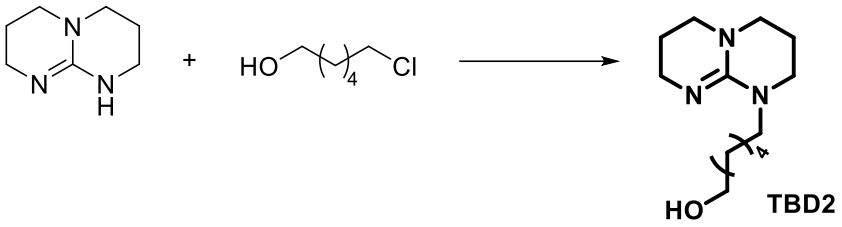

Approach a: In a 25 mL round bottom flask, 0.2784 g TBD (2.00 mmol, 1.00 eq.) were dissolved in 8.0 mL extra pure EtOH under N_2. After the addition of 0.2732 g 6-chloro-1-hexanol (2.00 mmol, 1.00 eq.), the reaction mixture was refluxed at 80°C for 23 h. The organic solvent was evaporated and the crude product was purified via recrystallization from MeOH (m = 0.2013 g, 42 %). Nevertheless, the ^{1}H and ^{13}C NMR spectra (Figure 6.6) showed no product formation.

Approach b: The reaction setup of approach a was repeated with dry THF as solvent at 70°C and a reaction time of 21 h. Again, the NMR analysis (Figure 6.6) revealed only resonances assigned to the starting materials.

In two additional attempts, both approach a and b were repeated with shorter reaction times (**approach c** with 7.5 h and **approach d** with 6 h). Yet again, no product formation was observed in the NMR spectra (Figure 6.6).

5.2.1.3 3,4,7,8-Tetrahydro-2*H*-pyrimido[1,2-*a*]pyrimidine-1(6*H*)-undecan-1-ol (**TBD3**)

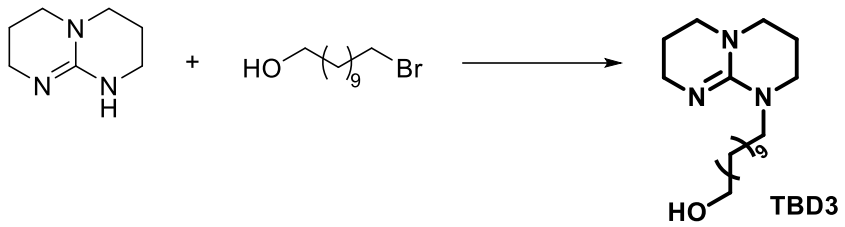

Approach a: In a 25 mL round bottom flask, 0.2784 g TBD (2.00 mmol, 1.00 eq.) were dissolved in 8.0 mL extra pure EtOH under N_2. Subsequently, 0.5024 g 11-bromo-1-undecanol (2.00 mmol, 1.00 eq.) were added to the TBD-solution and the reaction mixture was stirred at 80°C for 22 h. The solvent was evaporated and the crude product was purified via recrystallization from MeOH. Additionally, column chromatography (DCM / MeOH 99 : 1, silica) was conducted, yielding an orange viscous material (m = 0.0513 g, 8 %).

^{1}H NMR (400 MHz, $CDCl_3$) δ / ppm: 3.60 (m, 2H, *HO-C<u>H</u>$_2$-CH$_2$-*), 3.49-3.35 (m, 2H, *Br-C<u>H</u>$_2$-CH$_2$-*), 1.72 (m, 2H, *Br-CH$_2$-C<u>H</u>$_2$-*), 1.53 (m, 2H, *HO-CH$_2$-C<u>H</u>$_2$-*), 1.40-1.18 (m, 14H, *Br-(CH$_2$)$_2$-(C<u>H</u>$_2$)$_7$-(CH$_2$)$_2$-OH*).

Approach b: In a second attempt, another reaction as described in approach a was conducted with 0.1392 g TBD and a shorter reaction time of 6 h. The crude material was purified via recrystallization from MeOH, yielding an orange oil (m = 0.0985 g, 32 %).

^{1}H NMR (400 MHz, $CDCl_3$) δ / ppm: 3.68 (m, 2H, *HO-C<u>H</u>$_2$-CH$_2$-*), 3.58 (m, 2H, *-N-C<u>H</u>$_2$-CH$_2$-*), 3.37-3.19 (m, 8H, *-N-C<u>H</u>$_2$-CH$_2$-C<u>H</u>$_2$-N(H)-*), 2.00 (m, 4H, *-N-CH$_2$-C<u>H</u>$_2$-CH$_2$-N(H)-*), 1.80 (m, 2H, *-N-CH$_2$-C<u>H</u>$_2$-*), 1.53 (m, 2H, *HO-CH$_2$-C<u>H</u>$_2$-*), 1.44-1.15 (m, 14H, *-N-(CH$_2$)$_2$-(C<u>H</u>$_2$)$_7$-(CH$_2$)$_2$-OH*).

Approach c: The reaction for the synthesis of **TBD3** was repeated as in approach b with THF as solvent at 70°C with a reaction time of 6 h, yielding a dark orange oil (m = 0.1152 g, 37%).

^{1}H NMR (400 MHz, $CDCl_3$) δ / ppm: 3.68 (m, 2H, *HO-C<u>H</u>$_2$-CH$_2$-*), 3.58 (m, 2H, *-N-C<u>H</u>$_2$-CH$_2$-*), 3.37-3.19 (m, 8H, *-N-C<u>H</u>$_2$-CH$_2$-C<u>H</u>$_2$-N(H)-*), 2.00 (m, 4H, *-N-CH$_2$-C<u>H</u>$_2$-CH$_2$-N(H)-*), 1.80 (m, 2H, *-N-CH$_2$-C<u>H</u>$_2$-*), 1.53 (m, 2H, *HO-CH$_2$-C<u>H</u>$_2$-*), 1.44-1.15 (m, 14H, *-N-(CH$_2$)$_2$-(C<u>H</u>$_2$)$_7$-(CH$_2$)$_2$-OH*).

The NMR spectra of the approaches a-c are depicted in Figure 6.7.

5.2.2 Synthesis of the active-ester polymers

5.2.2.1 Copolymer **AEC1**

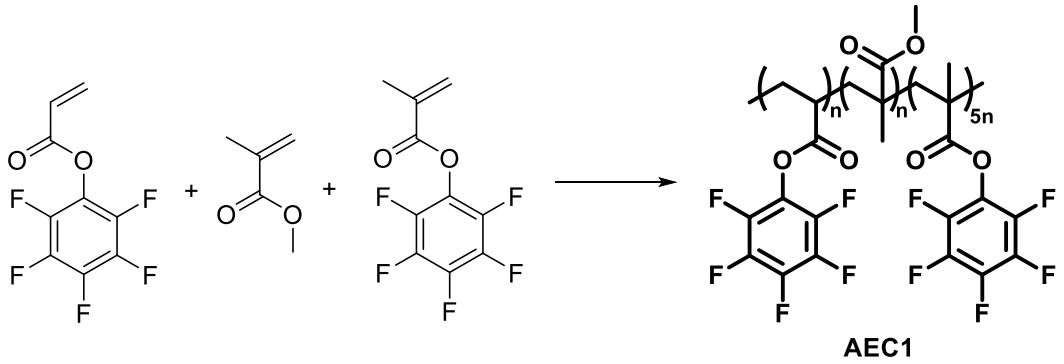

Under anhydrous conditions, 0.40 g PFP-MA (1.587 mmol, 5.00 eq.), 0.0756 g PFP-A (0.3170 mmol, 1.00 eq.) and 0.0317 g MMA (0.317 mmol, 1.00 eq.) were dissolved in 3 mL dry 1,4-dioxane. 3 mg AIBN (0.0190 mmol, 0.06 eq.) were dissolved in 3 mL dry 1,4-dioxane and were added to the reaction mixture. The reaction mixture was purged with N_2 for 30 min prior starting the reaction at 90°C. After 20 h, the reaction was stopped, and the reaction mixture was cooled to ambient temperature. The organic solvent was evaporated, and the residue was precipitated into ice cold MeOH, yielding a white solid (**AEC1**, 0.42 g).

SEC (THF): M_n = 6 500 g mol^{-1}, $Đ$ = 1.49 (Figure 6.4).

^{1}H NMR (500 MHz, $CDCl_3$) δ / ppm: 3.60 (m, 3H, *C<u>H</u>$_3$-O-CO-*), 2.37 – 0.78 (m, 13H, (*-C<u>H</u>$_2$-C$_q$)$_n$(-C<u>H</u>$_2$-C$_q$)$_m$(-C<u>H</u>$_2$-C<u>H</u>)$_o$-, -CO-C$_q$-C<u>H</u>$_3$*).

^{19}F NMR (471 MHz, $CDCl_3$) δ / ppm: -152.14 (m, 2F, *<u>F</u>$_{ortho}$*), -157.47 (m, 1F, *<u>F</u>$_{para}$*), -162.02 (m, 2F, *<u>F</u>$_{meta}$*).

The respective ^{1}H and ^{19}F chemical shift assignments are shown in Figure 6.3.

5.2.2.2 Copolymer **AEC2**

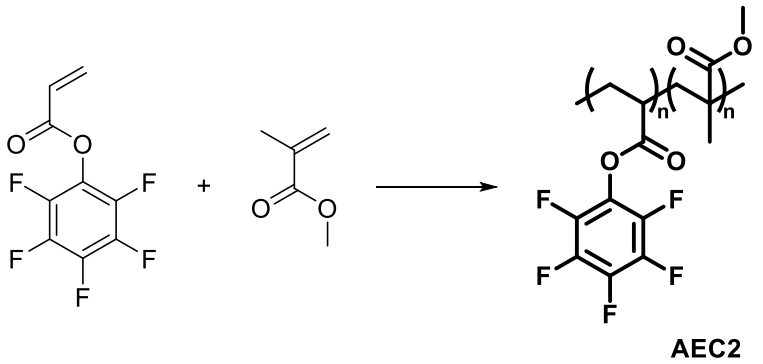

AEC2

Under anhydrous conditions, 0.2380 g PFP-A (1.00 mmol, 1.00 eq.) and 0.1001 g MMA (1.00 mmol, 1.00 eq.) were dissolved in 10 mL dry 1,4-dioxane. 10 mg AIBN were dissolved in 10 mL dry 1,4-dioxane and subsequently added to the reaction mixture. After purging with N_2 for 30 min, the reaction mixture was put in a preheated oil bath at 90°C. The reaction was stopped after 20 h and the reaction mixture was cooled to ambient temperature. The solvent was evaporated and the residue was precipitated into ice cold MeOH, yielding a white solid (**AEC2**, 0.81 g).

SEC (THF): M_n = 6 900 g mol^{-1}, $Đ$ = 2.12.

^{1}H NMR (500 MHz, $CDCl_3$) δ / ppm: 3.60 (m, 3H, *C<u>H</u>$_3$-O-CO-*), 2.37 – 0.78 (m, 8H, *(-C<u>H</u>$_2$-C<u>H</u>)$_n$(-C<u>H</u>$_2$-C$_q$)$_n$-, -CO-C$_q$-C<u>H</u>$_3$*).

^{19}F NMR (471 MHz, $CDCl_3$) δ / ppm: -152.14 (m, 2F, *<u>F</u>$_{ortho}$*), -157.47 (m, 1F, *<u>F</u>$_{para}$*), -162.02 (m, 2F, *<u>F</u>$_{meta}$*).

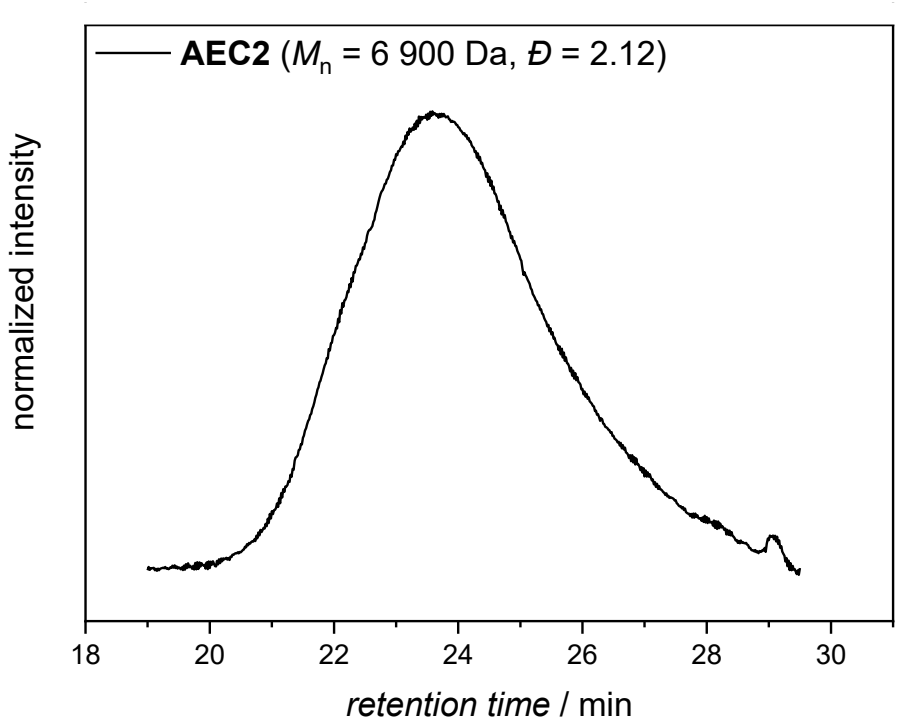

Figure 5.1: SEC elution trace of **AEC2** in THF at 30°C.

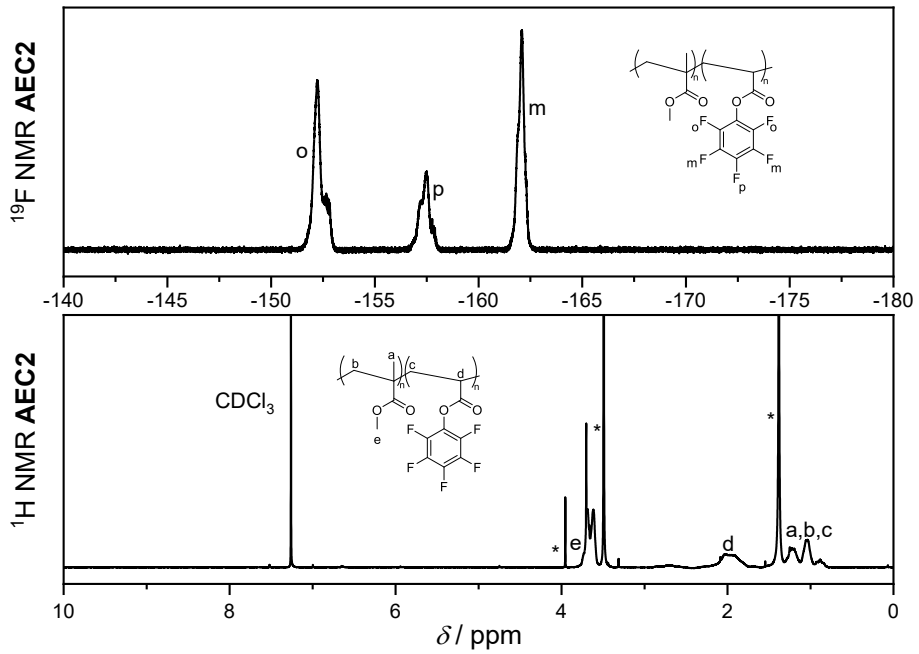

Figure 5.2: ^{1}H NMR (500 MHz) and ^{19}F NMR (471 MHz) spectra of **AEC2** in $CDCl_3$, respectively.

5.2.2.3 Copolymer **AEC3**

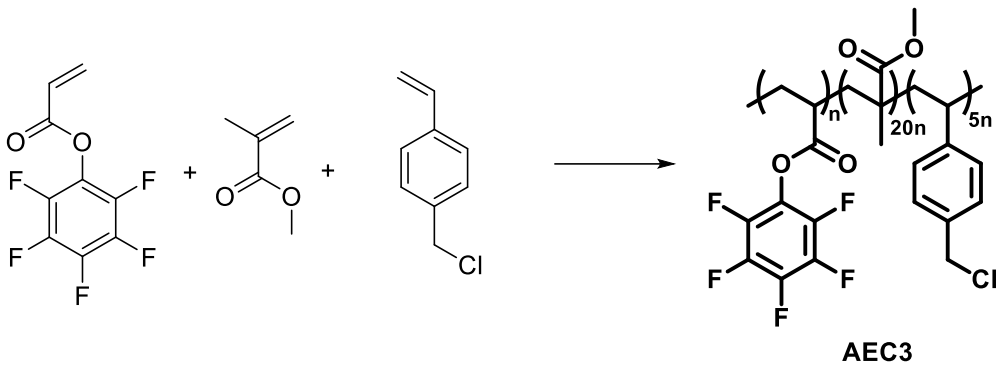

AEC3

Under anhydrous conditions, 0.7631 g VBC (5.0 mmol, 5.00 eq.), 0.2381 g PFP-A (1.00 mmol, 1.00 eq.) and 2.004 g MMA (20.00 mmol, 20.00 eq.) were dissolved in 10 mL dry 1,4-dioxane. 10 mg AIBN (0.06 mmol, 0.06 eq.) were dissolved in 10 mL dry 1,4-dioxane and were added to the reaction mixture. The reaction mixture was purged with N_2 for 1 h before being reacted at oil bath at 90°C. After 17 h, the reaction was stopped and the reaction mixture was cooled to ambient temperature. The solvent was evaporated and the residue was precipitated into ice cold MeOH, yielding a white solid (**AEC3**, 2.85 g).

SEC (THF): M_n = 14 600 g mol^{-1}, $Đ$ = 1.62.

^{1}H NMR (400 MHz, $CDCl_3$) δ / ppm: 7.23 (m, 2H, $\underline{H}_{arom.}$), 7.01 (m, 2H, $\underline{H}_{arom.}$), 4.50 (m, 2H, -C_q-$C\underline{H}_2$-*Cl*), 3.54 (m, 3H, -*CO-O-*$C\underline{H}_3$), 1.80 (m, 2H, *(-*CH_2-$C\underline{H}$*)*$_n$*(-*CH_2-C_q*)*$_m$*(-*CH_2-$C\underline{H}$*)*$_o$), 1.23-0.45 (m, 9H, $C\underline{H}_3$-C_q-, *(-*$C\underline{H}_2$-CH*)*$_n$*(-*$C\underline{H}_2$-C_q*)*$_m$*(-*$C\underline{H}_2$-CH*)*$_o$).

^{19}F NMR (377 MHz, $CDCl_3$) δ / ppm: -152.08 (s, 2F, $\underline{F}_{ortho}$), -157.64 (s, 1F, $\underline{F}_{para}$), -162.07 (s, 2F, $\underline{F}_{meta}$).

The respective ^{1}H and ^{19}F chemical shift assignments can be found in Figure 5.5 and Figure 5.6.

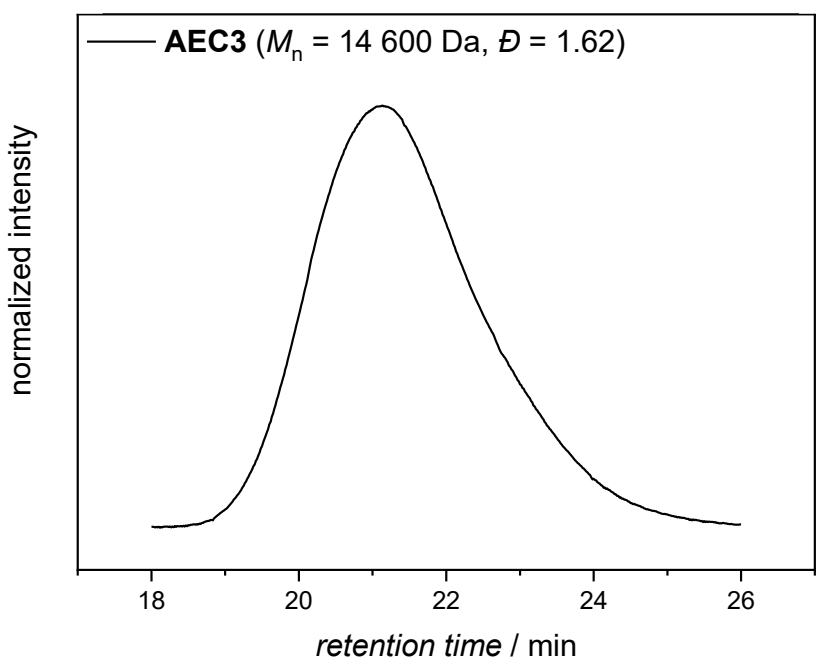

Figure 5.3: SEC elution trace of **AEC3** in THF at 30°C.

5.2.3 Synthesis of the luminol-polymers

5.2.3.1 Luminol-Polymer **LP1**

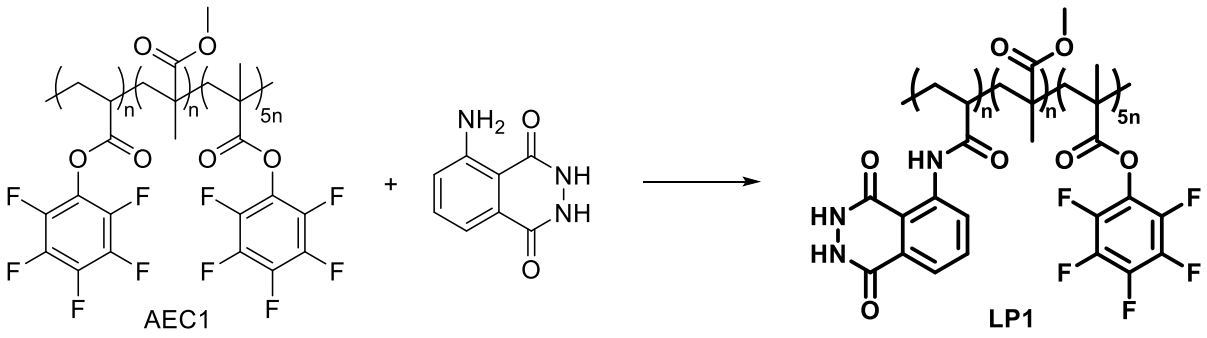

Under anhydrous conditions, 0.3384 g **AEC1** (0.2118 mmol of the PFP-A moiety, 1.00 eq.) were dissolved in 4 mL dry 1,4-dioxane. In a separate round bottom flask, 0.0938 g luminol (0.0938 mmol, 2.50 eq. with respect to the PFP-A moiety of the polymer backbone) and 0.15 mL TEA (0.1072 g, 1.0590 mmol, 5.00 eq. with respect to the PFP-A moiety of the polymer backbone) were dissolved in 2 mL dry DMSO, also under anhydrous conditions. The luminol – mixture was added to the dissolved polymer mixture and the reaction mixture was put in a preheated oil bath at 50°C. After 24 h, the reaction mixture was cooled to ambient temperature and the solvent was evaporated. Precipitation into ice cold MeOH yielded a yellow solid (**LP1**, 0.32 g).

SEC (THF): M_n = 7 400 g mol^{-1}, $Đ$ = 1.54 (Figure 6.4A).

^{1}H NMR (500 MHz, DMF) δ / ppm: 12.06 (s, 2H, -*CO-N<u>H</u>-N<u>H</u>-CO*-), 11.25 (s, 1H, -*CO-N<u>H</u>-C$_q$*-), 7.47 (m, 1H, *<u>H</u>$_{arom.}$*), 6.93 (m, 1H, *<u>H</u>$_{arom.}$*), 6.89 (m, 1H, *<u>H</u>$_{arom.}$*), 3.57 (m, 3H, *C<u>H</u>$_3$-O-CO*-), 2.36 – 1.08 (m, 13H, *-(C<u>H</u>$_2$-C$_q$)$_m$-(C<u>H</u>$_2$-C$_q$)$_n$-(C<u>H</u>$_2$-C<u>H</u>)$_o$-*, *C<u>H</u>$_3$-C$_q$-CO-O*-).

^{19}F NMR (471 MHz, DMSO) δ / ppm: -152.32 (m, 2F, *<u>F</u>$_{ortho}$*), -157.49 (m, 1F, *<u>F</u>$_{para}$*), -162.40 (m, 2F, *<u>F</u>$_{meta}$*).

The respective ^{1}H and ^{19} NMR spectra are depicted in Figure 6.3.

5.2.3.2 Luminol-Polymer **LP1'**

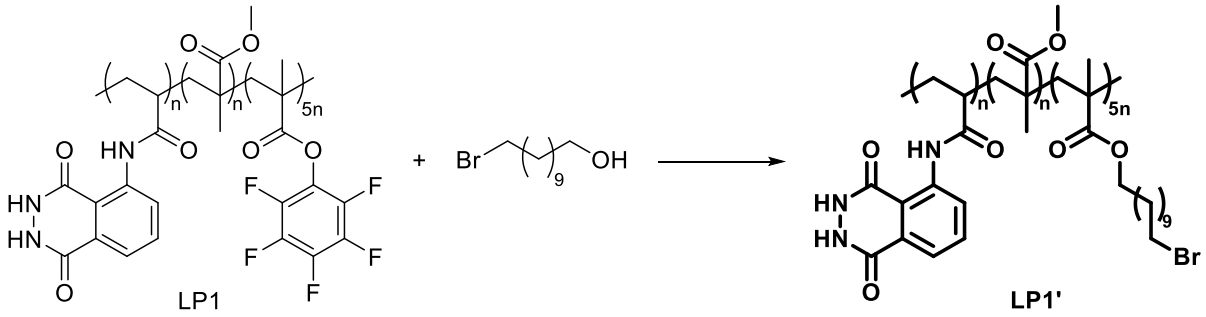

Under anhydrous conditions, 26.7 mg **LP1** (0.0324 mmol of the PFP-MA moiety, 1.00 eq.) were dissolved in dry 1,4-dioxane under N_2. In a separate vial, 27.1 mg 11-bromo-1-undecanol (0.0810 mmol with respect to the PFP-MA moieties in the polymer backbone, 2.50 eq.) and 16.4 mg TEA (0.1620 mmol with respect to the PFP-MA moieties in the polymer backbone, 5.00 eq.) were dissolved in dry DMSO. Subsequently, the DMSO-mixture was added to the **LP1**-solution and the reaction mixture was put in a pre-heated oil bath at 50°C. The reaction was stopped after 21 h and the solvent was evaporated. Precipitation into ice cold Et_2O yielded a yellow residue (**LP1'**), which was collected via centrifugation (0.0715 g).

SEC (THF): M_n = 8 900 g mol^{-1}, $Đ$ = 1.39 (Figure 5.4).

^{1}H NMR (500 MHz, DMF) δ / ppm: 11.88 (s, 2H, *-CO-N<u>H</u>-N<u>H</u>-CO*-), 9.78 (s, 1H, *-CO-N<u>H</u>-C$_q$*-), 7.67 (m, 2H, *<u>H</u>$_{arom.}$*), 7.24 (m, 1H, *<u>H</u>$_{arom.}$*), 3.88 ppm (m, 2H, *Br-C<u>H</u>$_2$-CH$_2$*-), 3.70 (m, 2H, *Br-(CH$_2$)$_{10}$-C<u>H</u>$_2$-O*-), 3.50 (m, 3H, *C<u>H</u>$_3$-O-CO*-), 1.98-1.74 ppm (m, 6H, *Br-CH$_2$-C<u>H</u>$_2$-(CH$_2$)$_6$-(C<u>H</u>$_2$)$_2$-CH$_2$-O*-), 1.38 – 1.12 (m, 25H, *Br-(CH$_2$)$_2$-(C<u>H</u>$_2$)$_6$-CH$_2$*), *-(C<u>H</u>$_2$-C<u>H</u>)$_n$-(C<u>H</u>$_2$-C$_q$)$_n$-(C<u>H</u>$_2$-C$_q$)$_{5n}$-*, *C<u>H</u>$_3$-C$_q$-CO-O*-).

^{19}F NMR (471 MHz, DMSO) δ / ppm: -157.49 (m, 1F, *<u>F</u>$_{para}$*), -162.40 (m, 2F, *<u>F</u>$_{meta}$*).

The assigned chemical shifts of the ^{1}H and ^{19}F resonances can be found in Figure 6.8.

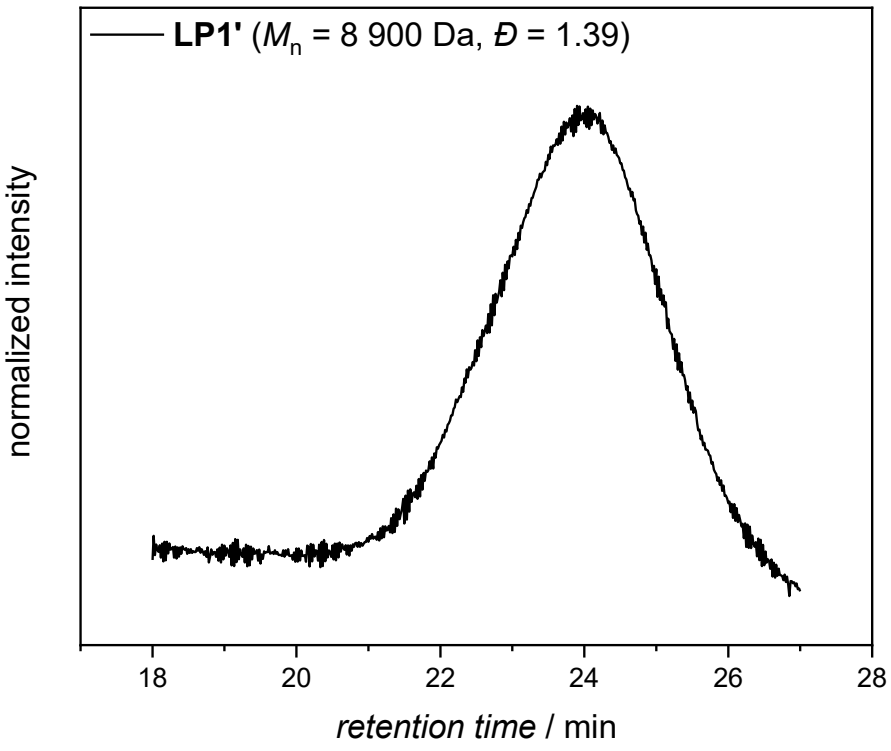

Figure 5.4: SEC elution trace of **LP1'** in THF at 30°C.

5.2.3.3 Luminol-Polymer **LP2**

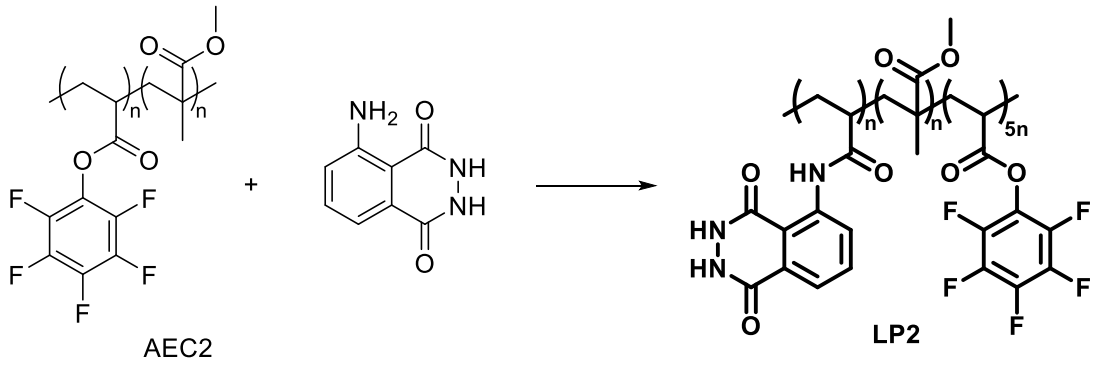

Under anhydrous conditions, 0.80 g **AEC2** (2.318 mmol of the PFP-A moiety, 1.00 eq.) were dissolved in 16 mL dry 1,4-dioxane. In a separate round bottom flask, 0.070 mg luminol (0.3940 mmol, 0.17 eq. with respect to the PFP-A moiety of the polymer backbone) and 0.64 mL TEA (0.4691 g, 4.6360 mmol, 2.00 eq. with respect to the PFP-A moiety of the polymer backbone) were dissolved in 8 mL dry DMSO, also under anhydrous conditions. The luminol – mixture was added to the dissolved polymer mixture and the reaction mixture was put in a preheated oil bath at 50°C. After 19 h, the reaction mixture was cooled to ambient temperature and the

solvent was evaporated. Precipitation into ice cold MeOH yielded a yellow solid (**LP2**, 0.24 g). SEC (DMAc): M_n = 11 300 g mol^{-1}, $Đ$ = 1.34 (Figure 6.4B).

^{1}H NMR (500 MHz, DMF) δ / ppm: 12.06 (s, 2H, -*CO-NH-NH-CO*-), 11.25 (s, 1H, -*CO-NH-C$_q$*-), 7.47 (m, 1H, *H$_{arom.}$*), 6.93 (m, 1H, *H$_{arom.}$*), 6.89 (m, 1H, *H$_{arom.}$*), 3.57 (m, 3H, *CH$_3$-O-CO*-), 2.36 – 1.08 (m, 11H, *(CH$_2$-CH)$_n$-(CH$_2$-C$_q$)$_n$-(CH$_2$-CH)$_{5n}$-*, *CH$_3$-C$_q$-CO-O*-).

^{19}F NMR (471 MHz, DMSO) δ / ppm: -152.32 (m, 2F, *F$_{ortho}$*), -157.49 (m, 1F, *F$_{para}$*), -162.40 (m, 2F, *F$_{meta}$*).

The assignment of the ^{1}H and ^{19}F resonances are illustrated in Figure 6.9 and Figure 6.10.

5.2.3.4 Luminol-Polymer **LP2'**

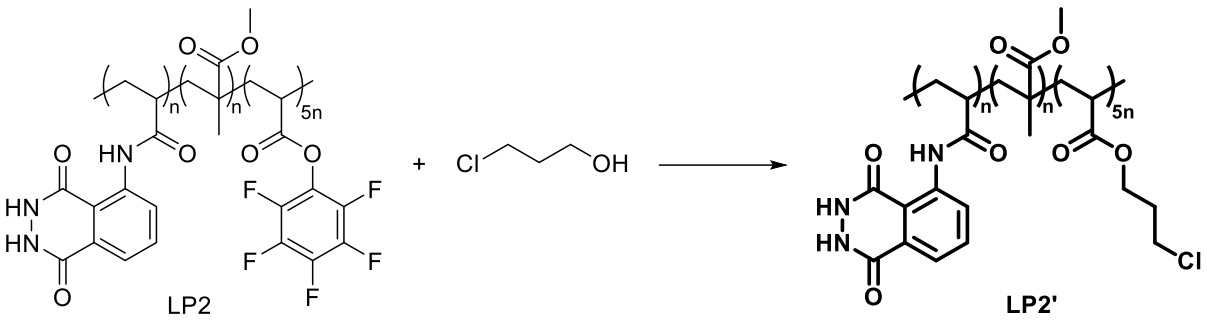

Under anhydrous conditions, 0.2360 g **LP2** (0.616 mmol of the PFP-A moiety) were dissolved in 5.8 mL 1,4-dioxane. In a separate vial, 0.1460 g 3-chloro-1-propanol (1.539 mmol with respect to the PFP-moieties in the polymer backbone) and 0.3120 g TEA (3.0780 mmol with respect to the PFP-A moieties in the polymer backbone) were dissolved in dry DMSO. The reaction mixture was purged with N_2 for 20 min and subsequently put in a pre-heated oil bath at 50°C. After 18 h, the reaction was stopped and the solvent was evaporated. The final product **LP2'** was obtained after precipitation in ice cold Et_2O (yield = 0.0930 g).

SEC (DMAc): M_n = 16 700 g mol^{-1}, $Đ$ = 1.44 (Figure 6.4B).

^{1}H NMR (500 MHz, DMF) δ / ppm: 11.9 (s, 2H, -*CO-NH-NH-CO*-), 11.25 (s, 1H, -*CO-NH-C$_q$*-), 7.47 (m, 1H, *H$_{arom.}$*), 6.93 (m, 1H, *H$_{arom.}$*), 6.89 (m, 1H, *H$_{arom.}$*), 3.80 (m, 2H, -*CO-O-CH$_2$-CH$_2$*-), 3.57 (m, 5H, *Cl-CH$_2$-CH$_2$-*, *CH$_3$-O-CO*-), 2.36 – 1.08 (m, 13H, *Cl-CH$_2$-CH$_2$*, *(CH$_2$-CH)$_n$(CH$_2$-C$_q$)$_n$-(CH$_2$-CH)$_{5n}$-*, *CH$_3$-C$_q$-CO-O*-).

^{19}F NMR (471 MHz, DMSO) δ / ppm: -152.32 (m, 2F, *F$_{ortho}$*), -157.49 (m, 1F, *F$_{para}$*), -162.40 (m, 2F, *F$_{meta}$*).

The assignment of the ^{1}H and ^{19}F resonances are illustrated in Figure 6.9 and Figure 6.10.

5.2.3.5 Luminol-Polymer **LP3**

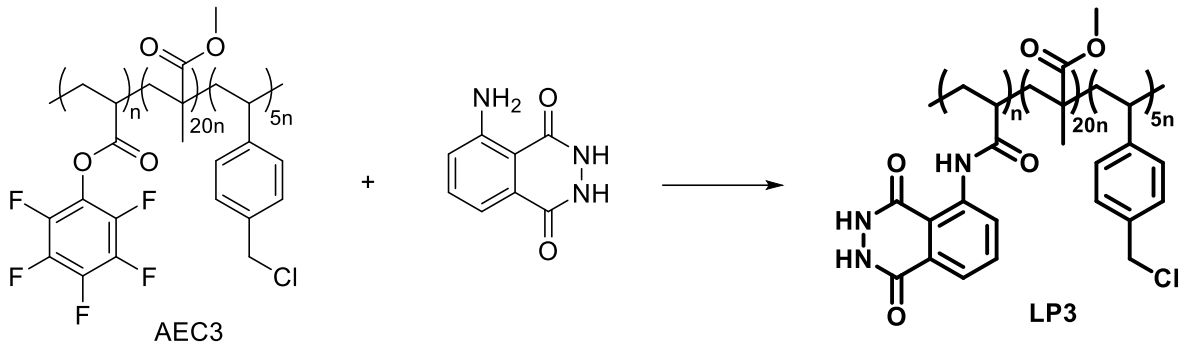

Under anhydrous conditions, 0.50 g **AEC3** (0.1608 mmol of the PFPA-moiety, 1.00 eq.) were dissolved in 1.7 mL dry 1,4-dioxane. In a separate round bottom flask, 0.0285 g luminol (0.1608 mmol, 1.00 eq. with respect to the PFP-A moiety of the polymer backbone) and 0.045 mL TEA (0.0325 g, 0.3216 mmol, 2.00 eq.) were dissolved in 0.9 mL dry DMSO under N_2. The luminol-mixture was added to the dissolved polymer mixture and the reaction mixture was put in a preheated oil bath at 50°C. After 21 h, the reaction mixture was cooled to ambient temperature and the solvent was evaporated. Precipitation into ice cold MeOH yielded **LP3** as a light yellow solid (0.42 g).

^{1}H NMR (400 MHz, DMSO) δ / ppm: 11.28 (m, 2H, -*CO-N*<u>*H*</u>-), 7.45 (m, 1H, <u>*H*</u>*arom.*), 7.29 (m, 2H, <u>*H*</u>*arom.*), 7.04 (m, 3H, <u>*H*</u>*arom.*, -*CO-N*<u>*H*</u>-), 6.91 (m, 1H, <u>*H*</u>*arom.*), 6.84 (m, 1H, <u>*H*</u>*arom.*), 4.69 (m, 2H, -C_q-*C*<u>*H*</u>$_2$-*Cl*), 3.47 (m, 3H, -*CO-O-C*<u>*H*</u>$_3$), 1.74 (m, 2H, *(-CH$_2$-C*<u>*H*</u>*)$_n$(-CH$_2$-C$_q$)$_m$(-CH$_2$-C*<u>*H*</u>*)$_o$*), 1.35-0.39 (m, 9H, , *C*<u>*H*</u>$_3$-C_q-, *(-C*<u>*H*</u>$_2$-*CH)$_n$(-C*<u>*H*</u>$_2$-C$_q$)$_m$(-C*<u>*H*</u>$_2$-*CH)$_o$*).

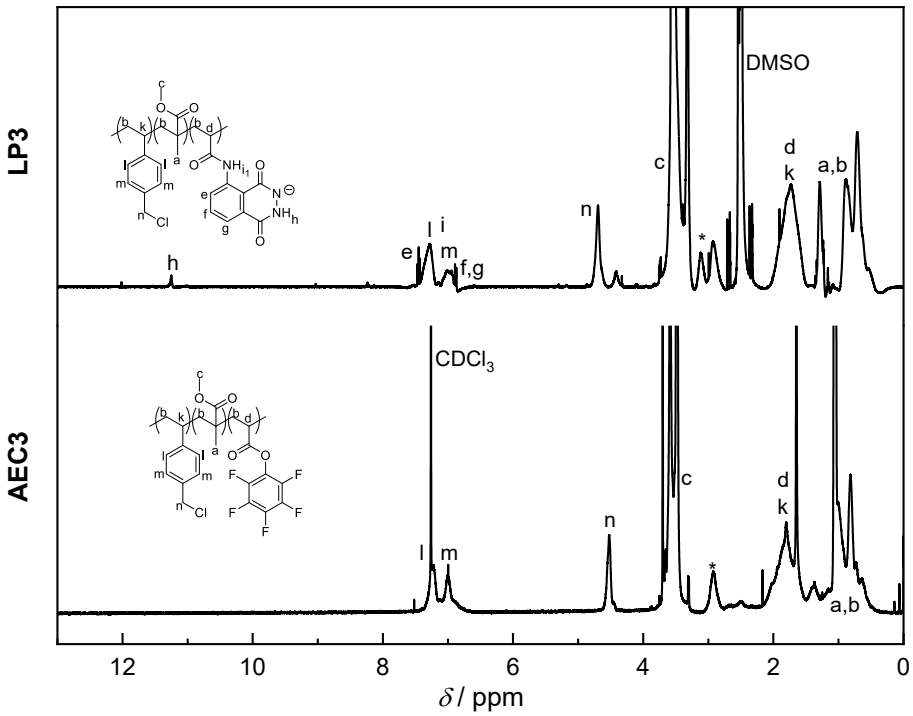

Figure 5.5: ^{1}H NMR (400 MHz) spectra of **AEC3** in $CDCl_3$ and **LP3** in DMSO-d_6.

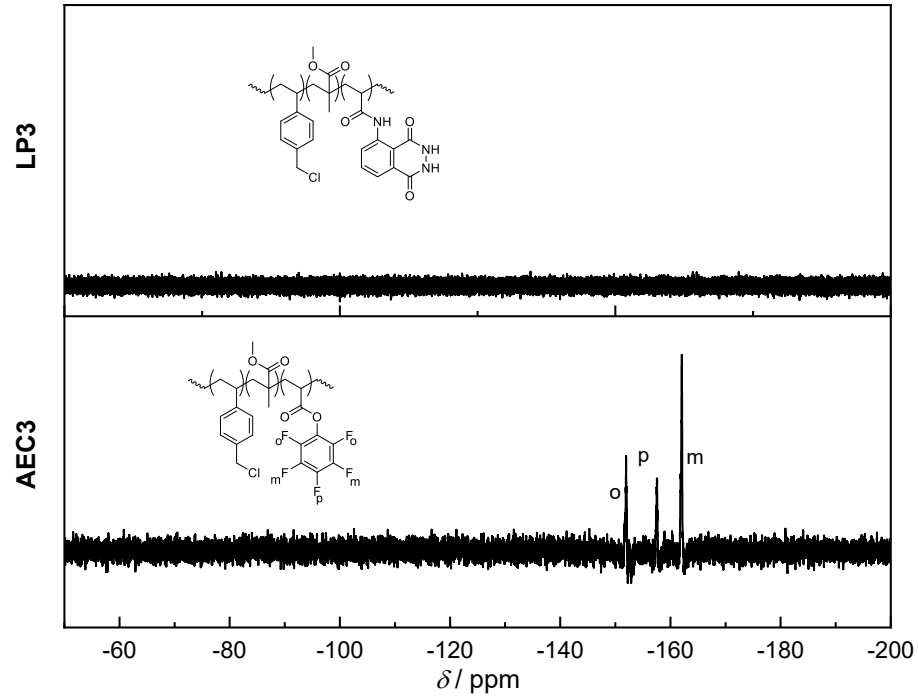

Figure 5.6: ^{19}F NMR (377 MHz) spectra of **AEC3** in $CDCl_3$ and **LP3** in DMSO-d_6.

5.2.4 Synthesis of the luminol-TBD-polymers

5.2.4.1 Luminol-TBD-Polymer **LTP1**

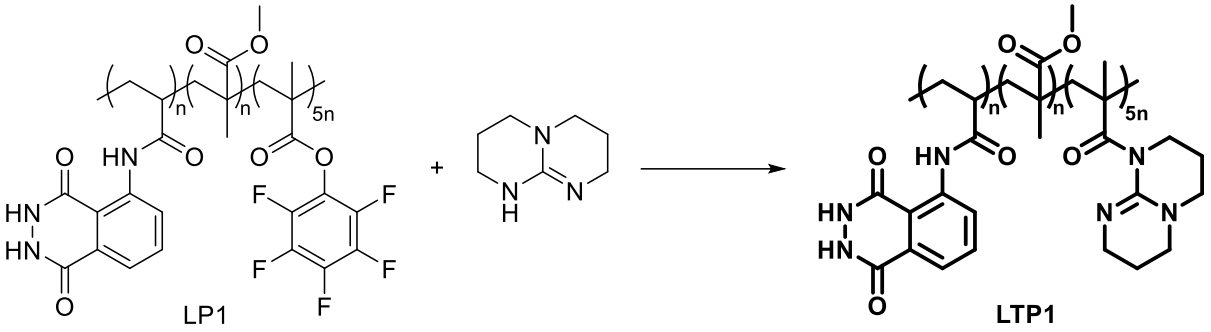

Under anhydrous conditions, 25.0 mg **LP1** (0.0303 mmol of the PFP-MA moiety, 1.00 eq.) were dissolved in 0.28 mL dry 1,4-dioxane under N_2. In a separate vial, 10.6 mg TBD (0.0758 mmol with respect to the PFP-MA moieties in the polymer backbone, 2.50 eq.) and 15.3 mg TEA (0.1515 mmol with respect to the PFP-MA moieties in the polymer backbone) were dissolved in dry DMSO. Subsequently, the TBD-mixture was added to the **LP1**-solution and the reaction mixture was put in a pre-heated oil bath at 50°C. The reaction was stopped after 20 h and the solvent was evaporated. The obtained material **LTP1** was not soluble in any organic solvent for further purification of analysis.

5.2.4.2 Luminol-TBD-Polymer **LTP1'**

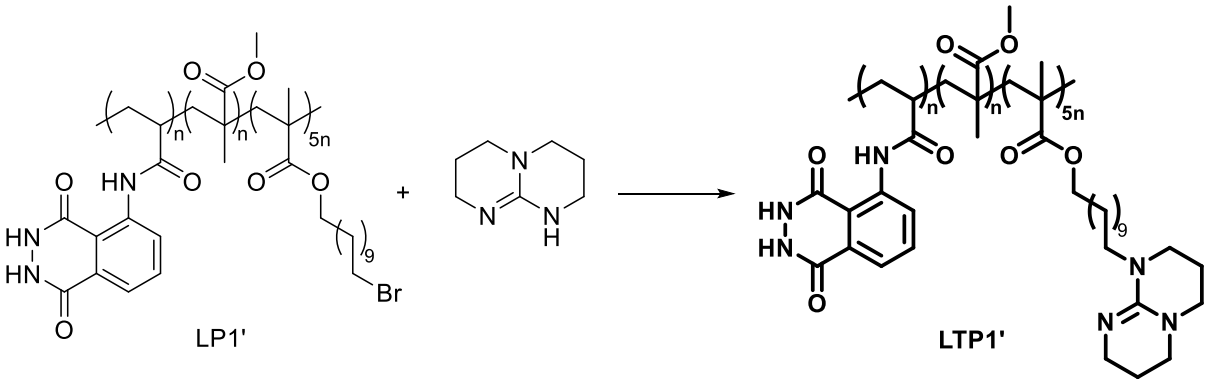

Under anhydrous conditions, 30.0 mg **LP1'** (0.0364 mmol of the Br-moiety, 1.00 eq.) were dissolved in 0.5 mL dry 1,4-dioxane under N_2. In a separate vial, 12.7 mg TBD (0.0910 mmol with respect to the PFP-MA moieties in the polymer backbone, 2.50 eq.) and 18.4 mg TEA (0.1820 mmol with respect to the PFP-MA moieties in the polymer backbone) were dissolved

in dry DMSO. Subsequently, the TBD-mixture was added to the **LP1'**-solution and the reaction mixture was put in a pre-heated oil bath at 50°C. The reaction was stopped after 18 h and the solvent was evaporated. The obtained material **LTP1'** was not soluble in any organic solvent for further purification of analysis.

5.2.4.3 Luminol-TBD-Polymer **LTP2**

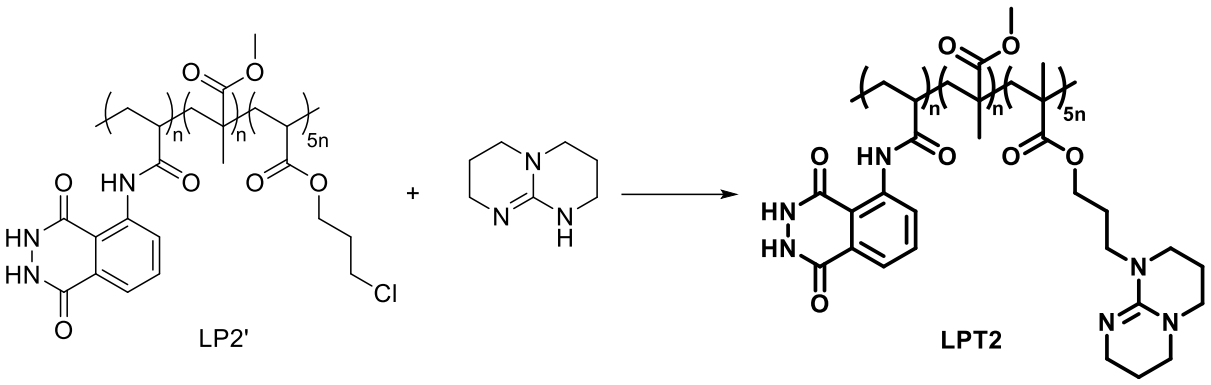

Under anhydrous conditions, 0.0930 g **LP2'** (0.1710 mmol of the Cl-moiety) and 0.0356 g TBD (0.2560 mmol with respect to the Cl-moieties in the polymer backbone, 1.50 eq.) were dissolved in 0.3 mL dry THF. The reaction mixture was put in a pre-heated oil bath at 70°C. After 25 h, the viscous, yellow materials was dissolved in 0.5 mL $CHCl_3$ and precipitated into ice cold Et_2O. The yellow residue was collected via centrifugation and dried under reduced pressure, yielding a yellow, sticky material (**LTP2**, m = 0.0753 g).

SEC (DMAc) = 5 200 g mol^{-1}, $Đ$ = 1.76.

^{1}H NMR (500 MHz, DMF) δ / ppm: 11.9 (s, 2H, -*CO-N*<u>*H*</u>*-N*<u>*H*</u>*-CO*-), 11.25 (s, 1H, -*CO-N*<u>*H*</u>*-*C_q-), 7.76 (s, 1H, -CH_2-*N*<u>*H*</u>*-CH*-), 7.47 (m, 1H, <u>*H*</u>$_{arom.}$), 6.93 (m, 1H, <u>*H*</u>$_{arom.}$), 6.89 (m, 1H, <u>*H*</u>$_{arom.}$), 6.13 (s, 1H, *-N-C*<u>*H*</u>*-NH-)*, 3.54 (m, 4H, -*CO-O-C*<u>*H*</u>$_2$-CH_2-*C*<u>*H*</u>$_2$-), 3.33 (m, 3H, *C*<u>*H*</u>$_3$*-O-CO*-), 3.15 (m, 8H, -*N-C*<u>*H*</u>$_2$-CH_2-*C*<u>*H*</u>$_2$*-N*-), 2.44 (m, 1H, -*(*CH_2-*C*<u>*H*</u>*)*$_n$-CH_2-, 1.86 (m, 2H, -*N-*CH_2-*C*<u>*H*</u>$_2$-), 1.76 (m, 4H, -*N-*CH_2-*C*<u>*H*</u>$_2$-CH_2*-N-),* 1.09 – 0.62 (m, 10H, *(C*<u>*H*</u>$_2$*-CH)*$_n$*-(C*<u>*H*</u>$_2$*-*C_q*)*$_n$*-(C*<u>*H*</u>$_2$*-C*<u>*H*</u>*)*$_{5n}$-, *C*<u>*H*</u>$_3$*-*C_q*-CO-O*-).

The ^{1}H NMR spectrum of **LTP2** with the chemical shift assignments is shown in Figure 6.9.

5.2.4.4 Luminol-TBD-Polymer **LTP3**

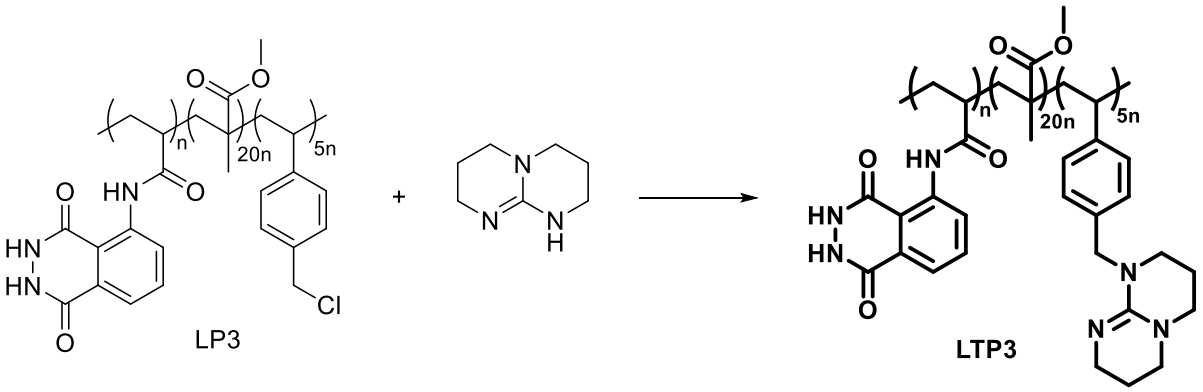

Under anhydrous conditions, 0.4226 g **LP3** (0.1359 mmol of the PFP-A moiety in the initial polymer **AEC3**, 1.00 eq.) were dissolved in 1.7 mL dry 1,4-dioxane. In a separate round bottom flask, 0.0946 g TBD (0.6795 mmol, 5.00 eq. with respect to the PFP-A moiety of the polymer backbone **AEC3**) and 0.038 mL TEA (0.0275 g, 0.2718 mmol, 5.00 eq. with respect to the PFP-A moiety of the polymer backbone **AEC3**) were dissolved in 0.9 mL dry DMSO under N_2. The TBD-mixture was added to the dissolved polymer mixture and the reaction mixture was put in a preheated oil bath at 50°C. After 20 h, the reaction mixture was cooled to ambient temperature and the solvent was evaporated. Precipitation into ice cold Et_2O yielded **LTP3** as a yellow solid (0.41 g).

^{1}H NMR (400 MHz, DMSO) δ / ppm: 8.52 (m, 1H, -CH_2-N$\underline{H}$-CH-), 7.33 (m, 1H, $\underline{H}_{arom.}$), 7.14 (m, 2H, -CO-N$\underline{H}$-), 7.01 (m, 3H, $\underline{H}_{arom.}$), 6.74 (m, 3H, $\underline{H}_{arom.}$), 6.10 (s, 2H, -C_q-C$\underline{H}_2$-N_t-), 3.47 (m, 3H, C$\underline{H}_3$-O-CO-), 3.26 (m, 8H, -N_t-C$\underline{H}_2$-CH_2-), 1.91-1.18 (m, 2H, (-CH_2-C$\underline{H}$)$_n$(-CH_2-C_q)$_m$(-CH_2-C$\underline{H}$)$_o$), 1.11-0.49 (m, 9H, C$\underline{H}_3$-C_q-, (-C$\underline{H}_2$-CH)$_n$(-C$\underline{H}_2$-C_q)$_m$(-C$\underline{H}_2$-CH)$_o$).

The chemical shift assignments are illustrated in Figure 3.4.

5.2.5 Procedure for the host-guest complexation

For the formation of the supramolecular complex **C1**, the luminol-TBD-polymer **LTP3** (1.00 eq., 0.02 g mL^{-1}) was dissolved in DMSO. After complete dissolving, the host-molecule Me-β-CD (5.20 eq.) was added. The solution was stirred at room temperature for 1 h.

5.2.6 1,6-Diisocyanohexane (DICH)

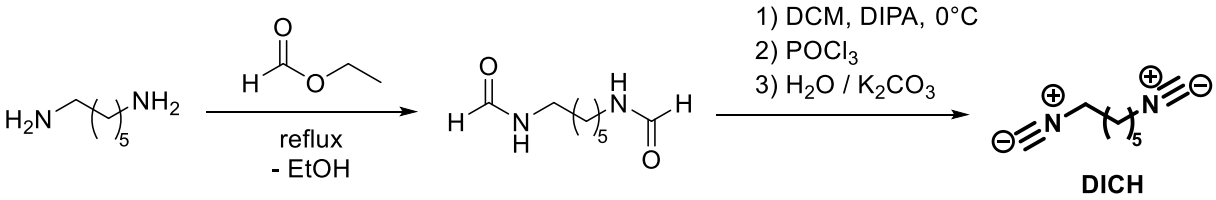

In a 250 mL round bottom flask, 10.0 g hexamethylenediamine (86.1 mmol, 1.00 eq.) and 172 mL ethyl formate (158 g, 2.02 mmol, 23.5 eq.) were heated under reflux (70°C). The reaction was stopped after 18 h and the solvent was removed under reduced pressure. Subsequently, the obtained formamide was suspended in 175 mL DCM. After the addition of 72.6 mL DIPA (52.5 g, 516 mmol, 6.00 eq), the suspension was cooled below 0°C with a liquid N_2 / acetone mixture. Slowly, 22.5 mL $POCl_3$ (36.9 g, 241 mmol, 2.80 eq.) were added dropwise, keeping the temperature of the reaction mixture steadily below 0°C. The reaction mixture was stirred for 2 h, in which a colour change from white to yellow was observed; the yellow mixture was poured into 500 mL ice water containing 100 g K_2CO_3 and stirred for one more hour. Then, the organic layer was separated, the aq. layer was extracted with DCM (3 x 50 mL) and the combined organic layers were dried over K_2CO_3. After removal of the K_2CO_3 via filtration over Celite, the solvent was evaporated. Further purification by column chromatography (hexane / EtOAc 5 : 1 → 2 : 1) and subsequent solvent removal yielded the DICH as light yellow oil (m = 8.35 g, 71 %).

^{1}H NMR (400 MHz, $CDCl_3$) δ / ppm: 3.27 (m, 4H, *CN-C<u>H</u>$_2$-*), 1.57 (m, 4H, *CN-CH$_2$-C<u>H</u>$_2$-*), 1.35 (m, 4H, *CN-CH$_2$-CH$_2$-C<u>H</u>$_2$-*).

^{13}C NMR (100 MHz, $CDCl_3$) δ / ppm: 155.28 (*<u>C</u>N-CH$_2$-*), 40.64 (*CN-<u>C</u>H$_2$-*), 28.07 (*CN-CH$_2$-CH$_2$-<u>C</u>H$_2$-*), 24.83 (*CN-CH$_2$-<u>C</u>H$_2$-*).

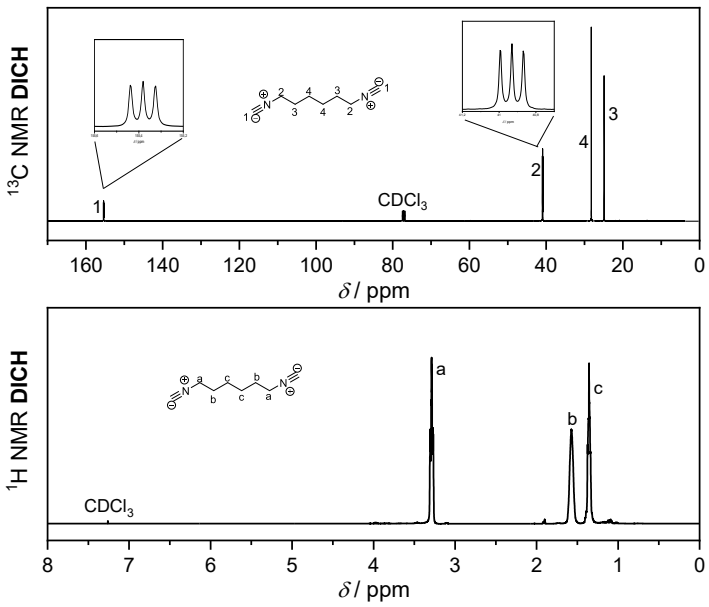

Figure 5.7: ^{1}H NMR (400 MHz) and ^{13}C NMR (100 MHz) spectra of **DICH** in $CDCl_3$.

5.2.7 Synthesis of the tetrazole-aldehyde derivatives

5.2.7.1 4-(2-(4-methoxyphenyl)-2*H*-tetrazol-5-yl)benzaldehyde (**T1**)

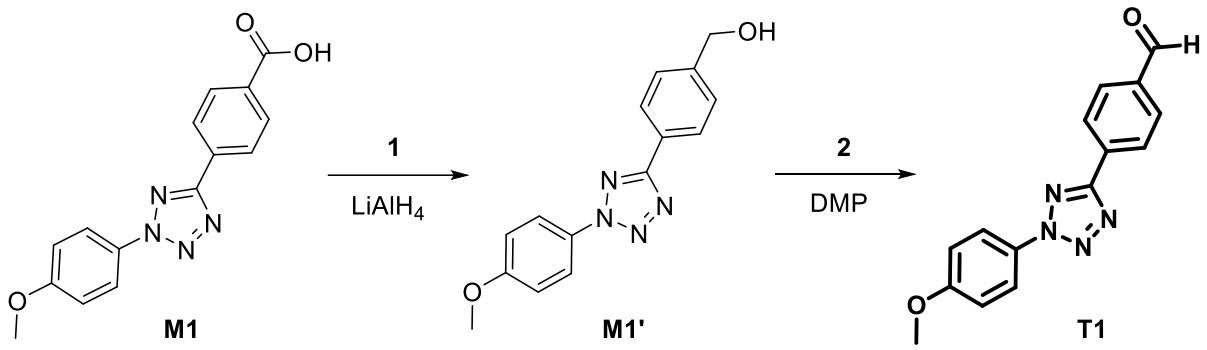

Step 1: Under anhydrous conditions, 1.0 g **M1** (3.3774 mmol, 1.00 eq.) were dissolved in 15 mL dry THF. In a separate flask, 0.1538 $LiAlH_4$ (4.0529 mmol, 1.20 eq.) were dispersed in 9 mL dry THF under N_2, before being cooled to 0°C. Very slowly, the **M1**-solution was added dropwise to the $LiALH_4$-suspension under continuous N_2-flow. The reaction mixture was stirred for 24 h at ambient temperature. Then, the mixture was cooled to 0°C again and 0.2 mL H_2O were slowly added to deactivate unreacted $LiAlH_4$, followed by the addition of 0.4 mL 10wt% NaOH and 0.6 mL H_2O. Subsequently, the salt was filtered off and washed several times

with THF. Removal of the solvent under reduced pressure yielded the tetrazole-alcohol **M1'** (m = 0.62 g, 64 %).

^{1}H NMR (400 MHz, DMSO) δ / ppm: 8.09 (m, 4H, *H*$_{arom}$), 7.52 (d, 2H, *H*$_{arom}$), 7.20 (d, 2H, *H*$_{arom.}$), 5.37 (m, 1H, *HO-CH*$_2$-), 4.59 (m, 2H, *HO-CH*$_2$-), 3.85 (s, 3H, *CH*$_3$*-O*-).

^{13}C NMR (100 MHz, DMSO) δ / ppm: 164. 37 (-*N-C*$_q$-*C*$_q$-), 160.43 (*CH*$_3$*-O-C*$_q$-), 145.56 (*HO-CH*$_2$-*C*$_q$-), 129.48 (-*N-C*$_q$-*C*$_q$-), 127.69 (-*C*$_q$-*CH*$_{arom}$-), 126.54 (-*C*$_q$-*CH*$_{arom}$-), 124.63 (-*N-C*$_q$—*CH*$_{arom}$-), 121.52 (-*C*$_q$-*CH*$_{arom}$-), 114.98 (-*C*$_q$-*CH*$_{arom}$-), 62.27 (*HO-CH*$_2$-*C*$_q$-), 55.65 (*CH*$_3$*-O-C*$_q$-).

Step 2: In a 25 mL round bottom flask, 0.6131 g **M1'** (2.1733 mmol, 1.00 eq.) were dissolved in 16 mL dry DCM under N_2. Subsequently, 1.1061 g Dess-Martin periodinane (DMP, 2.6080 mmol, 1.20 eq.) were added and the reaction mixture was stirred for 4 h at ambient temperature. Then, the solvent was removed under reduced pressure and the residue was dissolved in 60 mL EtOAc. After washing with sat. $NaHCO_3$, brine and H_2O (20 mL each), the organic layer was dried over $MgSO_4$. Finally, the product **T1** was obtained by evaporation of the solvent as dark orange solid (m = 0.5987 g, 98%).

^{1}H NMR (400 MHz, DMSO) δ / ppm: 10.10 (s, 1H, *H-CO-C*$_q$-), 8.37 (d, 2H, *H*$_{arom}$), 8.10 (m, 4H, *H*$_{arom}$), 7.21 (d, 2H, *H*$_{arom}$), 3.85 (s, 3H, *CH*$_3$*-O*-).

^{13}C NMR (100 MHz, DMSO) δ / ppm: 192.62 (*H-CO-C*$_q$-), 163.66 (-*N-C*$_q$-*C*$_q$-), 160.43 (*CH*$_3$*-O-C*$_q$-), 137.10 (*H-CO-C*$_q$-), 131.68 (-*N-C*$_q$-*C*$_q$-), 130.35 (-*C*$_q$-*CH*$_{arom}$-), 129.48 (-*N-C*$_q$—*CH*$_{arom}$-), 127.16 (-*C*$_q$-*CH*$_{arom}$-), 121.73 (-*C*$_q$-*CH*$_{arom}$-), 114.98 (-*C*$_q$-*CH*$_{arom}$-), 55.65 (*CH*$_3$*-O-C*$_q$-).

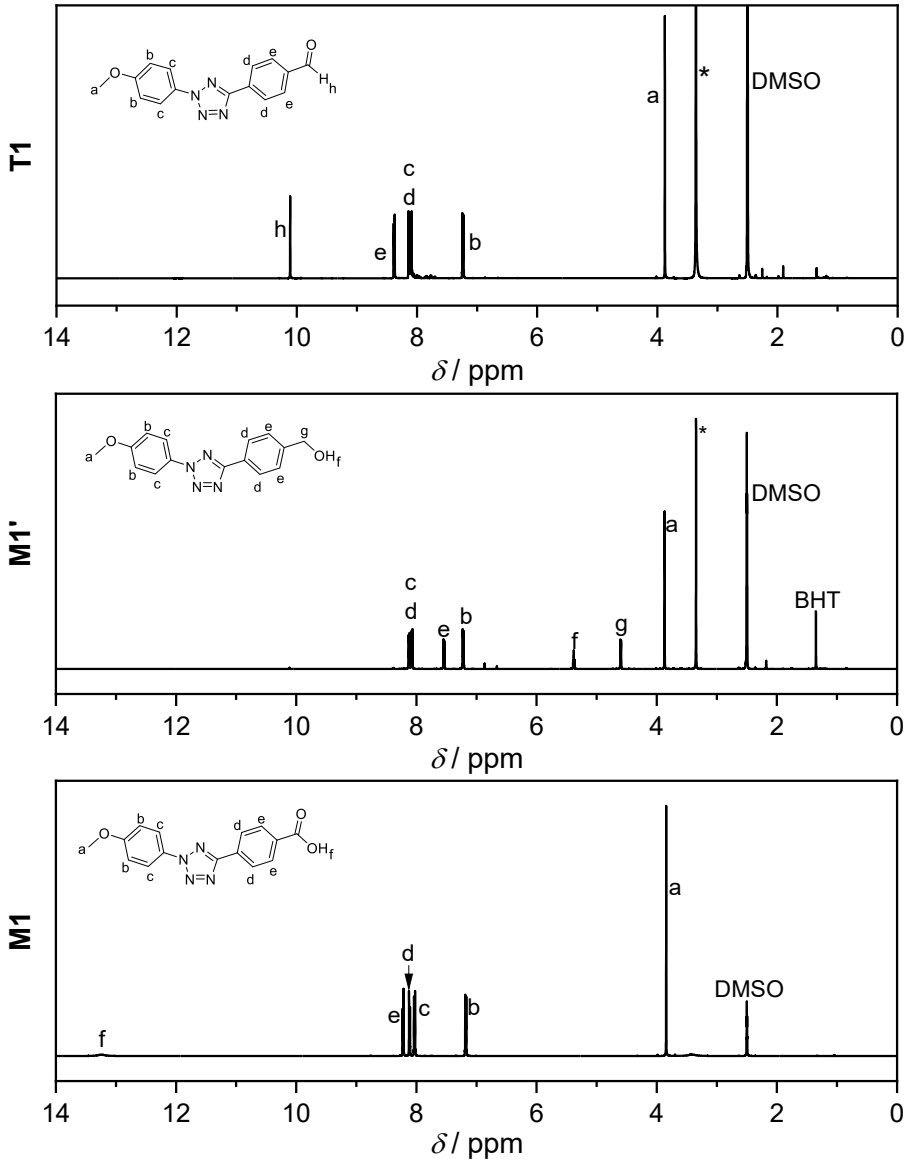

Figure 5.8: ^{1}H NMR (400 MHz) spectra of **M1**, **M1'** and **T1** in DMSO-d_6, respectively.

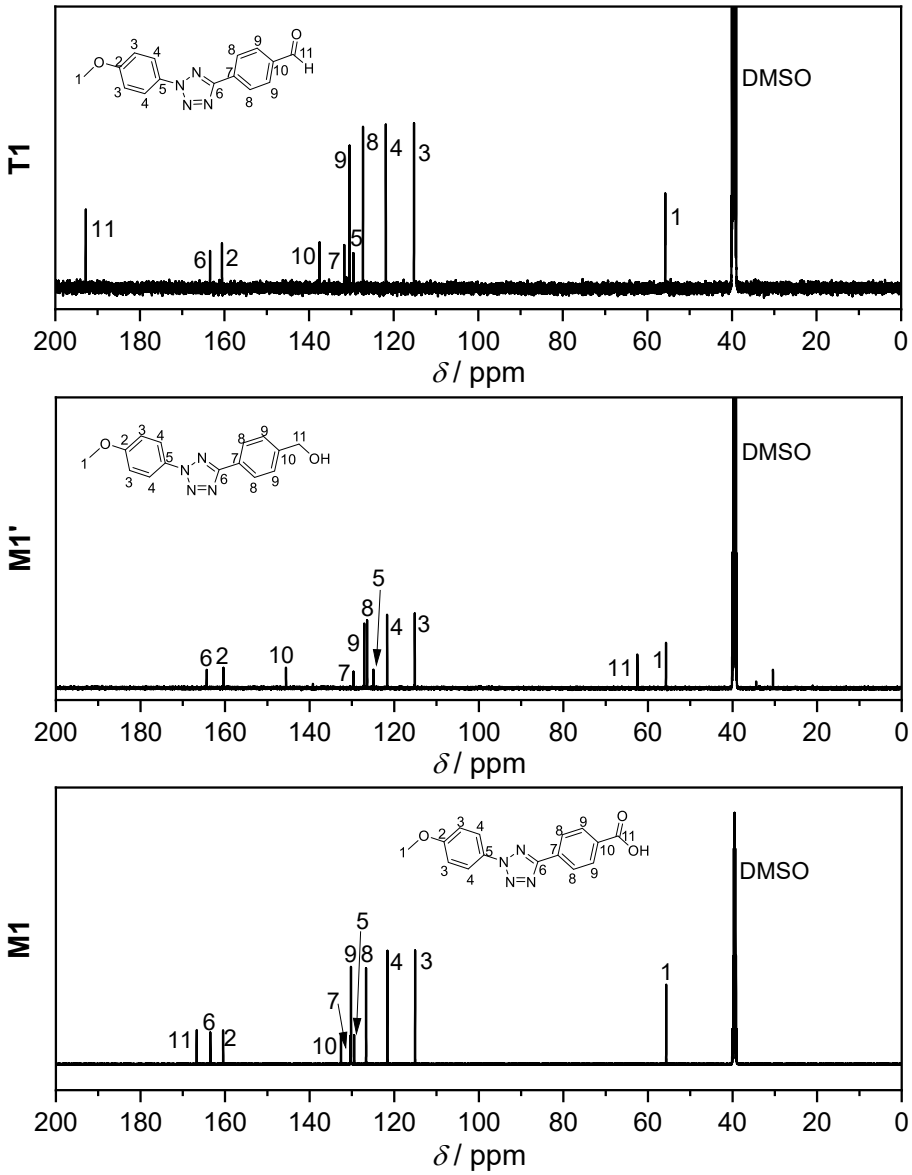

Figure 5.9: ^{13}C NMR (100 MHz) spectra of **M1**, **M1'** and **T1** in DMSO-d_6, respectively.

5.2.7.2 3-oxopropyl 4-(2-(4-methoxyphenyl)-2*H*-tetrazol-5-yl)benzoate (**T2**)

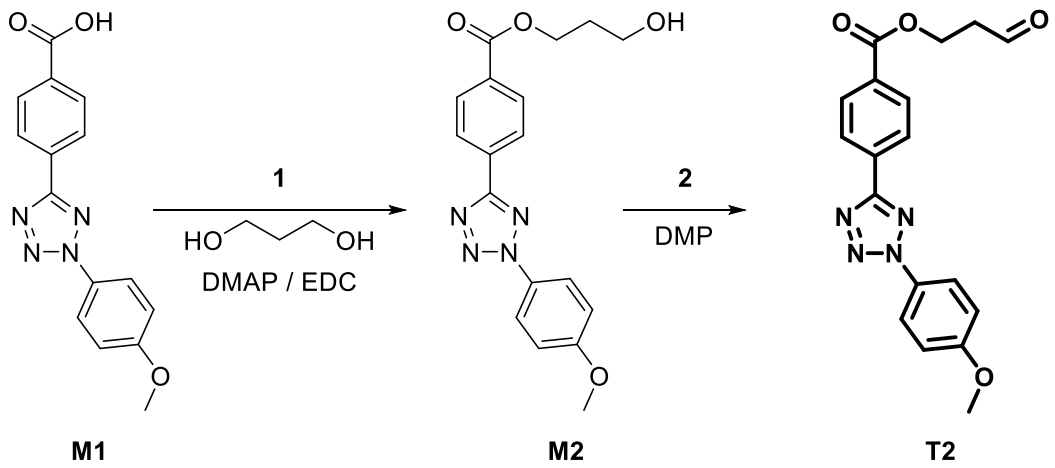

Step 1: Under anhydrous conditions, 0.5926 g **M1** (2.00 mmol, 1.00 eq.) and 0.0489 g DMAP (0.40 mmol, 0.20 eq.) were dissolved in 20 mL dry THF and 5 mL dry DCM. After the addition of 1.45 mL 1,3-propanediol (1.5220 g, 20.00 mmol, 10.00 eq.), the reaction mixture was cooled to 0°C and 0.4601 g EDC (2.40 mmol, 1.20 eq.) were added. The reaction mixture was allowed to come to ambient temperature and was stirred for 22 h. Subsequently, the reaction mixture was washed with 50 mL 5 wt% HCl, $NaHCO_3$ and brine, respectively. The organic layer was dried over $MgSO_4$ and the solvent was removed under reduced pressure, yielding **M2** as pale pink solid (m = 0.51 g, 72%).

^{1}H NMR (400 MHz, $CDCl_3$) δ / ppm: 8.32 (d, 2H, *H*$_{arom}$), 8.18 (d, 2H, *H*$_{arom}$), 8.09 (d, 2H, *H*$_{arom}$), 7.05 (d, 2H, *H*$_{arom}$), 4.51 (t, 2H, -*CO*-*O*-*CH*$_2$-), 3.89 (m, 3H, *CH*$_3$-*O*-), 3.80 (t, 2H, *HO*-*CH*$_2$-), 2.03 (m, 2H, *HO*-*CH*$_2$-*CH*$_2$-).

^{13}C NMR (100 MHz, $CDCl_3$) δ / ppm: 166.54 (-*O*-*CO*-*C*$_q$-), 163.83 (-*N*-*C*$_q$-*C*$_q$-), 160.38 (*CH*$_3$-*O*-*C*$_q$-), 132.02 (-*N*-*C*$_q$-*C*$_q$-), 130.17 (-*N*-*C*$_q$-*CH*$_{arom}$-, -*C*$_q$-*CH*$_{arom}$-, -*O*-*CO*-*C*$_q$-), 126.72 (-*C*$_q$-*CH*$_{arom}$), 121.99 (-*C*$_q$-*CH*$_{arom}$-), 114.71 (-*C*$_q$-*CH*$_{arom}$-), 62.20 (*HO*-*CH*$_2$-), 59.06 (-*CO*-*O*-*CH*$_2$-), 55.61 (*CH*$_3$-*O*-), 31.47 (*HO*-*CH*$_2$-*CH*$_2$-).

Step 2: In a 25 mL round bottom flask, 0.5098 g **M2** (1.4386 mmol, 1.00 eq.) were dissolved in 11 mL dry DCM under N_2. Subsequently, 0.7320 g DMP (1.7263 mmol, 1.20 eq.) were added and the reaction mixture was stirred for 4 h at ambient temperature. After removal of the solvent, the residue was dissolved in 20 mL DCM and washed with 20 mL sat. $NaHCO_3$, brine

and H_2O, respectively. The organic layer was dried over $MgSO_4$ and the solvent was evaporated, giving **T2** as pale yellow solid (m = 0.4985, 98%).

^{1}H NMR (400 MHz, $CDCl_3$) δ / ppm: 9.89 (s, 1H, *H-CO-*), 8.32 (d, 2H, H_{arom}), 8.15 (d, 2H, H_{arom}), 8.10 (d, 2H, H_{arom}), 7.05 (d, 2H, H_{arom}), 4.71 (t, 2H, *-CO-O-*CH_2-), 3.89 (m, 3H, CH_3-*O-*), 2.96 (m, 2H, *H-CO-*CH_2-).

^{13}C NMR (100 MHz, $CDCl_3$) δ / ppm: 199.08 (*H-*CO-), 165.94 (*-O-CO-*C_q-), 163.83 (*-N-*C_q-C_q-), 160.17 (CH_3-*O-*C_q-), 131.50 (*-N-*C_q-C_q-), 130.47 (*-N-*C_q-CH_{arom}-, *-*C_q-CH_{arom}-, *-O-CO-*C_q-), 126.72 (-C_q-CH_{arom}), 121.47 (-C_q-CH_{arom}-), 114.50 (-C_q-CH_{arom}-), 59.06 (*-CO-O-*CH_2-), 55.83 (CH_3-*O-*), 42.87 (*H-CO-*CH_2-).

The detailed chemical assignment of the ^{1}H and ^{13}C NMR resonances can be found in Figure 6.12.

5.2.7.3 2-oxoethyl 4-(2-(4-methoxyphenyl)-2*H*-tetrazol-5-yl)benzoate (**T3**)

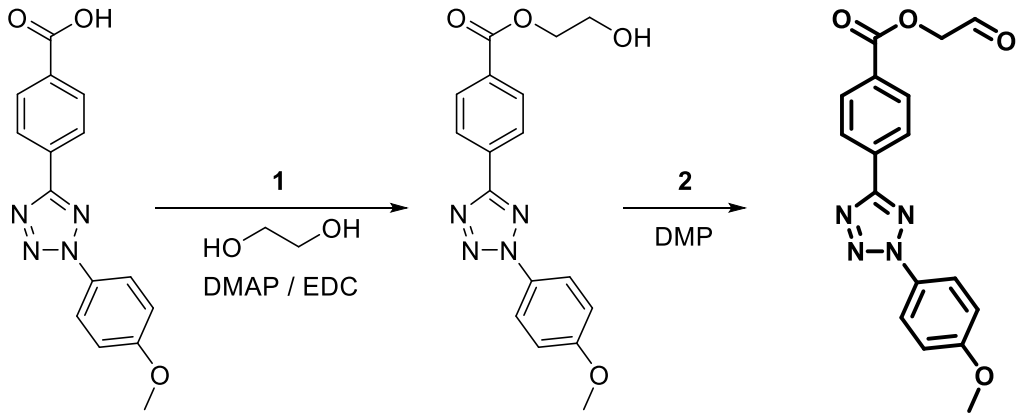

The synthesis of **T3** was conducted in a similar manner as for **T2** with 1,2-ethanediol instead of 1,3-propanediol.

After the first reaction step, **M3** was isolated as pale pink solid with a yield of 93 %.

^{1}H NMR (400 MHz, $CDCl_3$) δ / ppm: 8.35 (d, 2H, H_{arom}), 8.21 (d, 2H, H_{arom}), 8.09 (d, 2H, H_{arom}), 7.06 (d, 2H, H_{arom}), 4.52 (t, 2H, *-CO-O-*CH_2-), 4.00 (t, 2H, *HO-*CH_2-), 3.88 (m, 3H, CH_3-*O-*), 1.65 (m, 1H, *HO-*CH_2-).

^{13}C NMR (100 MHz, $CDCl_3$) δ / ppm: 166.25 (*-O-CO-*C_q-), 164.08 (*-N-*C_q-C_q-), 160.38 (CH_3-*O-*C_q-), 131.62 (*-N-*C_q-C_q-), 130.35 (*-N-*C_q-CH_{arom}-, *-*C_q-CH_{arom}-, *-O-CO-*C_q-), 126.88 (-C_q-CH_{arom}), 121.19 (-C_q-CH_{arom}-), 114.57 (-C_q-CH_{arom}-), 66.81 (CH_3-*O-*), 61.29 (*HO-*CH_2-), 55.89 (*HO-*CH_2-CH_2-).

The second reaction step yielded **T3** as yellow solid (76 %).

^{1}H NMR (400 MHz, $CDCl_3$) δ / ppm: 9.78 (s, 1H, *H-CO-CH$_2$-*), 8.36 (d, 2H, *H$_{arom}$*), 8.24 (d, 2H, *H$_{arom}$*), 8.10 (d, 2H, *H$_{arom}$*), 7.06 (d, 2H, *H$_{arom}$*), 5.29 (t, 2H, *-CO-O-CH$_2$-*), 3.92 (m, 3H, *CH$_3$-O-*).

^{13}C NMR ($CDCl_3$) δ / ppm: 195.65 (*H-CO-CH$_2$-*), 165.47 (*-O-CO-C$_q$-*), 164.29 (*-N-C$_q$-C$_q$-*), 160.73 (*CH$_3$-O-C$_q$-*), 132.11 (*-N-C$_q$-C$_q$-*), 130.55 (*-N-C$_q$-CH$_{arom}$-*, *-C$_q$-CH$_{arom}$-*, *-O-CO-C$_q$-*), 127.08 (*-C$_q$-CH$_{arom}$*), 121.19 (*-C$_q$-CH$_{arom}$-*), 114.65 (*-C$_q$-CH$_{arom}$-*), 69.10 (*CH$_3$-O-*), 55.73 (*H-CO-CH$_2$-*).

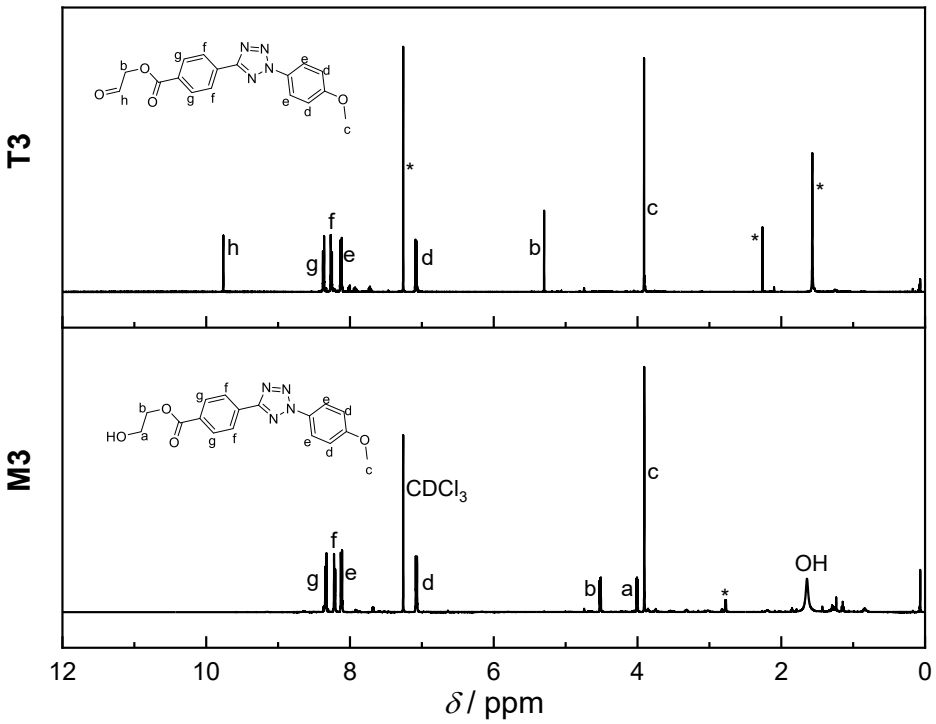

Figure 5.10: ^{1}H NMR (400 MHz) spectra of **M3** and **T3** in $CDCl_3$.

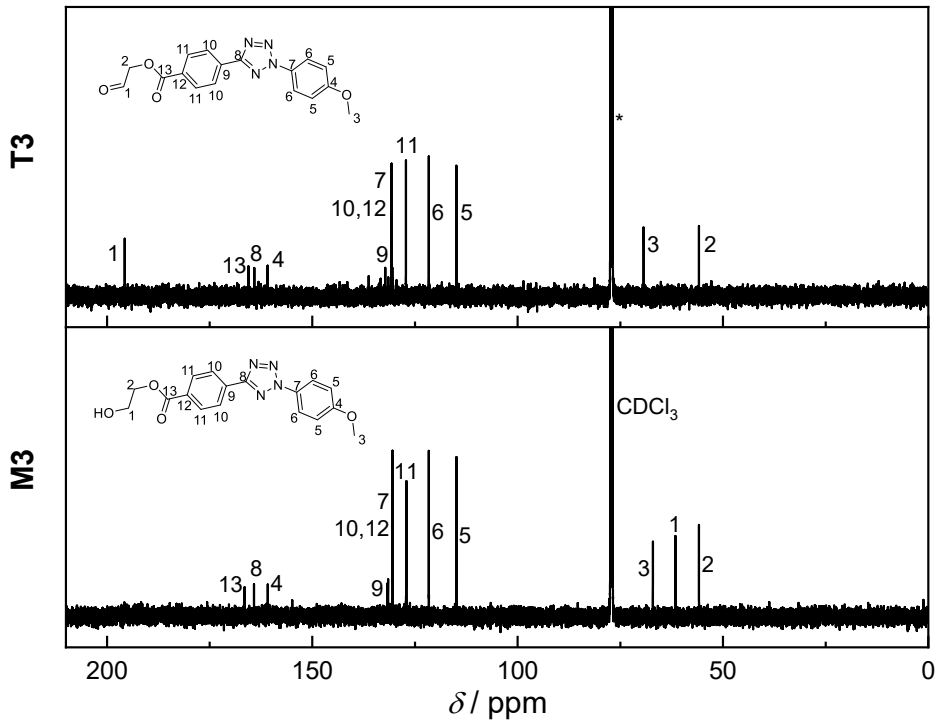

Figure 5.11: ^{13}C NMR (100 MHz) spectra of **M3** and **T3** in $CDCl_3$.

5.2.7.4 11-oxoundecyl 4-(2-(pyren-1-yl)-2*H*-tetrazol-5-yl)benzoate (**T5**)

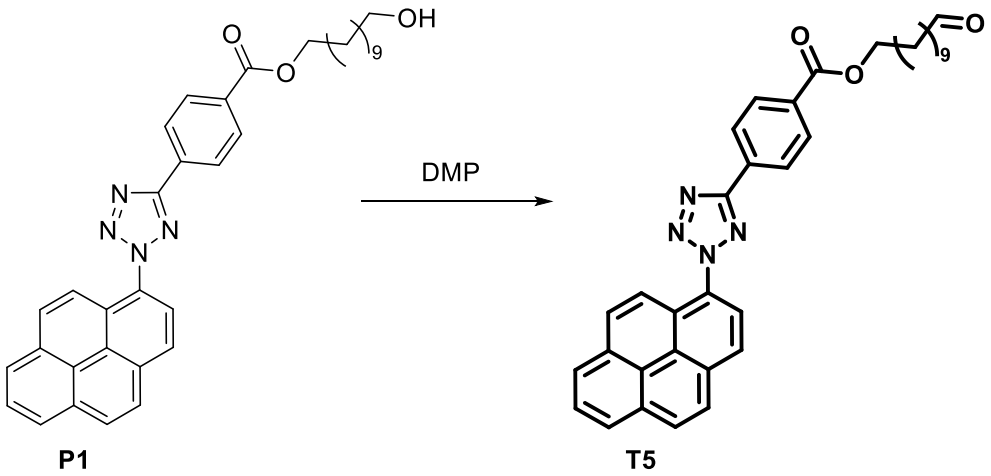

Under anhydrous conditions, 0.50 g **P1** (0.8917 mmol, 1.00 eq.) were dissolved in 6.5 mL dry DCM. Subsequently, 0.4538 g DMP (1.0700 mmol, 1.20 eq.) were added and the reaction mixture was stirred at ambient temperature for 5 h. After washing with $NaHCO_3$, NaCl and H_2O (20 mL each), the organic layer was dried over $MgSO_4$ and the solvent was evaporated. The product **T5** was obtained as red sticky material (m = 0.43 g, 86 %).

^{1}H NMR (400 MHz, DMSO) δ / ppm: 9.66 (s, 1H, *H-CO-CH$_2$-*), 8.61-7.74 (m, 13H, *H$_{arom}$-*), 4.31 (t, 2H, *-CO-O-CH$_2$-*), 1.73 (m, 2H, *-CO-O-CH$_2$-CH$_2$-*), 1.50 (m, 2H, *H-CO-CH$_2$-*), 1.42 (m, 4H, *HCO-O-CH$_2$-CH$_2$-*, *-CO-O-(CH$_2$)$_2$-CH$_2$-*), 1.28 (m, 10H, *-HCO-(CH$_2$)$_2$-(CH$_2$)$_5$-(CH$_2$)$_3$-O-*).

^{13}C NMR (100 MHz, DMSO) δ / ppm: 204.02 (*H-CO-CH$_2$-*), 165.42 (*-C$_q$-CO-O-*), 163.80 (*-N-C$_q$-C$_q$-*), 136.41-124.01 (*-C$_q$-CH$_{arom}$-*, *-C$_q$-C$_q$-*, *-N-C$_q$-*, *-N-C$_q$-C$_q$-*, *-O-CO-C$_q$-*), 55.16 (*-CO-O-CH$_2$-*), 43.04 (*HCO-CH$_2$-*), 32.85 (*-CO-O-CH$_2$-CH$_2$-*), 28.39 (*HCO-(CH$_2$)$_2$-(CH$_2$)$_4$-*), 25.23 (*-CO-O-(CH$_2$)$_3$-CH$_2$-*), 21.31 (*HCO-CH$_2$-CH$_2$-*), 19.82 (*-CO-O-(CH$_2$)$_2$-CH$_2$-*).

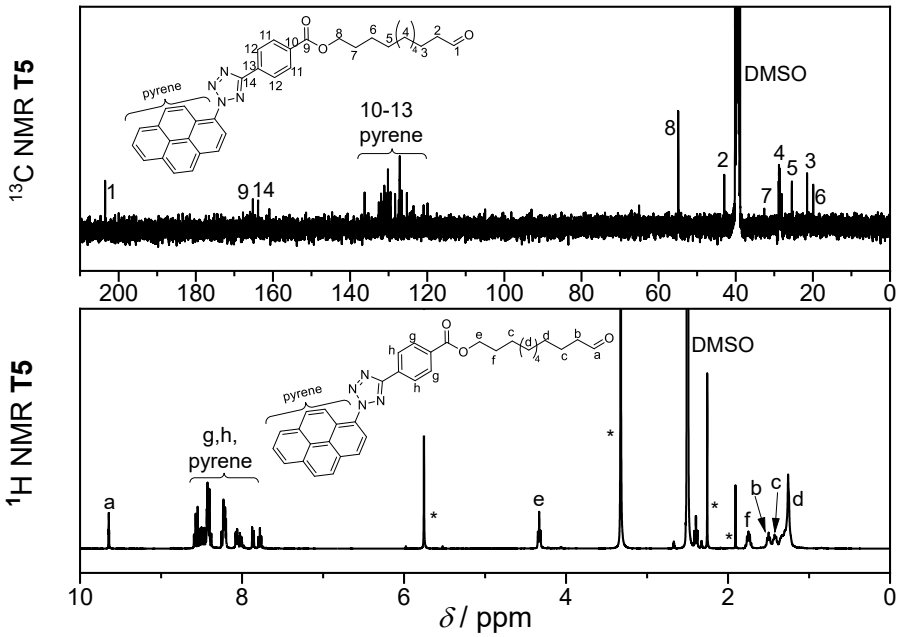

Figure 5.12: ^{1}H NMR (400 MHz) and ^{13}C NMR (100 MHz) spectra of **T5** in DMSO-d$_6$.

5.2.8 Passerini-MCP

5.2.8.1 General Procedure for the P-MCP

In a small crimp vial, 1.00 eq. of the bi-functional carboxylic acid and up to 3.00 eq. of the mono-functional aldehyde derivative were dissolved in a dry solvent (as stated in the respective synthesis procedures) with a concentration of c = 1 mmol mL^{-1} regarding the bi-functional carboxylic acid component. Subsequently, the reaction mixture was purged with N_2 for 5 min before adding 1.00 eq. DICH. The reaction mixture was purged again for 5 min with N_2 and then put in a pre-heated oil bath at 45°C (unless stated otherwise). Once the reaction was stopped, the reaction mixture was diluted with the smallest amount of solvent and

precipitated into ice cold MeOH. Drying of the residue under reduced pressure or in the vacuum oven yielded the respective products.

5.2.8.2 Synthesis of the Tetrazole-Polymer **TP1**

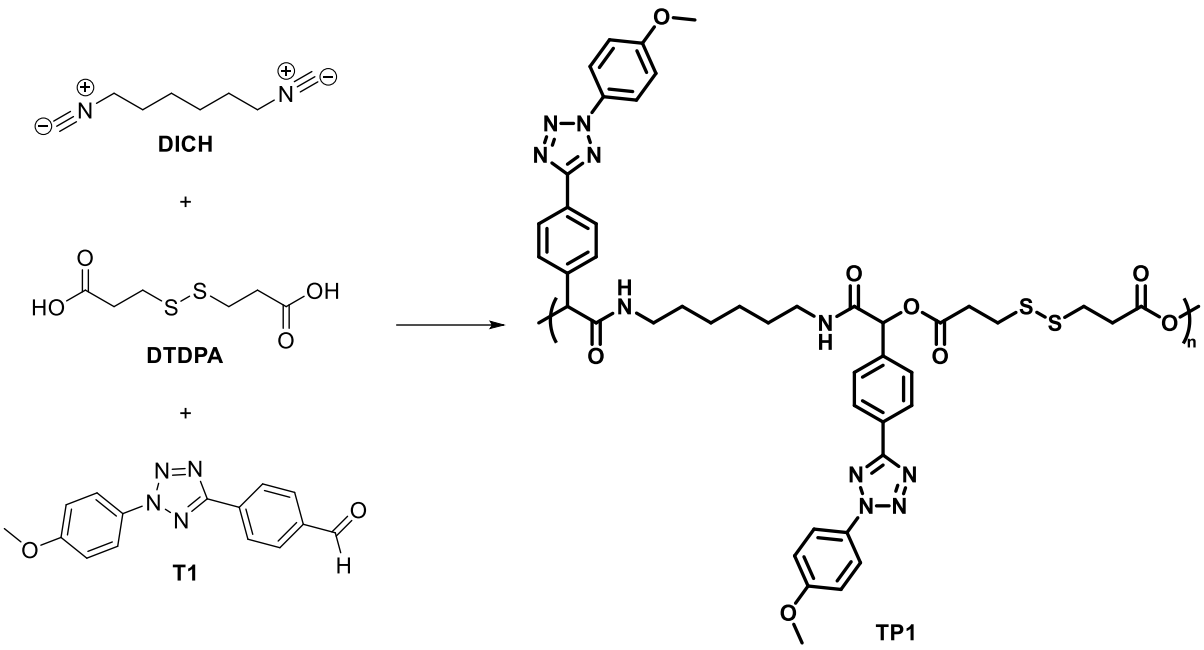

The synthesis of **TP1** was conducted according to the general procedure for the P-MCP with a ratio of DICH / DTDPA / **T1** 1 : 1 : 2.20 in DCM at 40°C. After 7 days, the reaction was stopped and precipitation into ice cold MeOH resulted in a light brown oily material.
SEC (THF): M_n = 1 200 g mol^{-1}, $Đ$ = 1.20 (Figure 6.11).

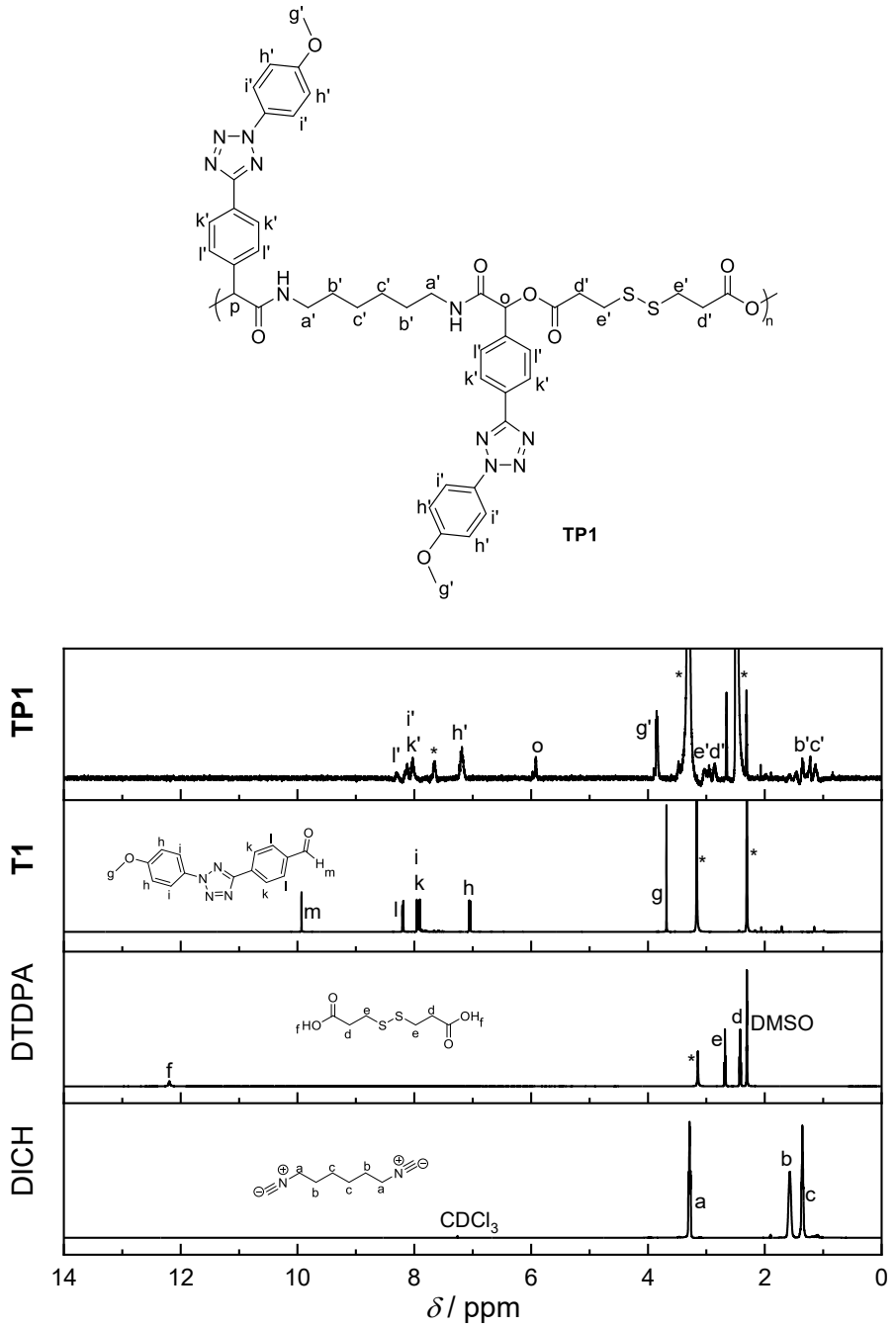

Figure 5.13: ^{1}H NMR (400 MHz) spectra of DICH in $CDCl_3$ and DTDPA, **T1** and **TP1** in DMSO-d_6, respectively.

5.2.8.3 Synthesis of the Tetrazole-Polymer **TP2**

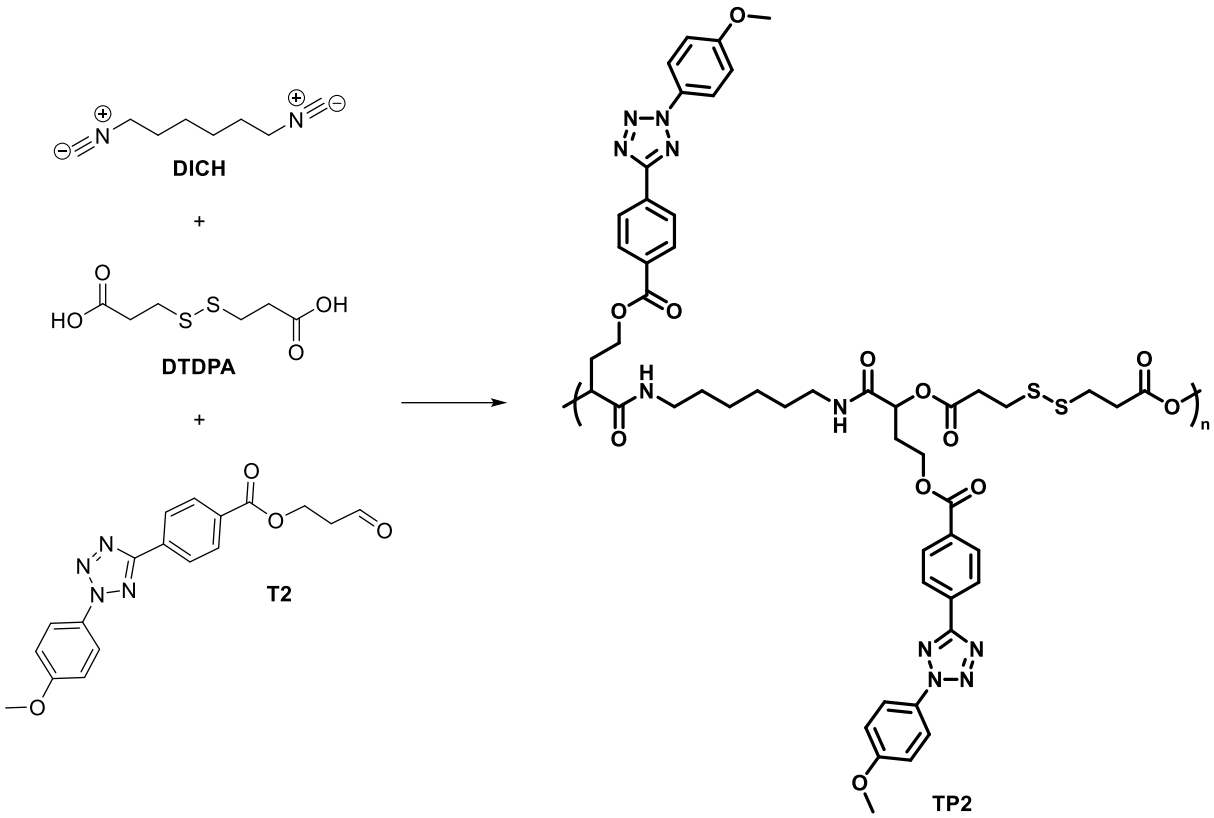

For the synthesis of **TP2**, several attempts with varying solvents and reaction times have been conducted as described in the general procedure for the P-MCP. The respective parameters and obtained values from SEC analysis (Figure 6.13) are collated in Table 5.1.

Table 5.1: Overview of the reaction conditions for the synthesis of **TP2** along the M_n and $Đ$ values for the respective entries obtained via SEC analysis (Figure 6.13). *Reaction conducted in the microwave.

Entry	solvent	ratio CHO / COOH / NC	reaction time	M_n [g mol^{-1}]	$Đ$
1a	DCM	3 : 1 : 1	24 h	1 200	1.17
1b	DCM	3 : 1 : 1	72 h	1 700	1.11
1c	DCM	3 : 1 : 1	6 d	1 100	1.28
2a	$CHCl_3$	3 : 1 : 1	3 d	2 000	1.93
2b	$CHCl_3$	2.25 : 1 : 1	6 d	1 700	1.05
2c*	$CHCl_3$	2 : 1 : 1	40 h	1 300	1.27
3a	$CHCl_3$ / THF	2.25 : 1 : 1	24 h	1 600	1.14
3b	$CHCl_3$ / THF	2.25 : 1 : 1	48 h	1 000	1.15
3c	$CHCl_3$ / THF	3 : 1 : 1	6 d	2 000	1.13
3d	$CHCl_3$ / THF	3 : 1 : 1	11 d	2 000	1.17
4a	Polarclean	2 : 1 : 1	24 h	1 300	1.10
4b	Polarclean	2 : 1 : 1	6 d	800	1.11
5	toluene / DCM	2.25 : 1 : 1	4 d	2 600	1.77
6	toluene / DMSO	2.25 : 1 : 1	1 d	2 300	1.03
7	1,2-dichlorobenzene	2.25 : 1 : 1	6 d	1 600	1.19

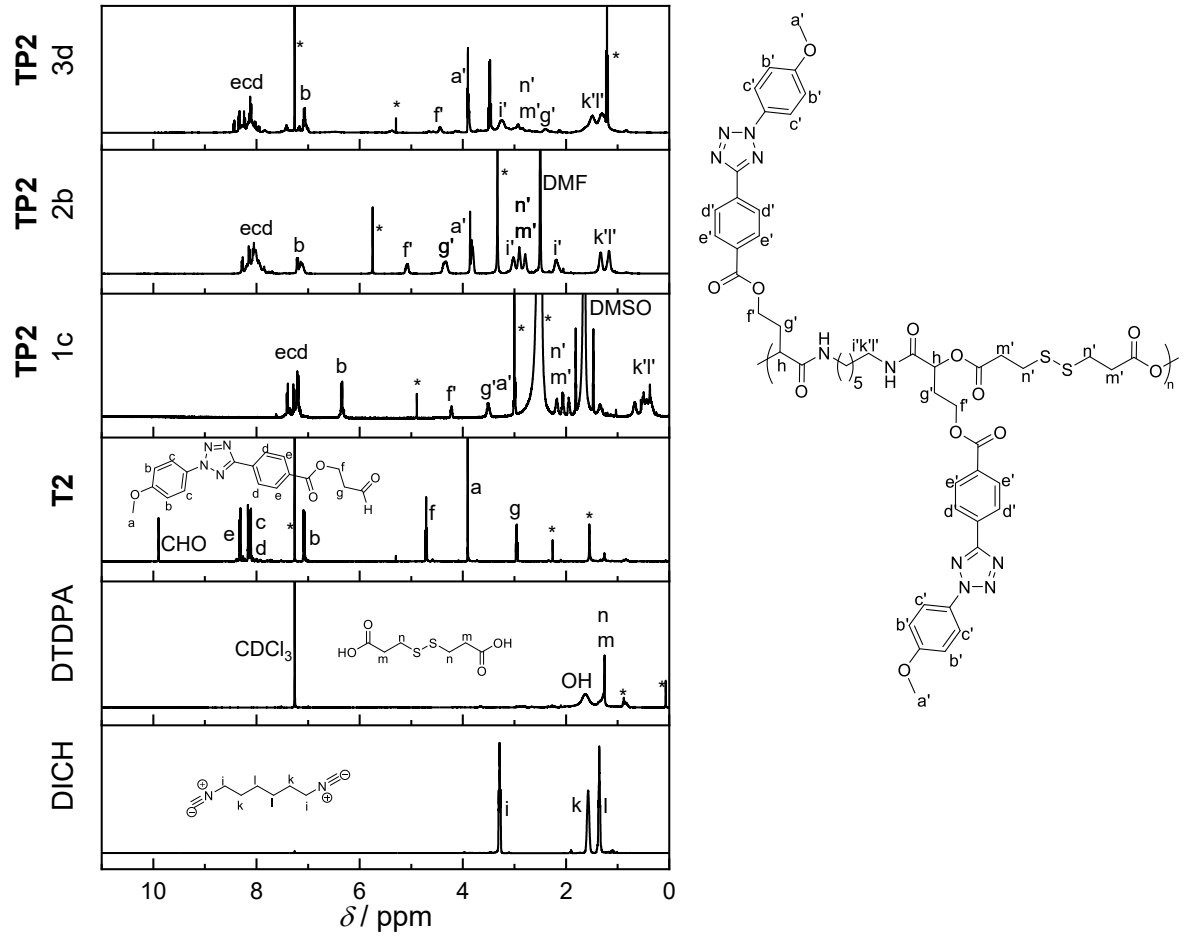

Figure 5.14: ^{1}H NMR (400 MHz) spectra of the starting materials applied for the synthesis of **TP2** and exemplary spectra of **TP2**. The spectra of DICH, CDTDPA, **T2** and entry 3d were recorded in $CDCl_3$, the spectrum of entry 1c in DMSO-d_6 and the one of entry 2b in DMF-d_7.

5.2.8.4 Synthesis of the Tetrazole-Polymers **TP3**-**TP4**

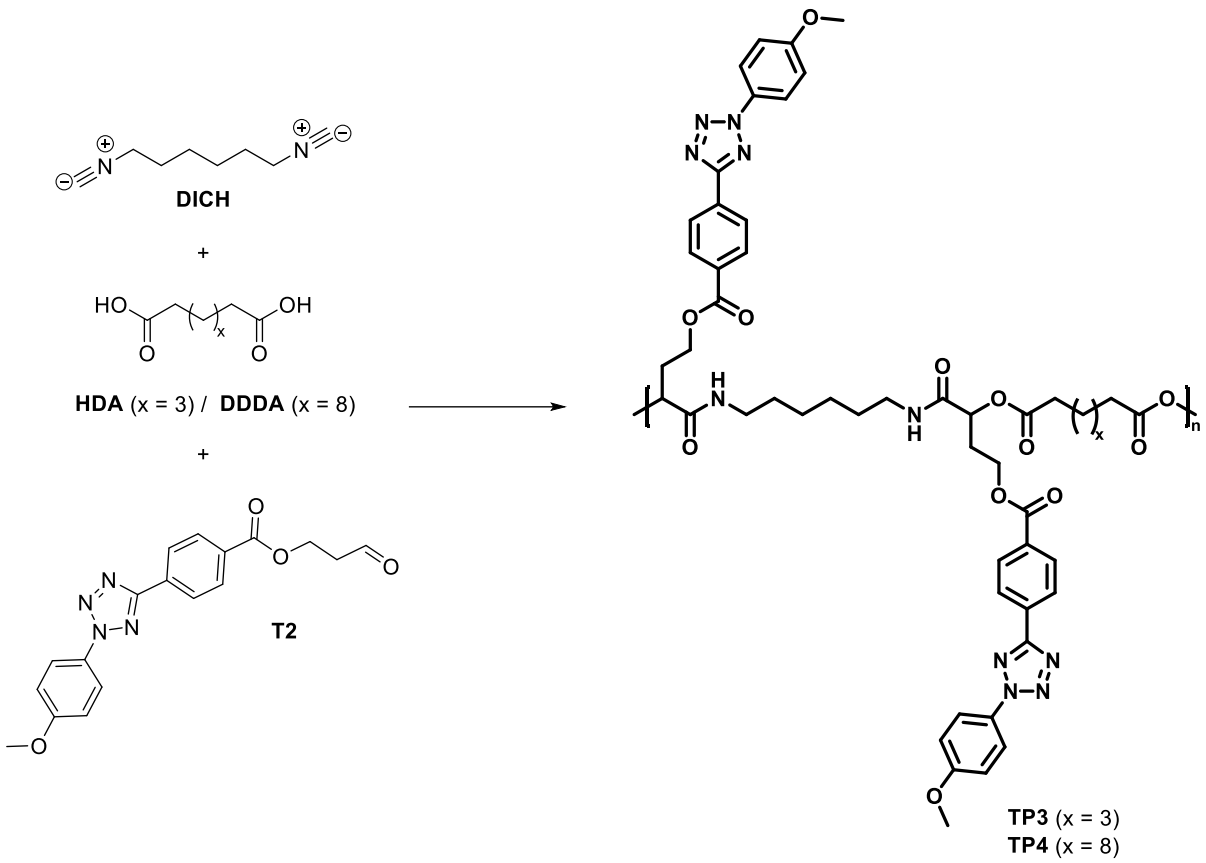

The reaction for the synthesis of **TP3** and **TP4** were conducted according to the general procedure for the P-MCP with either HDA or DDDA as bi-functional carboxylic acid. In both reactions, $CHCl_3$ was used as solvent with a ratio of the starting materials **T2** / DICH / -COOH 2 : 1 : 1. The reaction of **TP3** was stopped after 5 d, while the reaction of **TP4** was stopped after 4 d.

SEC (THF): M_n (**TP3**) = 2 800 g mol^{-1}, $Đ$ (**TP3**) = 1.53 (Figure 6.15).

M_n (**TP4**) = 4 100 g mol^{-1}, $Đ$ (**TP4**) = 1.84 (Figure 6.15).

5.2.8.5 Synthesis of the Tetrazole-Polymer **TP5**

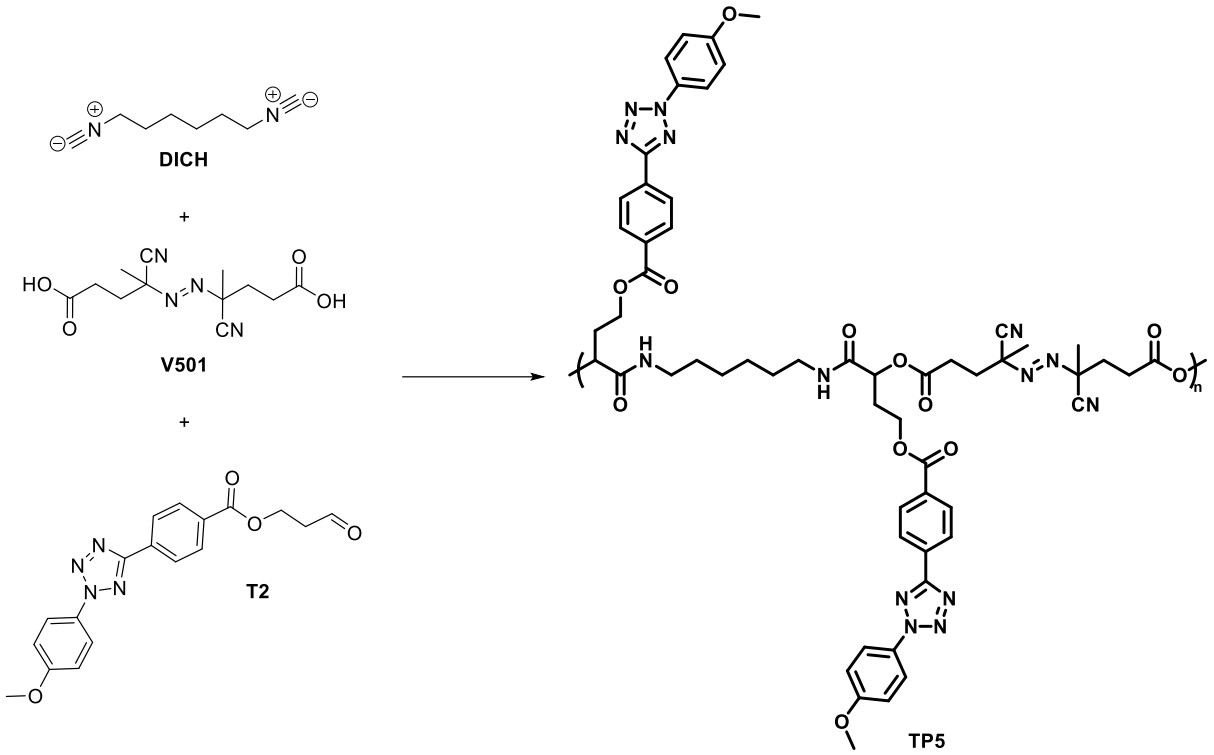

The tetrazole-polymer **TP5** was synthesised as described in the general reaction procedure for the P-MCP in $CHCl_3$ with a ratio of **T2** / DICH / V-501 2 : 1 : 1. The reaction was stopped after 2 d.

SEC (DMAc): M_n = 2 000 g mol^{-1}, $Đ$ = 1.16 (Figure 6.15).

5.2.8.6 Synthesis of the Azo-Polymer **AP1**

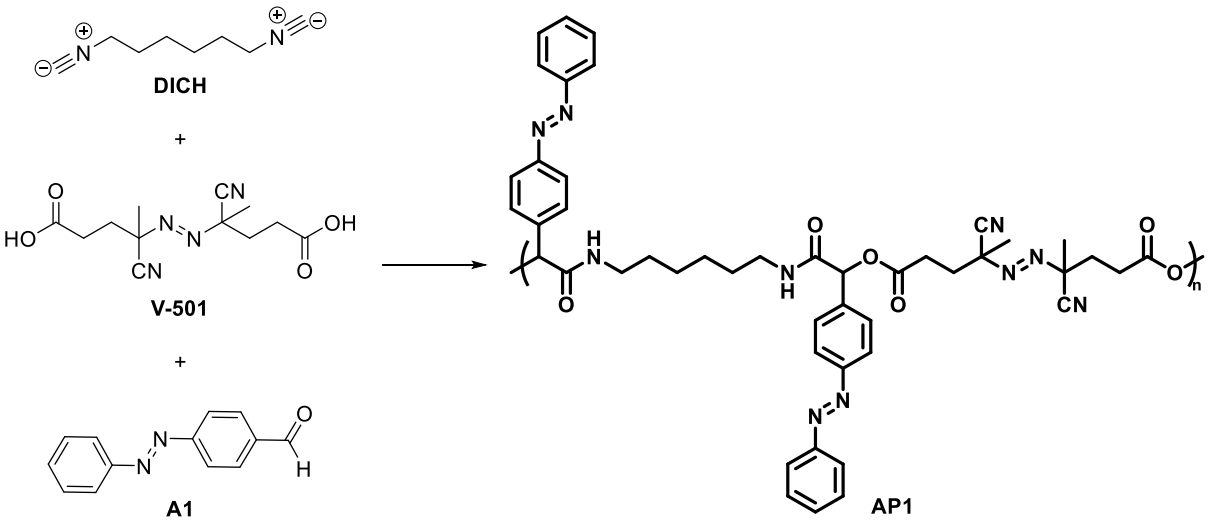

According to the general reaction procedure for the P-MCP, 2.00 eq. **A1**, 1.00 eq. DICH and 1.00 eq. V-501 were dissolved in 0.2 mL $CHCl_3$. After 1 h, 0.07 mL THF were added to increase the solubility of the reaction mixture. The reaction was stopped after 3 d and precipitated into ice cold MeOH. After letting the precipitate rest for 18 h at -22°C, the residue was decanted and the desired polymer **AP1** was obtained.

SEC (DMAc): M_n = 13 500 g mol^{-1}, $Đ$ = 1.26 (Figure 6.16).

^{1}H NMR (400 MHz, $CDCl_3$) δ / ppm: 7.89 (m, 8H, *H$_{arom}$*-), 7.59 (m, 4H, *H$_{arom}$*-), 7.44 (m, 4H, *H$_{arom}$*-), 7.24 (m, 2H, *H$_{arom}$*-), 6.91 (m, 2H, *-CO-NH-*), 6.10 (m, 2H, *-NH-CO-CH-O-*), 3.18 (m, 4H, *-CO-NH-CH$_2$-*), 2.92-1.97 (m, 8H, *-O-CO-(CH$_2$)$_2$-C$_q$-*), 1.75-0.72 (m, 14H, *-CO-NH-CH$_2$-(CH$_2$)$_2$-*, *-C$_q$-CH$_3$*).

The ^{1}H NMR spectrum is depicted in Figure 6.17.

5.2.9 Passerini-MCR

5.2.9.1 General Procedure for the P-MCR

In a small crimp vial, 1.00 eq of MAA and 1.00 eq. of the tetrazole-aldehyde were dissolved in a suitable solvent (e.g. DCM, $CHCl_3$, c = 1 mmol mL^{-1}). Subsequently, the crimp vial was sealed and the reaction mixture was purged with N_2 for 5 min. Then, 1.00 eq. PIC were added and the mixture was purged with N_2 for 5 additional min. Afterwards, the reaction mixture was stirred at 45°C, either on a conventional heating plate or in the microwave. Once the reaction

as stopped, the mixture was diluted with DCM and washed with NaCl and H_2O, respectively. The organic layer as dried over $MgSO_4$ and removal of the solvent under reduced pressure yielded the respective product.

5.2.9.2 Synthesis of the Tetrazole-Derivative **T4**

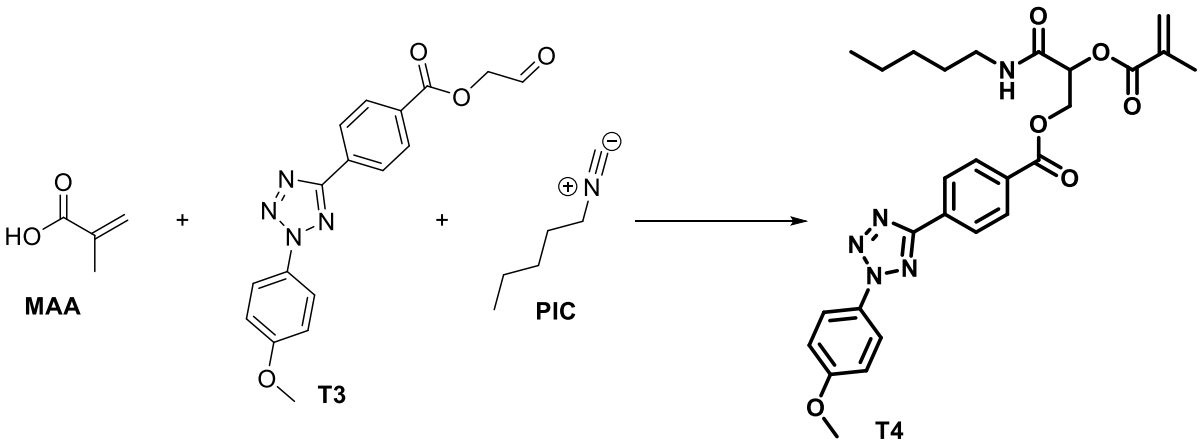

The first attempt was conducted according to the general procedure for the P-MCR on a conventional heating plate in DCM. After a reaction time of 40 h at 45°C on a conventional heating plate, **T4** was obtained as dark brown solid with a yield of 30 %.

In a second attempt, the reaction was repeated under similar conditions in the microwave at 45°C and a reaction time of 18 h in $CHCl_3$, yielding **T4** as yellow solid (65 %).

^{1}H NMR (400 MHz, $CDCl_3$) δ / ppm: 8.30 (d, 2H, *H$_{arom}$*), 8.13 (m, 4H, *H$_{arom}$*), 7.05 (d, 2H, *H$_{arom}$*), 6.19 (m, 1H, *CH$_3$-C$_q$-CH$_2$-*), 5.70 (m, 1H, *CH$_3$-C$_q$-CH$_2$-*), 5.64 (m, 1H, *-CO-O-CH-*), 4.89 (m, 1H, *-CO-O-CH-CH$_2$-*), 4.76 (m, 1H, *-CO-O-CH-CH$_2$-*), 3.89 (s, 3H, *CH$_3$-O-*), 3.31 (m, 2H, *-CO-NH-CH$_2$-*), 1.96 (m, 3H, *CH$_3$-C$_q$-CO-O-*), 1.57 (m, 2H, *-NH-CH$_2$-CH$_2$-*), 1.30 (m, 4H, *CH$_3$-(CH$_2$)$_2$-*), 0.87 (m, 3H, *CH$_3$-(CH$_2$)$_4$-*).

^{13}C NMR (100 MHz, $CDCl_3$) δ / ppm: 166.74 (*-NH-CO-CH-*), 165.58 (*-O-CO-C$_q$-CH$_3$*), 164.19 (*-C$_q$-CO-O-CH$_2$-*, *-N-C$_q$-C$_q$-*), 160.89 (*CH$_3$-O-C$_q$-*, *-C$_q$-CO-O-*), 135.58 (*-N-C$_q$-C$_q$-*), 131.55 (*CH$_3$-C$_q$-CO-O-*), 130.62 (*-C$_q$-CH$_{arom}$-*), 130.31 (*-N-C$_q$-CH$_{arom}$-*), 127.33 (*CH$_3$-C$_q$-CH$_2$-*), 127.02 (*-C$_q$-CH$_{arom}$*), 121.40 (*-C$_q$-CH$_{arom}$-*), 114.61 (*-C$_q$-CH$_{arom}$*), 71.98 (*-CO-O-CH-CH$_2$-*), 63.99 (*-CO-O-CH-CH$_2$-*), 55.74 (*CH$_3$-O-*), 39.46 (*-CO-NH-CH$_2$-*), 29.57 (*-CO-NH-CH$_2$-CH$_2$-*), 28.80 (*-CO-NH-(CH$_2$)$_2$-CH$_2$-*), 22.33 (*CH$_3$-CH$_2$-*), 18.45 (*CH$_3$-C$_q$-CO-O-*), 14.03 (*CH$_3$-CH$_2$-*).

The ^{1}H NMR spectrum is depicted in Figure 3.8, the ^{13}C NMR spectrum in Figure 6.18.

5.2.9.3 Synthesis of the Tetrazole-Derivative **T6**

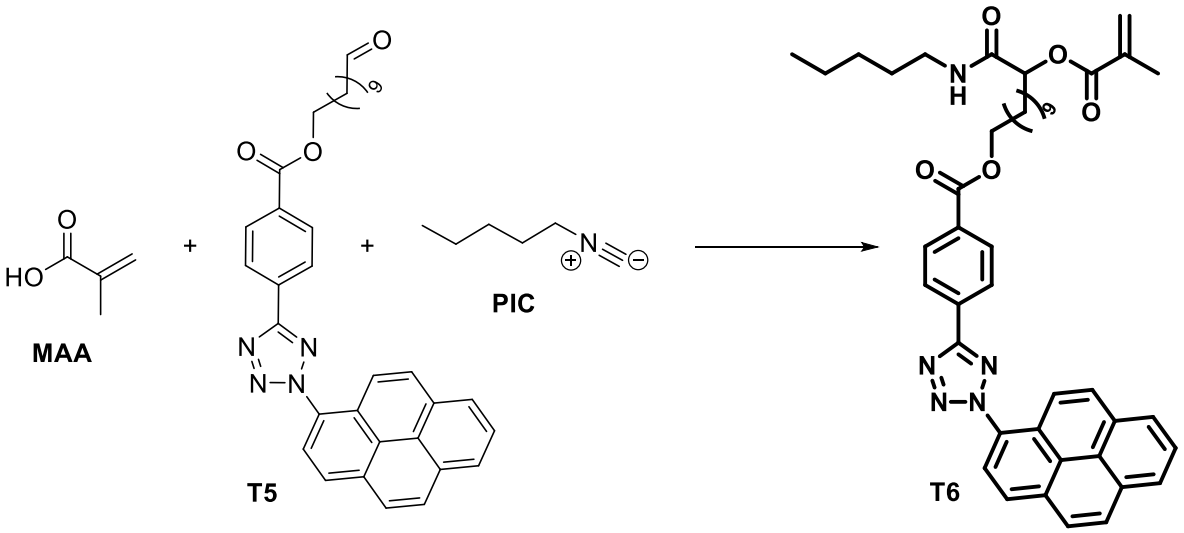

The reaction was conducted as described in the general reaction procedure for the P-MCR in the microwave at 45°C in $CHCl_3$. After 20 h, the reaction was stopped and **T6** was obtained as dark red-brown solid (79 %).

^{1}H NMR (400 MHz, $CDCl_3$) δ / ppm: 8.48-7.80 (m, 9H, *H$_{arom}$*-), 7.39 (m, 2H, *H$_{arom}$*-), 7.14 (m, 2H, *H$_{arom}$*-), 6,17 (m, 1H, *CH$_3$-C$_q$-CH$_2$*), 6.01 (m, 1H, *-CO-O-CH-CH$_2$-*), 5.67 (m, 1H, *CH$_3$-C$_q$-CH$_2$-*), 5.23 (m, 2H, *-CO-O-CH$_2$-CH$_2$-*), 4.37 (m, 2H, *-CO-O-CH$_2$-CH$_2$-*), 3.26 (m, 2H, *-CO-NH-CH$_2$-*), 1.98 (s, 3H, *CH$_3$-C$_q$-CH$_2$*), 1.80 (m, 2H, *-O-CH-CH$_2$-*), 1.47 (m, 2H, *-NH-CH$_2$-CH$_2$-*), 1.31 (m, 18H, *CH$_3$-(CH$_2$)$_2$-*, *-O-CH-CH$_2$-(CH$_2$)$_7$-*), 0.86 (m, 3H, *CH$_3$-(CH$_2$)$_4$-*).

^{13}C NMR (100 MHz, $CDCl_3$) δ / ppm: 169.67 (*-CH-CO-NH-*), 166.07 (*CH$_3$-C$_q$-CO-O-*), 164.57 (*-C$_q$-CO-O-CH$_2$-*), 161.34 (*-N-C$_q$-C$_q$-*), 141.79 (*-CH$_{arom}$-C$_q$-CO-*, *-N-C$_q$-CH$_{arom}$-*), 136.15 (*CH$_3$-C$_q$-CO-O-*, *-N-C$_q$-C$_q$-*), 133.29-121.32 (*CH$_3$-C$_q$-CH$_2$*, *-C$_q$-CH$_{arom}$-*, *-C$_q$-C$_q$-*, *-C$_q$-CH$_{arom}$-*), 74.46 (*-CO-O-CH-CH$_2$-*), 65.59 (*-CO-O-CH$_2$-CH$_2$-*), 39.36 (*-CO-NH-CH$_2$-*), 38.04 (*-CO-NH-CH$_2$-CH$_2$*), 32.11 (*-CO-O-CH$_2$-CH$_2$-*), 30.83 (*-O-CH-CH$_2$-*), 29.21 (*-O-CH-(CH$_2$)$_2$-(CH$_2$)$_5$-*, *CH$_3$-CH$_2$-CH$_2$-*), 26.31 (*-CO-O-(CH$_2$)$_2$-CH$_2$-*), 24.86 (*-O-CH-CH$_2$-CH$_2$-*), 22.71 (*CH$_3$-CH$_2$-*), 18.48 (*CH$_3$-C$_q$-CH$_2$*), 14.21 (*CH$_3$-(CH$_2$)$_4$-*).

The ^{1}H and ^{13}C NMR spectra are shown in Figure 3.9.

5.2.10 RAFT-Polymerization

5.2.10.1 General procedure for the RAFT polymerization

Under anhydrous conditions, 1.00 eq. of the tetrazole derivative, 7.00 eq. MMA and 0.5 eq. DTMP were dissolved in dry 1,4-dioxane (c = 1 mmol mL^{-1}). Subsequently, 0.06 eq. AIBN (from a stock solution in dry 1,4-dioxane with a concentration of c = 1 mg mL^{-1}) were added and the reaction mixture was purged with N_2 for 10 min. The reaction mixture was put in a pre-heated oil bath at 90°C and stirred for 2 h. Afterwards, the reaction was cooled to ambient temperature and the solvent was removed under reduced pressure. The residue was dissolved in a small amount of 1,4-dioxane and precipitated into ice cold MeOH. Finally, the respective polymers were obtained by filtration or centrifugation.

5.2.10.2 RAFT-Polymer **RP1**

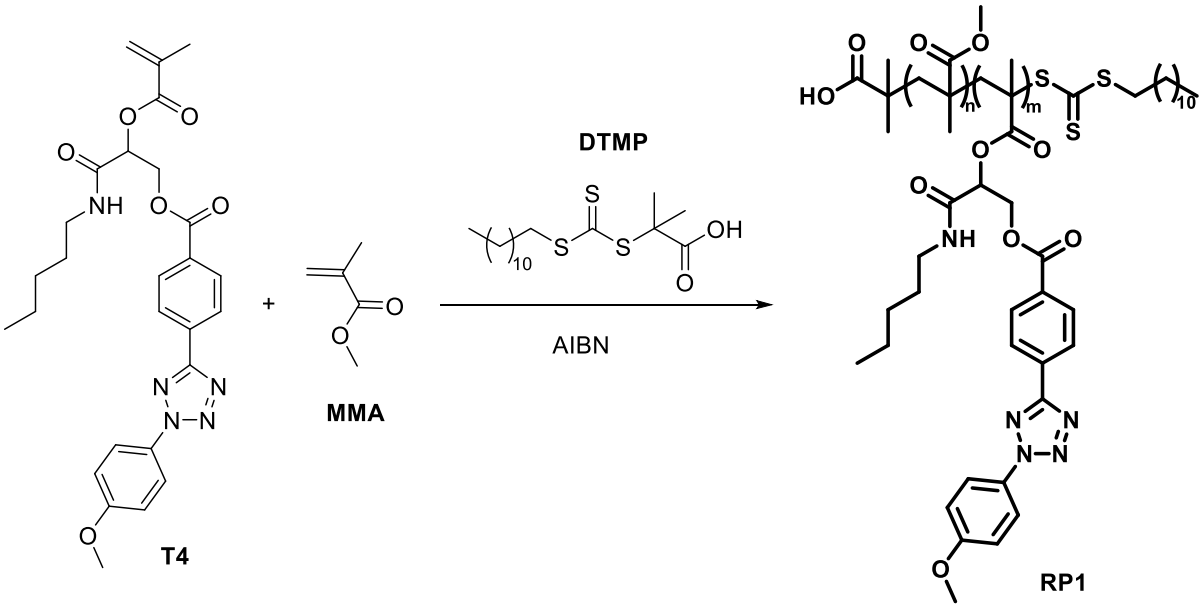

The reaction was conducted as described in the general reaction procedure for the RAFT polymerization with **T4** as tetrazole-derivative. After purification, the desired RAFT-polymer **RP1** was obtained as slightly yellow powder.

SEC (THF): M_n = 12 700 g mol^{-1}, $Đ$ = 1.22 (Figure 6.21).

^{1}H NMR (400 MHz, $CDCl_3$) δ / ppm: 8.23 (d, 2H, *H*$_{arom}$), 8.03 (m, 4H, *H*$_{arom}$), 6.99 (d, 2H, *H*$_{arom}$), 6.11 (m, 1H, -*CO-O-CH-*), 5.38 (m, 1H, -*CO-O-CH-CH$_2$-*), 4.69 (m, 1H, -*CO-O-CH-CH$_2$-*), 3.81 (m, 2H, -S-*CH$_2$-CH$_2$-*), 3.53 (s, 6H, *CH$_3$-O-*, *CH$_3$-O-CO-*), 3.23 (m, 2H, -*CO-NH-CH$_2$-*), 2.16-1.70 (m, 6H,

C<u>H</u>₃-C$_q$-CO-O-), 1.57 (m, 2H, *-NH-CH₂-C<u>H</u>₂-*), 1.40-1.01 (m, 28H, *CH₃-(C<u>H</u>₂)₂-*, *-(C<u>H</u>₂-C$_q$)$_n$-*), 0.92 (m, 6H, *HO-CO-C$_q$-(C<u>H</u>₃)₂-*), 0.74 (m, 6H, *C<u>H</u>₃-(CH₂)₄-*, *C<u>H</u>₃-(CH₂)₁₁-S-*).

The detailed assignment of the chemical shifts can be found in Figure 6.22.

5.2.10.3 RAFT-Polymer **RP2**

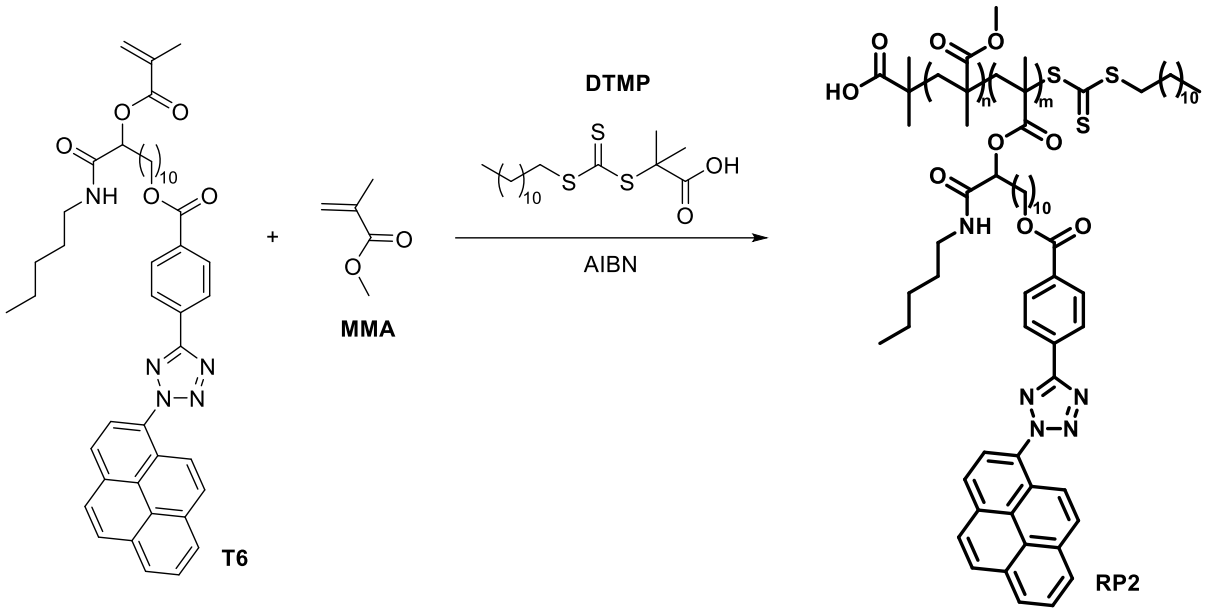

Processing of the RAFT-polymerization with **T6** as tetrazole-derivative yielded the RAFT-polymer **RP2** as pink solid.

SEC (THF): M_n = 12 900 g mol^{-1}, $Đ$ = 1.23 (Figure 6.21).

^{1}H NMR (400 MHz, $CDCl_3$) δ / ppm: 8.56-7.73 (m, 9H, *<u>H</u>$_{arom}$-*), 7.42 (m, 2H, *<u>H</u>$_{arom}$-*), 7.17 (m, 2H, *<u>H</u>$_{arom}$-*), 6.25 (m, 1H, *-CO-O-C<u>H</u>-CH₂-*), 5.39 (m, 2H, *-CO-O-C<u>H</u>₂-CH₂-*), 4.36 (m, 2H, *-CO-O-CH₂-C<u>H</u>₂-*), 3.63 (m, 3H, *C<u>H</u>₃-O-CO-*), 3.46 (m, 2H, *-S-C<u>H</u>₂-CH₂-*), 3.28 (m, 2H, *-CO-NH-C<u>H</u>₂-*), 2.19-1.63 (m, 8H, *C<u>H</u>₃-C$_q$-CO-*, *-O-CH-C<u>H</u>₂-*), 1.60-1.14 (m, 44H, *-NH-CH₂-C<u>H</u>₂-(CH₂)₂-*, *-(C<u>H</u>₂-C$_q$-)$_n$-*, *-O-CH-CH₂-(C<u>H</u>₂-)₇*, *CH₃-(C<u>H</u>₂)₁₀-*), 1.01 (m, 6H, *HO-CO-C$_q$-(C<u>H</u>₃)₂-*), 0.86 (m, 6H, *C<u>H</u>₃-(CH₂)₄-*, *C<u>H</u>₃-(CH₂)₁₁-S-*).

5.2.10.4 RAFT-Polymer **RP3**

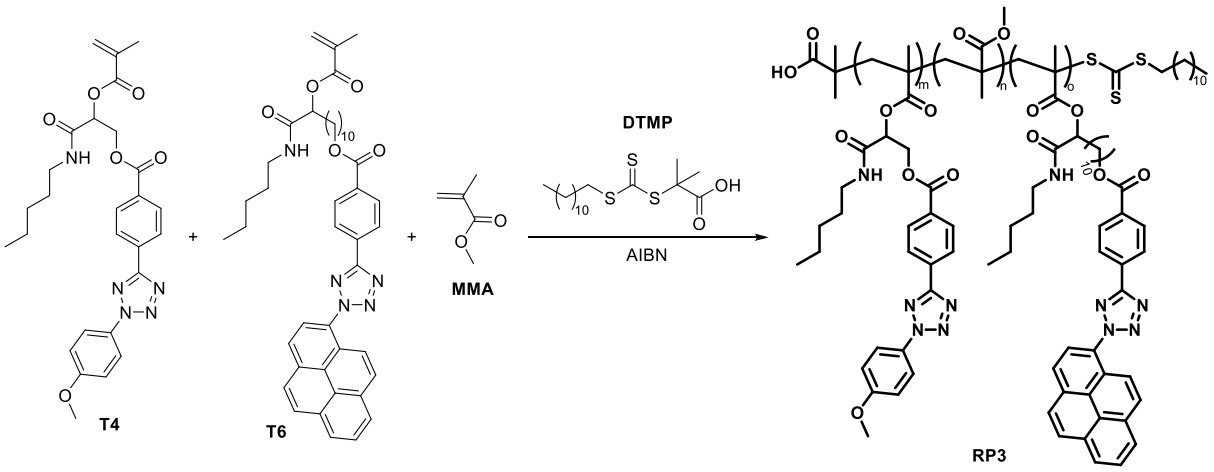

For the synthesis of **RP3**, the polymerization was conducted according to the general reaction procedure with both **T4** and **T6**. To maintain the amount of photo-sensitive moiety per wavelength (i.e. UV and Vis), a ratio of MMA / **T4** / **T6** 7 : 1 : 1 was chosen. The reaction yielded **RP3** as light pink solid.

SEC (THF): M_n = 11 400 g mol-1, $Đ$ = 1.41 (Figure 6.21).

^{1}H NMR (400 MHz, $CDCl_3$) δ / ppm: 8.50-7.89 (m, 19H, *H*$_{arom}$-), 7.06 (m, 2H, *H*$_{arom}$-), 6.18 (m, 2H, -*CO-O-CH-CH$_2$*-), 5.45 (m, 2H, -*CO-O-CH$_2$-CH*-), 4.76 (m, 2H, -*CO-O-CH$_2$-CH$_2$*-), 4.35 (m, 2H, -*CO-O-CH$_2$-CH$_2$*), 3.63 (m, 3H, *CH$_3$-O-CO*-), 3.89 (m, 2H, -*S-CH$_2$-CH$_2$*-), 3.58 (m, 6H, *CH$_3$-O*-), 3.28 (m, 2H, -*CO-NH-CH$_2$*-), 2.15-1.58 (m, 9H, *CH$_3$-C$_q$-CO*-), 1.50-1.10 (m, 52H, -*NH-CH$_2$-CH$_2$-(CH$_2$)$_2$*-, -*(CH$_2$-C$_q$-)$_n$*-, -*O-CH-CH$_2$-(CH$_2$-)$_7$*, *CH$_3$-(CH$_2$)$_{10}$*-), 1.00 (m, 6H, *HO-CO-C$_q$-(CH$_3$)$_2$*-), 0.83 (m, 9H, *CH$_3$-(CH$_2$)$_4$*-, *CH$_3$-(CH$_2$)$_{11}$-S*-).

The ^{1}H NMR spectrum of **RP3** is shown in Figure 6.24.

5.2.11 Photoreactions

5.2.11.1 General Procedure for the NITEC Reaction

In general, the respective RAFT polymer (1.00 eq. with respect to the theoretical amount of photo-sensitive unit) was dissolved in DCM with a concentration of c = 20 mg L^{-1}. Subsequently, 5.00 eq. of the bis-maleimide were added and the reaction mixture was put in the photoreactor displayed in Figure 5.15A. Depending on the photo-sensitive moiety, the reaction mixture was either irradiated with an Arimed B6 lamp (290-370 nm, Figure 5.15B) or

three Avonec 3W LED lamps (410-420 nm, Figure 5.15C) for 30 min. After removal of the solvent, the obtained folded polymer was analysed via SEC, ^{1}H NMR spectroscopy as well as UV/Vis and Fluorescence measurements.

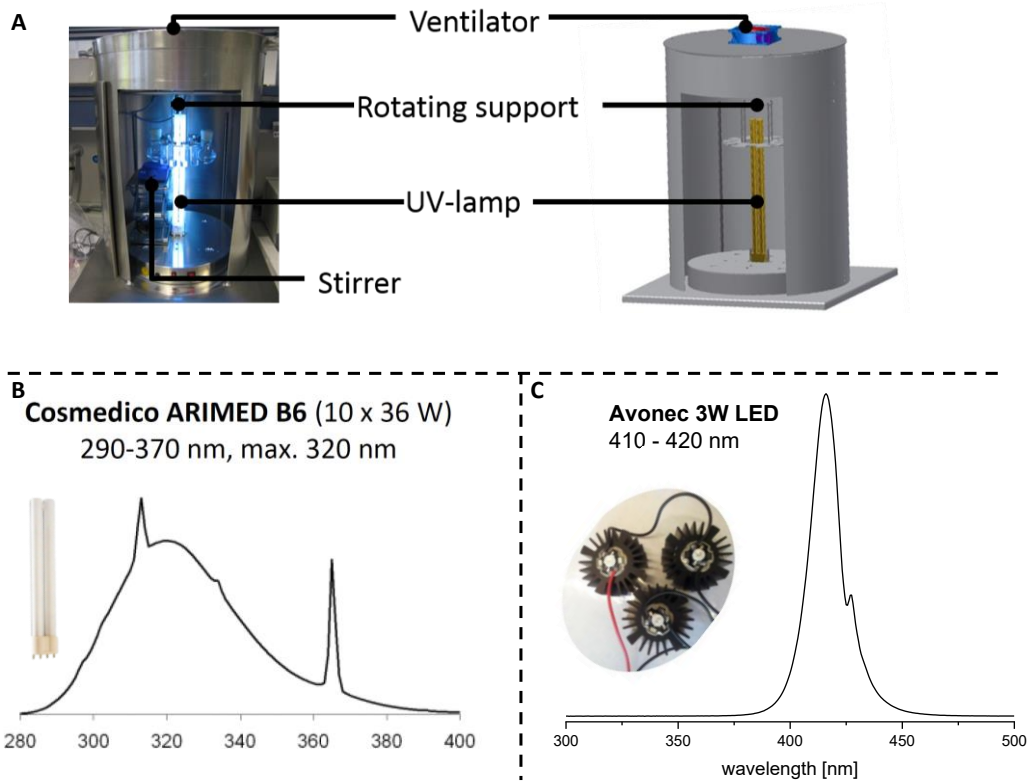

Figure 5.15A: Picture of the photoreactor equipped with a ventilator, rotating support, UV-lamp and magnetic stirrer. **B**: Emission spectrum of the Arimed B6 lamp chosen for the photoreactions in the UV-range (290-- 370 nm). **C**: Emission spectrum of the Avonec 3W LEDs taken for the photoreactions in the Vis-range (410 – 420 nm).

5.2.11.2 Folding of **RP1** in the UV-Range (**FP1, FP1'**)

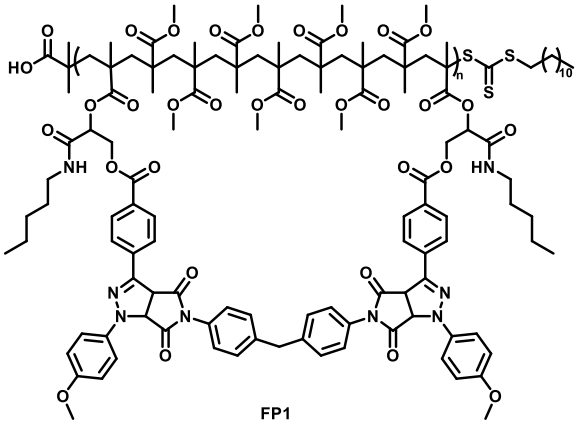

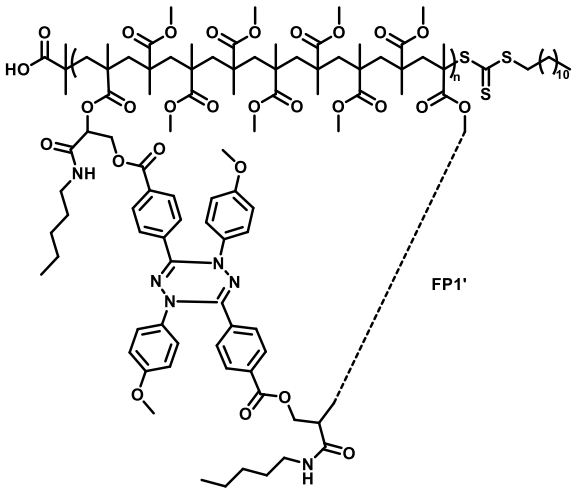

Irradiation of **RP1** at λ_{max} = 320 nm in the presence of the aromatic bis-maleimide crosslinker resulted in the formation of the highly fluorescent polymer **FP1**.

SEC (THF): M_n = 12 100 g mol^{-1}, $Đ$ = 1.34 (Figure 3.14).

The ^{1}H NMR spectrum of **FP1** can be found in Figure 3.12A.

If the reaction is repeated under similar conditions in the absence of the cross-linker, the non-fluorescent polymer FP1' is obtained.

SEC (THF): M_n = 12 400 g mol^{-1}, $Đ$ = 1.36 (Figure 3.14).

5.2.11.3 Folding of **RP2** in the Vis-Range (**FP2**)

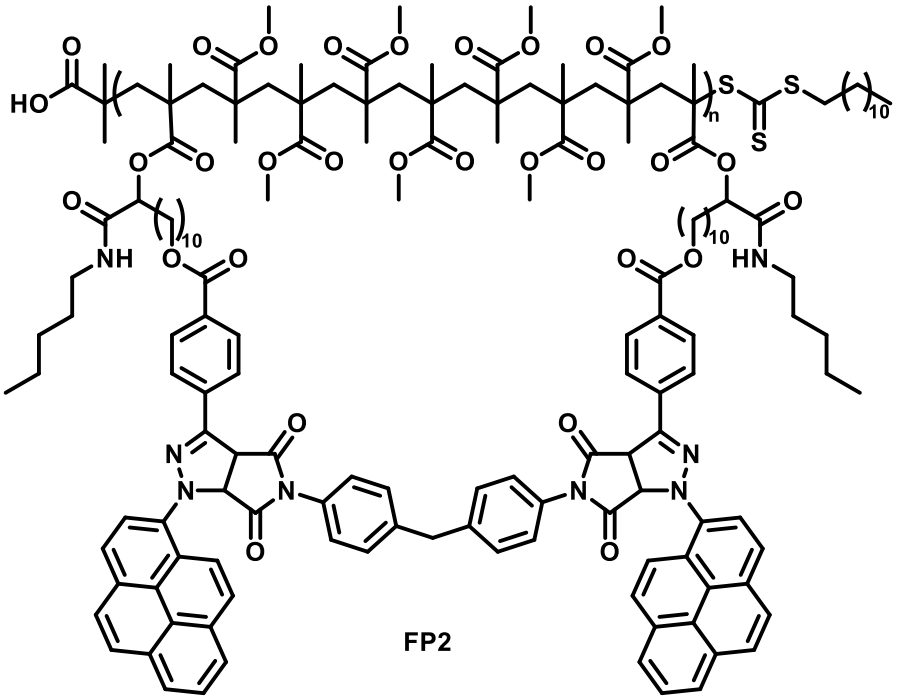

The RAFT polymer **RP2** was folded upon irradiation with Vis-light (410-420 nm) to obtain the folded polymer **FP2** with fluorescent properties.

SEC (THF): M_n = 12 200 g mol^{-1}, $Đ$ = 1.20.

In Figure 3.12B, the ^{1}H NMR spectrum is shown and the respective SEC elution trace is displayed in Figure 3.14.

5.2.11.4 Folding of **RP3** with Vis- and UV-Light (**FP3**, **FP3'**)

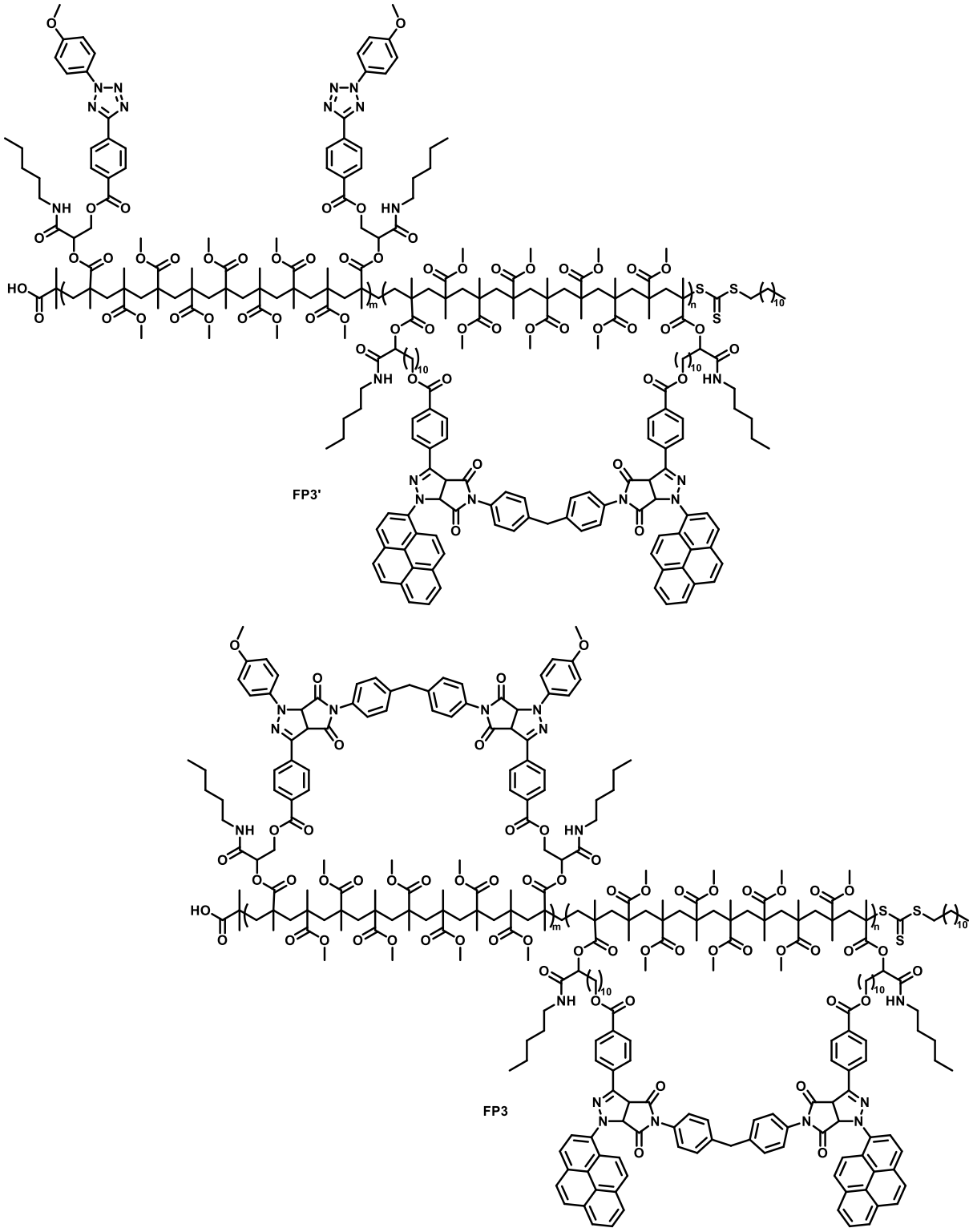

In order to fold the RAFT-polymer **RP3** in a *λ*-orthogonal manner, first the irradiation in the Vis-range (410-420 nm) was conducted, yielding **FP3'**.

SEC (THF): M_n = 10 400 g mol^{-1}, $Đ$ = 1.46.

Afterwards, the reaction was repeated with irradiation in the UV-range (λ_{max} = 320 nm), resulting in the completely folded polymer **FP3**. Both reactions were conducted for 30 min, respectively.

SEC (THF): M_n = 10 300 g mol^{-1}, $Đ$ = 1.46.

The ^{1}H NMR spectra of **FP3'** and **FP3** can be found in Figure 3.13, the SEC elution traces are shown in Figure 3.14.

5.3 Instrumentation

5.3.1 Nuclear Magnetic Resonance (NMR) Spectroscopy

The NMR spectra were recorded on Bruker Avance 400 MHz or 500 MHz indicated in the respective spectrum description. The spectra were referenced on residual solvent signal according to Nudelman et al[365]: 2.50 ppm for DMSO-d_6, 2.75 for DMF-d_7, 3.58 ppm for THF-d_8 and 7.26 ppm for $CDCl_3$. The deuterated solvents were purchased from Euriso-TOP and used without further purification.

5.3.2 Electron Paramagnetic Resonance (EPR) Spectroscopy

The spectra were recorded on a Magnet Tech MiniScope MS400 spectrometer at ambient temperature in DMSO. The following parameters were applied: B0-field = 336.9748 ± 10.1079 mT, sweep time = 30 s, modulation = 0.01 mT, microwave attenuation = 10.0 db, gain mantisse = 4, gain exponent = 1, number of points = 4096, number of passes = 1.

5.3.3 Nuclear Overhauser Effect Spectroscopy (NOESY)

The NOESY NMR spectra are recorded either on Bruker Avance II+ 600 MHz spectrometer equipped with a 5 mm BBI inversely detected $^{1}H,^{31}P$-^{109}Ag double resonance probehead with actively shielded z-gradient, on Bruker Avance III 600 MHz spectrometer with a 5 mm CPTCI inversely detected $^{1}H,^{13}C,^{15}N$ triple resonance cryogenically cooled probehead with actively shielded z-gradient or on Bruker Avance III 600 MHz spectrometer with a 5 mm TBI inversely detected ^{1}H, ^{31}P-^{109}Ag, ^{13}C double resonance probehead with actively shielded z-gradient. The respective frequencies are 600.19 MHz and 599.70 MHz and 600.19 MHz for proton frequency. The temperature is controlled with Bruker VT-unit or a Bruker Smart VT-Unit. The used NOESY pulse sequences are implemented in the spectrometer manufacturer software and are based on publications of Wagner[366] and Thrippleton.[367]

5.3.4 Ultraviolet-Visible (UV/Vis) Spectroscopy

The absorbance spectra were recorded on a Cary 100 UV-Visible Spectrometer (Agilent Technologies, USA) possessing a tungsten halogen light source (190 to 900 nm, accuracy +/- 2 nm) and a R928 PMT detector. For the measurement, the polymers were dissolved in the respective solvent with concentrations given in the description of the spectra. The samples were baseline corrected with respect to the pure solvent.

5.3.5 Chemiluminescence (CL) Measurements

Chemiluminescence spectra were recorded on a Varian Cary Eclipse fluorescence spectrometer in the Bio-/Chemiluminescence mode. The CL emission intensity was recorded in dependence on the wavelength from 300 to 800 nm (scan rate = 600 nm min^{-1}, averaging time = 0.1 s, emission slit = 5.0 nm, detector voltage = 800 V) with a luminol concentration of 7.5 x 10^{-2} mol L^{-1} for the small molecule model study and a polymer concentration of 3.25*10^{-4} mmol mL^{-1} for the supramolecular assembly.

5.3.6 Fluorescence Spectroscopy

The fluorescence spectra were recorded on a Varian Cary Eclipse fluorescence spectrometer. All spectra were recorded in quartz cuvettes at ambient temperature. The solvent, concentration and excitation wavelength is given in the description of the respective spectra.

5.3.7 Gas-Chromatography – Mass Spectrometry (GC-MS)

A Varian 431 GC instrument with a capillary column FactorFourTM VF-5 ms (30 m·0.25 mm·0.25 µm) and a Varian 210 ion trap mass detector were used. Scans were performed from 40 to 650 m/z at a rate of 1.0 scans·s^{-1}. The oven temperature program was: initial temperature 95 °C, hold for 1 min, ramp at 15 °C·min^{-1} to 200 °C, hold for 2 min, ramp at 15 °C·min^{-1} to 325 °C, hold for 5 min. Measurements were performed in split–split mode (split ratio 50:1) using helium as the carrier gas (flow rate 1.0 mL·min^{-1}).

5.3.8 Size-Exclusion Chromatography (SEC)

THF SEC: The apparent number average molar mass (M_n) and the molar mass distribution [$Đ$ (dispersity index) = M_w/M_n] values of the polymers were determined using a size exclusion chromatography (SEC) system equipped with Shimadzu LC20AD pump, Wyatt Optilab rEX refractive index detector and four PLgel 5µm Mixed-C columns. The characterization was performed at 30 °C in THF with a flow rate of 1.0 mL·min^{-1}. The molecular weight calibration was based on sixteen narrow molecular weight linear PMMA standards from Polymer Laboratories.

DMAc SEC: The analysis of the M_n and $Đ$ values in DMAc were performed on a Polymer Laboratories PLGPC 50 Plus Integrated System equipped with a PLgel 5 µm bead-size guard column (50 x 7.5 mm) followed by three PLgel 5 µm Mixed-C columns (300 x 7.5 mm) and a differential refractive index detector. As eluent, DMAc containing 0.03 wt% LiBr at 50°C with a flow rate of 1.0 mL min^{-1} was applied. The molecular weight calibration was based on PMMA standards from Polymer Laboratories.

5.3.9 Dynamic Light Scattering (DLS)

The apparent hydrodynamic diameters ($D_{h,app}$) were determined at 20 °C by means of a dynamic light scattering (DLS) analysis using a Zetasizer Nano ZS light scattering apparatus (Malvern Instruments, UK) equipped with He-Ne laser (at a wavelength of 633 nm, 4 mW). The Nano ZS instrument incorporates a non-invasive backscattering (NIBS) optic with a detection angle of 173°. The polymer solutions were prepared in the respective solvent (c = 1 mg mL^{-1}) and subsequently filtered into disposable micro cuvettes or quartz glass cuvettes. The prepared samples were stabilized prior to DLS analysis at an ambient temperature. All values of the apparent hydrodynamic diameter for each polymer mixture were averaged over three measurements (14 runs/measurement), and were automatically provided by the instrument using a cumulative analysis.

6 Appendix

In the following section, additional data are provided that are not displayed in Chapter 3.

6.1 Additional Figures of Chapter 3.1

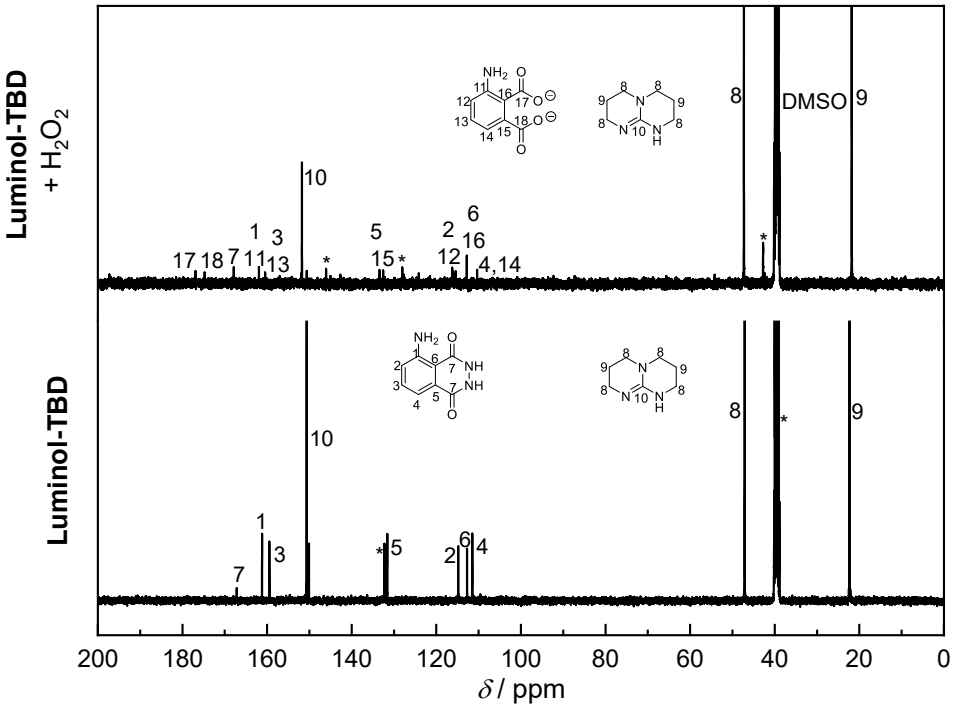

Figure 6.1: ^{13}C NMR (100 MHz) spectra of luminol-TBD and Luminol-TBD + H_2O_2 in DMSO-d_6.

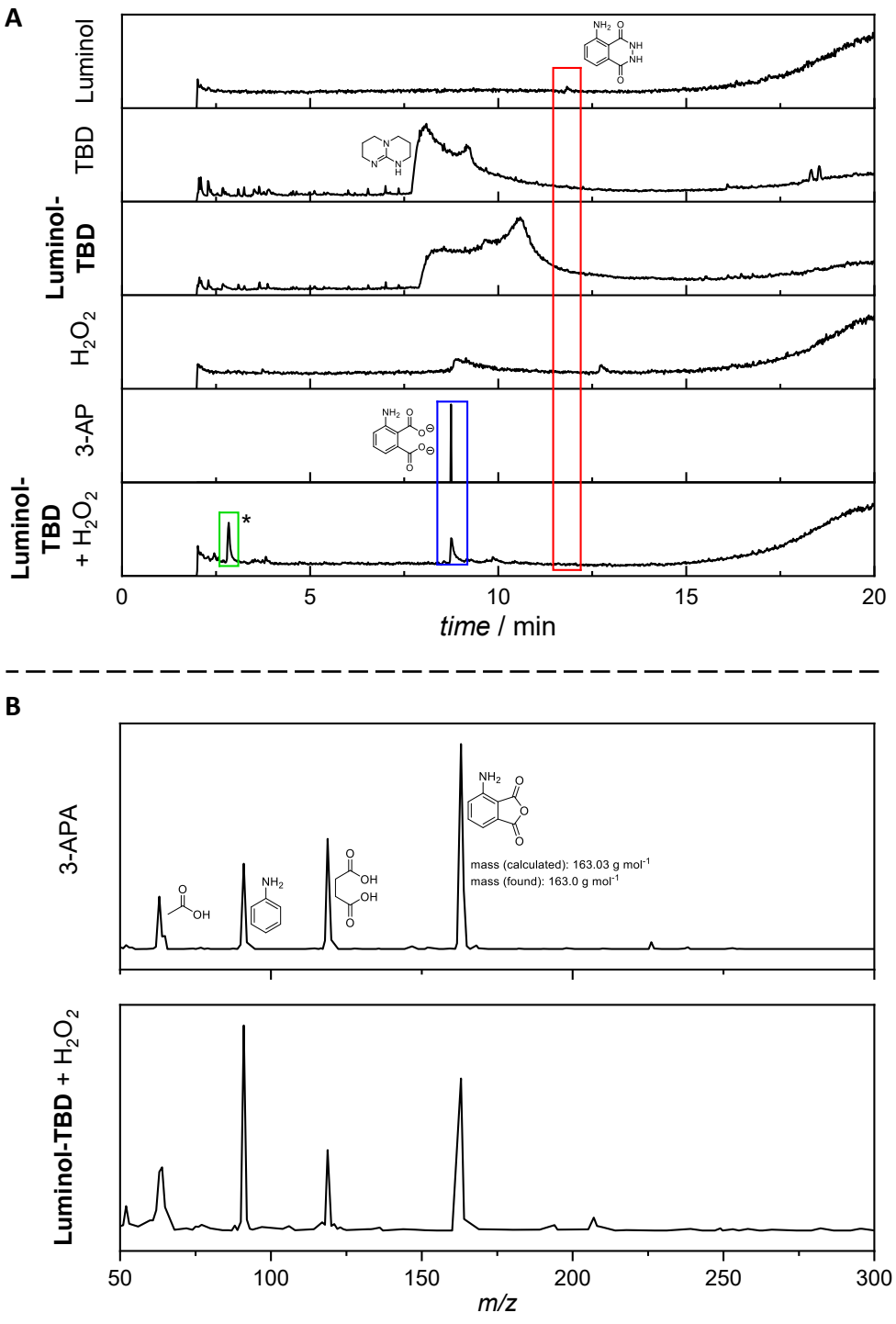

Figure 6.2A: GC chromatograms of luminol, TBD, luminol-TBD, H_2O_2, commercially available 3-APA and luminol-TBD+H_2O_2 in MeOH. **B**: MS spectra of 3-APA and luminol-TBD+H_2O_2 in MeOH.

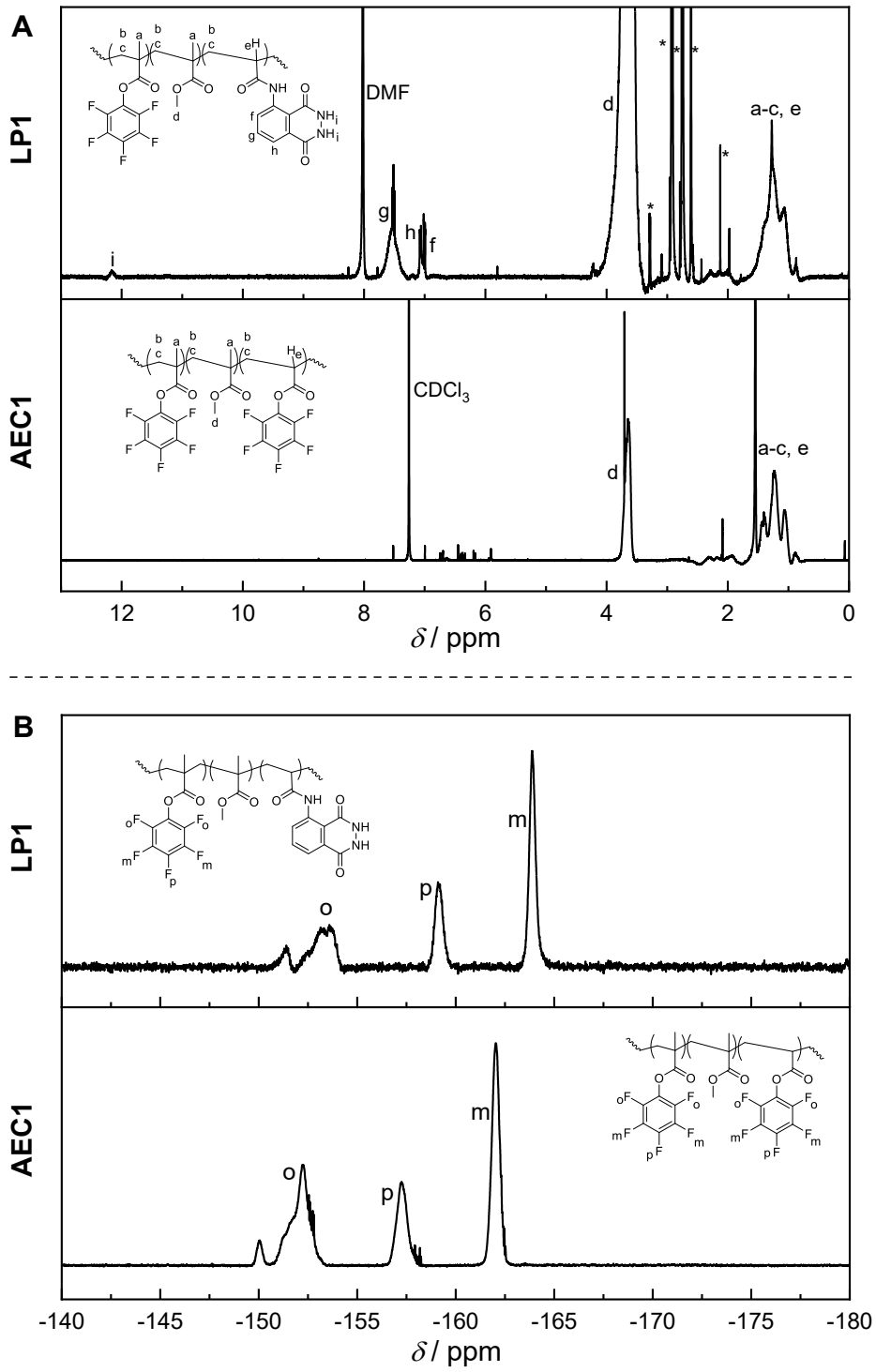

Figure 6.3A: ^{1}H NMR (400 MHz) spectra of **AEC1** in $CDCl_3$ and **LP1** in DMF at ambient temperature. **B**: ^{19}F NMR (377 MHz) spectra of **AEC1** in $CDCl_3$ and **LP1** in DMF at ambient temperature.

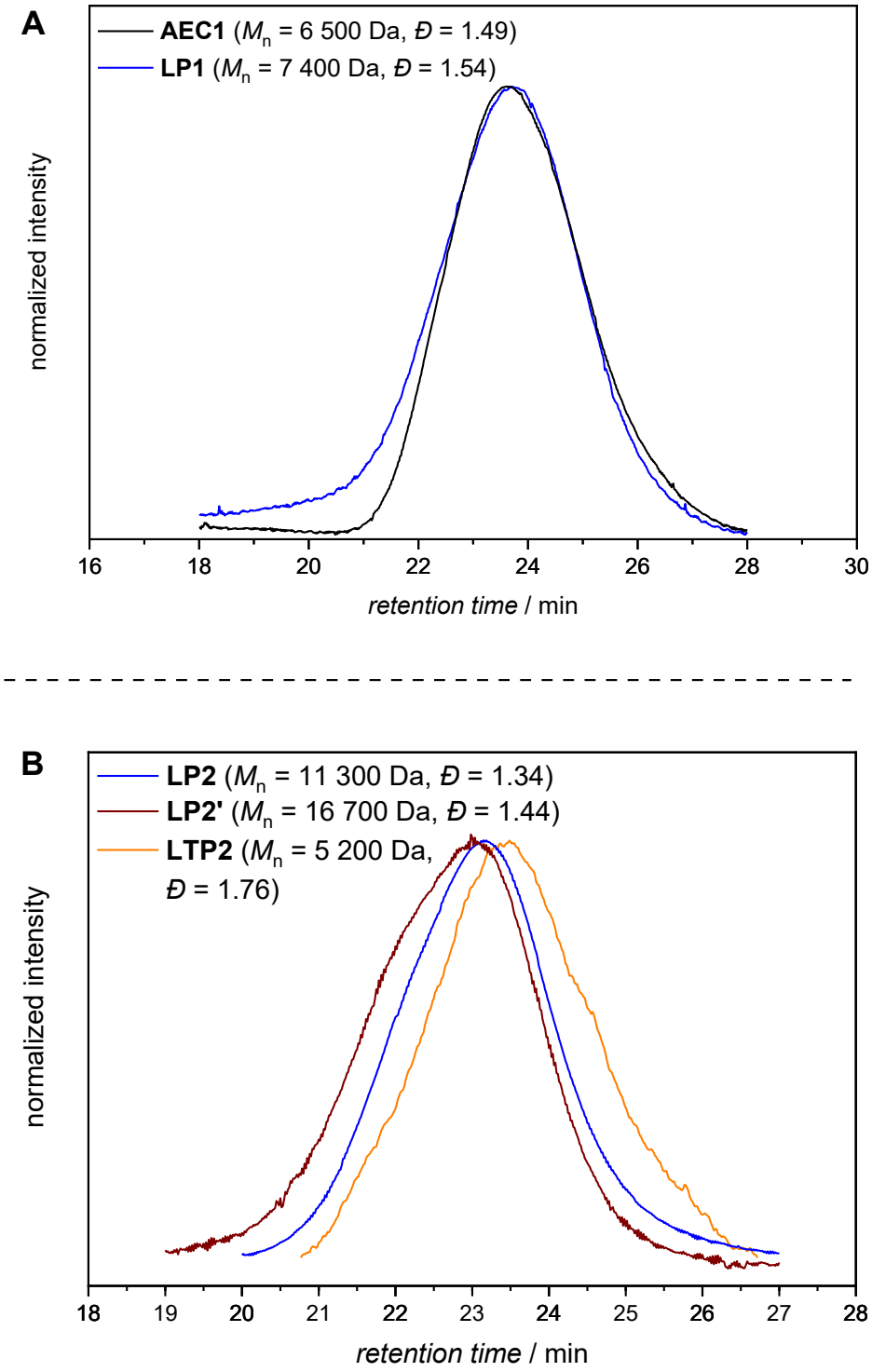

Figure 6.4A: SEC elution trace of **AEC1** and **LP1** in THF at 30°C. **B**: SEC elution trace of **LP2**, **LP2'** and **LTP2** in DMAc at 50°C.

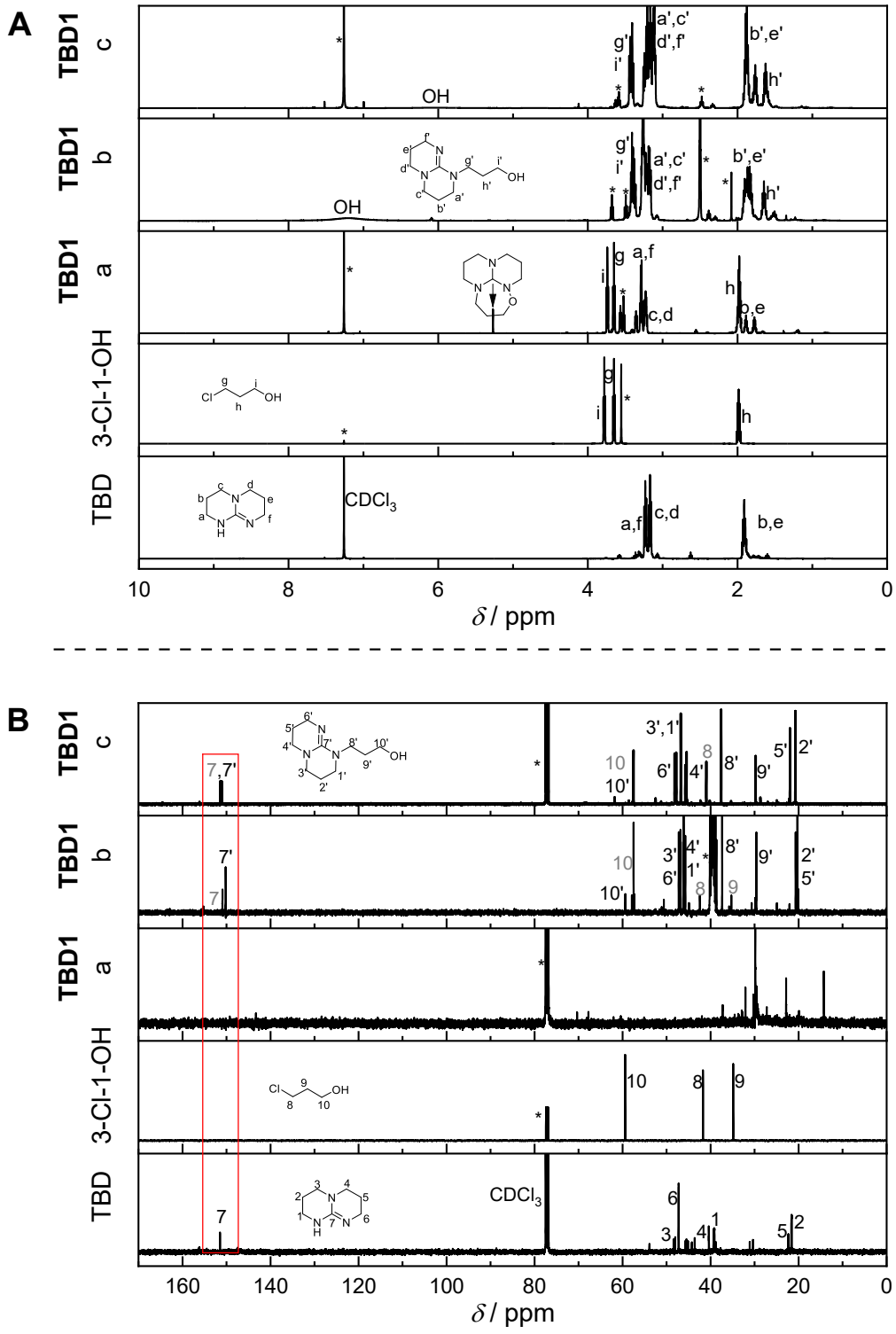

Figure 6.5A: ^{1}H NMR (400 MHz) and **B**: ^{13}C NMR (100 MHz) spectra of **TBD1a** and **c** in $CDCl_3$ and **TBD1b** in DMSO-d_6. The spectra were recorded after different experimental setups (a: THF, 24 h, b: THF, 18 h, c: EtOH, 70 h).

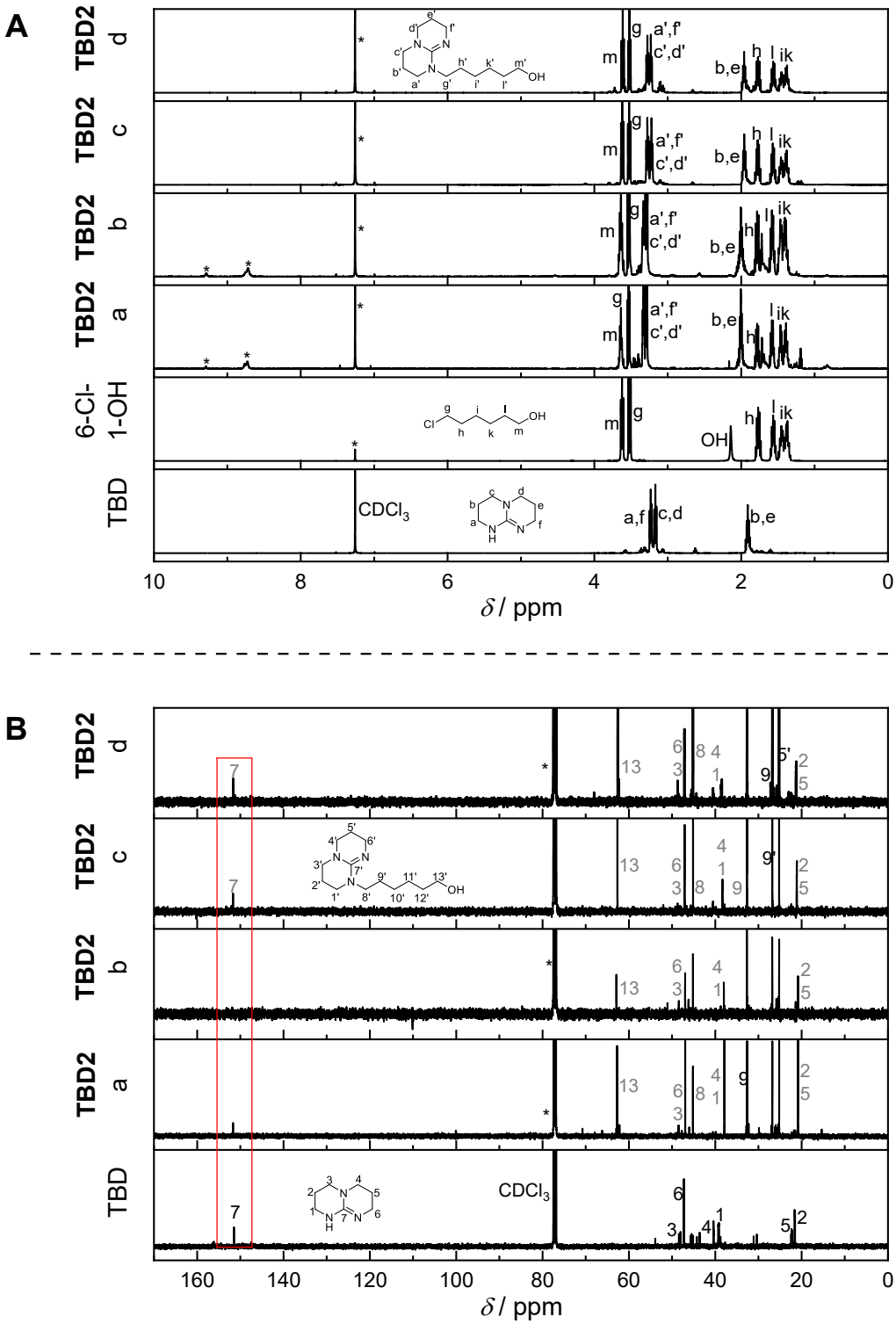

Figure 6.6A: ^{1}H NMR (400 MHz) and **B**: ^{13}C NMR (100 MHz) spectra of **TBD2** in $CDCl_3$ at ambient temperature. The spectra were recorded after different experimental setups (a: EtOH, 23 h, b: THF, 21 h, c: EtOH, 7.5 h, d: THF, 6h).

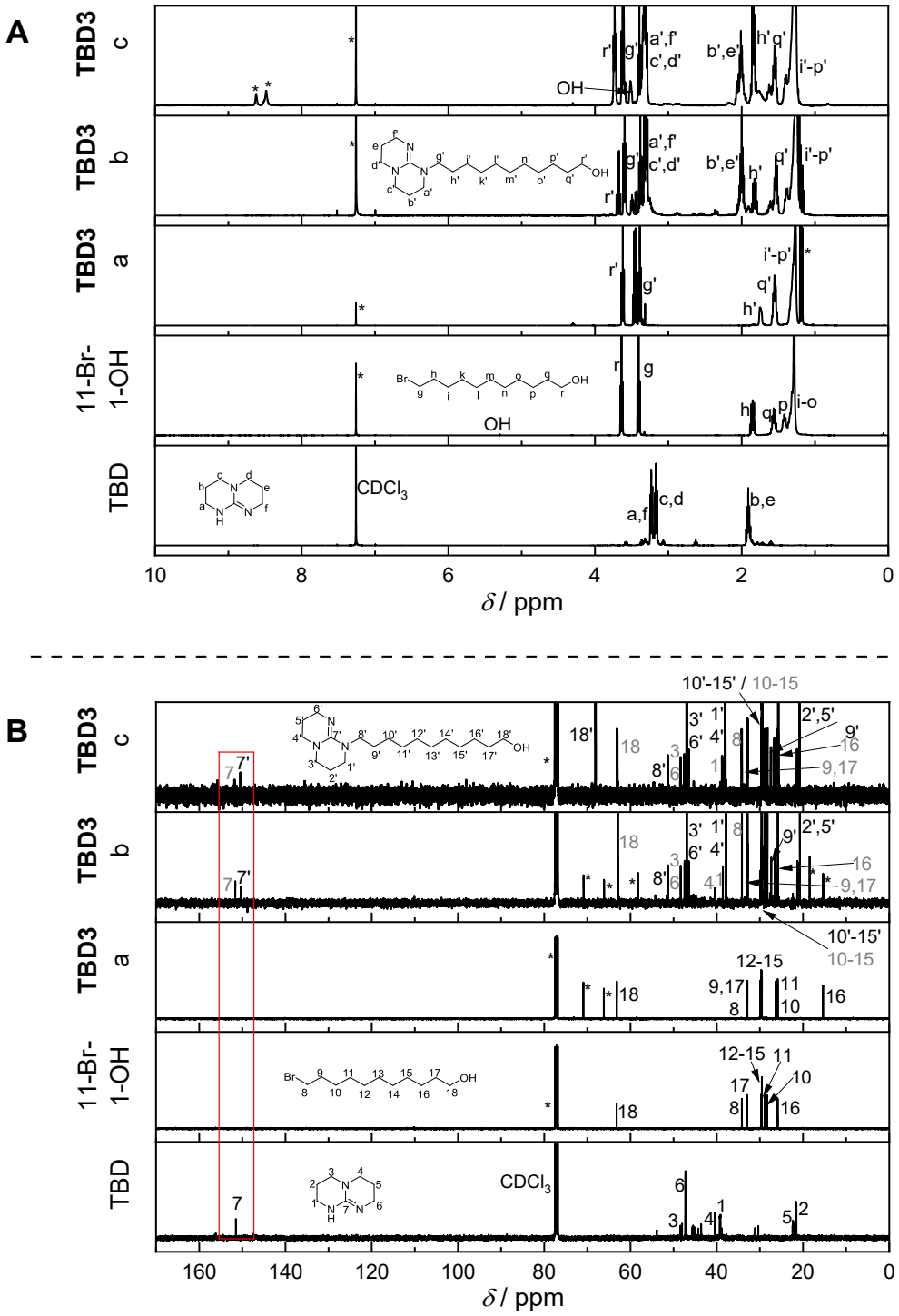

Figure 6.7A: ^{1}H NMR (400 MHz) and **B**: ^{13}C NMR (100 MHz) spectra of **TBD3** in $CDCl_3$ at ambient temperature. The spectra were recorded after different experimental setups (a: EtOH, 22 h, b: EtOH, 6 h, c: THF, 6 h).

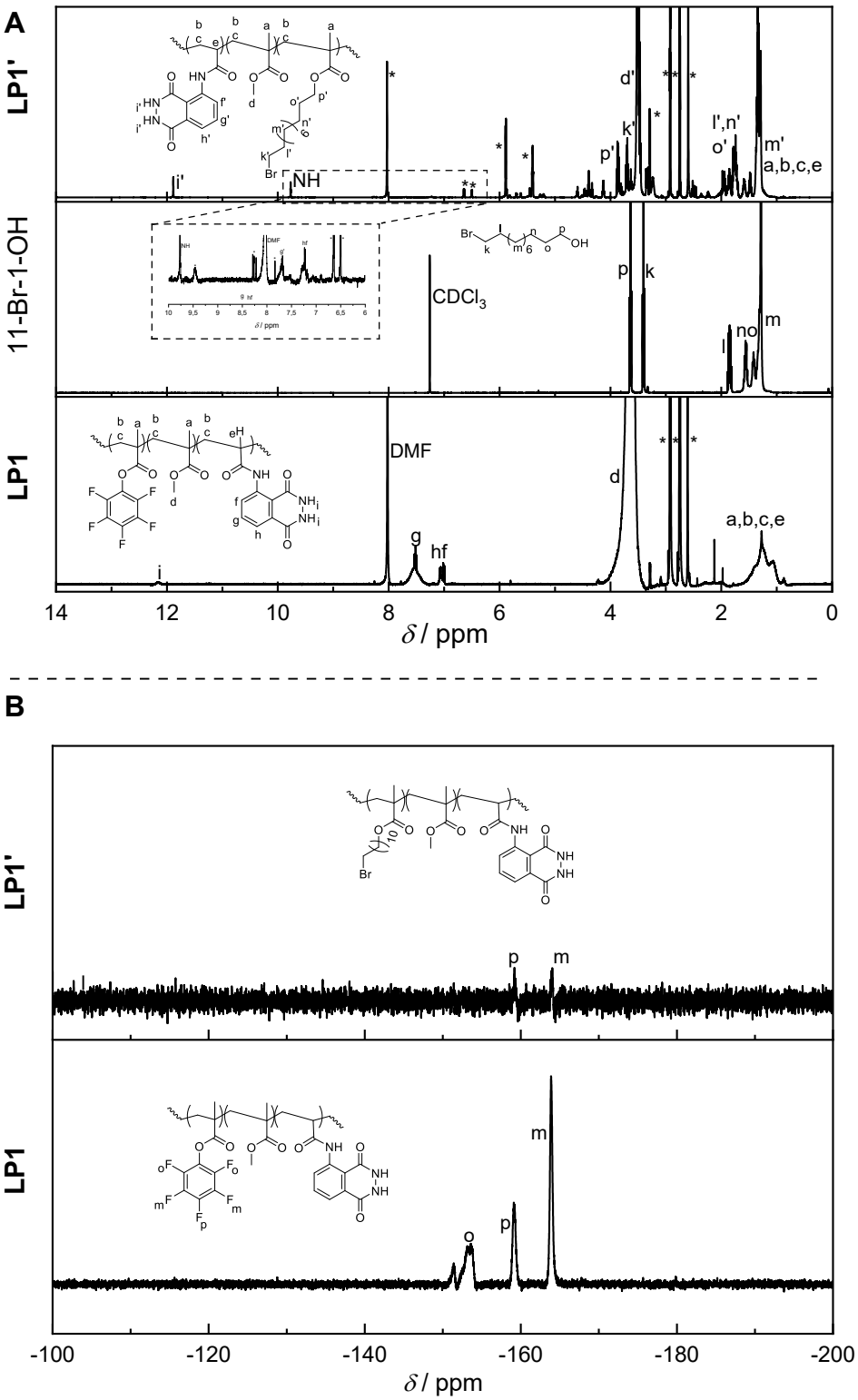

Figure 6.8A: ^{1}H NMR (400 MHz) and **B**: ^{19}F NMR (377 MHz) spectra of **LP1** and **LP1'** in DMF-d_7 at ambient temperature.

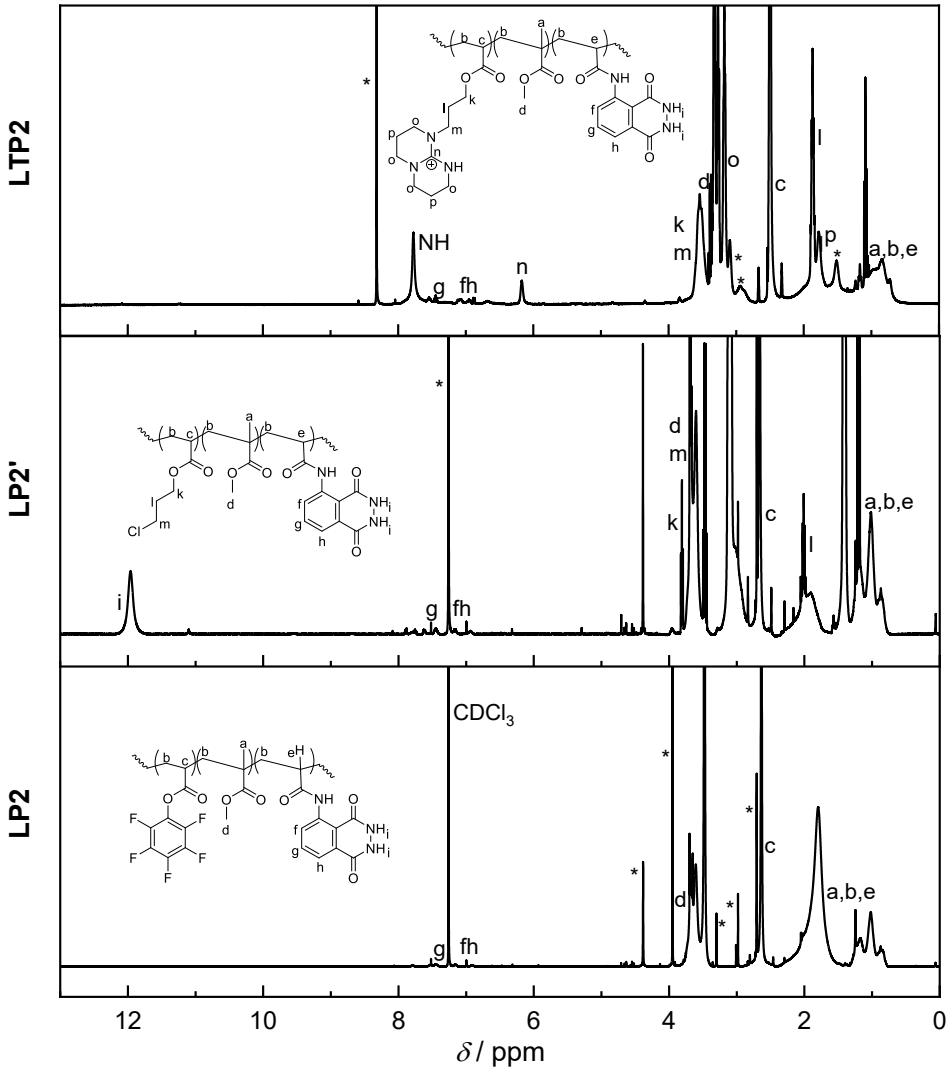

Figure 6.9: ^{1}H NMR (400 MHz) spectra of **LP2** and **LP2'** in $CDCl_3$ as well as **LTP2** in DMF-d_7.

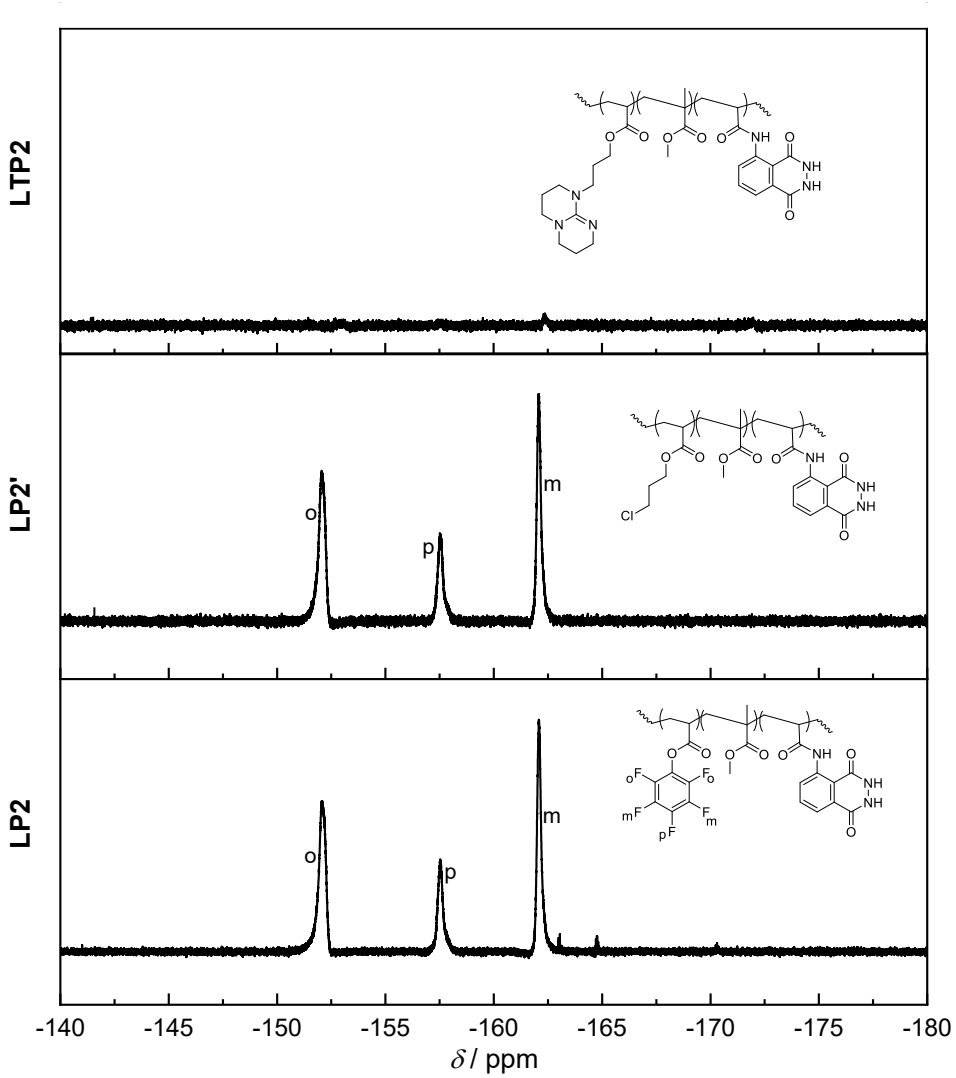

Figure 6.10: ^{19}F NMR (377 MHz) spectra of **LP2** and **LP2'** in $CDCl_3$ as well as **LTP2'** in DMF-d_7.

6.2 Additional Figures of Chapter 3.2

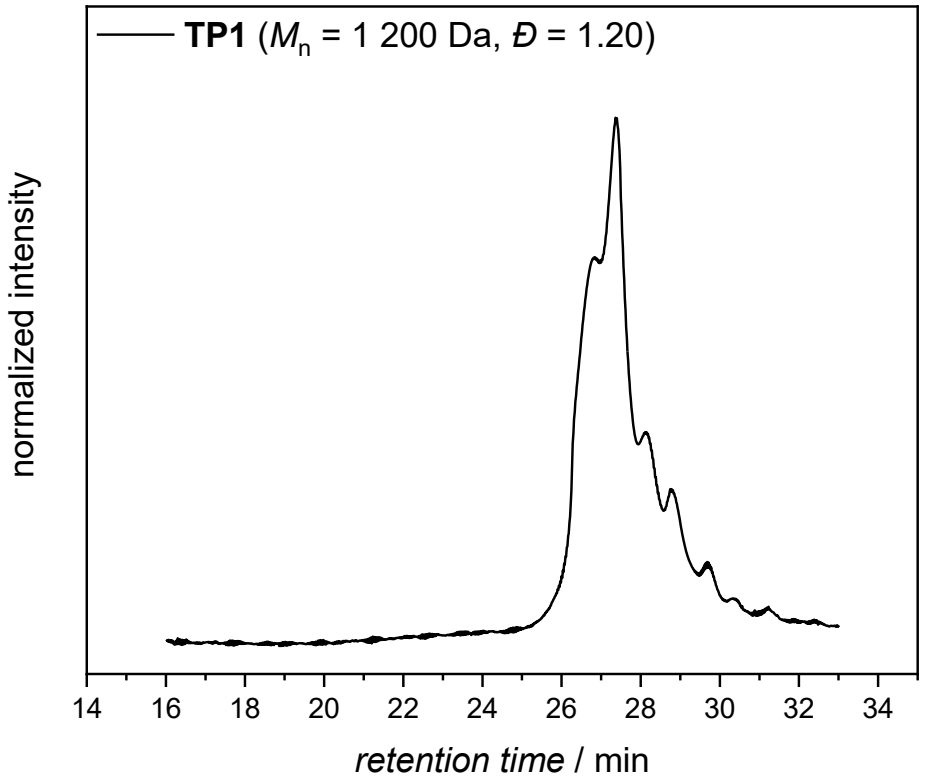

Figure 6.11: SEC elution trace of **TP1** in THF at 30°C.

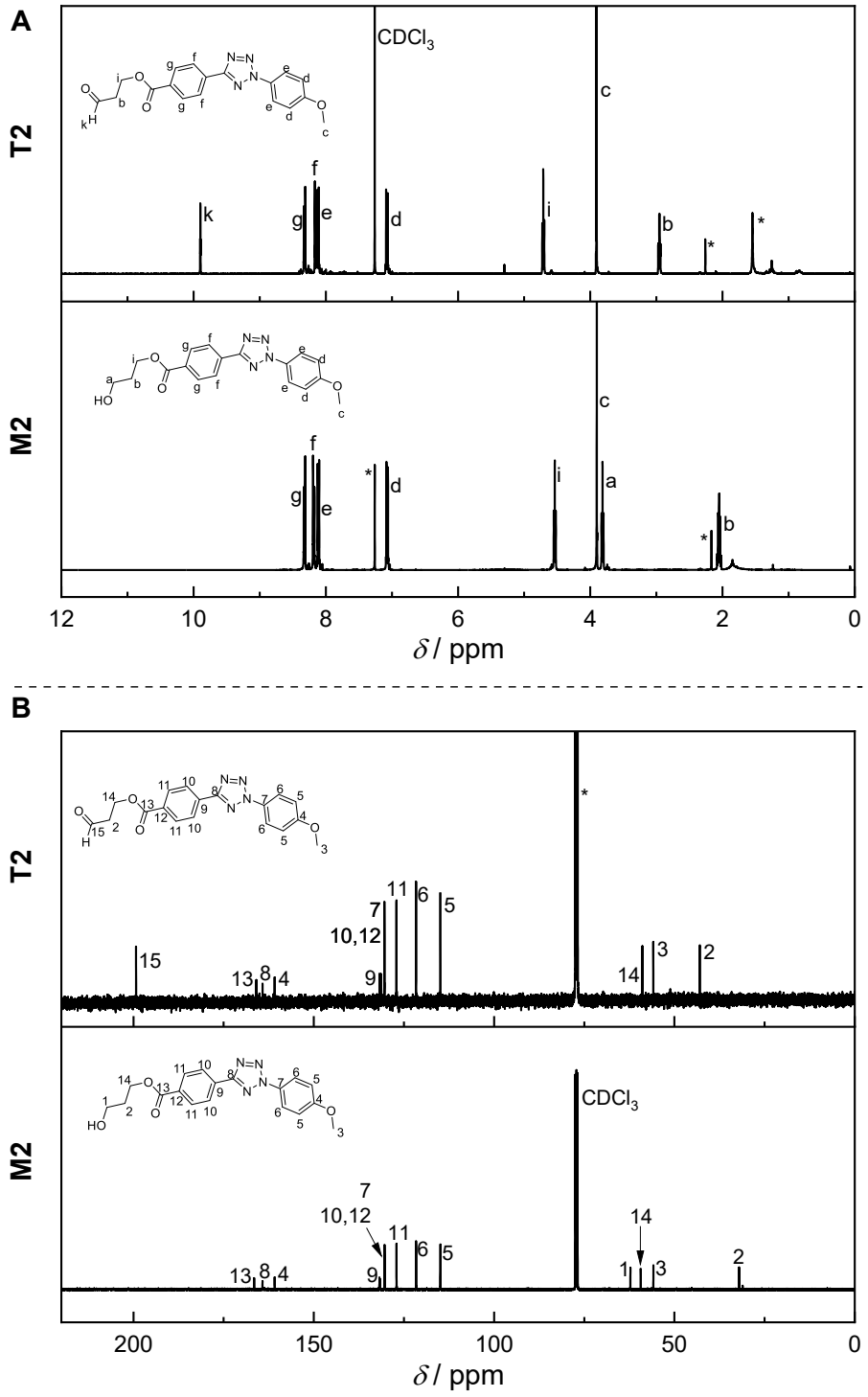

Figure 6.12A: ^{1}H NMR (400 MHz) and **B**: ^{13}C NMR (100 MHz) spectra of **M2** and **T2** in $CDCl_3$, respectively.

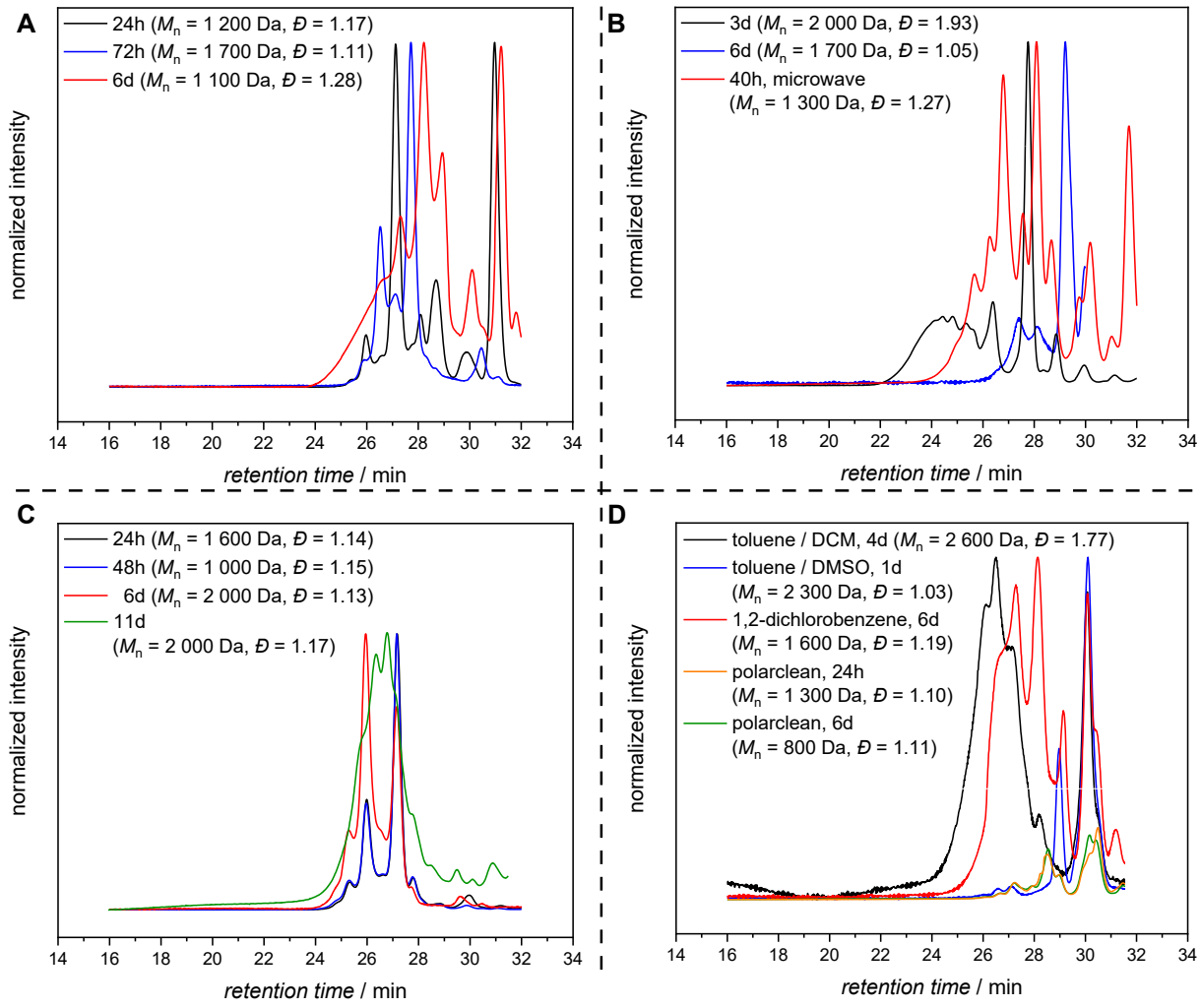

Figure 6.13: SEC elution traces of **TP2** for the different solvents applied in the P-MCP: DCM (**A**), $CHCl_3$ (**B**), $CHCl_3$ / THF (**C**) and other solvents (i.e. toluene / DCM, toluene / DMSO, 1,2-dichlorobenzene and polarclean) (**D**). All traces were recorded in THF at 30°C.

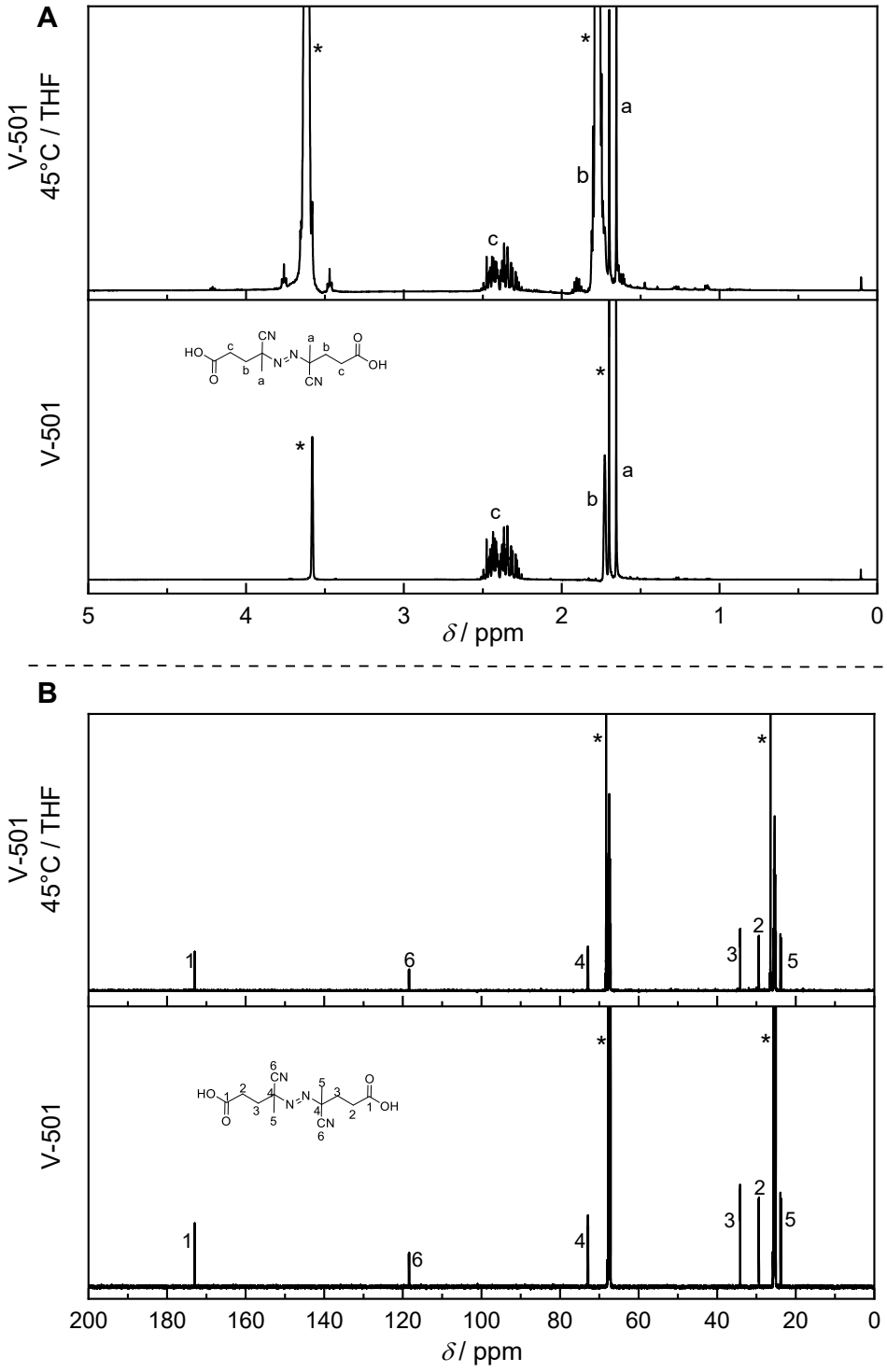

Figure 6.14A: ^{1}H NMR (400 MHz) and **B**: ^{13}C NMR (100 MHz) spectra of V-501 in THF-d_8 at ambient temperature and after heating at 45°C for 3 days, respectively.

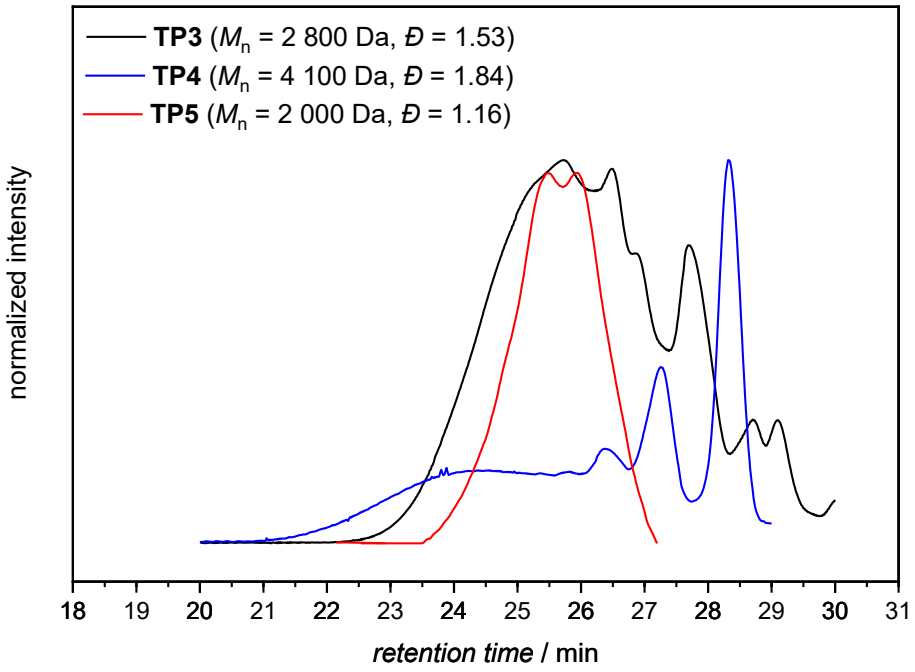

Figure 6.15: SEC elution traces of **TP3** and **TP4** in THF at 30°C and the SEC elution trace of **TP5** in DMAc at 50°C.

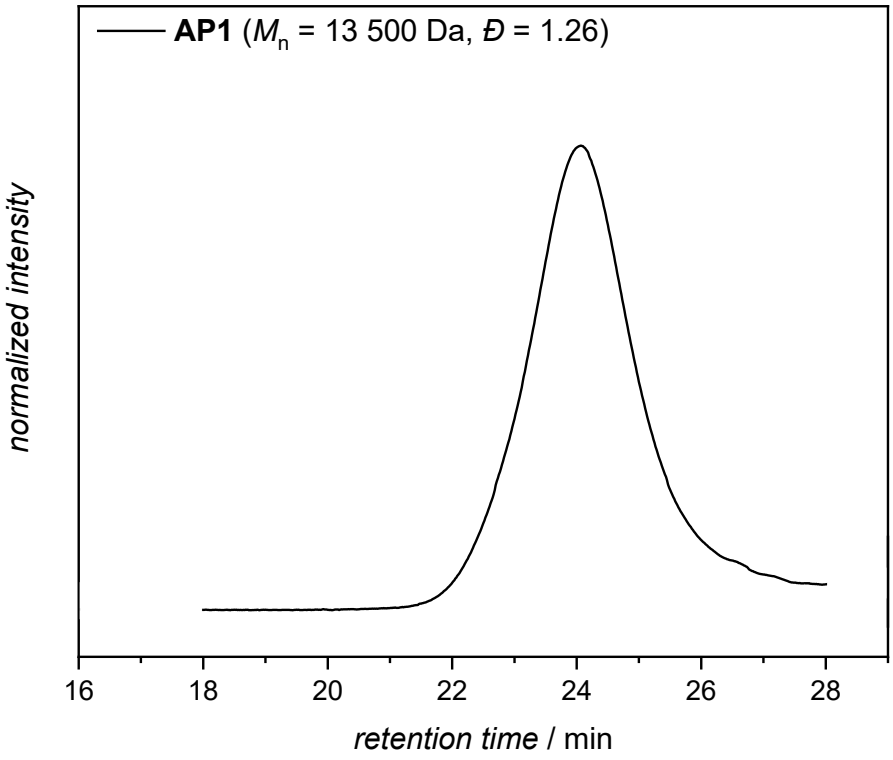

Figure 6.16: SEC elution trace of **AP1** in DMAc at 50°C.

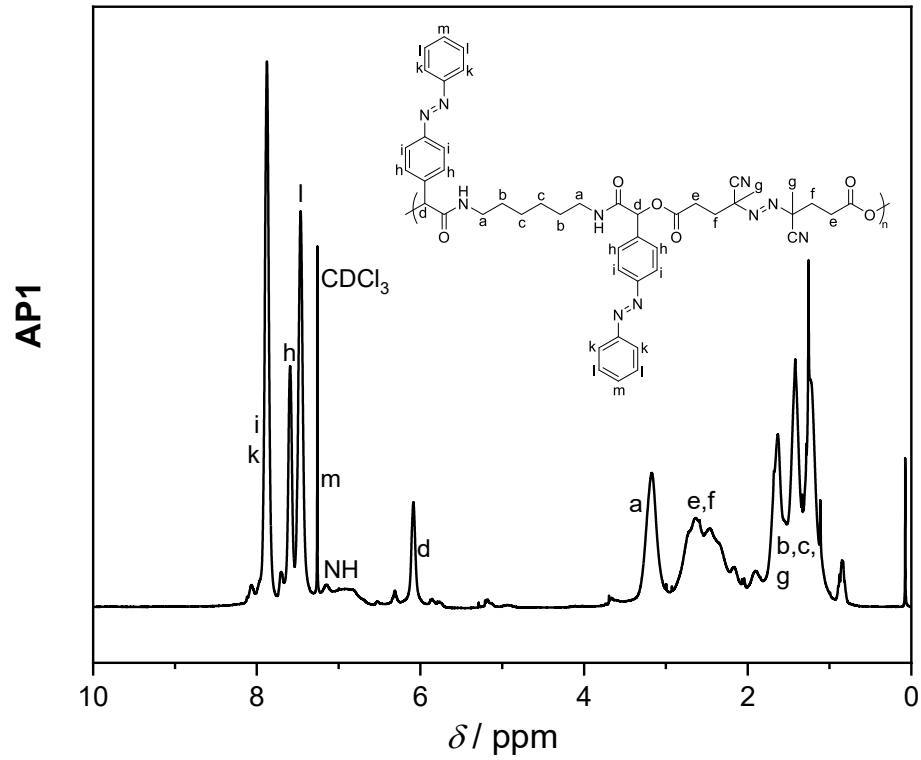

Figure 6.17: ^{1}H NMR (400 MHz) of **AP1** in $CDCl_3$.

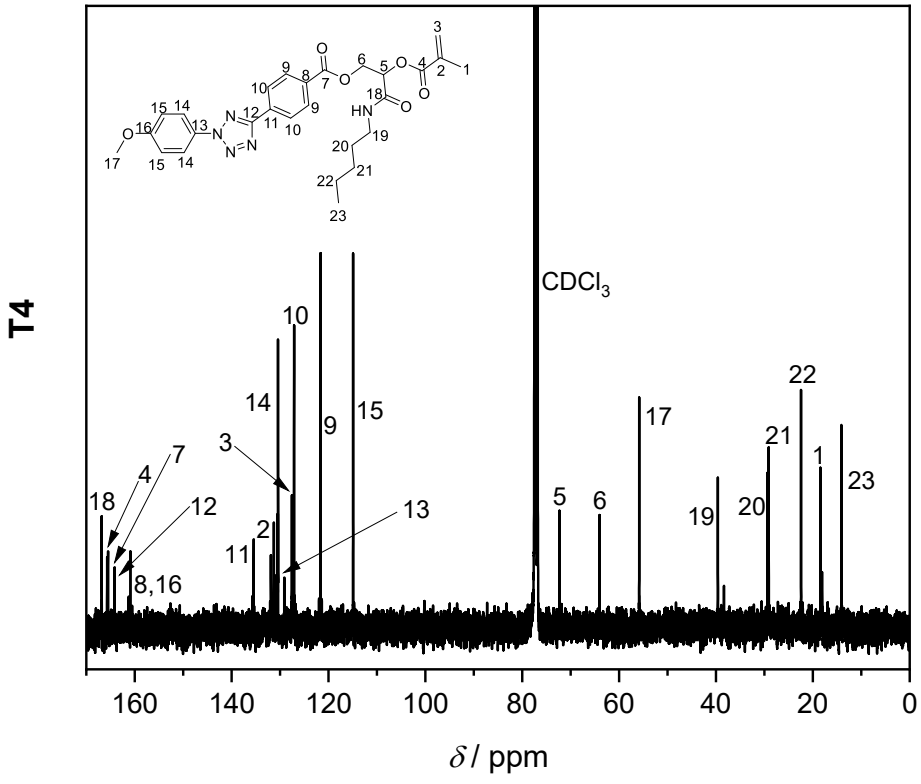

Figure 6.18: ^{13}C NMR (100 MHz) of **T4** in $CDCl_3$.

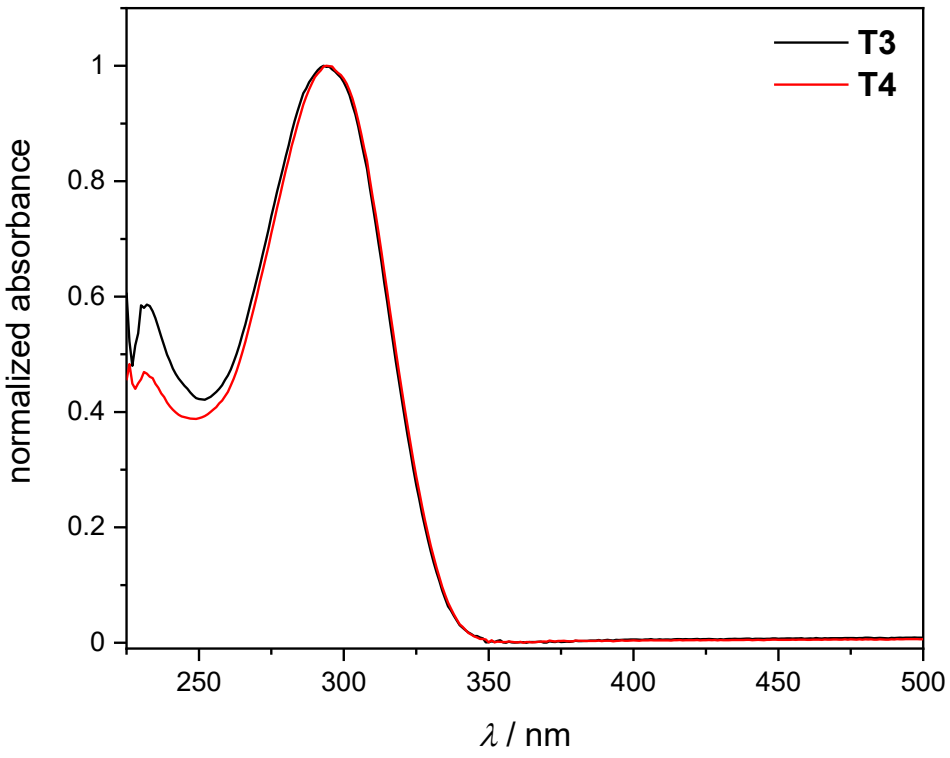

Figure 6.19: UV/Vis spectra of **T3** and **T4** in DCM at ambient temperature (c = 0.2 mg mL^{-1}).

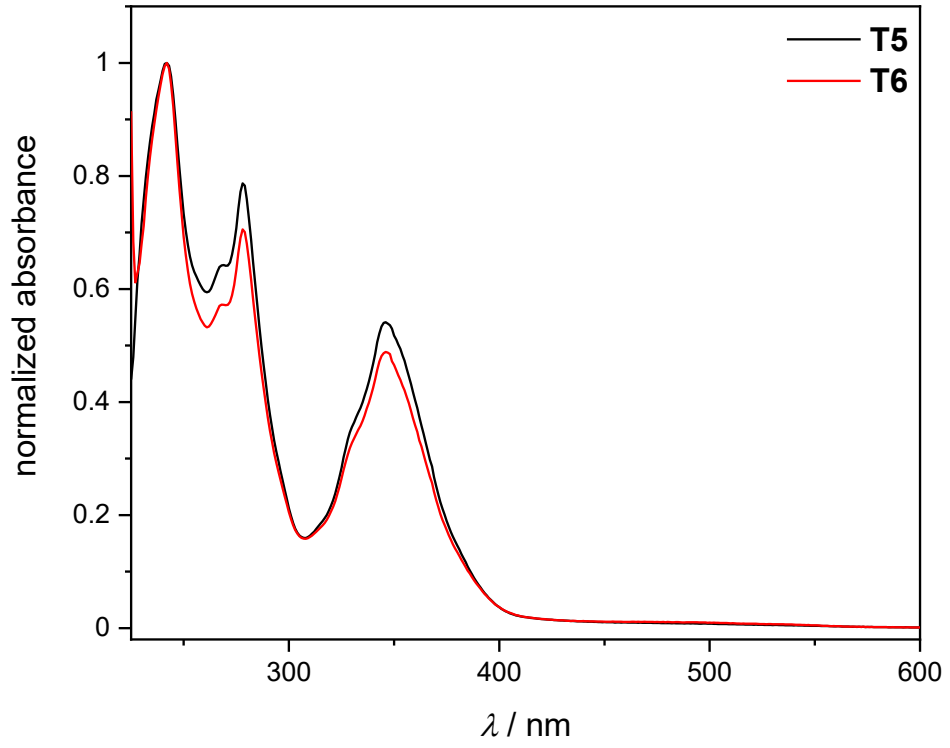

Figure 6.20: UV/Vis spectra of **T5** and **T6** in DCM at ambient temperature (c = 0.2 mg mL^{-1}).

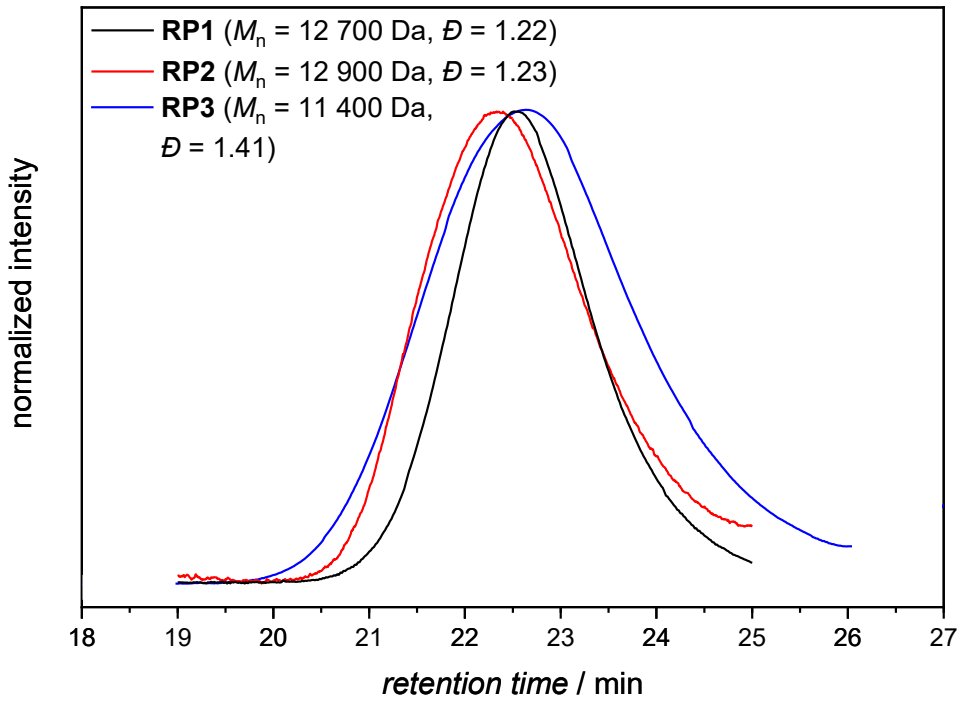

Figure 6.21: SEC elution traces of **RP1**, **RP2** and **RP3** in THF at 30°C.

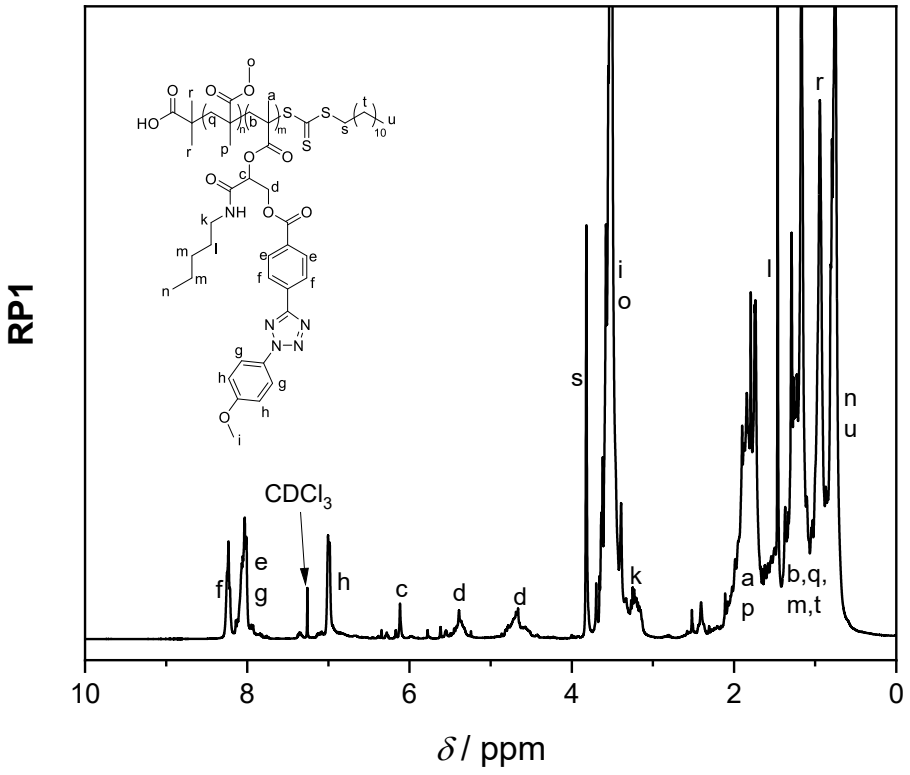

Figure 6.22: ^{1}H NMR (400 MHz) spectrum of **RP1** in $CDCl_3$.

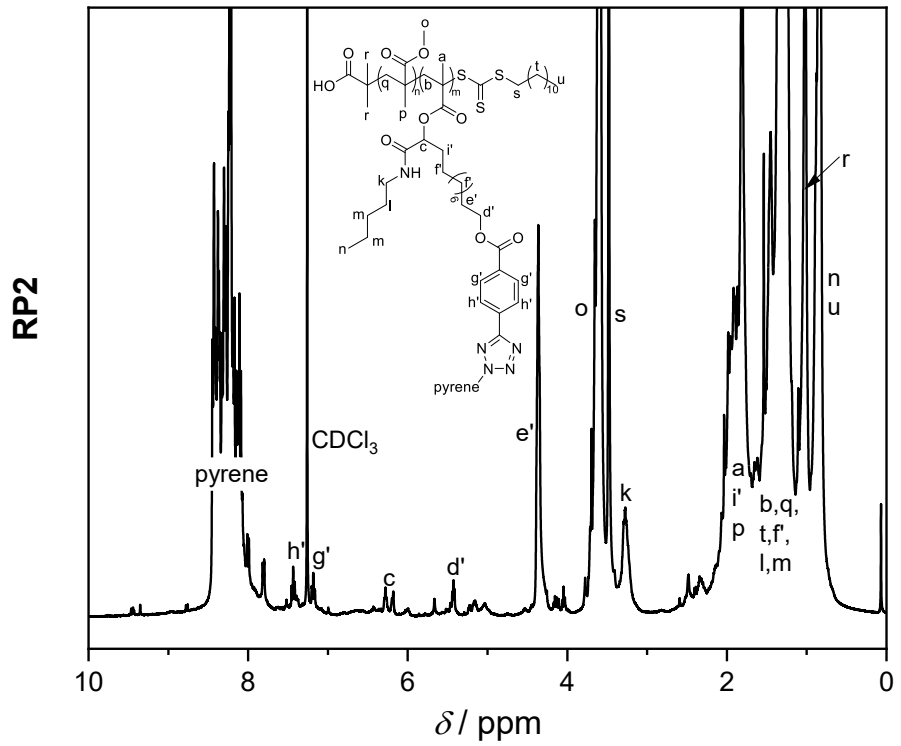

Figure 6.23: ^{1}H NMR (400 MHz) spectrum of **RP2** in $CDCl_3$.

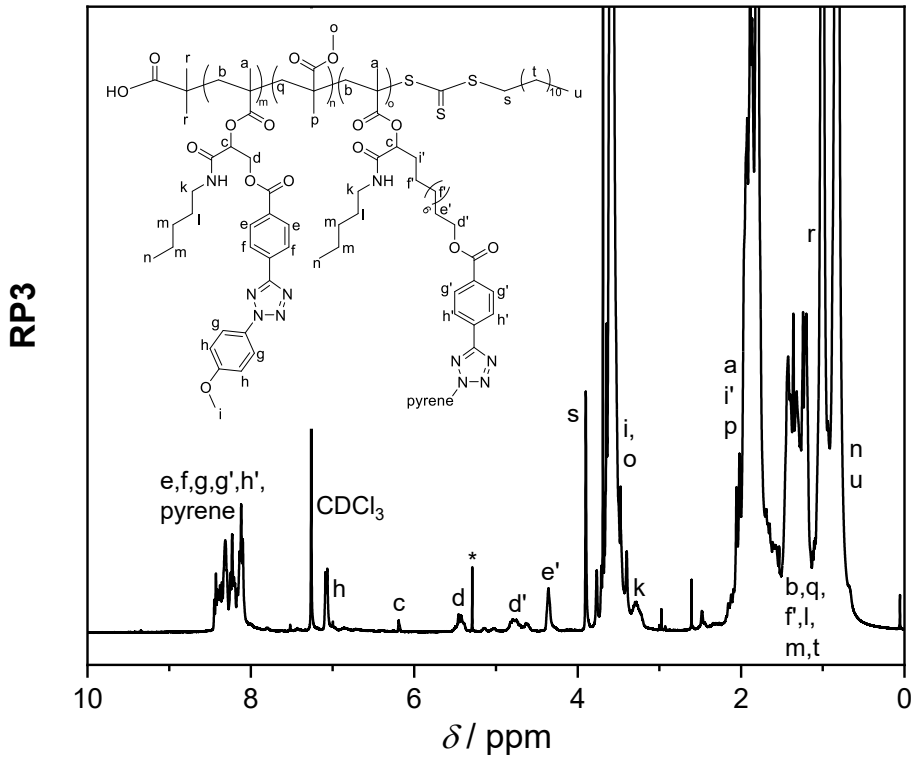

Figure 6.24: ^{1}H NMR (400 MHz) spectrum of **RP3** in $CDCl_3$.

6.3 List of Abbreviations

AA	L-ascorbic acid
AEC	active-ester copolymer
AIBN	2,2'-azobisisobutyronitrile
3-APA	3-aminophthalic acid
ATRP	atom transfer radical polymerization
Bis-Mal	bi-functional maleimide
BPO	benzyl peroxide
cat.	catalyst
CL	Chemiluminescence
CIEEL	chemical-induced electron-exchange luminescence
CuAAC	copper(I)-cat. alkyne-azide cycloadditions
Đ	dispersity
DBU	1,8-diazabicyclo[5.4.0]undec-7-ene
DCM	dichloromethane
DDDA	dodecanedioic acid
DFT	density functional theory
DICH	1,6-diisocyanohexane
DIPA	diisopropylamine
DLS	dynamic light scattering
DMAc	*N,N*-dimethylacetamide
DMAN	1,8-bis(dimethylamino)naphthalene
DMAP	4-Dimethylaminopyridine
DMF	*N,N*-dimehtyl formamide
DMP	Dess-Martin periodinane
DMPO	5,5,-dimethyl-1-pyrroline *N*-oxide
DMSO	dimethyl sulfoxide
DP_n	degree of polymerization
DPA	9,10-diphenylanthracence
DTBP	di-*tert*-butylperoxide
DTDPA	3,3'-dithiodipropionic acid

DTMP	2-(dodecylthiocarbonothioylthio)-2-methylpropionic acid
EDC	1-Ethyl-3-(3-dimethylaminopropyl)carbodiimide
EtOAc	ethyl acetate
EPR	electron-paramagnetic resonance
FRP	free radical polymerization
GC-MS	gas chromatography – mass spectrometry
HDA	heptanedioic acid
IC	Internal conversion
ISC	Intersystem crossing
LDA	lithium diisopropylamide
λ	wavelength
MAA	methacrylic acid
MCR	Multi-Component-Reaction
(Me-)β-CD	(methylated) β-cyclodextrin
M_n	molar number average
M_w	molar mass average
MMA	methyl methacrylate
NBS	*N*-bromosuccinimide
NIR	near infrared
NITEC	nitrile-imine mediated tetrazole-ene cycloaddition
NMP	nitroxide-mediated polymerization
NMR	nuclear magnetic resonance
NOESY	nuclear Overhauser effect spectroscopy
o-MBA	*ortho*-methyl benzaldehyde
PAT	pyrene-aryl-tetrazole
PIC	1-pentyl isocyanide
PG	protecting group
P-MCP	Passerini multi-component polymerization
P-MCR	Passerini multi-component reaction
PFP-A	pentafluorophenyl acrylate
PFP-MA	pentafluorophenyl methacrylate
PPM	post-polymerization modification

PO	peroxyoxalates
PS	polystyrene
RAFT	reversible addition-fragmentation chain transfer
ROS	reactive oxygen species
RDRP	reversible-deactivation radical polymerization
SEC	size exclusion chromatography
SOD	superoxide dismutase
TBD	1,5,7-triazabicyclo[4.4.0]dec-5-ene
TCPO	bis(2,4,6-trichlorophenyl)oxalate
TEA	triethylamine
THF	tetrahydrofuran
TMG	1,1,3,3-tetramethylguanidine
TMPD	2,2,6,6-tetramethyl-4-piperidone
TU	thiourea
UV	Ultraviolet
V-501	4,4’-azobis(4-cyanovaleric acid)
VBC	4-vinyl benzylchloride
Vis	Visible

6.4 List of Schemes

6.5 List of Figures

Bibliography

1. S. Wang; M. W. Urban. *Nat. Rev. Mater.* **2020**, *5*, 562.
2. J. A. McCune; S. Mommer; C. C. Parkins; O. A. Scherman. *Adv. Mater.* **2020**, *32*, 1906890.
3. J. F. Patrick; M. J. Robb; N. R. Sottos; J. S. Moore; S. R. White. *Nature* **2016**, *540*, 363.
4. C. M. Geiselhart; H. Mutlu; C. Barner-Kowollik. *Angew. Chem. Int. Ed.*, https://doi.org/10.1002/ anie.202012592.
5. P. Theato; B. S. Sumerlin; R. K. O'Reilly; I. I. I. T. H. Epps. *Chem. Soc. Rev.* **2013**, *42*, 7055.
6. G. Ge; Y. Lu; X. Qu; W. Zhao; Y. Ren; W. Wang; Q. Wang; W. Huang; X. Dong. *ACS Nano* **2020**, *14*, 218.
7. Y. Yang; D. Davydovich; C. C. Hornat; X. Liu; M. W. Urban. *Chem* **2018**, *4*, 1928.
8. Z. Deng; H. Wang; P. X. Ma; B. Guo. *Nanoscale* **2020**, *12*, 1224.
9. O. Speck; T. Speck. *Biomimetics* **2019**, *4*, 26.
10. B. Willocq; J. Odent; P. Dubois; J.-M. Raquez. *RSC Adv.* **2020**, *10*, 13766.
11. Q. Zhang; S. Niu; L. Wang; J. Lopez; S. Chen; Y. Cai; R. Du; Y. Liu; J.-C. Lai; L. Liu; C.-H. Li; X. Yan; C. Liu; J. B.-H. Tok; X. Jia; Z. Bao. *Adv. Mater.* **2018**, *30*, 1801435.
12. D. Döhler; P. Michael; W. H. Binder. *Acc. Chem. Res.* **2017**, *50*, 2610.
13. F. Zhang; P. Ju; M. Pan; D. Zhang; Y. Huang; G. Li; X. Li. *Corros. Sci.* **2018**, *144*, 74.
14. R. J. Wojtecki; M. A. Meador; S. J. Rowan. *Nat. Mater.* **2011**, *10*, 14.
15. X. K. D. Hillewaere; F. E. Du Prez. *Prog. Polym. Sci.* **2015**, *49-50*, 121.
16. M. Podgórski; B. D. Fairbanks; B. E. Kirkpatrick; M. McBride; A. Martinez; A. Dobson; N. J. Bongiardina; C. N. Bowman. *Adv. Mater.* **2020**, *32*, 1906876.
17. S. Billiet; X. K. D. Hillewaere; R. F. A. Teixeira; F. E. Du Prez. *Macromol. Rapid Commun.* **2013**, *34*, 290.
18. S. R. White; N. R. Sottos; P. H. Geubelle; J. S. Moore; M. R. Kessler; S. R. Sriram; E. N. Brown; S. Viswanathan. *Nature* **2001**, *409*, 794.
19. S. H. Cho; S. R. White; P. V. Braun. *Adv. Mater.* **2009**, *21*, 645.
20. O. Rifaie-Graham; E. A. Apebende; L. K. Bast; N. Bruns. *Adv. Mater.* **2018**, *30*, 1705483.
21. Y.-k. Kim; X. Wang; P. Mondkar; E. Bukusoglu; N. Abbott. *Nature* **2018**, *557*, 539.
22. J. V. Araujo; O. Rifaie-Graham; E. A. Apebende; N. Bruns, in *Bio-inspired Polymers*, The Royal Society of Chemistry, **2017**, pp. 354.
23. C. Calvino; C. Weder. *Small* **2018**, *14*, 1802489.
24. S. Chen; T. Han; Y. Zhao; W. Luo; Z. Zhang; H. Su; B. Z. Tang; J. Yang. *ACS Appl. Mater. Interfaces* **2020**, *12*, 4870.
25. J. Geng; W. Li; L. P. Smaga; N. R. Sottos; J. Chan. *Chem. Mater.* **2018**, *30*, 2198.
26. S. Shree; M. Dowds; A. Kuntze; Y. K. Mishra; A. Staubitz; R. Adelung. *Mater. Horiz.* **2020**, *7*, 598.
27. Y. Sagara; M. Karman; E. Verde-Sesto; K. Matsuo; Y. Kim; N. Tamaoki; C. Weder. *J. Am. Chem. Soc.* **2018**, *140*, 1584.
28. A. D. Das; G. Mannoni; A. E. Früh; D. Orsi; R. Pinalli; E. Dalcanale. *ACS Appl. Polym. Mater.* **2019**, *1*, 2990.
29. A. Giussani; P. Farahani; D. Martínez-Muñoz; M. Lundberg; R. Lindh; D. Roca-Sanjuán. *Chem. Eur. J.* **2019**, *25*, 5202.

30. K. K. Krzymiński; A. D. Roshal; P. B. Rudnicki-Velasquez; K. Żamojć. *Luminescence* **2019**, *34*, 512.
31. L. Delafresnaye; F. R. Bloesser; K. B. Kockler; C. W. Schmitt; I. M. Irshadeen; C. Barner-Kowollik. *Chem. Eur. J.* **2020**, *26*.
32. N. Hananya; D. Shabat. *ACS Cent. Sci.* **2019**, *5*, 949.
33. T. Zhang; Y. Li; Z. Zheng; R. Ye; Y. Zhang; R. T. K. Kwok; J. W. Y. Lam; B. Z. Tang. *J. Am. Chem. Soc.* **2019**, *141*, 5612.
34. A. M. Schenzel; N. Moszner; C. Barner-Kowollik. *Polym. Chem.* **2017**, *8*, 414.
35. A. Seeboth; D. Lötzsch; R. Ruhmann; O. Muehling. *Chem. Rev.* **2014**, *114*, 3037.
36. Y. Jia; S. Wang; W.-J. Wang; B.-G. Li; S. Zhu. *Macromolecules* **2019**, *52*, 7920.
37. R. W. Barber; M. E. McFadden; X. Hu; M. J. Robb. *Synlett* **2019**, *30*, 1725.
38. M. Li; Q. Zhang; Y.-N. Zhou; S. Zhu. *Prog. Polym. Sci.* **2018**, *79*, 26.
39. Q.-S. Tong; W. Xu; Q.-Y. Huang; Y.-R. Zhang; X.-X. Shi; H. Huang; H.-J. Li; J.-Z. Du; J. Wang. *Polym. Chem.* **2019**, *10*, 656.
40. J. M. Korde; B. Kandasubramanian. *Ind. Eng. Chem. Res.* **2019**, *58*, 9709.
41. E. Karshalev; R. Kumar; I. Jeerapan; R. Castillo; I. Campos; J. Wang. *Chem. Mater.* **2018**, *30*, 1593.
42. L. Mi; Y. Sun; L. Shi; T. Li. *ACS Appl. Mater. Interfaces* **2020**, *12*, 7879.
43. C. Zhao; H. Cui; J. Duan; S. Zhang; J. Lv. *Anal. Chem.* **2018**, *90*, 2201.
44. O. Green; T. Eilon; N. Hananya; S. Gutkin; C. R. Bauer; D. Shabat. *ACS Cent. Sci.* **2017**, *3*, 349.
45. M. Iranifam. *TrAC, Trends Anal. Chem.* **2014**, *59*, 156.
46. A. Roda, *Chemiluminescence and Bioluminescence: Past, Present and Future*, Royal Society of Chemistry, **2011**.
47. D. F. Roswell; E. H. White, in *Methods Enzymol., Vol. 57*, Academic Press, **1978**, pp. 409.
48. T. Martin; J. Fleissner; W. Milius; J. Breu. *Z. Anorg. Allg. Chem.* **2020**, *646*, 162.
49. W. Gu; H. Wang; L. Jiao; Y. Wu; Y. Chen; L. Hu; J. Gong; D. Du; C. Zhu. *Angew. Chem. Int. Ed.* **2020**, *59*, 3534.
50. P. Khan; D. Idrees; M. A. Moxley; J. A. Corbett; F. Ahmad; G. von Figura; W. S. Sly; A. Waheed; M. I. Hassan. *Appl. Biochem. Biotechnol.* **2014**, *173*, 333.
51. E. H. White; D. F. Roswell. *Acc. Chem. Res.* **1970**, *3*, 54.
52. F. McCapra. *Q. Rev. Chem. Soc.* **1966**, *20*, 485.
53. N. Corrigan; C. Boyer. *ACS Macro Lett.* **2019**, *8*, 812.
54. Q.-Q. Zhou; Y.-Q. Zou; L.-Q. Lu; W.-J. Xiao. *Angew. Chem. Int. Ed.* **2019**, *58*, 1586.
55. D. Cambié; F. Zhao; V. Hessel; M. G. Debije; T. Noël. *Angew. Chem. Int. Ed.* **2017**, *56*, 1050.
56. F. Politano; G. Oksdath-Mansilla. *Org. Process Res. Dev.* **2018**, *22*, 1045.
57. K. Jung; N. Corrigan; M. Ciftci; J. Xu; S. E. Seo; C. J. Hawker; C. Boyer. *Adv. Mater.* **2020**, *32*, 1903850.
58. M. Bilgi; D. Karaca Balta; B. A. Temel; G. Temel. *J. Polym. Sci., Part A: Polym. Chem.* **2018**, *56*, 2709.
59. I. Dashan; D. K. Balta; B. A. Temel; G. Temel. *Eur. Polym. J.* **2019**, *113*, 183.
60. C. Heiler; S. Bastian; P. Lederhose; J. P. Blinco; E. Blasco; C. Barner-Kowollik. *Chem. Commun.* **2018**, *54*, 3476.
61. T. S. Fischer; S. Spann; Q. An; B. Luy; M. Tsotsalas; J. P. Blinco; H. Mutlu; C. Barner-Kowollik. *Chem. Sci.* **2018**, *9*, 4696.
62. J. T. Offenloch; E. Blasco; S. Bastian; C. Barner-Kowollik; H. Mutlu. *Polym. Chem.* **2019**, *10*, 4513.

63. K. Hiltebrandt; M. Kaupp; E. Molle; J. P. Menzel; J. P. Blinco; C. Barner-Kowollik. *Chem. Commun.* **2016**, *52*, 9426.
64. S. Hurrle; A. Lauer; H. Gliemann; H. Mutlu; C. Wöll; A. S. Goldmann; C. Barner-Kowollik. *Macromol. Rapid Commun.* **2017**, *38*, 1600598.
65. N. Corrigan; M. Ciftci; K. Jung; C. Boyer. *Angew. Chem. Int. Ed.*, https://doi.org/10.1002/anie.201912001.
66. Y. Wang; W. J. Hu; W. Song; R. K. V. Lim; Q. Lin. *Org. Lett.* **2008**, *10*, 3725.
67. E. Blasco; Y. Sugawara; P. Lederhose; J. P. Blinco; A.-M. Kelterer; C. Barner-Kowollik. *ChemPhotoChem* **2017**, *1*, 159.
68. O. Olatunji, in *Natural Polymers: Industry Techniques and Applications* (Ed.: O. Olatunji), Springer International Publishing, Cham, **2016**, pp. 1.
69. S. Doppalapudi; S. Katiyar; A. J. Domb; W. Khan, in *Advanced Polymers in Medicine* (Ed.: F. Puoci), Springer International Publishing, Cham, **2015**, pp. 33.
70. G. Z. Papageorgiou. *Polymers (Basel)* **2018**, *10*, 952.
71. H. Staudinger. *Berichte der deutschen chemischen Gesellschaft (A and B Series)* **1920**, *53*, 1073.
72. *Nature* **1953**, *172*, 893.
73. A. S. Abd-El-Aziz; M. Antonietti; C. Barner-Kowollik; W. H. Binder; A. Böker; C. Boyer; M. R. Buchmeiser; S. Z. D. Cheng; F. D'Agosto; G. Floudas; H. Frey; G. Galli; J. Genzer; L. Hartmann; R. Hoogenboom; T. Ishizone; D. L. Kaplan; M. Leclerc; A. Lendlein; B. Liu; T. E. Long; S. Ludwigs; J.-F. Lutz; K. Matyjaszewski; M. A. R. Meier; K. Müllen; M. Müllner; B. Rieger; T. P. Russell; D. A. Savin; A. D. Schlüter; U. S. Schubert; S. Seiffert; K. Severing; J. B. P. Soares; M. Staffilani; B. S. Sumerlin; Y. Sun; B. Z. Tang; C. Tang; P. Théato; N. Tirelli; O. K. C. Tsui; M. M. Unterlass; P. Vana; B. Voit; S. Vyazovkin; C. Weder; U. Wiesner; W.-Y. Wong; C. Wu; Y. Yagci; J. Yuan; G. Zhang. *Macromol. Chem. Phys.* **2020**, *221*, 2000216.
74. H. Frey; T. Johann. *Polym. Chem.* **2020**, *11*, 8.
75. R. Mülhaupt. *Angew. Chem. Int. Ed.* **2004**, *43*, 1054.
76. D. Braun; H. Cherdron; M. Rehahn; H. Ritter; B. Voit, in *Polymer Synthesis: Theory and Practice: Fundamentals, Methods, Experiments* (Eds.: D. Braun, H. Cherdron, M. Rehahn, H. Ritter, B. Voit), Springer Berlin Heidelberg, Berlin, Heidelberg, **2013**, pp. 33.
77. G. Odian, *Principles of Polymerization*, Wiley, **2004**.
78. A. Rudin. *J. Chem. Educ.* **1969**, *46*, 595.
79. M. A. R. Meier; C. Barner-Kowollik. *Adv. Mater.* **2019**, *31*, 1806027.
80. J.-F. Lutz; M. Ouchi; D. R. Liu; M. Sawamoto. *Science* **2013**, *341*, 1238149.
81. J. De Neve; J. J. Haven; L. Maes; T. Junkers. *Polym. Chem.* **2018**, *9*, 4692.
82. A. Al Ouahabi; L. Charles; J.-F. Lutz. *J. Am. Chem. Soc.* **2015**, *137*, 5629.
83. A. C. Boukis; M. A. R. Meier. *Eur. Polym. J.* **2018**, *104*, 32.
84. S. Martens; A. Landuyt; P. Espeel; B. Devreese; P. Dawyndt; F. Du Prez. *Nat. Commun.* **2018**, *9*, 4451.
85. Y. Wang; C. Wu. *Biomacromolecules* **2018**, *19*, 1804.
86. D. J. Rucco; B. E. Barnes; J. B. Garrison; B. S. Sumerlin; D. A. Savin. *Biomacromolecules* **2020**, *21*, 5077.
87. C. Boyer; V. Bulmus; J. Liu; T. P. Davis; M. H. Stenzel; C. Barner-Kowollik. *J. Am. Chem. Soc.* **2007**, *129*, 7145.
88. J. Yang; I. Gitlin; V. M. Krishnamurthy; J. A. Vazquez; C. E. Costello; G. M. Whitesides. *J. Am. Chem. Soc.* **2003**, *125*, 12392.

89. J. Lawrence; S.-H. Lee; A. Abdilla; M. D. Nothling; J. M. Ren; A. S. Knight; C. Fleischmann; Y. Li; A. S. Abrams; B. V. K. J. Schmidt; M. C. Hawker; L. A. Connal; A. J. McGrath; P. G. Clark; W. R. Gutekunst; C. J. Hawker. *J. Am. Chem. Soc.* **2016**, *138*, 6306.
90. J. J. Haven; T. Junkers. *Polym. Chem.* **2019**, *10*, 679.
91. A. B. Chang; G. M. Miyake; R. H. Grubbs, in *Sequence-Controlled Polymers: Synthesis, Self-Assembly, and Properties, Vol. 1170*, American Chemical Society, **2014**, pp. 161.
92. W. R. Gutekunst; C. J. Hawker. *J. Am. Chem. Soc.* **2015**, *137*, 8038.
93. H. Frisch; B. T. Tuten; C. Barner-Kowollik. *Isr. J. Chem.* **2020**, *60*, 86.
94. B. Wei; W. Li; Z. Zhao; A. Qin; R. Hu; B. Z. Tang. *J. Am. Chem. Soc.* **2017**, *139*, 5075.
95. S. C. Solleder; K. S. Wetzel; M. A. R. Meier. *Polym. Chem.* **2015**, *6*, 3201.
96. S. C. Solleder; D. Zengel; K. S. Wetzel; M. A. R. Meier. *Angew. Chem. Int. Ed.* **2016**, *55*, 1204.
97. S. C. Solleder; R. V. Schneider; K. S. Wetzel; A. C. Boukis; M. A. R. Meier. *Macromol. Rapid Commun.* **2017**, *38*, 1600711.
98. T. T. Trinh; C. Laure; J.-F. Lutz. *Macromol. Chem. Phys.* **2015**, *216*, 1498.
99. M. Van De Walle; K. De Bruycker; J. P. Blinco; C. Barner-Kowollik. *Angew. Chem. Int. Ed.* **2020**, *59*, 14143.
100. M. Van De Walle; K. De Bruycker; T. Junkers; J. P. Blinco; C. Barner-Kowollik. *ChemPhotoChem* **2019**, *3*, 225.
101. W. Konrad; C. Fengler; S. Putwa; C. Barner-Kowollik. *Angew. Chem. Int. Ed.* **2019**, *58*, 7133.
102. N. Zydziak; W. Konrad; F. Feist; S. Afonin; S. Weidner; C. Barner-Kowollik. *Nat. Commun.* **2016**, *7*, 13672.
103. B. Yamada; P. B. Zetterlund, in *Handbook of Radical Polymerization* (Eds.: K. Matyjaszewski, T. P. Davis), Wiley-VCH Verlag GmbH & Co. KGaA, Weinheim, **2002**, pp. 117.
104. J. P. A. Heuts, in *Handbook of Radical Polymerization* (Eds.: K. Matyjaszewski, T. P. Davis), Wiley-VCH Verlag GmbH & Co. KGaA, Weinheim, **2002**, pp. 1.
105. M. D. Zammit; T. P. Davis; D. M. Haddleton; K. G. Suddaby. *Macromolecules* **1997**, *30*, 1915.
106. K. Matyjaszewski, in *Handbook of Radical Polymerization* (Eds.: K. Matyjaszewski, T. P. Davis), Wiley-VCH Verlag GmbH & Co. KGaA, Weinheim, **2002**, pp. 361.
107. K. Matyjaszewski; J. Spanswick. *Materials Today* **2005**, *8*, 26.
108. N. K. Singha; J. Mays, *Reversible Deactivation Radical Polymerization: Synthesis and Applications of Functional Polymers*, https://doi.org/10.1515/9783110643695, De Gruyter, **2020**.
109. W. Wang; J. Zhao; N. Zhou; J. Zhu; W. Zhang; X. Pan; Z. Zhang; X. Zhu. *Polym. Chem.* **2014**, *5*, 3533.
110. T. Fukuda; A. Goto; Y. Tsujii, in *Handbook of Radical Polymerization* (Eds.: K. Matyjaszewski, T. P. Davis), Wiley-VCH Verlag GmbH & Co. KGaA, Weinheim, **2002**, pp. 407.
111. K. Matyjaszewski; J. Xia, in *Handbook of Radical Polymerization* (Eds.: K. Matyjaszewski, T. P. Davis), Wiley-VCH Verlag GmbH & Co. KGaA, Weinheim, **2002**, pp. 523.
112. T. G. Ribelli; F. Lorandi; M. Fantin; K. Matyjaszewski. *Macromol. Rapid Commun.* **2019**, *40*, 1800616.
113. K. Matyjaszewski. *Macromolecules* **2012**, *45*, 4015.
114. C. J. Hawker, in *Handbook of Radical Polymerization* (Eds.: K. Matyjaszewski, T. P. Davis), Wiley-VCH Verlag GmbH & Co. KGaA, Weinheim, **2002**, pp. 463.

115. G. Moad; E. Rizzardo, in *Nitroxide Mediated Polymerization: From Fundamentals to Applications in Materials Science*, The Royal Society of Chemistry, **2016**, pp. 1.
116. H. R. Lamontagne; B. H. Lessard. *ACS Appl. Polym. Mater.* **2020**, *2*, 5327.
117. J. Chiefari;E. Rizzardo, in *Handbook of Radical Polymerization* (Eds.: K. Matyjaszewski, T. P. Davis), Wiley-VCH Verlag GmbH & Co. KGaA, Weinheim, **2002**, pp. 629.
118. S. Perrier. *Macromolecules* **2017**, *50*, 7433.
119. G. Moad. *Polym. Chem.* **2017**, *8*, 177.
120. G. Moad; C. Barner-Kowollik, in *Handbook of RAFT Polymerization* (Ed.: C. Barner-Kowollik), Wiley-VCH Verlag GmbH & Co. KGaA, Weinheim, **2008**, pp. 51.
121. D. J. Keddie; G. Moad; E. Rizzardo; S. H. Thang. *Macromolecules* **2012**, *45*, 5321.
122. R. Kakuchi. *Polymer Journal* **2019**, *51*, 945.
123. R. C. Cioc; E. Ruijter; R. V. A. Orru. *Green Chemistry* **2014**, *16*, 2958.
124. A. Dömling; A. D. AlQahatani, in *Multicomponent Reactions in Organic Synthesis* (Eds.: J. Zhu, Q. Wanf, M.-X. Wang), Wiley-VCH Verlag GmbH & Co. KGaA, **2014**, pp. 1.
125. C. G. Neochoritis; T. Zarganes-Tzitzikas; K. Katsampoxaki-Hodgetts; A. Dömling. *J. Chem. Educ.* **2020**, *97*, 3739.
126. A. Dömling; W. Wang; K. Wang. *Chem. Rev.* **2012**, *112*, 3083.
127. E. Marqués-López; R. P. Herrera, in *Multicomponent Reactions* (Eds.: R. P. Herrera, E. Marqués-López), Wiley-VCH Verlag GmbH & Co. KGaA, **2015**, pp. 306.
128. V. G. Santos; M. N. Godoi; T. Regiani; F. H. S. Gama; M. B. Coelho; R. O. M. A. de Souza; M. N. Eberlin; S. J. Garden. *Chem. Eur. J.* **2014**, *20*, 12808.
129. J. Wang; X. Liu; X. Feng. *Chem. Rev.* **2011**, *111*, 6947.
130. S. Saranya; N. A. Harry; K. K. Krishnan; G. Anilkumar. *Asian J. Org. Chem.* **2018**, *7*, 613.
131. E. D. Matveeva; N. S. Zefirov. *Dokl. Chem.* **2008**, *420*, 137.
132. X. Li; T. Wang; Y.-J. Lu; S. Ji; Y. Huo; B. Liu. *Org. Biomol. Chem.* **2018**, *16*, 7143.
133. S. Saranya; K. R. Rohit; S. Radhika; G. Anilkumar. *Org. Biomol. Chem.* **2019**, *17*, 8048.
134. M. A. Fouad; H. Abdel-Hamid; M. S. Ayoup. *RSC Adv.* **2020**, *10*, 42644.
135. E. Marqués-López; R. P. Herrera, in *Multicomponent Reactions* (Eds.: E. Marqués-López, R. P. Herrera), Wiley-VCH Veralg GmbH & Co. KGaA, **2015**, pp. 283.
136. J. G. Rudick; S. Shaabani; A. Dömling. *Front. Chem.* **2020**, *7*.
137. A. Dömling; I. Ugi. *Angew. Chem. Int. Ed.* **2000**, *39*, 3168.
138. M. Lakshminarasimhan; P. Madzelan; R. Nan; N. M. Milkovic; M. A. Wilson. *J Biol Chem* **2010**, *285*, 29651.
139. M. A. Mironov, in *Isocyanide Chemistry* (Ed.: V. G. Nenajdenko), Wiley-VCH Verlag GmbH & Co. KGaA, Weinheim, **2012**, pp. 35.
140. R. Ramozzi; N. Chéron; B. Braïda; P. C. Hiberty; P. Fleurat-Lessard. *New J. Chem.* **2012**, *36*, 1137.
141. A. Shaabani; A. Sarvary; A. Maleki, in *Isocyanide Chemistry* (Ed.: V. G. Nenajdenko), Wiley-VCH Verlag GmbH & Co. KGaA, Weinheim, **2012**, pp. 263.
142. L. A. Wessjohann; R. A. W. N. Filho; D. G. Rivera, in *Isocyanide Chemistry* (Ed.: V. G. Nenajdenko), Wiley-VCH Verlag GmbH & Co. KGaA, Weinheim, **2012**, pp. 233.
143. A. V. Gulevich; A. G. Zhdanko; R. V. A. Orru; V. G. Nenajdenko, in *Isocyanide Chemistry* (Ed.: V. G. Nenajdenko), Wiley-VCH Verlag GmbH & Co. KGaA, Weinheim, **2012**, pp. 109.
144. R. Ramozzi; K. Morokuma. *J. Org. Chem.* **2015**, *80*, 5652.
145. H. G. O. Alvim; E. N. da Silva Júnior; B. A. D. Neto. *RSC Adv.* **2014**, *4*, 54282.
146. I. Ugi; R. Meyr. *Chem. Ber.* **1961**, *94*, 2229.
147. R. H. Baker; D. Stanonis. *J. Am. Chem. Soc.* **1951**, *73*, 699.

148. O. Kreye; T. Tóth; M. A. R. Meier. *J. Am. Chem. Soc.* **2011**, *133*, 1790.
149. B. T. Tuten; L. De Keer; S. Wiedbrauk; P. H. M. Van Steenberge; D. R. D'hooge; C. Barner-Kowollik. *Angew. Chem. Int. Ed.* **2019**, *58*, 5672.
150. A. Sehlinger; M. A. R. Meier, in *Multi-Component and Sequential Reactions in Polymer Synthesis* (Ed.: P. Theato), Springer International Publishing, Cham, **2015**, pp. 61.
151. X.-X. Deng; L. Li; Z.-L. Li; A. Lv; F.-S. Du; Z.-C. Li. *ACS Macro Lett.* **2012**, *1*, 1300.
152. J. Zhang; M. Zhang; F.-S. Du; Z.-C. Li. *Macromolecules* **2016**, *49*, 2592.
153. A. E. J. de Nooy; G. Masci; V. Crescenzi. *Macromolecules* **1999**, *32*, 1318.
154. Y. Cui; M. Zhang; F.-S. Du; Z.-C. Li. *ACS Macro Lett.* **2017**, *6*, 11.
155. W. Lin; X. Guan; T. Sun; Y. Huang; X. Jing; Z. Xie. *Colloids Surf. B.* **2015**, *126*, 217.
156. L. Li; A. Lv; X.-X. Deng; F.-S. Du; Z.-C. Li. *Chem. Commun.* **2013**, *49*, 8549.
157. K. A. Günay; P. Theato; H.-A. Klok, in *Functional Polymers by Post-Polymerization Modification* (Eds.: P. Theato, H.-A. Klok), Wiley-VCH Verlag GmbH & Co. KGaA, Weinheim, **2013**, pp. 1.
158. M. A. Gauthier; M. I. Gibson; H.-A. Klok. *Angew. Chem. Int. Ed.* **2009**, *48*, 48.
159. E. Blasco; M. B. Sims; A. S. Goldmann; B. S. Sumerlin; C. Barner-Kowollik. *Macromolecules* **2017**, *50*, 5215.
160. N. K. Singha; H. Schlaad, in *Functional Polymers by Post-Polymerization Modification* (Eds.: P. Theato, H.-A. Klok), Wiley-VCH Verlag GmbH & Co. KGaA, Weinheim, **2013**, pp. 65.
161. G. Delaittre; L. Barner. *Polym. Chem.* **2018**, *9*, 2679.
162. C. M. Geiselhart; J. T. Offenloch; H. Mutlu; C. Barner-Kowollik. *ACS Macro Lett.* **2016**, *5*, 1146.
163. G. Delaittre; N. K. Guimard; C. Barner-Kowollik. *Acc. Chem. Res.* **2015**, *48*, 1296.
164. T. N. Gevrek; M. Arslan; A. Sanyal, in *Functional Polymers by Post-Polymerization Modification* (Eds.: P. Theato, H.-A. Klok), Wiley-VCH Verlag GmbH & Co. KGaA, Weinheim, **2013**, pp. 119.
165. R. Kakuchi; P. Theato, in *Functional Polymers by Post-Polymerization Modification* (Eds.: P. Theato, H.-A. Klok), Wiley-VCH Verlag GmbH & Co. KGaA, Weinheim, **2013**, pp. 45.
166. A. Das; P. Theato. *Chem. Rev.* **2016**, *116*, 1434.
167. Y. Pinyakit; T. Palaga; S. Kiatkamjornwong; V. P. Hoven. *J. Mater. Chem. B* **2020**, *8*, 454.
168. M. Eberhardt; R. Mruk; R. Zentel; P. Théato. *Eur. Polym. J.* **2005**, *41*, 1569.
169. A. Juris; P. Ceroni; V. Balzani, *Photochemistry and Photophysics: Concepts, Research, Applications*, Wiley-VCH Verlag GmbH & Co. KGaA, Weinheim, **2014**.
170. W.-D. Stohrer. *Photochemie* **1998**, https://doi.org/10.1002/3527603247.ch2, 5.
171. P. W. Atkins; J. De Paula, *Physikalische Chemie*, Wiley-VCH Verlag GmbH & Co. KGaA, Weinheim, **2014**.
172. P. J. Walla, in *Modern Biophysical Chemistry* (Ed.: P. J. Walla), Wiley-VCH Verlag GmbH & Co. KGaA, **2014**, pp. 13.
173. B. Wardle, *Principles and Applications of Photochemistry*, Wiley, **2009**.
174. A. Natarajan; C. K. Tsai; S. I. Khan; P. McCarren; K. N. Houk; M. A. Garcia-Garibay. *J. Am. Chem. Soc.* **2007**, *129*, 9846.
175. H. Trommsdorff. *Annalen der Pharmacie* **1834**, *11*, 190.
176. H. D. Roth. *Angew. Chem. Int. Ed.* **1989**, *28*, 1193.
177. M. W. H. Hoorens; W. Szymanski. *Trends Biochem. Sci* **2018**, *43*, 567.
178. E. Blasco; M. Wegener; C. Barner-Kowollik. *Adv. Mater.* **2017**, *29*, 1604005.
179. N. Hoffmann. *Chem. Rev.* **2008**, *108*, 1052.
180. A. B. Beeler. *Chem. Rev.* **2016**, *116*, 9629.

181. R. G. W. Norrish; C. H. Bamford. *Nature* **1937**, *140*, 195.
182. B. Marchetti; T. N. V. Karsili; M. N. R. Ashfold. *Phys. Chem. Chem. Phys.* **2019**, *21*, 14418.
183. M. D'Auria. *Photochem. Photobiol. Sci.* **2019**, *18*, 2297.
184. G. W. Breton; X. Vang. *J. Chem. Educ.* **1998**, *75*, 81.
185. H. I. Bernstein; W. C. Quimby. *J. Am. Chem. Soc.* **1943**, *65*, 1845.
186. V. X. Truong; F. Li; F. Ercole; J. S. Forsythe. *ACS Macro Lett.* **2018**, *7*, 464.
187. P. Jöckle; I. Lamparth; N. Moszner; C. Barner-Kowollik; A.-N. Unterreiner. *Polym. Chem.* **2020**, *11*, 3972.
188. C. E. Hoyle; C. N. Bowman. *Angew. Chem. Int. Ed.* **2010**, *49*, 1540.
189. A. B. Lowe. *Polym. Chem.* **2010**, *1*, 17.
190. N. B. Cramer; J. P. Scott; C. N. Bowman. *Macromolecules* **2002**, *35*, 5361.
191. N. ten Brummelhuis; C. Diehl; H. Schlaad. *Macromolecules* **2008**, *41*, 9946.
192. R. M. Hensarling; V. A. Doughty; J. W. Chan; D. L. Patton. *J. Am. Chem. Soc.* **2009**, *131*, 14673.
193. B. Yao; J. Mei; J. Li; J. Wang; H. Wu; J. Z. Sun; A. Qin; B. Z. Tang. *Macromolecules* **2014**, *47*, 1325.
194. A. B. Lowe. *Polymer* **2014**, *55*, 5517.
195. X. Zhang; W. Xi; C. Wang; M. Podgórski; C. N. Bowman. *ACS Macro Lett.* **2016**, *5*, 229.
196. W. Xi; H. Peng; A. Aguirre-Soto; C. J. Kloxin; J. W. Stansbury; C. N. Bowman. *Macromolecules* **2014**, *47*, 6159.
197. S. Chatani; T. Gong; B. A. Earle; M. Podgórski; C. N. Bowman. *ACS Macro Lett.* **2014**, *3*, 315.
198. T. Junkers. *Eur. Polym. J.* **2015**, *62*, 273.
199. D. E. Marschner; H. Frisch; J. T. Offenloch; B. T. Tuten; C. R. Becer; A. Walther; A. S. Goldmann; P. Tzvetkova; C. Barner-Kowollik. *Macromolecules* **2018**, *51*, 3802.
200. S. Telitel; E. Blasco; L. D. Bangert; F. H. Schacher; A. S. Goldmann; C. Barner-Kowollik. *Polym. Chem.* **2017**, *8*, 4038.
201. T. Krappitz; F. Feist; I. Lamparth; N. Moszner; H. John; J. P. Blinco; T. R. Dargaville; C. Barner-Kowollik. *Mater. Horiz.* **2019**, *6*, 81.
202. Y. Zheng; M. Micic; S. V. Mello; M. Mabrouki; F. M. Andreopoulos; V. Konka; S. M. Pham; R. M. Leblanc. *Macromolecules* **2002**, *35*, 5228.
203. J. He; L. Tremblay; S. Lacelle; Y. Zhao. *Soft Matter* **2011**, *7*, 2380.
204. T. K. Claus; S. Telitel; A. Welle; M. Bastmeyer; A. P. Vogt; G. Delaittre; C. Barner-Kowollik. *Chem. Commun.* **2017**, *53*, 1599.
205. M. Glassner; K. K. Oehlenschlaeger; A. Welle; M. Bruns; C. Barner-Kowollik. *Chem. Commun.* **2013**, *49*, 633.
206. T. Tischer; T. K. Claus; K. K. Oehlenschlaeger; V. Trouillet; M. Bruns; A. Welle; K. Linkert; A. S. Goldmann; H. G. Börner; C. Barner-Kowollik. *Macromol. Rapid Commun.* **2014**, *35*, 1121.
207. T. Pauloehrl; A. Welle; K. K. Oehlenschlaeger; C. Barner-Kowollik. *Chem. Sci.* **2013**, *4*, 3503.
208. O. Altintas; J. Willenbacher; K. N. R. Wuest; K. K. Oehlenschlaeger; P. Krolla-Sidenstein; H. Gliemann; C. Barner-Kowollik. *Macromolecules* **2013**, *46*, 8092.
209. J. T. Offenloch; S. Norsic; H. Mutlu; M. Taam; O. Boyron; C. Boisson; F. D'Agosto; C. Barner-Kowollik. *Polym. Chem.* **2018**, *9*, 3633.
210. K. K. Oehlenschlaeger; J. O. Mueller; N. B. Heine; M. Glassner; N. K. Guimard; G. Delaittre; F. G. Schmidt; C. Barner-Kowollik. *Angew. Chem. Int. Ed.* **2013**, *52*, 762.

211. A. Kerbs; P. Mueller; M. Kaupp; I. Ahmed; A. S. Quick; D. Abt; M. Wegener; C. M. Niemeyer; C. Barner-Kowollik; L. Fruk. *Chem. Eur. J.* **2017**, *23*, 4990.
212. A. F. Hirschbiel; W. Konrad; D. Schulze-Sünninghausen; S. Wiedmann; B. Luy; B. V. K. J. Schmidt; C. Barner-Kowollik. *ACS Macro Lett.* **2015**, *4*, 1062.
213. P. Mueller; M. M. Zieger; B. Richter; A. S. Quick; J. Fischer; J. B. Mueller; L. Zhou; G. U. Nienhaus; M. Bastmeyer; C. Barner-Kowollik; M. Wegener. *ACS Nano* **2017**, *11*, 6396.
214. J. P. Hooker; F. Feist; L. Delafresnaye; F. Cavalli; L. Barner; C. Barner-Kowollik. *Chem. Commun.* **2020**, *56*, 4986.
215. J. P. Hooker; F. Feist; L. Delafresnaye; L. Barner; C. Barner-Kowollik. *Adv. Funct. Mater.* **2020**, *30*, 1905399.
216. T. Laue; A. Plagens, *Namen- und Schlagwort-Reaktionen der Organsichen Chemie*, Vieweg + Teubner Verlag, Springer Fachmedien Wiesbaden GmbH, Wiesbaden, **2006**.
217. G. Bianchi; C. De Micheli; R. Gandolfi. *Angew. Chem. Int. Ed.* **1979**, *18*, 721.
218. R. K. V. Lim; Q. Lin. *Chem. Commun.* **2010**, *46*, 7993.
219. C. J. Dürr; P. Lederhose; L. Hlalele; D. Abt; A. Kaiser; S. Brandau; C. Barner-Kowollik. *Macromolecules* **2013**, *46*, 5915.
220. J.-F. Lutz. *Angew. Chem. Int. Ed.* **2007**, *46*, 1018.
221. H. B. Tinmaz; I. Arslan; M. A. Tasdelen. *J. Polym. Sci., Part A: Polym. Chem.* **2015**, *53*, 1687.
222. B. J. Adzima; Y. Tao; C. J. Kloxin; C. A. DeForest; K. S. Anseth; C. N. Bowman. *Nat. Chem.* **2011**, *3*, 256.
223. H. B. Song; A. Baranek; C. N. Bowman. *Polym. Chem.* **2016**, *7*, 603.
224. M. K. McBride; T. Gong; D. P. Nair; C. N. Bowman. *Polymer* **2014**, *55*, 5880.
225. A. Baranek; H. B. Song; M. McBride; P. Finnegan; C. N. Bowman. *Macromolecules* **2016**, *49*, 1191.
226. C. G. Neochoritis; T. Zhao; A. Dömling. *Chem. Rev.* **2019**, *119*, 1970.
227. R. Sustmann; R. Huisgen; H. Huber. *Chem. Ber.* **1967**, *100*, 1802.
228. V. Lohse; P. Leihkauf; C. Csongar; G. Tomaschewski. *J. Prakt. Chem. /Chem-Ztg* **1988**, *330*, 406.
229. C. Heiler; J. T. Offenloch; E. Blasco; C. Barner-Kowollik. *ACS Macro Lett.* **2017**, *6*, 56.
230. Z. Li; L. Qian; L. Li; J. C. Bernhammer; H. V. Huynh; J.-S. Lee; S. Q. Yao. *Angew. Chem. Int. Ed.* **2016**, *55*, 2002.
231. S.-L. Zheng; Y. Wang; Z. Yu; Q. Lin; P. Coppens. *J. Am. Chem. Soc.* **2009**, *131*, 18036.
232. Y. Zhang; W. Liu; Z. K. Zhao. *Molecules* **2014**, *19*, 306.
233. W. Feng; L. Li; C. Yang; A. Welle; O. Trapp; P. A. Levkin. *Angew. Chem. Int. Ed.* **2015**, *54*, 8732.
234. K. Livingstone; S. Bertrand; J. Mowat; C. Jamieson. *Chem. Sci.* **2019**, *10*, 10412.
235. K. Livingstone; S. Bertrand; A. R. Kennedy; C. Jamieson. *Chem. Eur. J.* **2020**, *26*, 10591.
236. Y. Y. Khine; R. Batchelor; R. Raveendran; M. H. Stenzel. *Macromol. Rapid Commun.* **2020**, *41*, 1900499.
237. Y. Sugawara; N. Jasinski; M. Kaupp; A. Welle; N. Zydziak; E. Blasco; C. Barner-Kowollik. *Chem. Commun.* **2015**, *51*, 13000.
238. L. Delafresnaye; N. Zaquen; R. P. Kuchel; J. P. Blinco; P. B. Zetterlund; C. Barner-Kowollik. *Adv. Funct. Mater.* **2018**, *28*, 1800342.
239. K. Piradashvili; J. Simon; D. Paßlick; J. R. Höhner; V. Mailänder; F. R. Wurm; K. Landfester. *Nanoscale Horiz.* **2017**, *2*, 297.
240. Y. Wang; C. I. Rivera Vera; Q. Lin. *Org. Lett.* **2007**, *9*, 4155.
241. S. Arndt; H.-A. Wagenknecht. *Angew. Chem. Int. Ed.* **2014**, *53*, 14580.
242. Z. Yu; L. Y. Ho; Z. Wang; Q. Lin. *Bioorg Med Chem Lett* **2011**, *21*, 5033.

243. P. Lederhose; K. N. R. Wüst; C. Barner-Kowollik; J. P. Blinco. *Chem. Commun.* **2016**, *52*, 5928.
244. L. Stolzer; A. Vigovskaya; C. Barner-Kowollik; L. Fruk. *Chem. Eur. J.* **2015**, *21*, 14309.
245. R. R. Batchelor; E. Blasco; K. N. R. Wuest; H. Lu; M. Wegener; C. Barner-Kowollik; M. H. Stenzel. *Chem. Commun.* **2018**, *54*, 2436.
246. M. Dietrich; G. Delaittre; J. P. Blinco; A. J. Inglis; M. Bruns; C. Barner-Kowollik. *Adv. Funct. Mater.* **2012**, *22*, 304.
247. E. Blasco; M. Piñol; L. Oriol; B. V. K. J. Schmidt; A. Welle; V. Trouillet; M. Bruns; C. Barner-Kowollik. *Adv. Funct. Mater.* **2013**, *23*, 4011.
248. A. Hufendiek; A. Carlmark; M. A. R. Meier; C. Barner-Kowollik. *ACS Macro Lett.* **2016**, *5*, 139.
249. J. T. Offenloch; J. Willenbacher; P. Tzvetkova; C. Heiler; H. Mutlu; C. Barner-Kowollik. *Chem. Commun.* **2017**, *53*, 775.
250. J. Willenbacher; K. N. R. Wuest; J. O. Mueller; M. Kaupp; H.-A. Wagenknecht; C. Barner-Kowollik. *ACS Macro Lett.* **2014**, *3*, 574.
251. E. Verde-Sesto; A. Blázquez-Martín; J. A. Pomposo. *Polymers (Basel)* **2019**, *11*, 1903.
252. E. Verde-Sesto; A. Arbe; A. J. Moreno; D. Cangialosi; A. Alegría; J. Colmenero; J. A. Pomposo. *Mater. Horiz.* **2020**, *7*, 2292.
253. A. M. Hanlon; C. K. Lyon; E. B. Berda. *Macromolecules* **2016**, *49*, 2.
254. M. Vacher; I. Fdez. Galván; B.-W. Ding; S. Schramm; R. Berraud-Pache; P. Naumov; N. Ferré; Y.-J. Liu; I. Navizet; D. Roca-Sanjuán; W. J. Baader; R. Lindh. *Chem. Rev.* **2018**, *118*, 6927.
255. T. H. Fereja; A. Hymete; T. Gunasekaran. *Int. Sch. Res. Notices* **2013**, *2013*, 1.
256. F. McCapra, in *Methods Enzymol., Vol. 305*, Academic Press, **2000**, pp. 3.
257. C. Dodeigne; L. Thunus; R. Lejeune. *Talanta* **2000**, *51*, 415.
258. K. B. Kockler; H. Frisch; C. Barner-Kowollik. *Macromol. Rapid Commun.* **2018**, *39*, 1800516.
259. L. Delafresnaye; C. W. Schmitt; L. Barner; C. Barner-Kowollik. *Chem. Eur. J.* **2019**, *25*, 12538.
260. A. Natrajan; D. Wen; D. Sharpe. *Org. Biomol. Chem.* **2014**, *12*, 3887.
261. M. Nakazono; Y. Oshikawa; M. Nakamura; H. Kubota; S. Nanbu. *J. Org. Chem.* **2017**, *82*, 2450.
262. S. Gnaim; O. Green; D. Shabat. *Chem. Commun.* **2018**, *54*, 2073.
263. M. E. Roth-Konforti; C. R. Bauer; D. Shabat. *Angew. Chem. Int. Ed.* **2017**, *56*, 15633.
264. O. Seven; F. Sozmen; I. Simsek Turan. *Sens. Actuators B Chem.* **2017**, *239*, 1318.
265. J. Sun; Z. Hu; S. Zhang; X. Zhang. *ACS Sensors* **2019**, *4*, 87.
266. D. Cui; J. Li; X. Zhao; K. Pu; R. Zhang. *Adv. Mater.* **2020**, *32*, 1906314.
267. B. A. Stoica; S. Bunescu; A. Neamtu; D. Bulgaru-Iliescu; L. Foia; E. G. Botnariu. *J. Forensic* **2016**, *61*, 1331.
268. T. I. Quickenden; C. P. Ennis; J. I. Creamer. *Luminescence* **2004**, *19*, 271.
269. D. L. Giokas; A. G. Vlessidis; G. Z. Tsogas; N. P. Evmiridis. *TrAC, Trends Anal. Chem.* **2010**, *29*, 1113.
270. L. Chen; Z. Zhang; X. Zhang; A. Fu; P. Xue; R. Yan. *Food Chem.* **2012**, *135*, 208.
271. W. Qin; Z. J. Zhang; F. C. Wang. *Fresenius J. Anal. Chem.* **1998**, *360*, 130.
272. R. B. Brundrett; E. H. White. *J. Am. Chem. Soc.* **1974**, *96*, 7497.
273. M. P. Algi; Z. Oztas; S. Tirkeş; A. Cihaner; F. Algi. *J. Fluoresc.* **2017**, *27*, 509.
274. D. Asil; A. Cihaner; A. M. Önal. *Electrochim. Acta* **2009**, *54*, 6740.
275. M. R. Nabid; S. S. Taheri; R. Sedghi; S. J. T. Rezaei. *Macromol. Res.* **2011**, *19*, 280.

276. D. Asil; A. Cihaner; F. Algı; A. M. Önal. *Electroanalysis* **2010**, *22*, 2254.
277. S. Deepa; K. Rajendrakumar. *ChemistrySelect* **2019**, *4*, 1158.
278. B. S. Johnson; W. J. Ward, (Ed.: N. C. f. B. Information), NALCO CHEMICAL CO, **1997**.
279. H. Zhang; C. Smanmoo; T. Kabashima; J. Lu; M. Kai. *Angew. Chem. Int. Ed.* **2007**, *46*, 8226.
280. H. N. Choi; J. H. Han; J. A. Park; J. M. Lee; W.-Y. Lee. *Electroanalysis* **2007**, *19*, 1757.
281. Y. B. Tsaplev. *J. Anal. Chem.* **2012**, *67*, 506.
282. P. Muller. *Pure Appl. Chem.* **1994**, *66*, 1077.
283. T. Ishikawa; L. M. Harwood. *Synlett* **2013**, *24*, 2507.
284. J. Verkade. *Angew. Chem. Int. Ed.* **2009**, *48*, 9221.
285. I. Kaljurand; J. Saame; T. Rodima; I. Koppel; I. A. Koppel; J. F. Kögel; J. Sundermeyer; U. Köhn; M. P. Coles; I. Leito. *J. Phys. Chem. A* **2016**, *120*, 2591.
286. T. Ishikawa, *Superbases for Organic Synthesis: Guanidines, Amidines, Phosphazenes and Related Organocatalysts*, https://doi.org/10.1002/9780470740859.fmatter, Wiley-VCH Verlag GmbH & Co. KGaA, **2009**.
287. L. A. Ruiz-Cantu; A. K. Pearce; L. Burroughs; T. M. Bennett; C. E. Vasey; R. Wildman; D. J. Irvine; C. Alexander; V. Taresco. *Macromol. Chem. Phys.* **2019**, *220*, 1800459.
288. R. C. Pratt; B. G. G. Lohmeijer; D. A. Long; R. M. Waymouth; J. L. Hedrick. *J. Am. Chem. Soc.* **2006**, *128*, 4556.
289. D. Simoni; M. Rossi; R. Rondanin; A. Mazzali; R. Baruchello; C. Malagutti; M. Roberti; F. P. Invidiata. *Org. Lett.* **2000**, *2*, 3765.
290. B. A. Trofimov; E. F. Sagitova; O. V. Petrova; L. N. Sobenina; I. A. Ushakov; A. V. Vashchenko. *Tetrahedron Lett.* **2017**, *58*, 2209.
291. W. Ye; J. Xu; C.-T. Tan; C.-H. Tan. *Tetrahedron Lett.* **2005**, *46*, 6875.
292. N. Porahmad; R. Baharfar. *Res. Chem. Intermed.* **2018**, *44*, 305.
293. C. Volpe; S. Meninno; A. Capobianco; G. Vigliotta; A. Lattanzi. *Adv. Synth. Catal.* **2019**, *361*, 1018.
294. A. Singh; B. Ganguly. *New J. Chem.* **2008**, *32*, 210.
295. D. Simoni; R. Rondanin; M. Morini; R. Baruchello; F. P. Invidiata. *Tetrahedron Lett.* **2000**, *41*, 1607.
296. H. Sabet-Sarvestani; H. Eshghi; M. Izadyar. *Struct. Chem.* **2017**, *28*, 675.
297. J. E. Taylor; S. D. Bull; J. M. J. Williams. *Chem. Soc. Rev.* **2012**, *41*, 2109.
298. D. Castagnolo; S. Schenone; M. Botta. *Chem. Rev.* **2011**, *111*, 5247.
299. J.-P. Schermann, in *Spectroscopy and Modeling of Biomolecular Building Blocks* (Ed.: J.-P. Schermann), Elsevier, Amsterdam, **2008**, pp. 211.
300. C. Alonso-Moreno; A. Antiñolo; F. Carrillo-Hermosilla; A. Otero. *Chem. Soc. Rev.* **2014**, *43*, 3406.
301. J. W. Shaw; D. H. Grayson; I. Rozas, in *Guanidines as Reagents and Catalysts I* (Ed.: P. Selig), Springer International Publishing, Cham, **2017**, pp. 1.
302. A. Demjén; A. Angyal; J. Wölfling; L. G. Puskás; I. Kanizsai. *Org. Biomol. Chem.* **2018**, *16*, 2143.
303. T. Ishikawa; T. Kumamoto. *Synthesis* **2006**, *2006*, 737.
304. M. K. Kiesewetter; M. D. Scholten; N. Kirn; R. L. Weber; J. L. Hedrick; R. M. Waymouth. *J. Org. Chem.* **2009**, *74*, 9490.
305. M. P. Coles. *Dalton Transactions* **2006**, 10.1039/B515490A, 985.
306. O. Mahé; D. Frath; I. Dez; F. Marsais; V. Levacher; J.-F. Brière. *Org. Biomol. Chem.* **2009**, *7*, 3648.
307. J. Ma; X. Zhang; N. Zhao; A. S. N. Al-Arifi; T. Aouak; Z. A. Al-Othman; F. Xiao; W. Wei; Y. Sun. *J. Mol. Catal. A: Chem.* **2010**, *315*, 76.

308. A. Horváth. *Tetrahedron Lett.* **1996**, *37*, 4423.
309. A. M. Funhoff; C. F. van Nostrum; M. C. Lok; M. M. Fretz; D. J. A. Crommelin; W. E. Hennink. *Bioconjugate Chem.* **2004**, *15*, 1212.
310. K. E. S. Locock; T. D. Michl; J. D. P. Valentin; K. Vasilev; J. D. Hayball; Y. Qu; A. Traven; H. J. Griesser; L. Meagher; M. Haeussler. *Biomacromolecules* **2013**, *14*, 4021.
311. N. J. Treat; D. Smith; C. Teng; J. D. Flores; B. A. Abel; A. W. York; F. Huang; C. L. McCormick. *ACS Macro Lett.* **2012**, *1*, 100.
312. O. Christiaens; M. G. Tardajos; Z. L. Martinez Reyna; M. Dash; P. Dubruel; G. Smagghe. *Front. Physiol.* **2018**, *9*.
313. S. Matsukawa; T. Harada; S. Yasuda. *Org. Biomol. Chem.* **2012**, *10*, 4886.
314. J. Zhu, in *Encyclopedia of Reagents for Organic Synthesis*, **2003**, https://doi.org/10.1002/047084289X.rn00330.
315. F. Fringuelli; F. Pizzo; C. Vittoriani; L. Vaccaro. *Eur. J. Org. Chem.* **2006**, *2006*, 1231.
316. S. Matsukawa; S. Fujikawa. *Tetrahedron Lett.* **2012**, *53*, 1075.
317. Y. Takashima; A. Harada. *J. Inclusion Phenom. Mol. Recognit. Chem.* **2017**, *88*, 85.
318. X. Yan; F. Wang; B. Zheng; F. Huang. *Chem. Soc. Rev.* **2012**, *41*, 6042.
319. J. Zhang; H. Qiu; T. He; Y. Li; S. Yin. *Front. Chem.* **2020**, *8*.
320. K. Liu; Y. Jiang; Z. Bao; X. Yan. *CCS Chemistry* **2019**, *1*, 431.
321. C. D. Gutsche; B. Dhawan; K. H. No; R. Muthukrishnan. *J. Am. Chem. Soc.* **1981**, *103*, 3782.
322. E. S. Español; M. M. Villamil. *Biomolecules* **2019**, *9*, 90.
323. M. Y. Hur; I. Hwang; K. Kim, in *Cucurbiturils and Related Macrocycles*, The Royal Society of Chemistry, **2020**, pp. 1.
324. G. Crini. *Chem. Rev.* **2014**, *114*, 10940.
325. R. Challa; A. Ahuja; J. Ali; R. K. Khar. *AAPS PharmSciTech* **2005**, *6*, E329.
326. G. Crini; S. Fourmentin; É. Fenyvesi; G. Torri; M. Fourmentin; N. Morin-Crini, in *Cyclodextrin Fundamentals, Reactivity and Analysis* (Eds.: S. Fourmentin, G. Crini, E. Lichtfouse), Springer International Publishing, Cham, **2018**, pp. 1.
327. N. Song; X.-Y. Lou; L. Ma; H. Gao; Y.-W. Yang. *Theranostics* **2019**, *9*, 3075.
328. L.-L. Tan; Y.-W. Yang. *J. Inclusion Phenom. Mol. Recognit. Chem.* **2015**, *81*, 13.
329. T. Kumpulainen; M. R. Panman; B. H. Bakker; M. Hilbers; S. Woutersen; A. M. Brouwer. *J. Am. Chem. Soc.* **2019**, *141*, 19118.
330. X. Han; G. Liu; S. H. Liu; J. Yin. *Org. Biomol. Chem.* **2016**, *14*, 10331.
331. A. R. Hedges. *Chem. Rev.* **1998**, *98*, 2035.
332. B. Tian; J. Liu. *New J. Chem.* **2020**, *44*, 9137.
333. G. Tiwari; R. Tiwari; A. K. Rai. *J Pharm Bioallied Sci* **2010**, *2*, 72.
334. M. Singh; R. Sharma; U. C. Banerjee. *Biotechnol. Adv.* **2002**, *20*, 341.
335. B. V. K. J. Schmidt; C. Barner-Kowollik. *Angew. Chem. Int. Ed.* **2017**, *56*, 8350.
336. E. M. M. Del Valle. *Process Biochem.* **2004**, *39*, 1033.
337. S. V. Kurkov; T. Loftsson. *Int. J. Pharm.* **2013**, *453*, 167.
338. J. W. Steed;J. L. Atwood, *Supramolecular Chemistry*, https://doi.org/10.1002/9780470740880.fmatter, John Wiley & Sons, Ltd, **2009**.
339. A. Zarepour; A. Zarrabi; K. L. Larsen. *Int. J. Nanomed.* **2019**, *14*, 7017.
340. L. Zhao; S. Hao; Q. Zhai; H. Guo; B. Xu; H. Fan. *Soft Matter* **2017**, *13*, 3099.
341. T.-W. Chuo; T.-C. Wei; Y.-L. Liu. *J. Polym. Sci., Part A: Polym. Chem.* **2013**, *51*, 3395.
342. B. V. K. J. Schmidt; M. Hetzer; H. Ritter; C. Barner-Kowollik. *Macromolecules* **2013**, *46*, 1054.
343. S. Saha; T. Ray; S. Basak; M. N. Roy. *New J. Chem.* **2016**, *40*, 651.

344. R. Kataky; P. M. Kelly; D. Parker; A. F. Patti. *J. Chem. Soc. Perk. Trans. 2* **1994**, https//doi.org/ 10.1039/P29940002381, 2381.
345. R. Maeztu; G. Tardajos; G. González-Gaitano. *J. Phys. Chem. B* **2010**, *114*, 2798.
346. C. M. Geiselhart, Self-Reporting Chemiluminescent Systems, Master thesis, Karlsruher Institut für Technologie (KIT) (Karlsruhe), **2017**.
347. C. M. Geiselhart; H. Mutlu; P. Tzvetkova; C. Barner-Kowollik. *Polym. Chem.* **2020**, *11*, 4213.
348. C. M. Geiselhart; C. W. Schmitt; P. Jöckle; H. Mutlu; C. Barner-Kowollik. *Sci. Rep.* **2019**, *9*, 14519.
349. S. Tshepelevitsh; A. Kütt; M. Lõkov; I. Kaljurand; J. Saame; A. Heering; P. G. Plieger; R. Vianello; I. Leito. *Eur. J. Org. Chem.* **2019**, *2019*, 6735.
350. M. Tassi; E. Bartollini; P. Adriaensens; L. Bianchi; B. Barkakaty; R. Carleer; J. Chen; D. K. Hensley; A. Marrocchi; L. Vaccaro. *RSC Adv.* **2015**, *5*, 107200.
351. J. P. Hooker; L. Delafresnaye; L. Barner; C. Barner-Kowollik. *Mater. Horiz.* **2019**, *6*, 356.
352. L. Delafresnaye; J. P. Hooker; C. W. Schmitt; L. Barner; C. Barner-Kowollik. *Macromolecules* **2020**, *53*, 5826.
353. Y.-Z. Wang; X.-X. Deng; L. Li; Z.-L. Li; F.-S. Du; Z.-C. Li. *Polym. Chem.* **2013**, *4*, 444.
354. W. Lin; W. Zhang; T. Sun; S. Liu; Y. Zhu; Z. Xie. *ACS Appl. Mater. Interfaces* **2017**, *9*, 29612.
355. J.-M. Noy; M. Koldevitz; P. J. Roth. *Polym. Chem.* **2015**, *6*, 436.
356. M. Ingold; G. V. López; W. Porcal. *ACS Sustain. Chem. Eng.* **2014**, *2*, 1093.
357. A. Kokel; C. Schäfer; B. Török, in *Green Chemistry and Chemical Engineering* (Eds.: B. Han, T. Wu), Springer New York, New York, NY, **2019**, pp. 573.
358. M. Ingold; R. Dapueto; S. Victoria; G. Galliusi; C. Batthyàny; M. Bollati-Fogolín; D. Tejedor; F. García-Tellado; J. M. Padrón; W. Porcal; G. V. López. *Eur. J. Med. Chem.* **2018**, *143*, 1888.
359. D. Estupiñán; T. Gegenhuber; J. P. Blinco; C. Barner-Kowollik; L. Barner. *ACS Macro Lett.* **2017**, *6*, 229.
360. D. Sahoo; V. Narayanaswami; C. M. Kay; R. O. Ryan. *Biochemistry* **2000**, *39*, 6594.
361. K. Hayashi; Y. Mitsuyoshi; T. Kamei; T. Shimanouchi; K. Suga; Y. Okamoto; H. Nakamura; H. Umakoshi. *ACS Omega* **2018**, *3*, 3572.
362. R. D. Pensack; R. J. Ashmore; A. L. Paoletta; G. D. Scholes. *J. Phys. Chem. C* **2018**, *122*, 21004.
363. Y. Ji; J. Sweeney; J. Zoglio; D. J. Gorin. *J. Org. Chem.* **2013**, *78*, 11606.
364. J. T. Lai; D. Filla; R. Shea. *Macromolecules* **2002**, *35*, 6754.
365. G. R. Fulmer; A. J. M. Miller; N. H. Sherden; H. E. Gottlieb; A. Nudelman; B. M. Stoltz; J. E. Bercaw; K. I. Goldberg. *Organometallics* **2010**, *29*, 2176.
366. R. Wagner; S. Berger. *Journal of Magnetic Resonance, Series A* **1996**, *123*, 119.
367. M. J. Thrippleton; J. Keeler. *Angew. Chem. Int. Ed.* **2003**, *42*, 3938.

Acknowledgements

It would have never been possible for me to complete this PhD thesis without the help and support of all the people accompanying me during the last years, therefore

"I can no other answer make but thanks, and thanks, and ever thanks…."

(William Shakespeare)

First and foremost, I want to thank my supervisor Prof. Christopher Barner-Kowollik for the opportunity to work on this fascinating project within the macroarc group. Thank you for the outstanding mentorship and the everlasting support while working simultaneously on two different continents. Our meetings were always highly motivating and inspiring to solve all the countless problems and challenges that came around. I also want to thank you for the chance to spent an amazing time at the Queensland University of Technology in Brisbane. It was a great pleasure to do this PhD thesis under your supervision.

At the same time, my warmest gratitude goes to Dr. Hatice Mutlu. I would have never been able to finish this work without your never ending optimism and infinite pool of ideas to eventually make things work. I highly appreciate the many hours you spent improving manuscripts and discussing over and over again the replies for the reviewers' comments. Despite your own problems and obstacles your door was always open and I could always count on your advice and support. Besides the work however, recreation time was an essential part since our first meeting more than 5 years ago and it was always a lot of fun. Thank you so much for everything!

Furthermore, I want to thank Dr. Anja Goldmann, Dr. Eva Blasco, Dr. Patrick Hodapp, Dr. Laura Delafresnaye, Dr. Dominik Voll, Dr. Maria Schneider, Katharina Elies, Birgit Huber, Evelyn Stühring and Martina Ritter for their organizational and technical support during my PhD time. A special thanks goes to Dr. Pavleta Tzvetkova for the NOESY measurements. Thanks for your valuable time and the fruitful discussions about the results. In this regard, I also want to thank Dr. Aaron Micallef for the support with the EPR measurements and evaluation of the data.

Moreover, I would like to thank IBG-I, the ComPlat group, Prof. M. A. R. Meier and Prof. P. Théato for the access to all the additional chemicals and analytical devices.

I gratefully acknowledge the “Deutsche Akademische Austauschdienst” (DAAD) for the financial support during my research stay at the Queensland University in Brisbane.

A big thanks goes of course to the whole macroarc team at both the KIT and the QUT node for a great atmosphere. Thanks for all the cheerful coffee breaks, barbeques, group trips and PhD parties. Here, I also want to thank the members of AK Théato (especially Edgar, Martin and Sergej) for the invitations to their group activities and for the funny times at campus south.
I am especially thankful for all the great people that were working in the Soft Matter Lab at campus north in the last years: Nicholas, Silvana, Diego, Federica, Sylvain, Birgit, Hatice, Timo, Daniel, Tiep, Jan, Patrick H. and Marc. Thanks for an amazing working atmosphere, which was based on team work, refreshing lunch- and coffee breaks, cakes, Glühwein and all the other things I forgot to mention here. I very much enjoyed working with you!

In addition, I want to thank my fellow students (particularly Larissa, Sergej, Sara, Yannic and Tanja) who made the hole study time an unforgettable experience. Thanks for all the fun during the many lectures and lab courses, study sessions for exams, sleeping accommodations and not to forget the visits to the Christmas markets, parties and birthday celebrations, to mention just a few.
Likewise, I’m grateful to all my friend from outside the KIT and their continuous support within the last years. From relaxing weekends, barbeques, holidays, hiking trips, a short coffee in between to the many other experiences and activities I could gain the energy and motivation to finally complete this PhD project.

Last but definitely not least, my greatest thanks goes to my family. Thank you so much for your everlasting support and encouragement. I know I can always count on you no matter what. You’re amazing!